2015

Molecular Modeling Assisted Design and Synthesis of Unsymmetrical Anthracene Isoxazole Small Molecule Anti-tumor Agents

Nathan S. Duncan
The University of Montana

Molecular Modeling Assisted Design and Synthesis of Unsymmetrical Anthracene

Isoxazole Small Molecule Anti-tumor Agents

By

NATHAN SCOTT DUNCAN

B.S. Biochemistry, Missouri Southern State University, Joplin, Missouri, 2010
M.S. Medicinal Chemistry, University of Montana, Missoula, Montana, 2013

Dissertation

presented in partial fulfillment of the requirements
for the degree of

Doctorate of Philosophy
in Medicinal Chemistry

The University of Montana
Missoula, Montana

May 2015

Approved by:

Sandy Ross, Dean of The Graduate School
Graduate School

Nicholas R. Natale, Director, Medicinal Chemistry Program
Department of Biomedical and Pharmaceutical Sciences

Howard D. Beall
Department of Biomedical and Pharmaceutical Sciences

Donald Stierle
Department of Biomedical and Pharmaceutical Sciences

Keith Parker
Department of Biomedical and Pharmaceutical Sciences

Orion B. Berryman
Department of Chemistry & Biochemistry

"Molecular Modeling Assisted Design and Synthesis of Unsymmetrical Anthracene Isoxazole

Small Molecule Anti-tumor Agents"

Chairperson: Nicholas R. Natale

Co-Chairperson: Howard D. Beall, Donald Stierle, Keith Parker, Orion B. Berryman

There are several isoxazoles in general medical practice and their metabolic fate and disposition is well known, and thus, this heterocyclic ring is often considered among the privileged scaffolds or templates for drug design and discovery. Many examples can be found of 3-aryl-isoxazoles which in theory have a chiral axis, yet actual experimental examples of direct determinations of isoxazole rotational barriers are few and far between. The dihedral angle of the 3-aryl to isoxazole bond in antibacterials of the oxacillin series increased with substitution in the 2- and 6- positions of the phenyl. Although his calculated barrier was low, this implied that atropisomers are possible for unsymmetrical substitution. The chirality of these systems differs from that of other compounds as their configuration is inverted by rotation about single bonds and can be accomplished by thermal equilibration. Thus, depending on the barrier to rotation, some of these atropisomers may only be isolated at low temperatures, if at all.

Recognition of the chiral elements, helicity and sugar morphology, of DNA by a small chiral molecule has long been an area of interest for the design of new antitumor medicines. It is expected that chiral atropisomers would exhibit a significant eudismic ratio when the functional groups of the chiral small molecule addresses the chiral portion of the molecular target. Our working hypothesis is based on docking studies with our putative molecular target G4-DNA, and indicates a eudismic ratio for atropisomers which arises precisely from the functional group which renders the molecule axially chiral. The study described herein propose to characterize at atomic resolution the first such atropisomerc isoxazole interacting with G4, an interaction that spans the domain interface from the G-tetrad deck to the sugar phosphate backbone, thus providing a rigorous framework for the development of selectivity among the major classes of G4 structures.

The goal is rational design of therapeutic aryl isoxazoles in which the barrier to stereochemical inversion (rotation) can be tailored to the application. By this means, we can probe the efficacy (binding efficiency) of potential drugs locked in a particular atropisomeric form *vs* freely/restricted rotating at physiological temperatures. In the course of these studies we have prepared analogs with enhanced bioactivity in the sub-micromolar to nanomolar range, which in principle contain a chiral axis. It is important for our current study to experimentally elucidate these conformational dynamics, and knowledge of such dynamics will be useful in the broader impact sense of providing energetic benchmarks for others in the field.

ACKNOWLEDGEMENT

TABLE OF CONTENTS

List of Figures

List of Charts

List of Tables

List of Schemes

Chapter 1

Isoxazoles in the PDB

1.1 Introduction

It is commonly accepted that a majority of the published work in organic chemistry involved at least one heterocyclic ring. Heterocycles can play a pivotal role not only as goals in synthesis, but as mediators of synthetic transformations. Isoxazoles are unique in their chemical behavior not only among heterocyclic compounds in general but also among related azoles. This is because isoxazoles possess the typical properties of aromatic systems, which are in fact rather pronounced in these derivatives, together with high lability of the ring under certain conditions, particularly route to liberate the latent functionality. From a purely formal point of view isoxazole can be considered an analog of pyridine just as furan is an analog of benzene. Such formal analogy is to some extent valid; for isoxazole resembles pyridine more than other heterocyclic compounds as far as chemical properties are concerned. It differs from pyridine in undergoing more readily electrophilic substitutions reactions and possessing a more labile ring this relationship thus resembles that between furan and benzene.

The isoxazole ring appears in several drugs in general medical practice, and is found routinely in drug discovery leads, to the point where some consider it a privileged scaffold. The literature on crystallography has continued to expand at an accelerating pace in recent years, and it seemed that a summary of the observed interactions of the isoxazole moiety with biological targets could be useful to those involved in design and discovery. Especially intriguing in light of the fact that most medicinal chemists use some form of molecular modelling, is that a collection of the observed interactions could prove useful in assessment of hypothesis generation.

The current review covers isoxazole ligands in the Protein data bank (PDB) reviewed April 27, 2015, there were 174 isoxazole containing ligands and 215 discreet drug-receptor interactions deposited and released to the PDB. There has been classic work on topics such as sulfamethoxazole, beta-lactams, antivirals, and the AMPA receptor, as well as intense recent interest in topics such as BRD, FXR, kinases and HSP90. We have attempted to describe here the most essential interactions defining the potential role of an isoxazole in drug-receptor interactions. The full analysis of the data set is summarized in the Table, and a more detailed comprehensive discussion will appear in an invited review to *Future Medicinal Chemistry.*

1.2 Types of interactions

Our general discussion of interactions will begin with common modes of interaction that have

been observed in coordination chemistry[1].
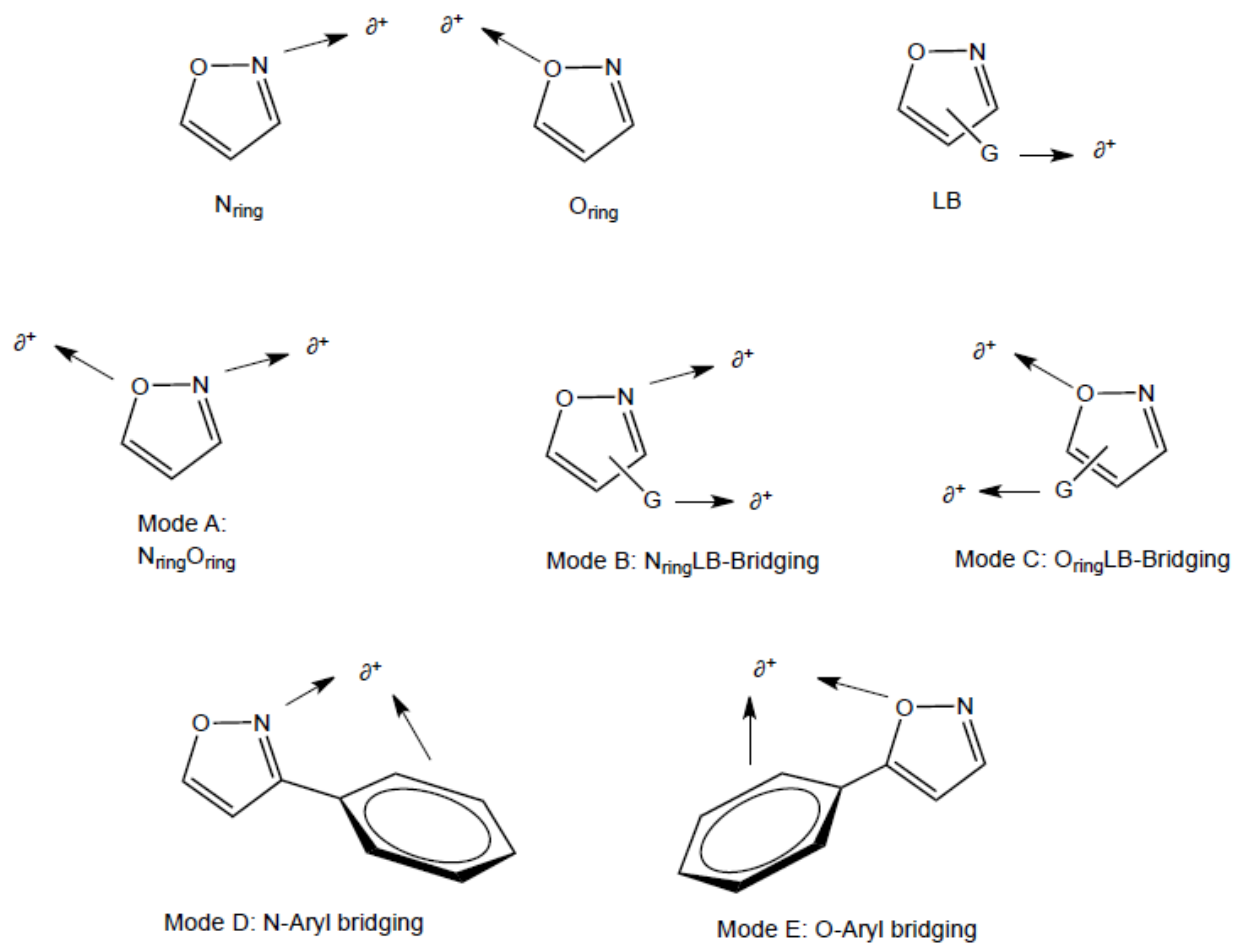
Chart 1-1. Isoxazole binding modes observed in metal complexes, generalized to interactions with Lewis Acids $\partial+$. In the Munsey review, conjugated amino groups were considered in the coordination chemistry with metals, here generalized to conjugated Lewis bases (LB). Reprinted with permission from reference 1.

The depiction of three dimensional shape in two dimensions is often a difficult undertaking,

however, the Stierand and Rarey notation used on the PDB is the best current solution[2].
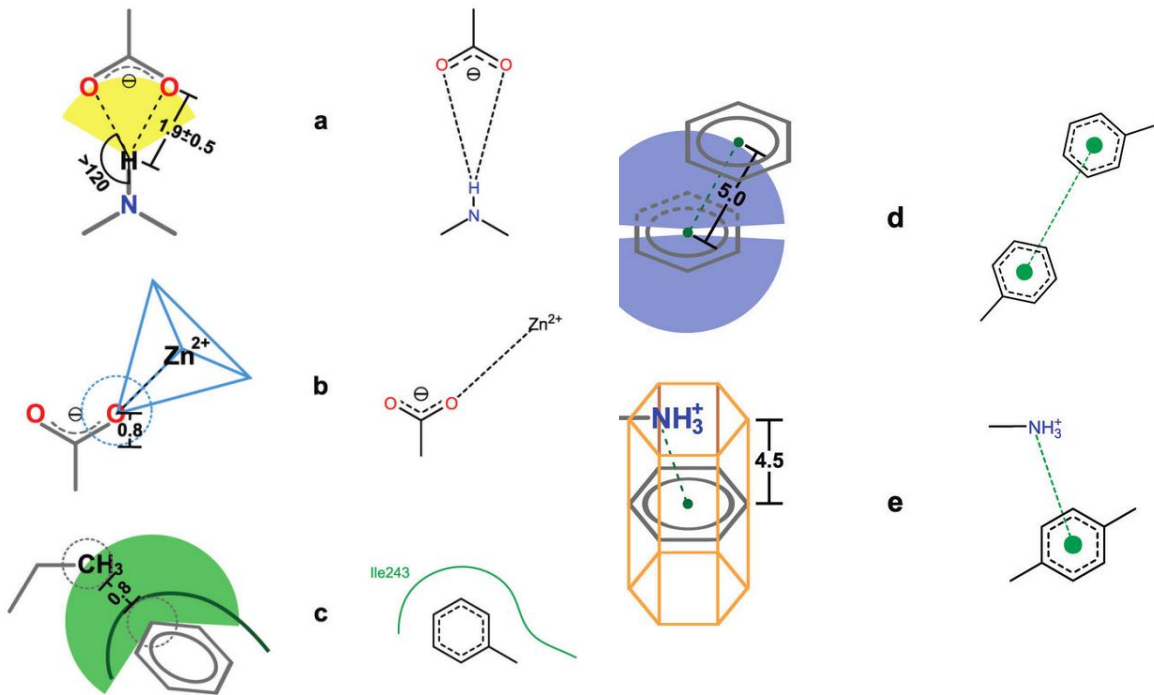
Chart 1-2. The ligand interactions in the protein data bank are based on the graphic nomenclature. Reprinted with permission from reference 2.

1.3 Sulfamethoxazole

Dihydropteroate synthase enzyme in bacteria has been a target for many years to help combat bacterial infections in both gram-positive and gram-negative organisms. Since bacteria have to synthesize folic acid for DNA synthesis, targeting this enzyme would allow for selective toxicity to bacterial cells. Sulfa drugs interrupt this essential folate pathway by competing with
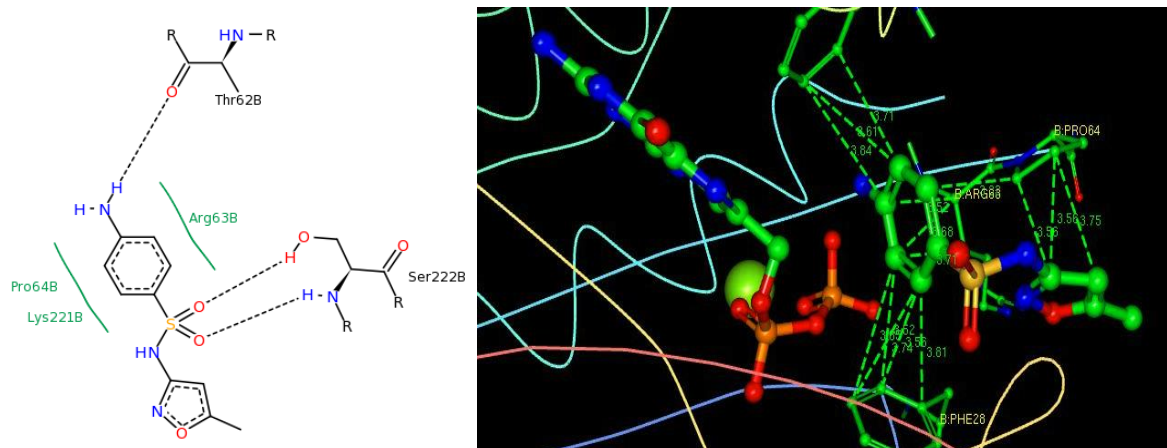
Figure 1-1. Sulfamethoxazole interactions with dihydropteroate synthase. Left, image from the RCSB PDB of PDB ID 3TZF. Right, *Ligand Explorer* reveals hydrophobic interactions with the isoxazole. Yun, M.K., Wu, Y., Li, Z., Zhao, Y., Waddell, M.B., Ferreira, A.M., Lee, R.E., Bashford, D., White, S.W. Catalysis and sulfa drug resistance in dihydropteroate synthase. Science. 2012. 335: 1110-1114.

the 4-Aminobenzoic acid (PABA) precursor. Sulfamethoxazole was the first isoxazole containing drug to hit the market. The first dihydropteroate synthase crystallized with sulfamethoxazole appeared in 2012. The 5-methyl-3- sulfonamide isoxazole plays a role as a spacer for anchoring two hydrogen bonds with one each of the carbonyl groups of the sulfone to Ser222B[3], and Ligand Explorer reveals direct isoxazole hydrophobic interactions that are seen for the C3 and C4 carbons of the isoxazole with Proline 64 (Figure 1-1).

1.4 Beta-lactamase

β-Lactamases are one of the most recognizable and most widely prescribed antibiotics used to treat a number of bacterial infections. β-Lactamases, such as penicillins, cephalosporins,
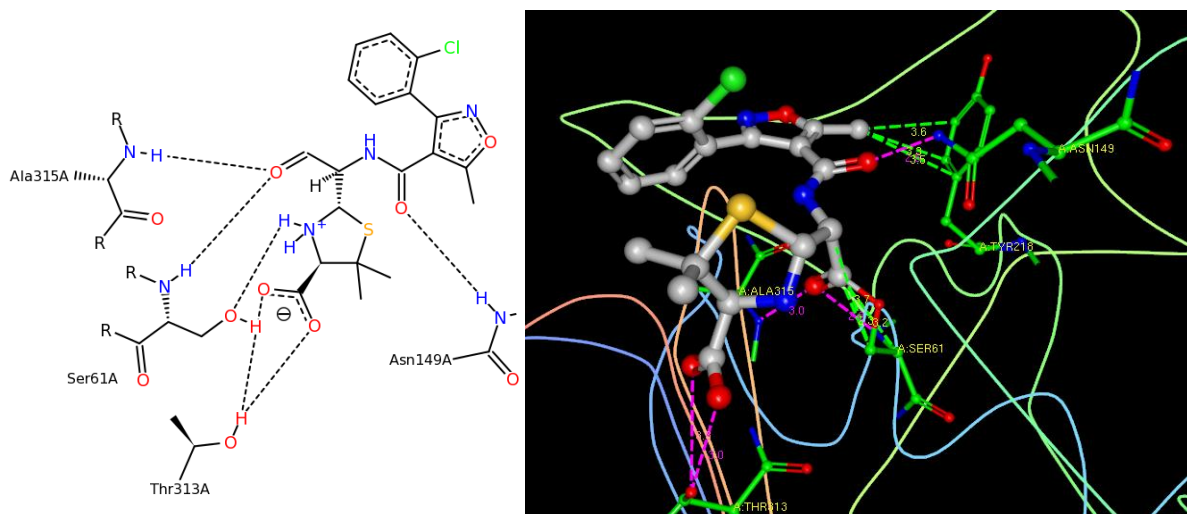
Figure 1-2. Cloxacillin interactions with β-lactamase. Left, image from the RCSB PDB of PDB ID 1FCM. Left, interaction map and Right, *Ligand Explorer* reveals hydrophobic interactions with the isoxazole. Patera, A., Blaszczak, L.C., Shoichet, B.K. Crystal structures of Substrate and Inhibitor Complexes with AmpC-Lactamase: Possible Implications for Substrate-Assisted Catalysis. J.Am.Chem.Soc. 2000, 122: 10504-10512.

and carbapenems work by inhibiting cell wall synthesis inhibiting of the peptidoglycan layer in the cell wall. β -lactam analogs preserve the β-lactam core of the drug but explore diverse functionality of the amide bond substituents to help understand the different pharmacological profiles and different bacterial spectra of action. However, different levels of resistance to β-lactamases comes with such a diverse pharmacophore, as well as, the added concern of overuse and misuse of these drugs.[4, 5]

Lactamases are categorized into three classes (A, B, and C) with many subclasses. While class B enzymes use a zinc-based mechanism for hydrolysis as opposed to a nucleophilic serine-based two-step mechanism for class A and C, the potential problem lies in the covalent bond that β-lactams form with such diverse β-lactamases[4,5]. However, as more classes of β–lactamases

being discovered and characterized, the diversity in their substrate selectivity profiles became apparent.

With many β-lactamases having been crystallized with antibiotics containing isoxazoles (Chart 1-3), a ligand interactions diagram can start unfolding. Many of the interactions that occur with isoxazole in the binding pocket are aliphatic hydrophobic interactions of the C5-methyl-isoxazole and isoxazole-aryl, although direct isoxazole interactions were noted in 1NYY (Figure 1-2). Another interesting case comes from Patera (2000) when they crystallized cloxacillin (open-form) with in beta-lactamase not only showing hydrophobic interactions of the C5-methyl-isoxazole with Tyr218, but also the *first known resolved axially chiral 3-aryl- isoxazole* found in the literature. With continued efforts, the structural bases for isoxazole containing β-lactamase antibiotics structure-activity-relationship will continue to grow and become well understood and remain areas of intense investigation.
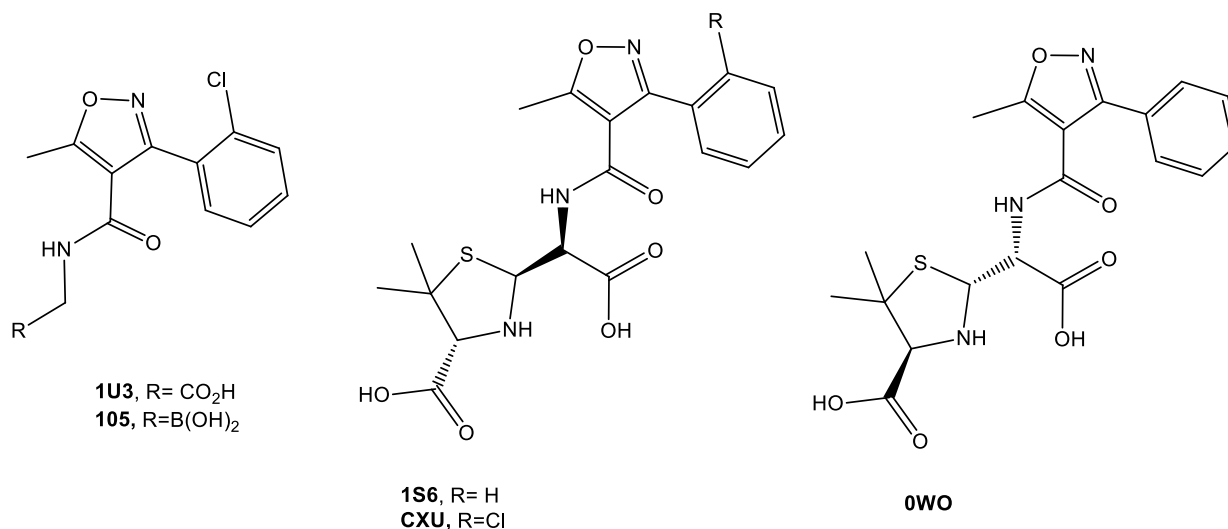
Chart 1-3. Ligands containing isoxazole moieties of β-lactamase.

7

1.5 Rhinovirus

Small icosahedral RNA viruses that are a part of the *Picornaviridae* family, including the rhinoviruses are the most common and leading viral infection in humans for upper respiratory tract infections, also known as the common cold. Human rhinoviruses are composed of a capsid, that contains four viral proteins VP1, VP2, VP3 and VP4 consisting of 60 copies of each. VP1, VP2, and VP3 form the major part of the protein capsid with 8 anti-parallel-barrels. The smaller VP4 protein has a polypeptide chain and lies at the internal surface of the capsid. Rhinoviruses have a surface "canyon" which is the binding site for many surface molecules. Below the floor of the "canyon" within the VP-1 barrel, lies a hydrophobic pocket which is hypothesized to play a role in maintaining the capsid stability. Thus, effort into building a small molecule to stabilize the capsid via binding in the hydrophobic space (Figure 1-3, shown below) to an extent that the
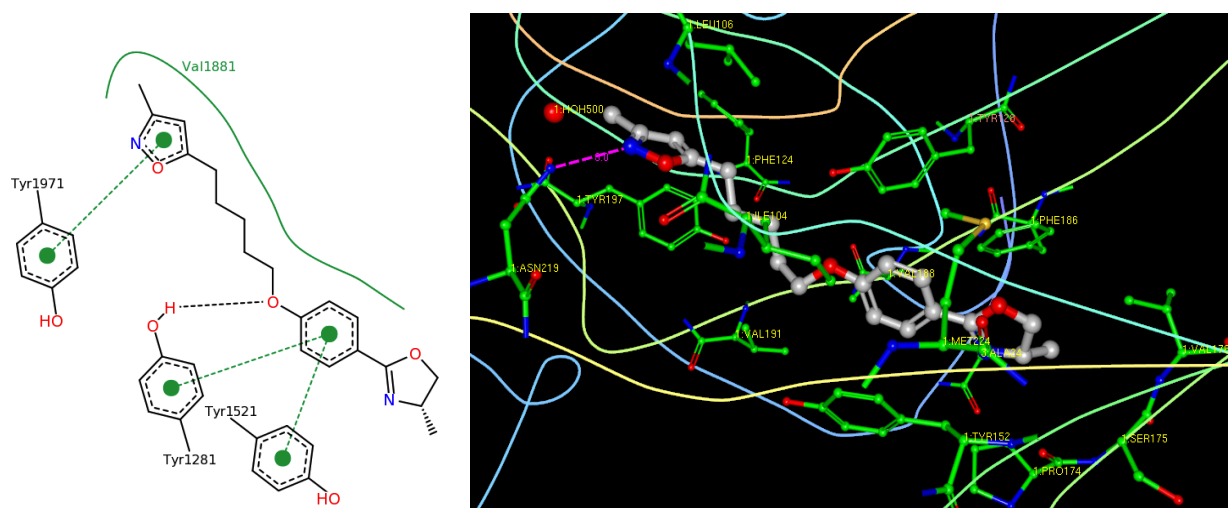
virus cannot release its RNA

Figure 1-3. W56 ligand interactions of Antiviral human rhinovirus 14. Left, image from the RCSB PDB of PDB ID 2RS5. Right, *Ligand Explorer* reveals N_{ring}-H-Bond –Asn219 and p-Ring-Isox-π-Leu106/Phe124 interactions with the isoxazole. Badger, J., Minor, I., Oliveira, M.A., Smith, T.J., Rossmann, M.G. Proteins 1989, 6: 1-19.

into the target cell is underway. A new development in antiviral drugs came when Pleconaril

made to clinical trials. Although the FDA did reject the new-drug application due to safety concerns, although it is under further investigation, it is a breakthrough in the sense that small molecules could be designed to bind in the hydrophobic pocket to prevent RNA release (Chart 1-4 and 1-5).[6, 7]
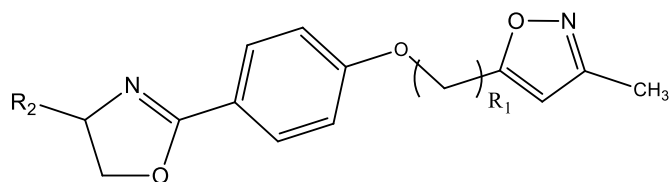
W35. R_1=5, R_2=H
W71. R_1=7, R_2=H
W56. R_1=5, R_2=(S)-CH$_3$
W8R. R_1=7, R_2=(R)-CH$_3$
W84. R_1=7, R_2=(S)-CH$_3$
W59. R_1=7, R_2=(S)-CH$_2$CH$_3$

= R   W01

= R   W02

= R   W03
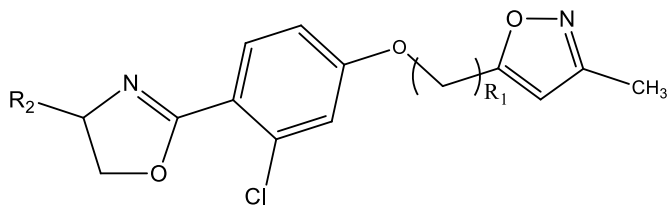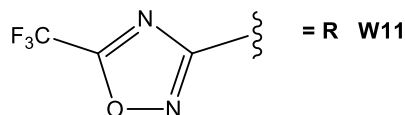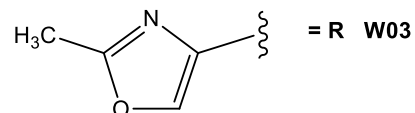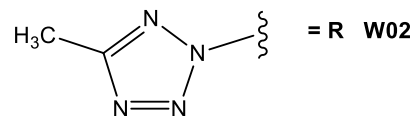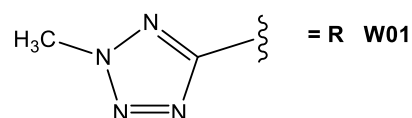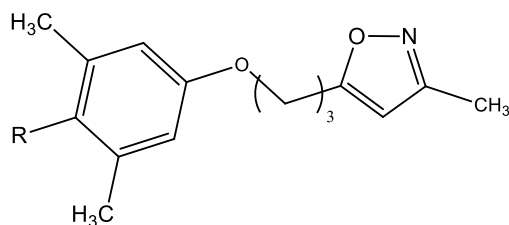
W33. R_1=5, R_2=H
W43. R_1=7, R_2= (S)-CH$_3$

= R   W11

Chart 1-4. Isoxazole ligands for rhinovirus.
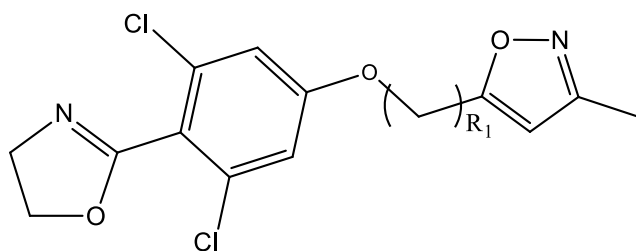
W91. R$_1$=3, R$_2$=CH$_3$
W54. R$_1$=5, R$_2$=CH$_3$
W33. R$_1$=5, R$_2$=
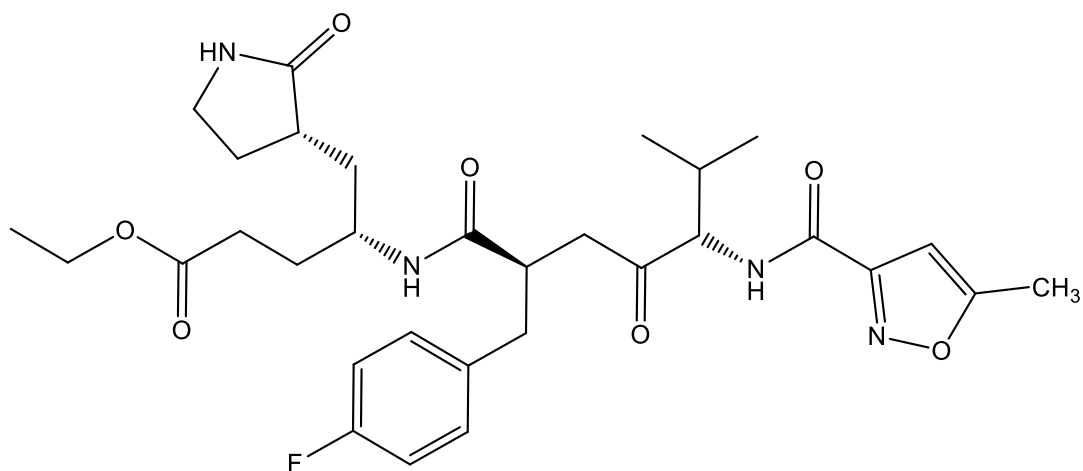
AG7

Chart 1-5. Isoxazole ligands for rhinovirus.

1.6 MMP

Matrix metalloproteinases (MMPs) are part of a large family of proteases that are zinc-dependent endopeptidases. Collectively, MMPs degrade all kinds of extracellular matrix proteins and participate in connective tissue remodeling and in numerous other physiological processes[8]. With MMPs being implicated in multiple pathways, extensive efforts to develop new and more
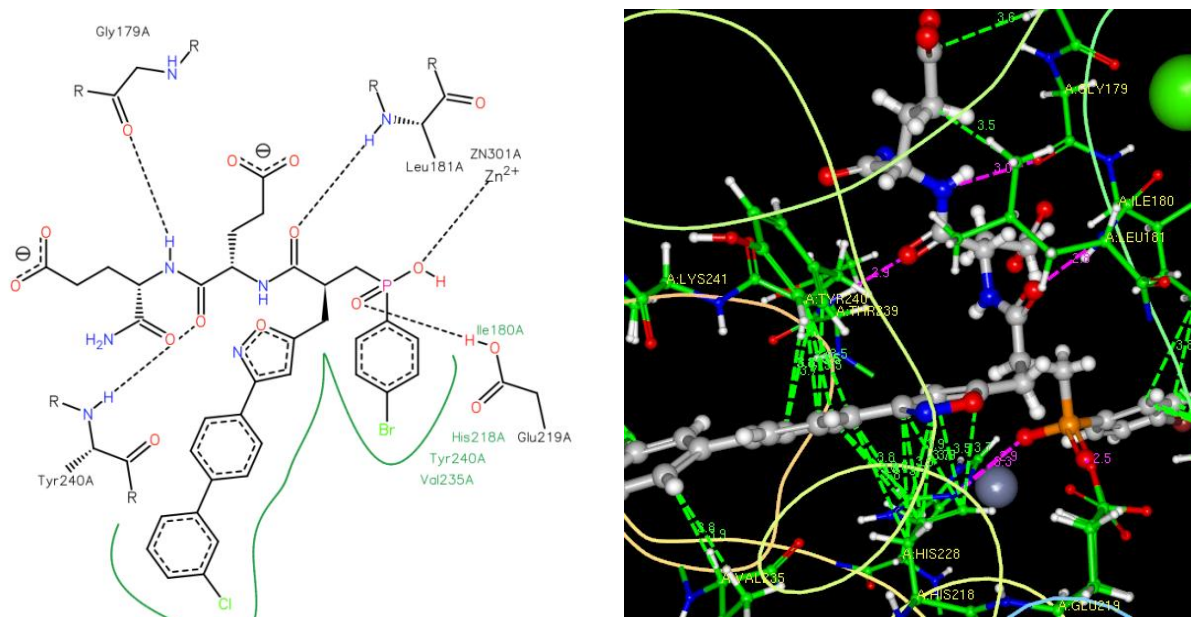
Figure 1-4. R47 ligand interactions with matrix metalloproteinase 12. Left, image from the RCSB PDB of PDB ID 4GQL. Right, *Ligand Explorer* reveals π-Ring-Isox- π -His218; C3-Ph-Tyr240/His218 interactions with the isoxazole. Czarny, B., Stura, E.A., Devel, L., Vera, L., Cassar-Lajeunesse, E., Beau, F., Calderone, V., Fragai, M., Luchinat, C., Dive, V. J.Med.Chem. 2013, 56: 1149-1159.

potent inhibitors is a target for a variety of therapeutic applications with the initial broad-spectrum inhibitor, a synthetic inhibitor, showed disappointing results in clinical trials[9]. The first MMP inhibitor containing an isoxazole was shown in 2007 for MMP9, since then only literature has been seen for MMP12 with the most recent derivatives by Czarny[10] (Chart 1-6) showing sub-nano-molar to pico-molar activity is attainable. The isoxazole side chain extends deep into the cavity of MMP-12 and ring stacks on the His218 imidazole ring (Figure 1-4, shown above).
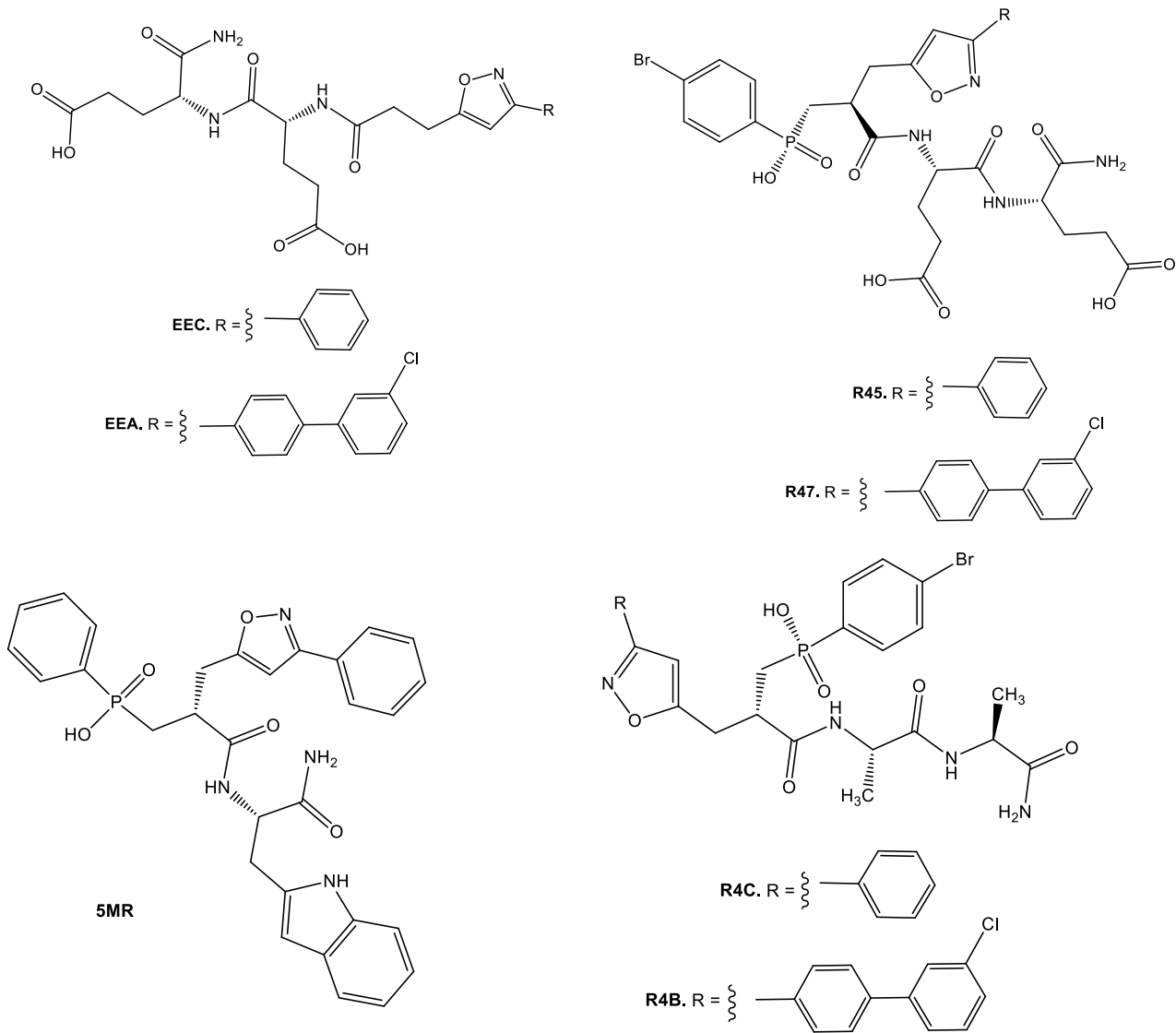
Chart 1-6. Isoxazole ligands at the matrix metalloproteinases (MMP).

1.7 Heat Shock Protein 90 (HSP90)

Heat shock protein 90 (HSP90) has a complex function involving homodimerization, assisting protein folding, stabilizes proteins against heat stress and aids in protein degradation.
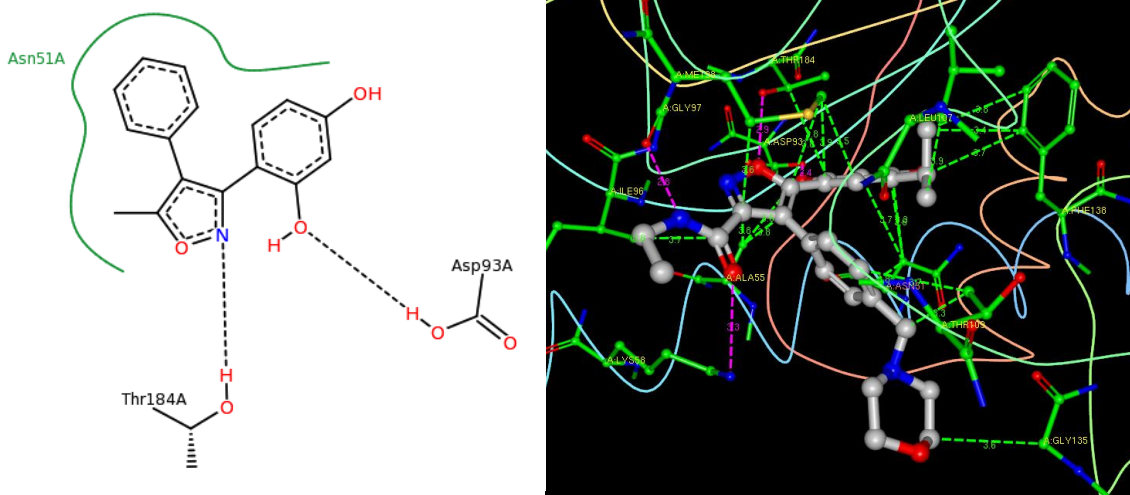
Figure 1-5. 2JG ligand interactions with HSP90. Left, image from the RCSB PDB of PDB ID 2VCI. Right, *Ligand Explorer* reveals N_{ring}-H-Bond–Thr184 interactions with the isoxazole. Brough, P.A., Aherne, W., Barril, X., Borgognoni, J., Boxall, K., Cansfield, J.E., Cheung, K.M., Collins, I., Davies, N.G.M., Drysdale, M.J., Dymock, B., Eccles, S.A., Finch, H., Fink, A., Hayes, A., Howes, R., Hubbard, R.E., James, K., Jordan, A.M., Lockie, A., Martins, V., Massey, A., Matthews, T.P., Mcdonald, E., Northfield, C.J., Pearl, L.H., Prodromou, C., Ray, S., Raynaud, F.I., Roughley, S.D., Sharp, S.Y., Surgenor, A., Walmsley, D.L., Webb, P., Wood, M., Workman, P., Wright, L. J.Med.Chem. 2008, 51: 196.

The chaperone cycle is driven by hydrolysis of ATP to ADP with a binding pocket in the N-terminal domain, in which most inhibitors are bound within. The dysregulation of pathways involving stabilizing a number of proteins that play a key role in assisting survival, proliferation, invasion and metastasis is why HSP90 inhibitors are investigated as potential anti-cancer drugs. HSP90 is expressed in normal cell homeostatis, comprising 1-2% of total cellular protein, however, many theories have been proposed for rationales for selectively of HSP90 in cancer cells versus normal cells [11]. A group from Vernalis[11], found that bioisoteric replacement of a pyrazole with 3,4-diaryl isoxazole-5-carboxamides resulted in potent anticancer activity (Figure

1-5, shown above). The crystal structure revealed binding at the ATP binding pocket of heat shock protein 90 (HSP90). Key interactions include Oring-hydrogen bond with Thr184 and hydrophobic interactions of Met98 with the isoxazole ring (Chart 1-7).
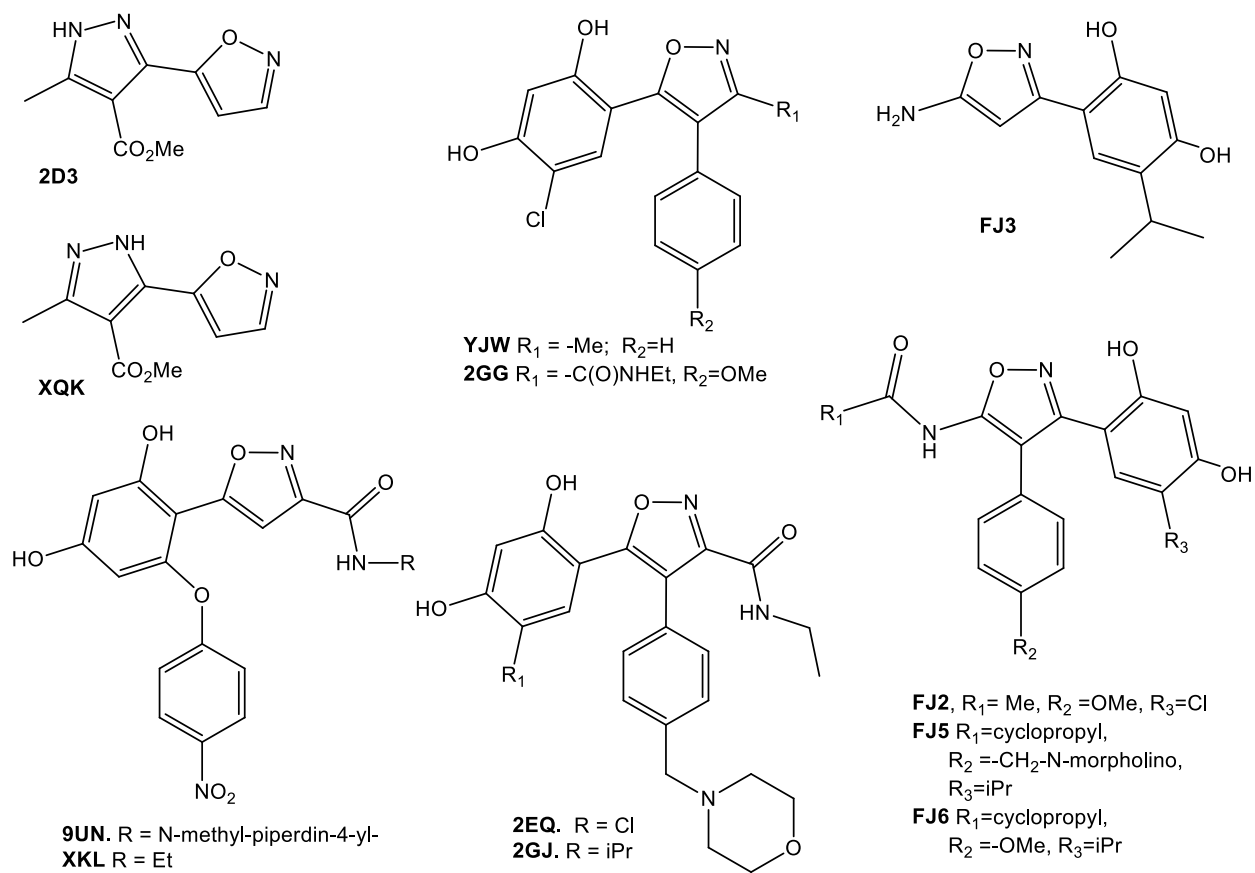
Chart 1-7. Isoxazole ligands for chaperone protein Heat Shock Protein 90 (HSP90).

14

1.8 Farnesoid X receptor (FXR)

The farnesoid X receptor (FXR), also known as, the bile acid receptor (BAR), is a part of a large nuclear receptor family which regulates gene transcription. Just like other nuclear receptors, FXR, when activated, translocated to the nucleus, forms a dimer and binds to a response element of DNA, which up- or down-regulates the expression of certain genes. FXR is expressed highly in the liver and intestine and to a less extent in gallbladder, kidney and adrenal
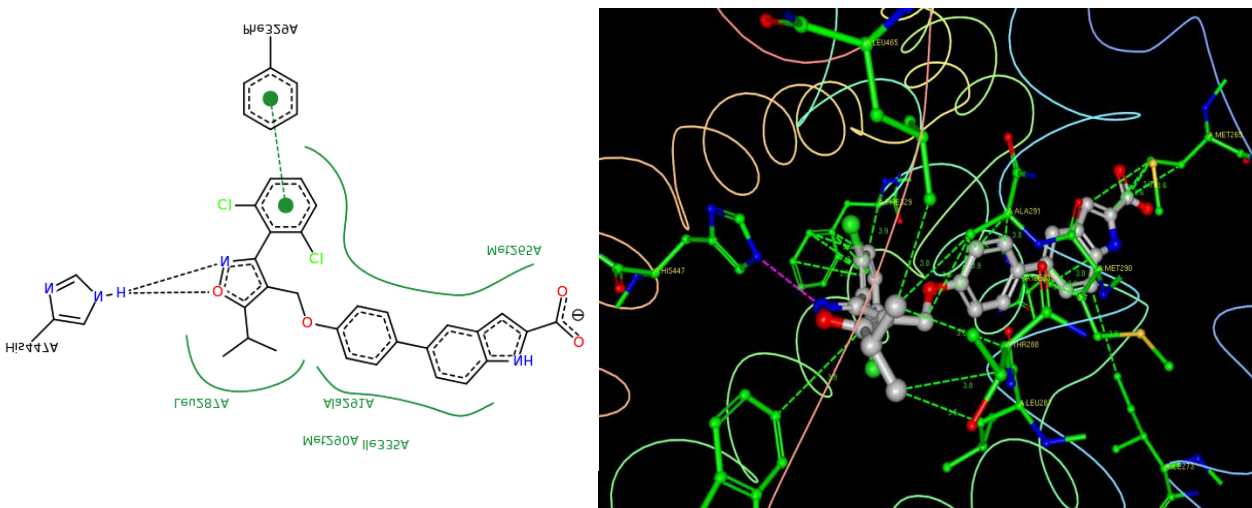
Figure 1-6. 034 ligand interactions with FXR. Left, image from the RCSB PDB of PDB ID 3RVF. Right, *Ligand Explorer* reveals Bifurcated-N_{ring}-O_{ring}-H-bond-Asn447A, π-Ring-C3-Cl$_2$-Ph-π-Phe329A and C5-iPr-Leu387A interactions with the isoxazole. Akwabi-Ameyaw, A., Caravella, J.A., Chen, L., Creech, K.L., Deaton, D.N., Madauss, K.P., Marr, H.B., Miller, A.B., Navas, F., Parks, D.J., Spearing, P.K., Todd, D., Williams, S.P., Wisely, G.B. Bioorg.Med.Chem.Lett. 2011, 21: 6154-6160.

glands. FXR is a key controller of bile acid homeostasis, as well as, helps maintain glucose homeostasis. With such diverse functions, FXR has the potential in many aspects of health practices, such as: inflammatory bowel disease, diabetes, obesity, and liver cancer among other possibilities. This first isoxazole continuing FXR inhibitor in the literature was found to be from Akwabi-Ameyaw[12] in 2008. Since then, many other groups have come out with additional potent isoxazole containing inhibitors for FXR[13–17] (Chart 1-8). Interesting binding interactions came

from Akwabi-Ameyaw[14] (Figure 1-6) showing a bifurcated N_{ring}-O_{ring}-H-bond with Asn447A and additional hydrophobic interactions with π-Ring-C3-Cl$_2$-Ph-π, π-Phe329A and C5-iPr-Leu387A.
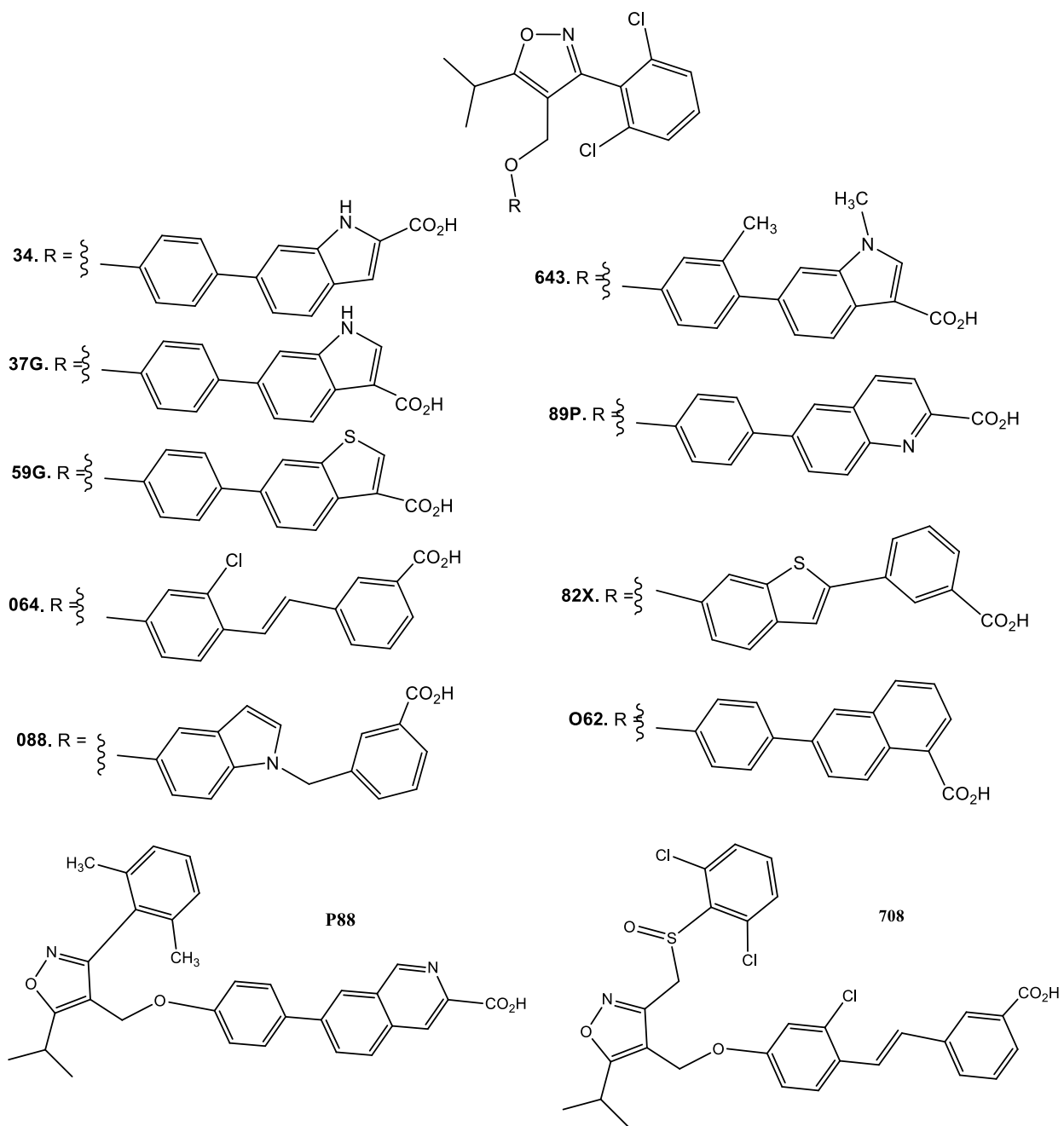
Chart 1-8. Isoxazole ligands at the Farnesoid X Receptor (FXR).

1.9 Human angiotensin-I converting enzyme (hACE)

Human angiotensin-I converting enzyme (hACE) is a well-accepted agent used for the treatment of hypertension, electrolyte homeostasis, and related cardiovascular diseases. ACE enzyme is a membrane-bound zinc metalloprotease having two primary functions: the first, catalyzing the conversion of a peptide hormone that acts a potent vasoconstrictor, and two, degrades a potent vasodilator.[18] With a majority of the commercially available ACE inhibitors being designed back in the 1970s, a second generation of ACE inhibitors (Chart 1-9) that has enhanced selectively without the undesirable side effects will be boosted by the availability of high resolution structures currently being published. One example comes from Masuyer[19] showing hydrophobic interactions to both Val380A and Val518A (Figure 1-7).
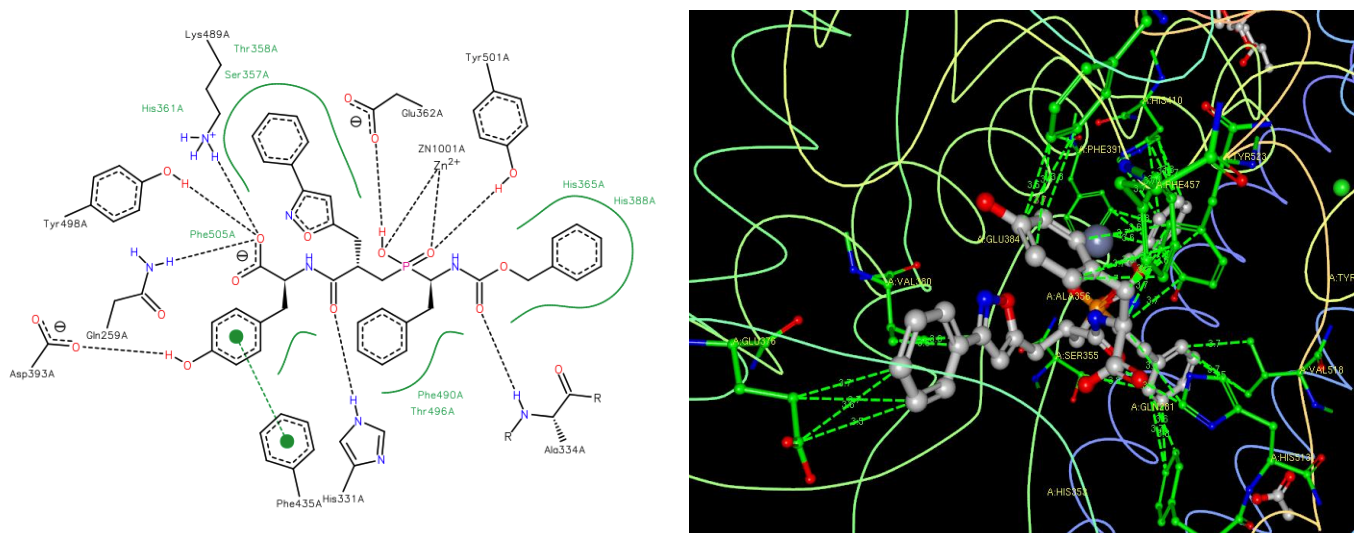
Figure 1-7. 3EF ligand interactions with hACE. Left, image from the RCSB PDB of PDB ID 4CA5. Right, *Ligand Explorer* reveals Val380A and Val518A hydrophobic interactions with the isoxazole. Masuyer, G., Akif, M., Czarny, B., Beau, F., Schwager, S.L., Sturrock, E.D., Isaac, R.E., Dive, V., Acharya, K.R. FEBS J. 2014, 281: 943.

3ES
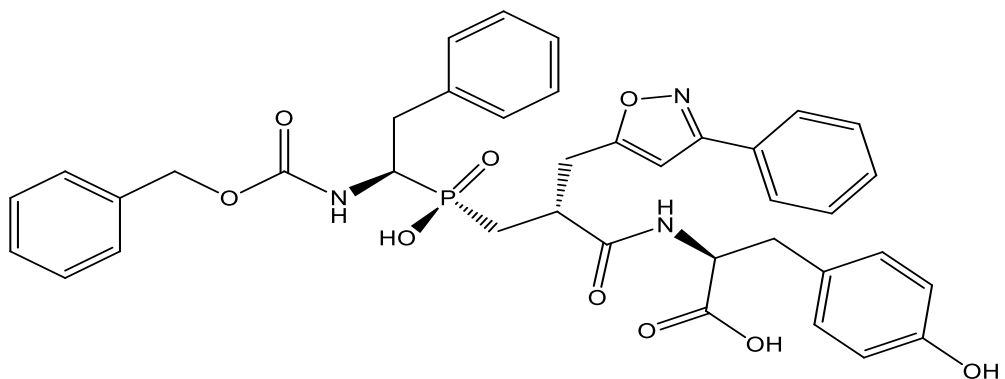
3EF
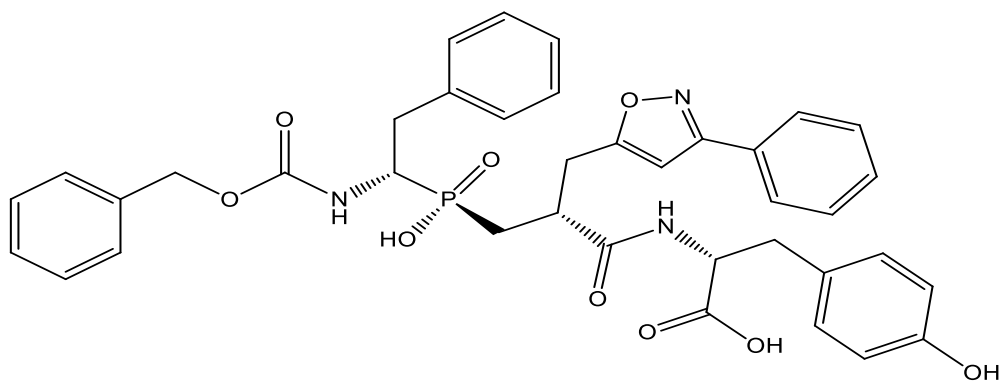
Chart 1-9. Isoxazole ligands at the human angiotensin converting enzyme (hACE).

1.10 Bromodomain (BRD)

The bromodomain protein module, which binds to acetylated lysine, is emerging as an important epigenetic therapeutic target. Conway and colleagues reported the structure-guided optimization of 3,5-dimethylisoxazole derivatives to develop potent inhibitors of the BET (bromodomain and extra terminal domain) bromodomain family with good ligand efficiency[20]. The first bromodomain crystallized with an isoxazole ligand appeared in 2011, and since then there has been intense activity in the area, with 28 structures. The 3, 5-dimethyl isoxazole plays a bioisosteric role for the endogenous acetyl lysine group at the BRDs (Chart 1-10), and the

majority of
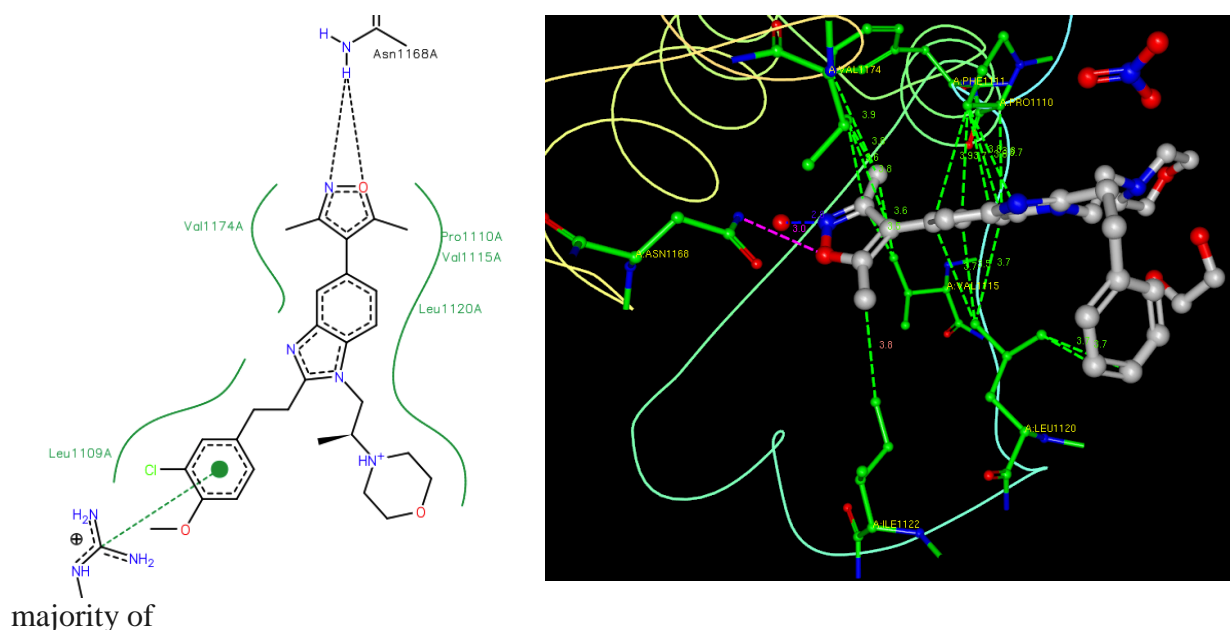
Figure 1-8. 2LO ligand interactions with bromodomain. Left, image from the RCSB PDB of PDB ID 4NR5. Right, *Ligand Explorer* reveals bifurcated-N_{ring}-O_{ring}-H-bond-Asn1168A and C5-Me-Pro1110A interactions with the isoxazole. Filippakopoulos, P., Picaud, S., Felletar, I., Hay, D., Fedorov, O., Martin, S., Pike, A.W., Von Delft, F., Brennan, P., Arrowsmith, C.H., Edwards, A.M., Bountra, C., Knapp, S. 2015, TBP.

structures in the literature at the time of this review contain this moiety. Commonly found is an anchoring hydrogen bond to the isoxazole ring oxygen (Figure 1-8, shown above), although considering distances in many of the structure indicate that both oxygen and nitrogen may lie

19

within interaction distance, as in 2LO-4NR7, which shows a bifurcated Nring-Oring Mode A interaction with an aspartame residue which usually binds the acetylated lysine.

A9P R₂=R₃=R₄=R₅=R₆=H
1H2 R₃= OH R₅ = (R)-CH(OH)Ph
1H3 R₃= OH R₅ = (S)-CH(OH)Ph
ODR R₃=OCH₂CH₃ R₅ = (R)-CH(OH)CH₃
KRG R₃=OCH₂CH₃; R₅= CO₂H
36Z R₃=NH₂ R₅ =CO₂Me
37N R₃=NHSO₂Ph R₅=CO₂H
A9N R₃=SO₂NH(cycloprop-2-en-1-yl); R₄=CH₃
P9M R₃=SO₂NH(cyclopentyl); R4=CH₃

1XA R= NH₂
A9O R=Et

0Q1 (R)

3P2

WDR

S5B R₁=R₂=CH
UTH R₁=N R₂=CH
9BM R₁=CH R₂=N R₃=OMe

1GH

2LK R₁=CH₂-p-C₆H₄Cl
2LL R₁= CH₂CH₂-N-Morpholine
    R₂= CH₂CH₂C₆H₅
2LO R₁=(R)CH₂CH(CH₃)-N-Morpholine
    R₂= CH₂CH₂-3-Cl,4-MeO-C₆H₃

9B6

1A6

Chart 1-10. Isoxazole ligands of Bromodomains (BRD).

1.11 AMPA Receptor

The α-amino-3-hydroxy-5-methyl-4-isoxazolepropionic acid receptor (AMPA receptor or AMPAR) is a transmembrane receptor for glutamate that is part of a large ionotropic glutamate receptor (iGluR) family that mediates fast synaptic transmission in the central nervous system (CNS). AMPARs are comprised of four subtypes of iGluRs: GluR1 through GluR4, which combine to form tetramers consisting of symmetric 'dimer of dimers' of GluR2 and either GluR1, GluR3 or GluR4. Each AMPAR has four sites to which an agonist (*i.e.* glutamate) can bind, one for each subunit. The structural studies performed by Gouaux (among others) has led to a very thorough Structure Activity Relationship (SAR) for ligands binding to GluR2 based on co-crystallographic studies on the S1S2J construct.[21] The structural studies performed by Gouaux (among others) has led to a very thorough Structure Activity Relationship (SAR) for ligands binding (Char 1-11) to GluR2 based on co-crystallographic studies on the S1S2J construct.[22] AMPA crystallized at GluR2 is perhaps the classic bridging Mode B interactions of the N_{ring}-H-Bond with Glu193C with additional C3-OH-H-Bond with Thr143C (Figure 1-9, shown below).
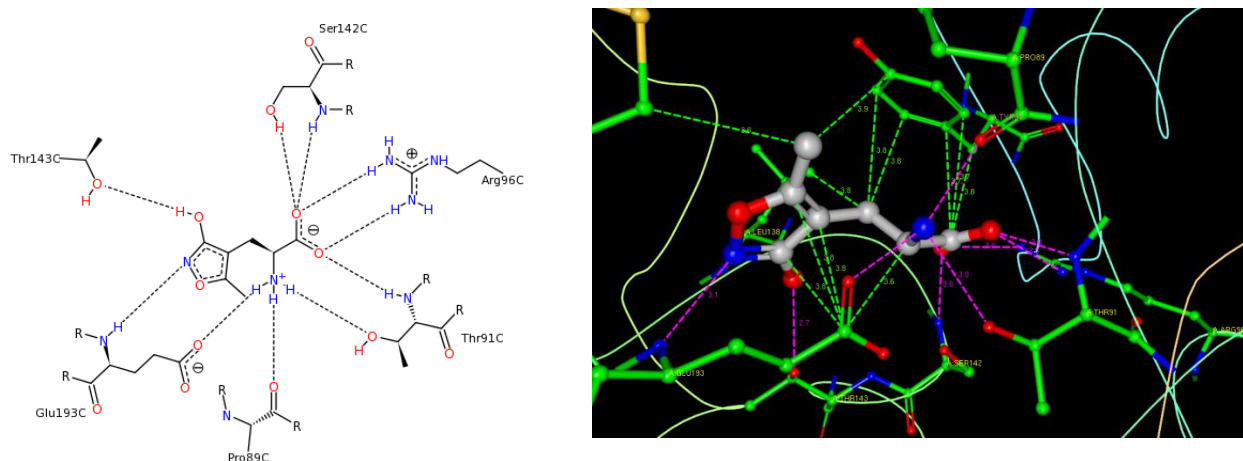
Figure 1-9. AMPA ligand interactions with AMPAR. Left, image from the RCSB PDB of PDB ID 1FTM. Right, *Ligand Explorer* reveals N_{ring}-H-Bond -Glu193C; C3-OH-H-Bond-Thr143C interactions with the isoxazole. Armstrong, N., Gouaux, E. Neuron 2000, 28: 165-181.
.

BRH
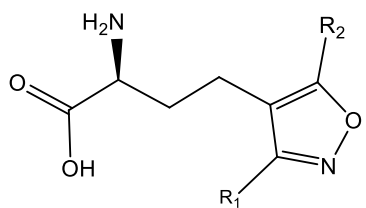
AMQ. R$_1$=OH, R$_2$=CH$_3$
AM1. R$_1$=CO$_2$H, R$_2$=CH$_3$
SHI. R$_1$=OH, R$_2$=H
CE2. R$_1$=OH, R$_2$=C(CH$_3$)$_3$
BN1. R$_1$=OH, R$_2$=2-methyl-1,2,3,4-tetrazol-5-yl
MP9. R$_1$=OH, R$_2$=2-(phenylmethyl)-1,2,3,4-tetrazol-5-yl]-1,2-oxazol-4-yl
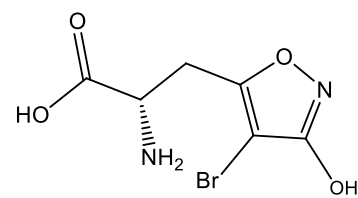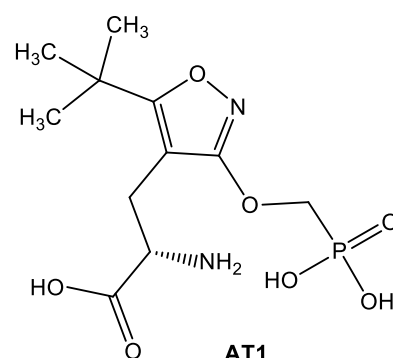
AT1

Chart 1.11. Isoxazole ligands at AMPAR**.**

1.12 Kinases

Over the past 15 years, protein kinases have become and proven to be an important class of drug targets for the pharmaceutical industry. With many already FDA approved and hundreds more undergoing development and clinical trials to treat an assortment of disease ranging from: cancer, anti-inflammatory diseases, and signaling networks that control the immune system, there is plenty of drive that suggests that there will be a surge of interest in this area for many years to come (Chart 1-12 a-d). One example being ERK2, small molecule inhibitors have been targeted in oncology clinical development across multiple disease indications. Kang, Stuckey
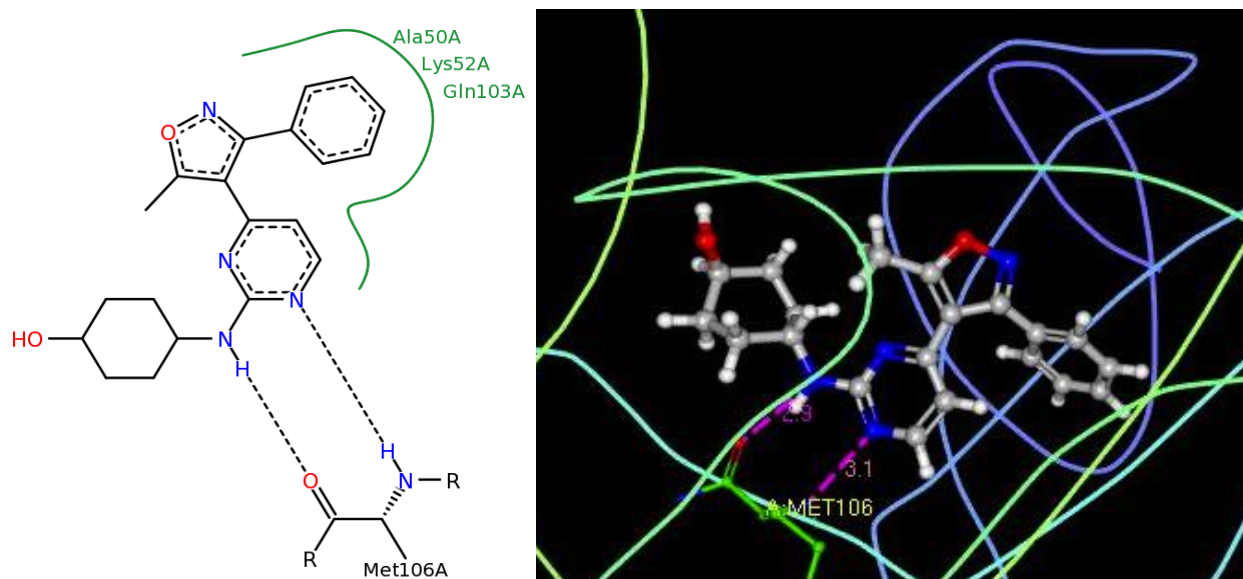
Figure 1-10. E75 ligand interactions with ERK2. Left, image from the RCSB PDB of PDB ID 4FUX. Right, *Ligand Explorer* reveals C3-Ph-Ala50A interactions with the isoxazole. Kang, Y.N., Stuckey, J.A., Xie, X. TBP.

and Xie have solved two ERK2 crystal structures containing inhibitors with isoxazole groups, although they are in press. One of them 4FUX (Figure 1-10) contains an amino-pyrimidine moiety analogous to that reported by Ward[23] for covalent adduct 4ZZM, and both show a similar backbone interaction with methionine. A hydrophobic interaction of VAL47 with the C-3 of the

isoxazole ring was observed, as well as interactions of the LYS52 methylenes with the C3 phenyl.
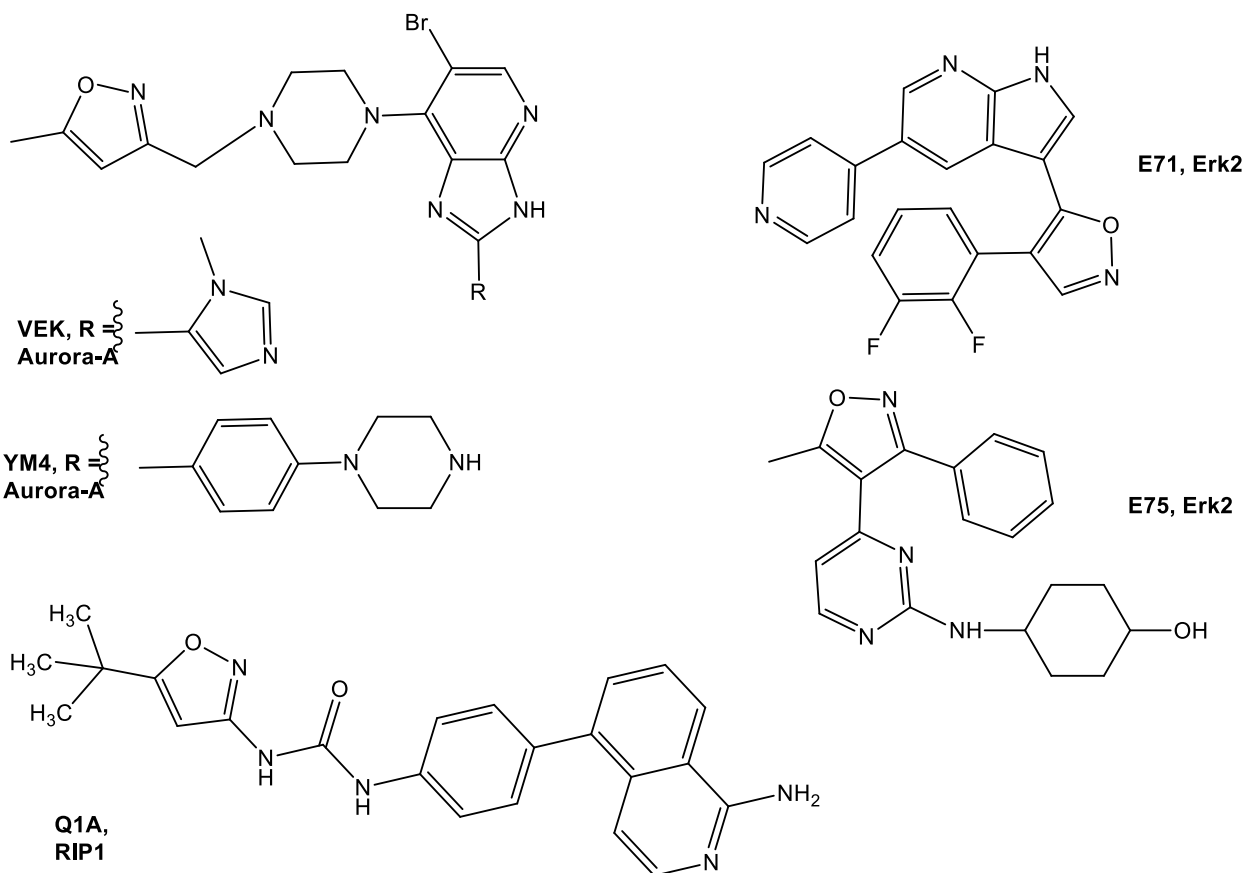
Chart 1-12a. Ligands containing isoxazole moieties of kinase proteins.
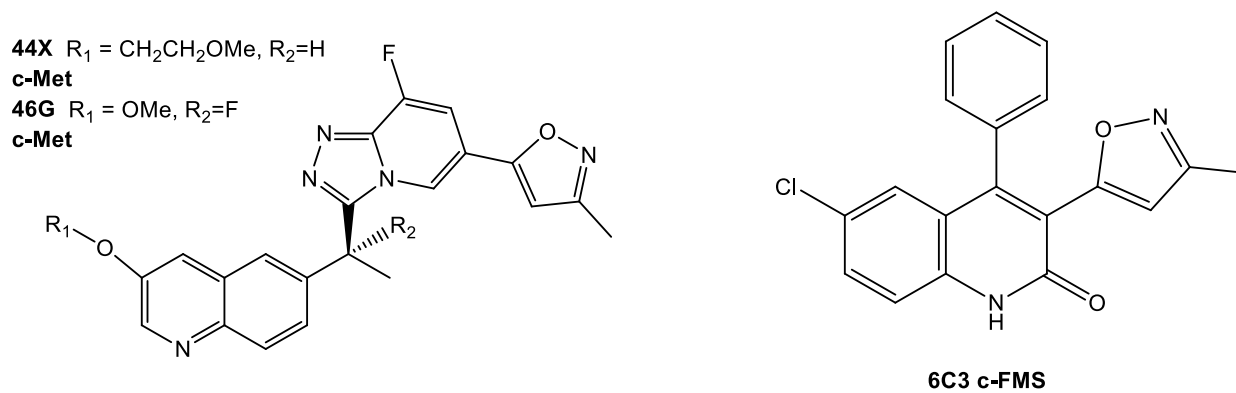
Chart 1-12b. Ligands containing isoxazole moieties of kinase proteins.

2M2. R_1=H, R_2=H, R_3=H
2K5. R_1=OCH$_3$, R_2=OCH$_3$
FGFR

2K7. R_1=OCH$_3$, R_2=OCH$_3$, R_3=H
0S9. R_1=H, R_2=H, R_3=Br
FGFR

0S8. FGFR
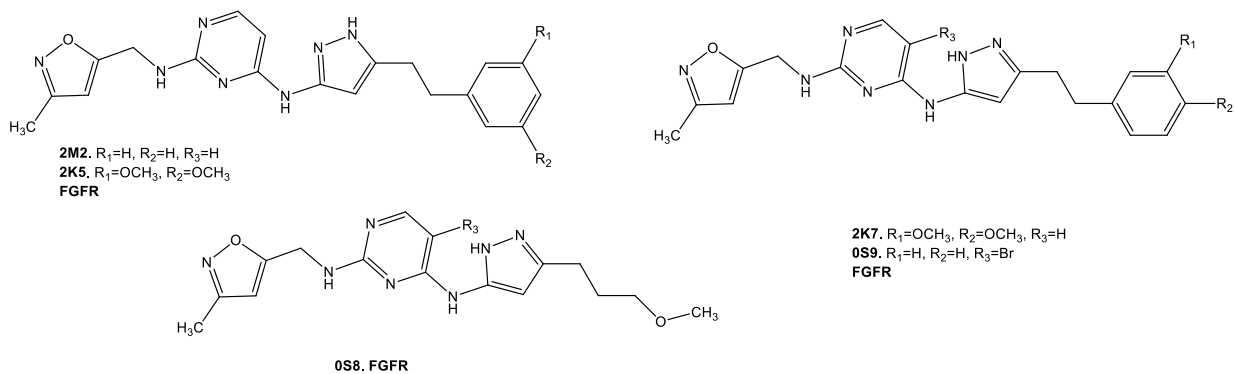
Chart 1-12c. Ligands containing isoxazole moieties of FGFR kinase proteins.

AAV
p38 MAP

FMJ
p38 MAP

39P
p38 MAP

OCG
p38 MAP
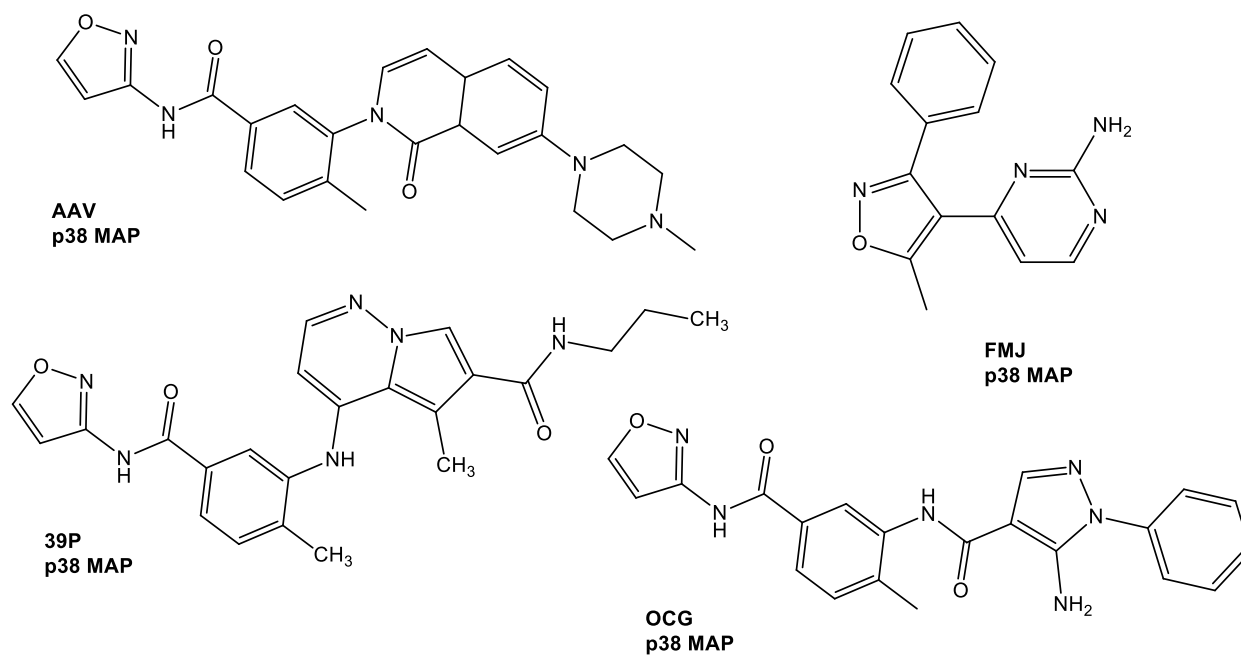
Chart 1-12d. Ligands containing isoxazole moieties of p38 kinase proteins.

1.13 Conclusion

The isoxazole ring appears in several drugs in general medical practice, and is found routinely in drug discovery leads, to the point where some consider it a privileged scaffold. The literature on crystallography has continued to expand at an accelerating pace in recent years, and it seemed that a summary of the observed interactions of the isoxazole moiety with biological targets could be useful to those involved in design and discovery. Especially intriguing in light of the fact that most medicinal chemists use some form of molecular modelling, is that a collection of the observed interactions could prove useful in critical assessment of hypothesis generation. Isoxazoles play four major roles as seen in the PDB: first, they serve as bioisoteres as seen in sulfamethoxazole; second, the serve as a spacer as seen in HSP90 derivatives with hydrophobic interactions; third, the isoxazole ring as direct interaction in the binding site, the most notably a bifurcated N_{ring}-O_{ring} hydrogen bond in AMPA, FXR and HIV integrase; and fourth, an isoxazole being used as a prodrug as seen in Leflunomide (Chapter 5), a immunosuppressive disease-modifying anti-rheumatic drug (DMARD). There are several isoxazoles in general medical practice, and their metabolic fate and disposition is well known (Chapter 5), and thus, this heterocyclic ring is often considered among the privileged scaffolds or templates for drug design and discovery.

References

(1)   Munsey, M. S.; Natale, N. R. The Coordination Chemistry of Isoxazoles. *Coord. Chem. Rev.* **1991**, *109* (2), 251–281.

(2)   Stierand, K.; Rarey, M. Drawing the PDB: Protein−Ligand Complexes in Two Dimensions. *ACS Med. Chem. Lett.* **2010**, *1* (9), 540–545.

(3)   Yun, M.-K.; Wu, Y.; Li, Z.; Zhao, Y.; Waddell, M. B.; Ferreira, A. M.; Lee, R. E.; Bashford, D.; White, S. W. Catalysis and Sulfa Drug Resistance in Dihydropteroate Synthase. *Science* **2012**, *335* (6072), 1110–1114.

(4)   Caselli, E.; Powers, R. A.; Blaszczak, L. C.; Wu, C. Y. E.; Prati, F.; Shoichet, B. K. Energetic, Structural, and Antimicrobial Analyses of β-Lactam Side Chain Recognition by β-Lactamases. *Chem. Biol.* **2001**, *8* (1), 17–31.

(5)   June, C. M.; Vallier, B. C.; Bonomo, R. A.; Leonard, D. A.; Powers, R. A. Structural Origins of Oxacillinase Specificity in Class D β-Lactamases. *Antimicrob. Agents Chemother.* **2014**, *58* (1), 333–341.

(6)   Badger, J.; Minor, I.; Oliveira, M. A.; Smith, T. J.; Rossmann, M. G. Structural Analysis of Antiviral Agents That Interact with the Capsid of Human Rhinoviruses. *Proteins Struct. Funct. Bioinforma.* **1989**, *6* (1), 1–19.

(7)   Zhang, Y.; Simpson, A. A.; Ledford, R. M.; Bator, C. M.; Chakravarty, S.; Skochko, G. A.; Demenczuk, T. M.; Watanyar, A.; Pevear, D. C.; Rossmann, M. G. Structural and Virological Studies of the Stages of Virus Replication That Are Affected by Antirhinovirus Compounds. *J. Virol.* **2004**, *78* (20), 11061–11069.

(8)   Tochowicz, A.; Maskos, K.; Huber, R.; Oltenfreiter, R.; Dive, V.; Yiotakis, A.; Zanda, M.; Bode, W.; Goettig, P. Crystal Structures of MMP-9 Complexes with Five Inhibitors:

Contribution of the Flexible Arg424 Side-Chain to Selectivity. *J. Mol. Biol.* **2007**, *371* (4), 989–1006.

(9)   Coussens, L. M.; Fingleton, B.; Matrisian, L. M. Matrix Metalloproteinase Inhibitors and Cancer—Trials and Tribulations. *Science* **2002**, *295* (5564), 2387–2392.

(10)   Czarny, B.; Stura, E. A.; Devel, L.; Vera, L.; Cassar-Lajeunesse, E.; Beau, F.; Calderone, V.; Fragai, M.; Luchinat, C.; Dive, V. Molecular Determinants of a Selective Matrix Metalloprotease-12 Inhibitor: Insights from Crystallography and Thermodynamic Studies. *J. Med. Chem.* **2013**, *56* (3), 1149–1159.

(11)   Brough, P. A.; Aherne, W.; Barril, X.; Borgognoni, J.; Boxall, K.; Cansfield, J. E.; Cheung, K.-M. J.; Collins, I.; Davies, N. G. M.; Drysdale, M. J.; Dymock, B.; Eccles, S. A.; Finch, H.; Fink, A.; Hayes, A.; Howes, R.; Hubbard, R. E.; James, K.; Jordan, A. M.; Lockie, A.; Martins, V.; Massey, A.; Matthews, T. P.; McDonald, E.; Northfield, C. J.; Pearl, L. H.; Prodromou, C.; Ray, S.; Raynaud, F. I.; Roughley, S. D.; Sharp, S. Y.; Surgenor, A.; Walmsley, D. L.; Webb, P.; Wood, M.; Workman, P.; Wright, L. 4,5-Diarylisoxazole Hsp90 Chaperone Inhibitors: Potential Therapeutic Agents for the Treatment of Cancer. *J. Med. Chem.* **2008**, *51* (2), 196–218.

(12)   Akwabi-Ameyaw, A.; Bass, J. Y.; Caldwell, R. D.; Caravella, J. A.; Chen, L.; Creech, K. L.; Deaton, D. N.; Jones, S. A.; Kaldor, I.; Liu, Y.; Madauss, K. P.; Marr, H. B.; McFadyen, R. B.; Miller, A. B.; III, F. N.; Parks, D. J.; Spearing, P. K.; Todd, D.; Williams, S. P.; Wisely, G. B. Conformationally Constrained Farnesoid X Receptor (FXR) Agonists: Naphthoic Acid-Based Analogs of GW 4064. *Bioorg. Med. Chem. Lett.* **2008**, *18* (15), 4339–4343.

(13)   Akwabi-Ameyaw, A.; Bass, J. Y.; Caldwell, R. D.; Caravella, J. A.; Chen, L.; Creech, K. L.; Deaton, D. N.; Madauss, K. P.; Marr, H. B.; McFadyen, R. B.; Miller, A. B.; Navas III, F.;

Parks, D. J.; Spearing, P. K.; Todd, D.; Williams, S. P.; Bruce Wisely, G. FXR Agonist Activity of Conformationally Constrained Analogs of GW 4064. *Bioorg. Med. Chem. Lett.* **2009**, *19* (16), 4733–4739.

(14)   Akwabi-Ameyaw, A.; Caravella, J. A.; Chen, L.; Creech, K. L.; Deaton, D. N.; Madauss, K. P.; Marr, H. B.; Miller, A. B.; Navas III, F.; Parks, D. J.; Spearing, P. K.; Todd, D.; Williams, S. P.; Wisely, G. B. Conformationally Constrained Farnesoid X Receptor (FXR) Agonists: Alternative Replacements of the Stilbene. *Bioorg. Med. Chem. Lett.* **2011**, *21* (20), 6154–6160.

(15)   Bass, J. Y.; Caldwell, R. D.; Caravella, J. A.; Chen, L.; Creech, K. L.; Deaton, D. N.; Madauss, K. P.; Marr, H. B.; McFadyen, R. B.; Miller, A. B.; Parks, D. J.; Todd, D.; Williams, S. P.; Wisely, G. B. Substituted Isoxazole Analogs of Farnesoid X Receptor (FXR) Agonist GW4064. *Bioorg. Med. Chem. Lett.* **2009**, *19* (11), 2969–2973.

(16)   Bass, J. Y.; Caravella, J. A.; Chen, L.; Creech, K. L.; Deaton, D. N.; Madauss, K. P.; Marr, H. B.; McFadyen, R. B.; Miller, A. B.; Mills, W. Y.; Navas III, F.; Parks, D. J.; Smalley Jr., T. L.; Spearing, P. K.; Todd, D.; Williams, S. P.; Wisely, G. B. Conformationally Constrained Farnesoid X Receptor (FXR) Agonists: Heteroaryl Replacements of the Naphthalene. *Bioorg. Med. Chem. Lett.* **2011**, *21* (4), 1206–1213.

(17)   Feng, S.; Yang, M.; Zhang, Z.; Wang, Z.; Hong, D.; Richter, H.; Benson, G. M.; Bleicher, K.; Grether, U.; Martin, R. E.; Plancher, J.-M.; Kuhn, B.; Rudolph, M. G.; Chen, L. Identification of an N-Oxide Pyridine GW4064 Analog as a Potent FXR Agonist. *Bioorg. Med. Chem. Lett.* **2009**, *19* (9), 2595–2598.

(18)   Akif, M.; Schwager, S. L.; Anthony, C. S.; Czarny, B.; Beau, F.; Dive, V.; Sturrock, E. D.; Acharya, K. R. Novel Mechanism of Inhibition of Human Angiotensin-I-Converting Enzyme (ACE) by a Highly Specific Phosphinic Tripeptide. *Biochem. J.* **2011**, *436* (1), 53–59.

(19)   Masuyer, G.; Akif, M.; Czarny, B.; Beau, F.; Schwager, S. L. U.; Sturrock, E. D.; Isaac, R. E.; Dive, V.; Acharya, K. R. Crystal Structures of Highly Specific Phosphinic Tripeptide Enantiomers in Complex with the Angiotensin-I Converting Enzyme. *FEBS J.* **2014**, *281* (3), 943–956.

(20)   Hewings, D. S.; Fedorov, O.; Filippakopoulos, P.; Martin, S.; Picaud, S.; Tumber, A.; Wells, C.; Olcina, M. M.; Freeman, K.; Gill, A.; Ritchie, A. J.; Sheppard, D. W.; Russell, A. J.; Hammond, E. M.; Knapp, S.; Brennan, P. E.; Conway, S. J. Optimization of 3,5-Dimethylisoxazole Derivatives as Potent Bromodomain Ligands. *J. Med. Chem.* **2013**, *56* (8), 3217–3227.

(21)   Natale, N.; Magnusson, K.; Nelson, J. Can Selective Ligands for Glutamate Binding Proteins Be Rationally Designed? *Curr. Top. Med. Chem.* **2006**, *6* (8), 823–847.

(22)   Armstrong, N.; Gouaux, E. Mechanisms for Activation and Antagonism of an AMPA-Sensitive Glutamate Receptor. *Neuron* **2000**, *28* (1), 165–181.

(23)   Ward, R. A.; Colclough, N.; Challinor, M.; Debreczeni, J. E.; Eckersley, K.; Fairley, G.; Feron, L.; Flemington, V.; Graham, M. A.; Greenwood, R.; Hopcroft, P.; Howard, T. D.; James, M.; Jones, C. D.; Jones, C. R.; Renshaw, J.; Roberts, K.; Snow, L.; Tonge, M.; Yeung, K. Structure-Guided Design of Highly Selective and Potent Covalent Inhibitors of ERK1/2. *J. Med. Chem.* **2015**, *58* (11), 4790–4801.

Table 1.-1 Crystallography or NMR of Isoxazole Binding Proteins.

PDB Ligand No.	Target	PDB Accession No.	Resolution	Ligand Interactions	Reference
AMQ	AMPAR-GluR2	1FTM	1.7	N_{ring}-H-Bond -Glu193C; C3-OH-H-Bond-Thr143C	Armstrong, 2000
	GluR2-L483Y	1LB8	2.3	N_{ring}-H-Bond-Glu193B; C3-OH-H-Bond-Thr143B	Sun, 2002
		1MY2	1.8	N_{ring}-H-Bond -Glu193C; C3-OH-H-Bond-Thr143C	Jin, 2003
	GluR2-L650T	1P1Q	2.0	N_{ring}-H-Bond -Glu193C; C3-OH-H-Bond-Thr143C	Armstrong, 2003
	GluR2-L650T	1P1U	2.0	C3-OH-H-Bond-Ser142B	Armstrong, 2003
	GluR2-L483Y-L650T	1P1W	1.8	N_{ring}-Glu193B; C3-OH-H-Bond-Thr143B	Armstrong, 2003
	GluR3	3DP4	2.11	N_{ring}-H-Bond -Glu193A; C3-OH-H-Bond-Thr143A	Ahmed, 2008
	GluR4	3FAT	1.90	N_{ring}-H-Bond -Glu191A; C3-OH-H-Bond-Thr141A	Kasper, 2008
AM1	GluR2	1M5E	1.46	N_{ring}-H-Bond -Glu193A; C3-COOH-H-Bond-Thr143A	Hogner, 2002
	GluR2	1M5F	1.95	C3-COOH-H-Bond-Thr143A	Hogner, 2002
AT1	GluR2	1N0T	2.10	Ring-Isox-Glu193	Hogner, 2003
	GluR5	1VSO	1.85	Bridged H_2O-O_{ring}/ N_{ring}	Hald, 2007
BRH	GluR2	1M5C	1.65	N_{ring}-H-Bond -Thr143A	Hogner, 2002
	GluR2	1M5D	1.73	N_{ring}-H-Bond –Thr143A; C3-OH-H-Bond-Glu193A	Hogner, 2002
CE2	GluR2	1NNK	1.85	N_{ring}-H-Bond –Thr140A; C3-OH-H-Bond-Thr140A(OH/NH)	Lunn, 2003
	GluR2	1NNP	1.90	N_{ring}-H-Bond –Thr140A; C3-OH-H-Bond-Thr140A(OH/NH)	Lunn, 2003
MP9	GluR2	2P2A	2.26	N_{ring}-H-Bond –Thr140B; C3-OH-H-Bond-Thr140A(NH)	Vogenson, 2007
SHI	GluR2	1MQD	1.46	N_{ring}-H-Bond -Glu190A; C3-OH-H-Bond-Thr140A	Kasper, 2002
	GluR2	1MS7	1.97	N_{ring}-H-Bond -Glu190A; C3-OH-H-Bond-Thr140A	Kasper, 2002
BN1	AMPAR-GluR2	1M5B	1.85	N_{ring}-H-Bond-Thr143(OH); C3-OH-H-Bond-Backbone-NH-Thr143	Hogner, 2002
		1MXV	1.95	AMPA, BrW 10mM	Jin, 2003
		1MXW	1.9	AMPA, BrW 1mM	Jin, 2003
		1MXX	2.0	AMPA, BrW 100uM	Jin, 2003
		1MXY	1.95	AMPA, BrW 10uM	Jin, 2003
		1MXZ	1.9	AMPA, BrW 1uM	Jin, 2003
		1MY0	1.9	AMPA, BrW 100nM	Jin, 2003
		1MY1	1.9	AMPA, BrW 10nM	Jin, 2003
		1MY2	1.8	AMAPA, Zn2+	Jin, 2003

Code	PDB	Protein	Resolution	Interactions	Reference
3EF	4CA5	hACE	1.85	Val380A; Val518A	Masuyer, 2014
	4CA6	hACE	1.91	Ser357A; Thr358A	Masuyer, 2014
	4CA7	AnCE, drosophilia	1.82	Phe363A	Masuyer, 2014
3ES	2XY9	hACE	1.97	Glu376A; Val380A	Akif, 2011
	2XYD	hACE	2.15	Thr496A	Akif, 2011
	4CA8	AnCE, drosophilia	1.99		Masuyer, 2014
1A6	4HXO	Bromodomain hBRD4	1.76	O_{ring}-H-bond-Asn140A	Zhao, 2013
1H2	4J0R	Bromodomain hBRD4	1.72	O_{ring}-H-bond-Asn140A	Hewings, 2013
1H3	4J0S	Bromodomain hBRD4	1.84	O_{ring}-5-NH_2-double-H-bond-Asn140A	Hewings, 2013
1XA	4LR6	Bromodomain hBRD4	1.29	O_{ring}-H-bond-Asn140A	Gehling, 2013
1GH	3ZYU	Bromodomain hBRD4	1.5	O_{ring}-H-bond-Asn140A	Dawson, 2011
	4ALG	Bromodomain hBRD2	1.6	O_{ring}-H-bond-Asn110A; C3-Me-Val57A	Seal, 2012
KRG	3SVH	Bromodomain hCREBBP	1.8	π-Ring-π-Tyr1102A	Flippakopoulos, TBP
0Q1	4GPJ	Bromodomain hBRD4	1.6	O_{ring}-H-bond-Asn140A; C5-Me-Ileu146A	Hay, TBP
36Z	4TTE	Bromodomain-ATAD2A	1.8	O_{ring}-H-bond-Asn1064A; C3-Me-Val1013A	Poncet-Montange, 2015
37N	4TU4	Bromodomain ATAD2A	1.73	O_{ring}-H-bond-Asn1064A; C3-Me-Val1008A	Poncet-Montange, 2015
A9N	4A9N	Bromodomain hBRD2	1.85	O_{ring}-H-bond-Asn156A; C3-Me-Pro98A	Bamborough, 2012
A9O	4A9O	Bromodomain hBRD2	1.78	O_{ring}-H-bond-Asn156A; C3-Me-Pro98A; C5-Et-Leu108A	Bamborough, 2012
A9P	4ALH	Bromodomain hBRD2	1.97	O_{ring}-H-bond-Asn156A; C3-Me-Pro98A; C5-Me-Leu108A	Bamborough, 2012
P9M	4A9M	Bromodomain hBRD2	2.06	O_{ring}-H-bond-Asn156A; C3-Me-Pro98A	Bamborough, 2012
S5B	4AKN	Bromodomain hBRD2	1.82	O_{ring}-H-bond-Asn156A; C3-Me-Val103A	Seal, 2012
	4BW1	Bromodomain hBRD4	1.4	O_{ring}-H-bond-Asn140A; C3-Me-Pro82A; C5-Me-Ileu146A	Mirguet, 2014
3P2	4WIV	Bromodomain hBRD4	1.56	O_{ring}-H-bond-Asn140A; C5-Me-Leu92A; C3-Me-Pro82A	McKeown, 2014
UTH	4BW2	Bromodomain hBRD4	1.92	O_{ring}-H-bond-Asn140A; C5-Me-Leu92A	Mirguet, 2014
WDR	3SVF	Bromodomain hBRD4	1.98	O_{ring}-H-bond-Asn140A; C5-Me-Leu92A; C3-Me-Ileu146A	Flippakopoulos, TBP
ODR	3SVG	Bromodomain hBRD4	1.68	O_{ring}-H-bond-Asn140A; C3-Me-Ileu146A; C5-Me-Leu82A	Flippakopoulos, TBP
2LK	4NR4	Bromodomain hCREBBP	1.69	O_{ring}-H-bond-Asn1168A; C3-Me-Val1115A; C5-Me-Val1174A	Flippakopoulos, TBP
2LL	4NR5	Bromodomain hCREBBP	1.66	Bifurcated-N_{ring}-O_{ring}-H-bond-Asn1168A; C5-Me-Pro1110A	Flippakopoulos, TBP
	4NR8	Bromodomain hBRD4	1.63	O_{ring}-H-bond-Asn140A; C3-Me-Leu92A; C5-Me-Ileu46A	Flippakopoulos, TBP

Ligand	PDB	Target	Res	Interactions	Reference
2LO	4NR7	Bromodomain hCREBBP	1.2	Mode A: Bifurcated-N_{ring}-O_{ring}-H-bond-Asn1168A C3-Me-Val1174A; C5-Me-Pro1110A	Flippakopoulos, TBP
9B6	4BW4	Bromodomain hBRD4	1.67	O_{ring}-H-bond-Asn140A	Mirguet, 2014
9BM	4BW3	Bromodomain hBRD4	1.5	O_{ring}-H-bond-Asn140A; C3-Me-Pro82A	Mirguet, 2014
34	3RVF	Farnesoid X Receptor	3.1	Bifurcated-N_{ring}-O_{ring}-H-bond-Asn447A	Akwabi-Ameyaw, 2011
064	3DCT	Farnesoid X Receptor	2.5	π-Ring-C3-Cl_2-Ph-π-Phe329A; C5-iPr-Leu387A	Akwabi-Ameyaw, 2008
O62	3DCU	Farnesoid X Receptor	2.95	π-Ring-C3-Cl_2-Ph-π-Phe329A; C5-iPr-Leu287A & Ala291A	Akwabi-Ameyaw, 2008
82X	3HC5	Farnesoid X Receptor	2.6	π-Ring-C3-Cl_2-Ph-π-Phe329A; C3-Cl_2-Ph-Phe329A; N_{ring}-H-bond-His447A	Akwabi-Ameyaw, 2009
088	3HC6	Farnesoid X Receptor	3.2	C5-iPr-Leu387A C3-Cl_2-Ph-Met265A, Met290A, Ala291A, Met328A, Ile335A	Akwabi-Ameyaw, 2009
37G	3RUU	Farnesoid X Receptor	2.5	N_{ring}-H-bond-His447A, C5-iPr-Leu287A π-Ring-C3-Cl_2-Ph-π-Phe329A; C3-Cl_2-Ph-Met290A	Akwabi-Ameyaw, 2011
59G	3RUT	Farnesoid X Receptor	3.0	N_{ring}-H-bond-His447A; C5-iPr-Leu287A π-Ring-C3-Cl_2-Ph-π-Phe329A; C3-Cl_2-Ph-Met290A	Akwabi-Ameyaw, 2011
643	3FXV	Farnesoid X Receptor	2.26	π-Ring-C3-Cl_2-4-pyridyl-π-Phe333A; C3-Cl_2-N-4-pyridyl-H□bond-Tyr373A;	Feng, 2009
708	3GD2	Farnesoid X Receptor	3.2	N_{ring}-H-bond-His447A; C5-iPr--Leu287A C3-Cl_2-Ph-methylene-sulfoxide-ille352A & Met365A	Bass, 2009
P88	3P88	Farnesoid X Receptor	2.95	π-Ring-C3-Cl_2-Ph-π-Phe329A N_{ring}-H-bond-His447A; C5-iPr-Ala291A	Bass, 2011
89P	3P89	Farnesoid X Receptor	2.3	N_{ring}-H-bond-His447A; π-Ring-C3-Cl_2-Ph-π -Phe329A C3-Cl_2-Ph-Leu287A	Bass, 2011
2EQ	2VCJ	HSP90	2.5	Spacer for 3,4 and 5 substituents	Brough, 2008
2GJ	2VCI	HSP90	2.0	Spacer for 3,4 and 5 substituents	Brough, 2008
2GG	2UWD	HSP90	1.9	Spacer for 3,4 and 5 substituents	Sharp, 2008
9UN	4B7P	HSP90	1.7	Spacer or 3,4 and 5 substituents	Fogliatto, 2013
XKL	4BQJ	HSP90	2.0	Spacer or 3,4 and 5 substituents	Brasca, 2013
XQK	2YEI	HSP90	2.2	Phe138A; π-Ring-Isox--π-Tyr139A co-crystal with XQI	Roughley, 2011
	2YEJ	HSP90	2.2	Phe138A; co-crystal with XQI	Roughley, 2011
2D3	2YE8	HSP90	2.3	Phe138A	Roughley, 2011
YJW	2YJW	HSP90	1.61	N_{ring}-H-bond-Thr184A; 4-Ph- π-cation-Lys58A	Vallee, 2011
YK2	2YK2	HSP90	1.74	N_{ring}-H-bond-Thr184A; C5-Me & 4-Ph Asn51A	Vallee, 2011

Code	PDB ID	Target	Resolution	Interaction	Reference
FJ2	4LWE	HSP90	1.5	Spacer or 3, 4 and 5 substituents	Li, 2014
FJ3	4LWF	HSP90	1.75	N_{ring}-H-bond-Thr184A; Met98A	Li, 2014
FJ5	4LWH	HSP90	1.7	N_{ring}-H-bond-Thr184A;	Li, 2014
FJ6	4LWI	HSP90	1.7	N_{ring}-H-bond-Thr184A;	Li, 2014
AAV	4AAC	Kinase, p38a MAPK	2.5	π-Ring-Isox-π-Phe1169A	Brown, 2012
OCG	3OCG	Kinase-p38a			
39P	3MVM	Kinase-p38a			
FMJ	3FMJ	Kinase-p38a			
YM4	2X6E	Kinase, Aurora-A	3.35	C3-CH$_2$-Leu139A; C5-CH$_3$-Leu263A	Bavetsias, 2010
VEK	4B0G	Kinase, Aurora-A	2.5	C3-CH$_2$-Val13947A; C5-CH$_3$-Leu263A	Bavetsias, 2012
E71	4FV9	Kinase, ERK2	2.11	C3-H-Ala50A	Kang, 2012
E75	4FUX	Kinase, ERK2	2.2	C3-Ph-Ala50A	Kang, 2012
44X	4XYF	Kinase c-Met	1.85	π-Ring-Isox-π-Tyr1230A	Peterson, 2015
46G	4XMO	Kinase c-Met	1.75	π-Ring-Isox-π-Tyr1230A	Peterson, 2015
6C3	2I0V	Kinase c-FMS	2.8	C3-Me-Ala800A	Schubert, 2007
0S8	4F64	Kinase-FGFR	2.05	C5-CH$_2$-Val492	Norman 2012
0S9	4F65	Kinase-FGFR	2.26	hydrophobic-Leu630; C5-CH$_2$-Val492	Norman 2012
2K5	4NK9	Kinase-FGFR	2.57	C3-CH$_3$-Leu630; C5-CH$_2$-Gly485/Leu484/Val495	Klein, 2014
2K7	4NKA	Kinase-FGFR	2.19	C3-CH$_3$-Leu630	Klein, 2014
2M2	4NKS	Kinase-FGFR	2.50	C3-CH$_3$-Leu630/Ala640	Klein, 2014
Q1A	4NEU	Kinase-RIP1	2.57	hydrophobic-Asp156/Met67; C5-t-butyl-Leu70/Val75	Harris, 2013
M3I	3RCI	Cyclophillin D	1.44	Mode B: LB=NH$_2$-H-Bonds-Asn144X	Colliandre, 2012
MIO	3RDA	Cyclophillin D	1.07	N_{ring}-H-Bond-Arg97X	Colliandre, 2012
3SD	3SDI	Proteosome 20S			
W56	2RS5	Human Rhinovirus 14	3.00	N_{ring}-H-Bond –Asn219; p-Ring-Isox-π-Leu106/Phe124	Badger 1989
W59	2RS3	Human Rhinovirus 14	3.00	π-Ring-Isox-π-Phe186	Badger 1989
W8R	2RR1	Human Rhinovirus 14	3.00	π-Ring-Isox-π-Phe186	Badger 1989
W35	1RUC	Human Rhinovirus 14	3.10	π-Ring-Isox-π-Tyr197/Leu106	Hadfield 1995
	1RUE		2.90	π-Ring-Isox-π-Tyr197/Leu106	Hadfield 1995
	1RUG		3.00	π-Ring-Isox-π-Tyr197/Leu106	Hadfield 1995
	2R06		3.00	π-Ring-Isox-π-Tyr197/Leu106	Badger 1989
W11-3	4WM7	Human Enterovirus D68	2.32	π-Ring-Isox-π-Tyr193	Liu 2015
	1NA1		3.30	π-Ring-Isox-π-Tyr197/Leu106	Zhang 2004

Compound	Virus / Enzyme	PDB	Res (Å)	Interactions	Reference
		1NCQ	2.50	π-Ring-Isox-π-Tyr197/Leu106	Zhang 2004
		1NCR	2.70	π-Ring-Isox-π-Tyr190/Leu100/Met214	Zhang 2004
		1ND3	2.80	π-Ring-Isox-π-Tyr197/Met214	Zhang 2004
		1C8M	2.80	π-Ring-Isox-π-Tyr190/Leu100	Chakravarty TBP
W33	Human Rhinovirus 14	2R07	3.00	π-Ring-Isox-π-Tyr197/Leu106	Badger 1989
W42	Human Rhinovirus 14	1R08	3.00	π-Ring-Isox-π-Leu106	Badger 1989
W43	Human Rhinovirus 14	2RM2	3.00	π-Ring-Isox-π-Phe186/Tyr152	Badger 1989
W54	Human Rhinovirus 14	2HWC	3.00	π-Ring-Isox-π-Tyr197/Leu106	Kim 1993
		2HWE	3.80	π-Ring-Isox-π-Leu103	Kim 1993
W91	Human Rhinovirus 14	2HWB	3.00	π-Ring-Isox-π-Leu106	Kim 1993
		2HWD	3.80	π-Ring-Isox-π-Leu106	Kim 1993
W01	Human Rhinovirus 16	1QJU	2.80	π-Ring-Isox-π-Tyr190/Leu100/Met214	Hadfield 1999
W02	Human Rhinovirus 16	1QJX	2.80	π-Ring-Isox-π-Tyr190/Leu100/Met214	Hadfield 1999
W03	Human Rhinovirus 16	1QJY	2.80	π-Ring-Isox-π-Tyr190/Met214	Hadfield 1999
W71	Human Enterovirus A71	3ZFF	3.40	π-Ring-Isox-π-Phe155; C3-Me-Ile24/Val179	Plevka 2013
		3ZFG	3.20	π-Ring-Isox-π-Phe155/Val190; C3-Me-Ile24/Val179	Plevka 2013
	Coxsackie virus A9	1D4M	2.90	π-Ring-Isox-π-Tyr192; C3-Me-Leu216	Hendry 1999
	Poliovirus type 3	1PIV	2.90	π-Ring-Isox-π-Tyr112/Phe238; C3-Me-Tyr112/Phe238	Hiremath 1995
		2R04	3.00	π-Ring-Isox-π–Tyr197	Badger 1989
W84	Human Rhinovirus 14	1RUD	2.90	π-Ring-Isox-π-Phe186/Try152; C3-Me-Ser175/Val176	Hadfield 1995
		1RUH	3.00	π-Ring-Isox-π-Phe186/Try152; C3-Me-Ser175/Val176	Hadfield 1995
		1RUI	3.00	π-Ring-Isox-π-Phe186/Try152; C3-Me-Ser175/Val176	Hadfield 1995
		2RS1	3.00	π-Ring-Isox-π-Phe186/Try152; C3-Me-Ser175/Val176	Badger 1989
AG7	Human Enterovirus A71	4GHT	1.96	π-Ring-Isox-π-Leu125/Phe170; C5-Me-Leu125	Wu 2013
	Human Enterovirus 93 3C	3RUO	1.50	π-Ring-Isox-π-Phe170; C5-Me-Leu125	Costenaro 2011
		3QZQ	1.70	π-Ring-Isox-π-Leu125/Phe170; C5-Me-Leu125/Phe170	Wang 2011
		3QZR	1.04	π -Ring-Isox-π-Leu125/Phe170; C5-Me-Leu125/Phe170	Wang 2011
		3R0F	1.31	π-Ring-Isox-π–Leu125/Phe170	Wang 2011
		3SJI	1.80	π-Ring-Isox-π-Leu125; C5-Me-Leu125	Lu 2011
		3SJO	1.70	π-Ring-Isox-π-Phe170; C5-Me-Phe170	Lu 2011
	Type 2 Rhinovirus	1CQQ	1.85	π-Ring-Isox-π-Phe170; C5-Me-Ile125/Phe170	Matthews 1999
105	Beta-lactamase	1NYY	1.90	no interactions	Wang 2003
		1JWZ	1.80	π-Ring-Isox-π-Tyr105; C5-Me-Ala237/Gly238/Met69	Wang 2002

Ligand	PDB	Protein	Interaction	Resolution	Reference
1S6	1FSY	Beta-lactamase	C5-Me-Tyr221	1.75	Caselli 2001
	4JXG		C5-Me-Tyr221	1.65	Docter TBP
	4MLL		π-Ring-Isox-π-Leu255; C5-Me-Gly216; C3-Ph-Gly238/Ser237	1.37	June 2014
1U3	4F94	Beta-lactamase-glysine	C5-Me-Trp221; C3-Ph-Leu 168	2.40	June TBP
	4KZ5		C5-Ph-Tyr221; N_{ring}-H-bond-Asn152; Bridged H_2O-O_{ring}	1.35	Barelier 2014
CXU	4R1G	Beta-lactamase	C5-Me-Trp720/Thr893; C3-Ph-Trp791/His718	1.92	Filippova TBP
	1FCM		C5-Me-Tyr218	2.46	Patera 2000
0WO	4EYB	Beta-lactamase	π-Ring-Isox-π-Gly69; C5-Me-Leu65/Trp93 C3-Ph-His122/Met154/Gln123	1.16	King 2012
0W0	4FSF	Penicillin binding protein	π-Ring-Isox-π-Val333; Bridged H_2O-O_{ring}/ N_{ring}	2.20	Mitton-Fry 2012
CXV	3MZD	Penicillin binding protein	π-Ring-Isox-π-Ser86	1.90	Nicola 2010
BI7	2JKH	Factor Xa	π-Ring-Isox-π-Val333; Bridged H_2O-N_{ring}	1.25	Salonen 2009
IIA	2BOH	Factor Xa	π-Ring-Isox-π-Gln192/Cys191	2.20	Nazare 2005
IIB	2BQ6	Factor Xa	π-Ring-Isox-π-Gln192	3.00	Nazare 2005
XWG	2Y5F	Factor Xa	π-Ring-Isox-π-Cys191; Bridged H_2O-N_{ring}	1.29	Salonen 2012
VYR	4BTT	Factor Xa	no interactions	2.59	Meneyrol 2013
2FN	4N3L	Factor Xa	π-Ring-Isox-π-Cys191	1.94	Belviso 2014
5MR	2OVZ	MMMP9	π-Ring-Isox-π-His401; C3-Ph-His401/Tyr423/Met422	2.00	Tochowicz 2007
EEA	3LIL	MMP12	π-Ring-Isox-π-His218/Try240; C3-Ph-Tyr240/Val235	1.80	Devel 2010
EEC	3LIR	MMP12	π-Ring-Isox-π-His218/Try240; C3-Ph-Lys241/Tyr240/Val235	1.90	Devel 2010 Devel235
R47	4GQL	MMP12	π-Ring-Isox-π-His218; C3-Ph-Tyr240/His218	1.15	Czarny 2013
R4B	4GR0	MMP12	π-Ring-Isox-π-His218; C3-Ph-Tyr240/His218	1.50	Czarny 2013
R4C	4GR8	MMP12	π-Ring-Isox-π-His218; C3-Ph-Thr239/Thr240/His218	1.30	Czarny 2013
R45	4GR3	MMP12	π-Ring-Isox-π-His218/ Tyr240; C3-Ph-Tyr240/Thr239	1.49	Czarny 2013
A2Y	2LY0	Influenza A	π-Ring-Isox-π-Val27	NMR	Wang 2013
0MM	3TG6	Influenza A	π-Ring-Isox-π-Tyr52/Trp104; C3-Ph-Tyr52/ Tyr313	3.00	Edavettal TBP
0MF	4DYA	Influenza A	π-Ring-Isox-π-Tyr52/Trp104; C3-Ph-Tyr52/ Tyr313	2.75	Lewis TBP
0MH	4DYB	Influenza A	π-Ring-Isox-π-Tyr52/Trp104; C3-Ph-Tyr313	2.80	Lewis TBP
0MR	4DYN	Influenza A	π-Ring-Isox-π-Tyr52/Trp104; C3-Ph-Tyr52/ Tyr313	2.40	Lewis TBP
0MS	4DYP	Influenza A	π-Ring-Isox-π-Tyr52/Trp104; C3-Ph-Tyr52/ Tyr313	2.82	Lewis TBP

Code	Target	Resolution	Interactions	Reference
MOK	HIV integrase	2.00	C4-COO-H-Bond –Ser195; π-Ring-Isox-π-Glu198	Wielens 2013
MPK	HIV integrase	2.30	C4-CH2OH-H-Bond –Ser195/Asn184	Wielens 2013
0NK	HIV integrase	1.90	π-Ring-Isox-π-Glu198; C4-CH2-π-His185/Ser195 C3-CH2OH-H-Bond –Asp202/Thr206; π-Ring-Isox-π-Glu198/Gly197/Ile204; C4-Ph-Gly197/Pro109/Trp108	Wielens 2013
AF8	HIV protease	1.50	Bifurcated-N$_{ring}$-O$_{ring}$-H-bond-Asp30; π-Ring-Isox-π-Ile47	Altman TBP
F71	HIV protease	1.75	π-Ring-Isox-π-Ile47	Altman TBP

Chapter 2

Synthesis of New Quinolinequinone Derivatives and Preliminary

Exploration of their Cytotoxic Properties

Reprinted with permission from Charles M. Keyari, Alison K. Kearns, Nathan S. Duncan*,

Emily A. Eickholt, Geoffrey Abbott, Howard D. Beall, and Philippe Diaz. Synthesis of New

Quinolinequinone Derivatives and Preliminary Exploration of their Cytotoxic Properties. *J. Med.*

Chem. 2013, 56, 3806−3819. dx.doi.org/10.1021/jm301689x. Copyright 2015 American

Chemical Society.

*Role of author was contribution of computational modeling

2.1 Introduction

Lavendamycin (Figure 2-1) is a quinolinequinone antibiotic with antitumor activity first

isolated from *Streptomyces lavendulae* by Balitz et al. in 1982.[1,2] It is structurally related to

streptonigrin, which was first isolated from Streptomyces flocculus.[3,4] Streptonigrin is known for

its potent cytotoxic properties, antitumor activity, in vitro and in vivo antiviral properties, and
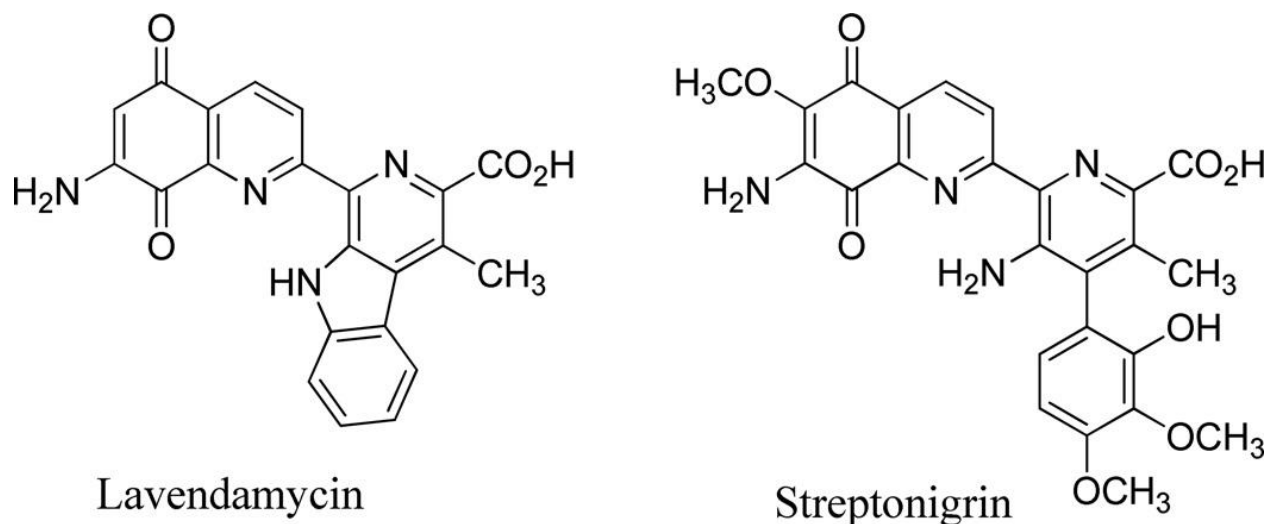
Figure 2-1. Natural quinolinequinone antibiotics.

potent, broad-spectrum antimicrobial properties. Although lavendamycin is not suitable for clinical use due to its toxicity, its analogues are less toxic and hence have potential as antitumor agents.[5] Recent findings[6–11] suggest that some indolequinones and quinolinequinones are excellent substrates for the quinone reductase enzyme NAD(P)H:quinone oxidoreductase 1 (NQO1) and are selectively cytotoxic to cancer cell lines that overexpress NQO1. NQO1 is a ubiquitous flavoenzyme that catalyzes the two-electron reduction of quinones to hydroquinones, and it is highly expressed in many solid tumors.[12] This forms the basis for the synthesis of novel quinolinequinones structurally related to lavendamycin as potential NQO1-directed antitumor agents.

Behforouz et al.[13] first demonstrated that 7-aminoquinoline-5,8-diones can be efficiently prepared from commercially available 8-hydroxy-2-methylquinoline. Fryatt et al.[7] also showed that, by starting with 6-methoxyquinoline, 6-methoxy-2-chloroquinoline-5,8-dione was prepared, and subsequent palladium(0)-catalyzed reaction with boronic acids gave novel quinolinequinones under reflux for 24 h. Furthermore, in 2004,[14] arylboronic acids were shown to be more reactive than their counterparts, the arylpinacolboronate esters, when reacted with indole bromides in Suzuki couplings under reflux. The lower reactivity was attributed to steric factors in the arylpinacolboronate esters. Also, 3-arylindazoles have been synthesized by the reaction of haloindazoles (3-bromoindazole and 3-iodoindazole) with arylboronic acids under Pd(0) catalysis in Suzuki-type cross couplings.[15] The reaction times ranged from 1 to 18 h under reflux conditions. In this study we report a direct, more efficient approach to 7-aminoquinoline quinones starting from commercially available 7-amino-8-hydroxyquinoline under microwave conditions where the reaction times are shorter. Computational, metabolism, and cytotoxicity studies on the quinoline-5,8-diones are also described.

2.2 Chemistry

The synthesis commenced with nitration of 5-chloro-8-hydroxyquinoline under HNO_3/H_2SO_4 according to a procedure reported by Musser et al.[16] to give the 5-chloro-7-nitro-8-hydroxyquinoline (1) in good yield (79%). Hydrogenation under Pd/C catalysis at 40−50 psi
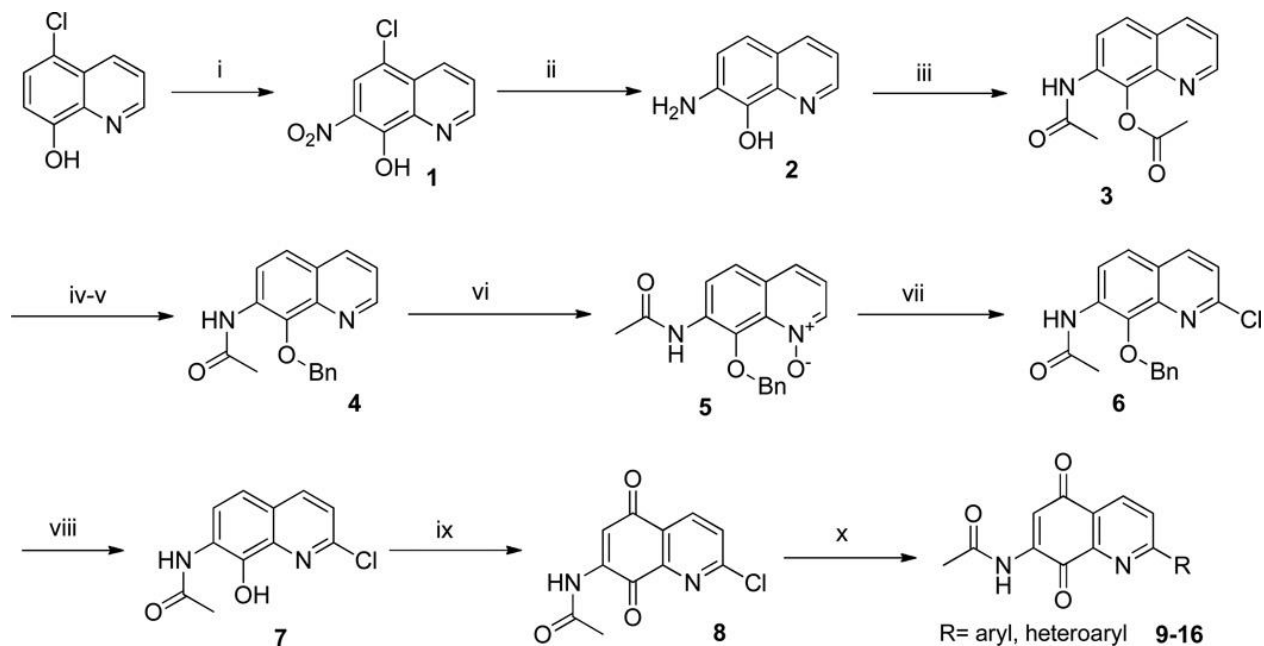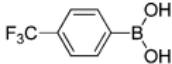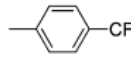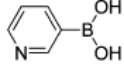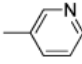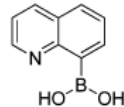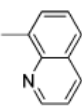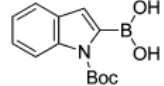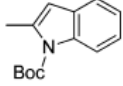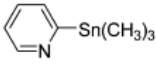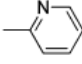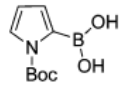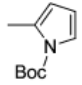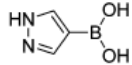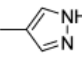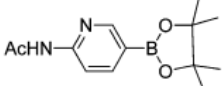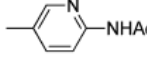
Scheme 2-1. a.Reagents and conditions: (i) HNO_3/H_2SO_4; (ii) H_2/Pd−C, MeOH, 40−50 psi, overnight; (iii) CH_3COCl, DIEA, THF, 2 h; (iv) H_2O/MeOH, reflux, 1 h; (v) BnBr, K_2CO_3, DMF, 50 °C, 24 h; (vi) mCPBA, $ClCH_2CH_2Cl$, 48 h; (vii) $POCl_3$, $CHCl_3$, reflux, 2 h; (viii) $BCl_3 \cdot SMe_2$, CH_2Cl_2, overnight; (ix) Fremy's salt, rt, 1 h; (x) $RB(OH)_2$, $Pd(PPh_3)_4$, 110−140 °C, μW 20−25 min.

not only reduced the nitro group to the free amine but also removed the chloride to provide the desired 7-amino-8-hydroxyquinoline (2) in excellent yield (99%). A direct approach to the amino alcohol 2 involves heating a mixture of 8-hydroxyquinoline and N-methyl-N-phenylhydrazine at 90 °C, albeit very low yields were obtained.[17] Our attempt to synthesize the amino alcohol by heating in a microwave between 130 and 160 °C did not improve the yield.

Acetylation proceeded smoothly where both the amino and hydroxyl groups were protected. The resulting diacetylated product (3) was hydrolyzed in MeOH/H2Ounder reflux to

form 7-acetamido-8-hydroxyquinoline. Subsequent benzylation of the free hydroxyl was effected by reaction with BnBr/K$_2$CO$_3$ in N,N-dimethylformamide (DMF) at 50 °C for 24 h to give the

R-X	Reaction conditions	R		Yield (%)
F$_3$C—⬡—B(OH)$_2$	Pd(PPh$_3$)$_4$, DME/Na$_2$CO$_3$ 140°C, 20 min	—⬡—CF$_3$	(9)	70
pyridin-3-yl-B(OH)$_2$	Pd(PPh$_3$)$_4$, DME/Na$_2$CO$_3$ 120°C, 20 min	pyridinyl	(10)	41
quinolin-8-yl-B(OH)$_2$	Pd(PPh$_3$)$_4$, DME/Na$_2$CO$_3$ 120°C, 20 min	quinolinyl	(11)	51
N-Boc-indol-2-yl-B(OH)$_2$	Pd(PPh$_3$)$_4$, DME/Na$_2$CO$_3$ 110°C, 25 min	N-Boc-indolyl	(12)	67
pyridin-2-yl-Sn(CH$_3$)$_3$	*Pd(PPh$_3$)$_4$, p-dioxane 120°C, 20 min	pyridinyl	(13)	71
N-Boc-pyrrol-2-yl-B(OH)$_2$	Pd(PPh$_3$)$_4$, DME/Na$_2$CO$_3$ 110°C, 25 min	N-Boc-pyrrolyl	(14)	53
pyrazol-4-yl-B(OH)$_2$	Pd(PPh$_3$)$_4$, DME/Na$_2$CO$_3$ 120°C, 20 min	pyrazolyl	(15)	42
AcHN-pyridin-5-yl-Bpin	PdCl$_2$(dppf), p-dioxane,K$_3$PO$_4$ 120°C,30 min	pyridinyl-NHAc	(16)	27

[a]Asterisk indicates Stille coupling reaction.

Table 2-1. Suzuki Couple Products. Asterisk indicates Stille coupling reaction.

7-acetamido-8-benzyloxyquinoline (4) in 90% yield. Oxidation with m-chloroperoxybenzoic acid (mCPBA) in 1,2-dichloroethane at room temperature (rt) for 48 h gave the N-oxide (5) in 82% yield.[18] The key intermediate in the synthesis, 2-chloro-7- acetamido-8-benzyloxyquinoline

(6), was obtained in 62% yield by refuxing the N-oxide with $POCl_3$ in $CHCl_3$.[19] The high regioselectivity of the reaction can be rationalized in terms of sterics as well as formation of an oxyphosphorane adduct anion in a rapid concerted mechanism.[20] We also attempted to reflux the N-oxide 5 with SO2Cl2 as reported in literature,[9] but this only resulted in massive decomposition of the starting material. Deprotection of the benzyl group was effected with $BCl_3 \cdot SMe_2$ in CH_2Cl_2 and subsequent oxidation with Fremy's salt [potassium nitrosodisulfonate, $(KO_3S)_2NO$] gave 7-acetamido-2-chloroquinoline-5,8-dione (8) in 71% yield.[7] The results are summarized in Scheme 2.1 above.

After successful formation of quinolinequinone 8, the stage was now set for Suzuki coupling chemistry. This was accomplished by reaction with different boronic acids under Pd(0) catalysis in a microwave as illustrated in Table 2-1. Generally, the reactions were complete within 20−30 min in good yields except for the arylboronate ester, where only 27% of the product (16) was obtained. The mechanistic details of the reaction have been well studied, with oxidative addition, transmetalation, and reductive elimination being the most critical steps.[21] Interestingly, 7-amino-2-(2-pyridyl)quinoline-5,8-dione was prepared in nine steps starting from 3-hydroxybenzoic acid where the key step was a Friedlander condensation of 2-acetylpyridine and 2-amino-3-benzyloxy-4-bromobenzaldehyde to give 8-benzyloxy-7-bromo-2-(2′-pyridyl)quinoline.[22] Although this seems an attractive strategy, the method lacks the flexibility needed to create a library of lavendamycin analogues.

The final step in the synthesis involved removal of the acetate protecting group, which was effected by reaction with H_2SO_4/MeOH at rt. The tert-butyloxycarbonyl (Boc)-protected derivatives were also subjected to trifluoroacetic acid (TFA)/CH_2Cl_2 at rt for 2 h to provide the 7-acetamido derivatives.
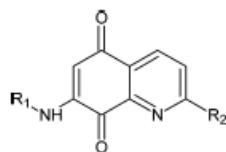
No.	R1	R2	Reduction rate by hNQO1 (µmol cyt c reduced /min/mg NQO1	Oxygen Consumption (µmol/min/mg NQO1)	Reduction Potential ($E_{1/2}$(V) vs Fc)
9	CH_3CO	(4-CF₃-phenyl)	4.5 +/- 0.5	5.2 +/- 1.0	-1.93 nr[d]
10	CH_3CO	(3-pyridyl)	25 +/- 4	-	-1.17, -1.92 nr
11	CH_3CO	(8-methylquinolinyl)	7.0 +/- 0.3	-	-1.18, -1.68, -1.77
13	CH_3CO	(2-methylpyridyl)	480 +/- 200	34 +/- 3	-1.90 nr
15	CH_3CO	(pyrazolyl)	16 +/- 1	-	-1.08, -1.36, -1.58
17	CH_3CO	(indolyl)	2.8 +/- 0.2	-	-1.10, -1.60, -1.94
18	CH_3CO	(pyrrolyl)	31 +/- 9	-	-
19	H	(4-CF₃-phenyl)	78 +/- 7	-	-
20	H	(3-pyridyl)	170 +/- 30	-	-1.99 nr
21	H	(indolyl)	80 +/- 8	-	-1.84 nr
22	H	(8-methylquinolinyl)	18 +/- 6	-	-1.53, -1.65
23	H	(2-pyridyl)	71 +/- 13	-	-1.85 nr
24	H	(pyrrolyl)	120 +/- 10	8.5 +/- 1.6	-

Table 2-2. Reduction Rates[a] and Oxygen Consumption[b] as a Result of Quinoline-5,8-Dione Metabolism by Recombinant Human NQO1 and Electrochemical Reduction Potentials versus Ferrocene[c,d]. [a]Spectrophotometric assay with cytochrome c as terminal electron acceptor (550 nm). [b]Oxygen concentration monitored via an oxygen electrode. [c]$E_{1/2}$ values calculated as (Epc+Epa)/2 are average values from voltammograms recorded atpotential sweep rate of 50 mV/s. Epc = cathodic peak potential; Epa = anodic peak potential. [d]nr = nonreversible, anodic peak only.

2.3 Electrochemistry

Eletrochemistry was performed to compare the electrochemical behavior of the quinolinequinones with their reduction rates by NQO1, and the data are shown in Table 2-2. Tetrahydrofuran (THF) was used as the solvent for all compounds except 15, which was run in dimethyl sulfoxide (DMSO). The compounds were run against an Ag/AgCl electrode and cathodic and anodic peak potentials, Epc and Epa, respectively, were measured at a potential sweep rate of 50 mV/s, and the midpoint of the peak potentials was used to determine E1/2 values, (Epc + Epa)/2. Unfortunately, many of the analogues did not show reversible electrochemistry, and in some cases there were multiple somewhat difficult, but some conclusions can be drawn. For instance, most of the acetylated quinolinequinones had a reduction peak between −1.08 and −1.18 V, an indication that they are easier to reduce than the nonacetylated compounds due to the presence of this electron-withdrawing group. This is consistent with what we reported previously for lavendamycins. However, there was no correlation between reduction potentials and reduction rates by NQO1, in line with previous publications on this topic.[6–8, 23, 24] This suggests that steric interactions are more likely to be predictive of substrate efficiency than reduction potentials.

2.4 NMR Spectroscopy and Spectrophotometry

Complexation of zinc(II) triflate by compounds 13, 19, 22, and 23 was studied by 1H NMR spectroscopy. No new peaks were observed in the NMR spectra, indicating that free and complexed forms of zinc(II) triflate were in a rapid exchange relative to NMR time scale. The aromatic region of the NMR spectrum of compound 19 in THF-d8 at room temperature is shown in Figure 2-2.

There was a small difference in chemical shifts of H-2′ (moving upfield) and H-3 (moving downfield) after addition of 1 equiv of zinc(II) triflate to the NMR solution (Table S1, Supporting Information, and Figure 2-2) whereas the changes in δ of the other protons were barely noticeable. The biggest change in δ of H-2′ (−0.04 ppm) and H-3′ (+0.07 ppm) occurs after addition of 10 equiv of Zn(SO3CF3)2. This suggests that weak binding occurs at low Zn2+ concentration.
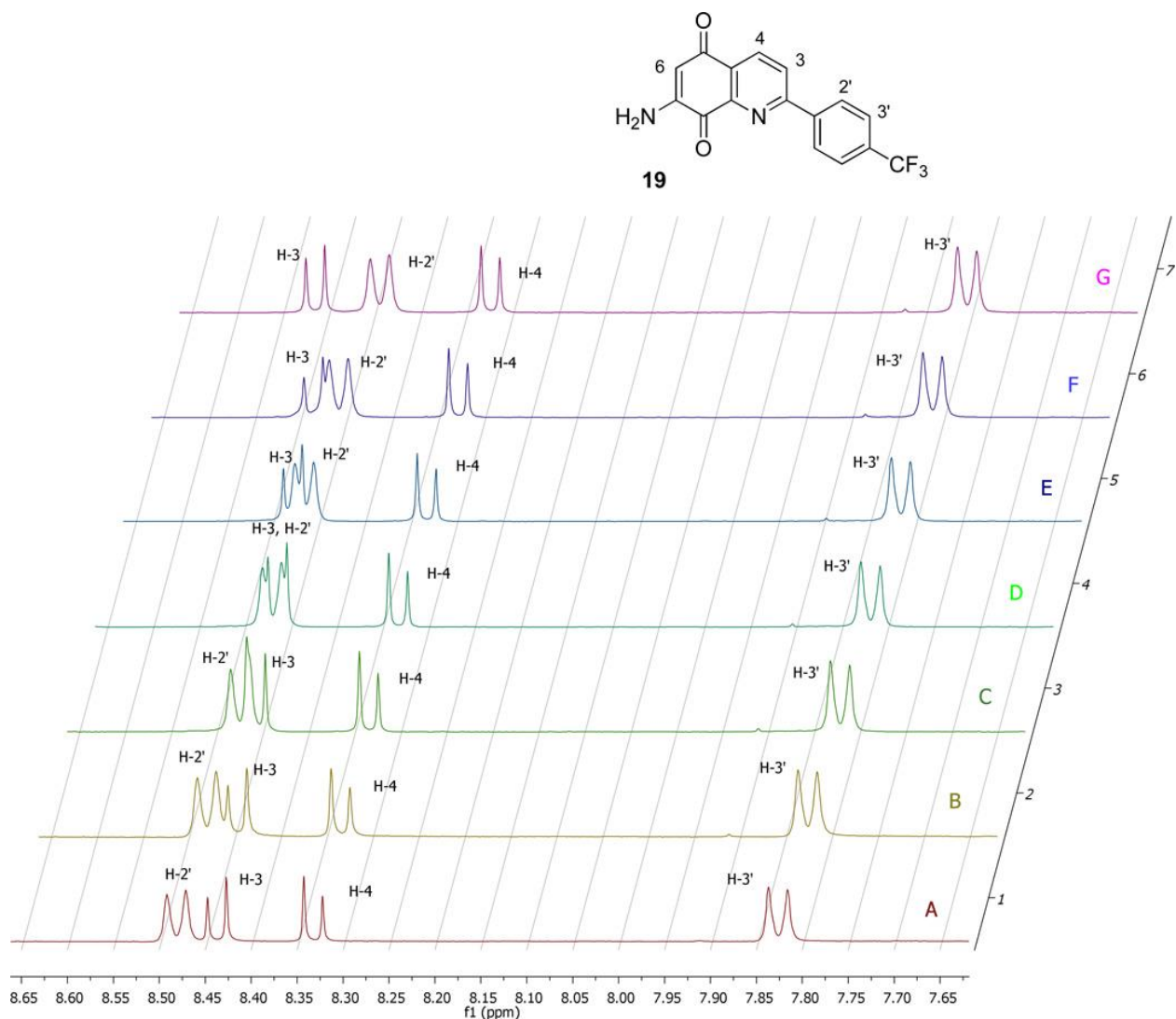
Figure 2-2. proton region of NMR spectrum of 19 upon addition of increasing equivalents of Zn(SO3CF3)2 in THF-d8. Note the change in δ of H-2′and H-3 upon addition of Zn2+. Equivalents of Zn2+: A = 0, B = 1, C = 2, D = 3, E = 4, F = 5, and G = 10.

In contrast, addition of only 1 equiv of Zn(SO3CF3)2 to compound 22 caused larger chemical shift variations of all the protons (Table S2, Supporting Information, and Figure 2-3).
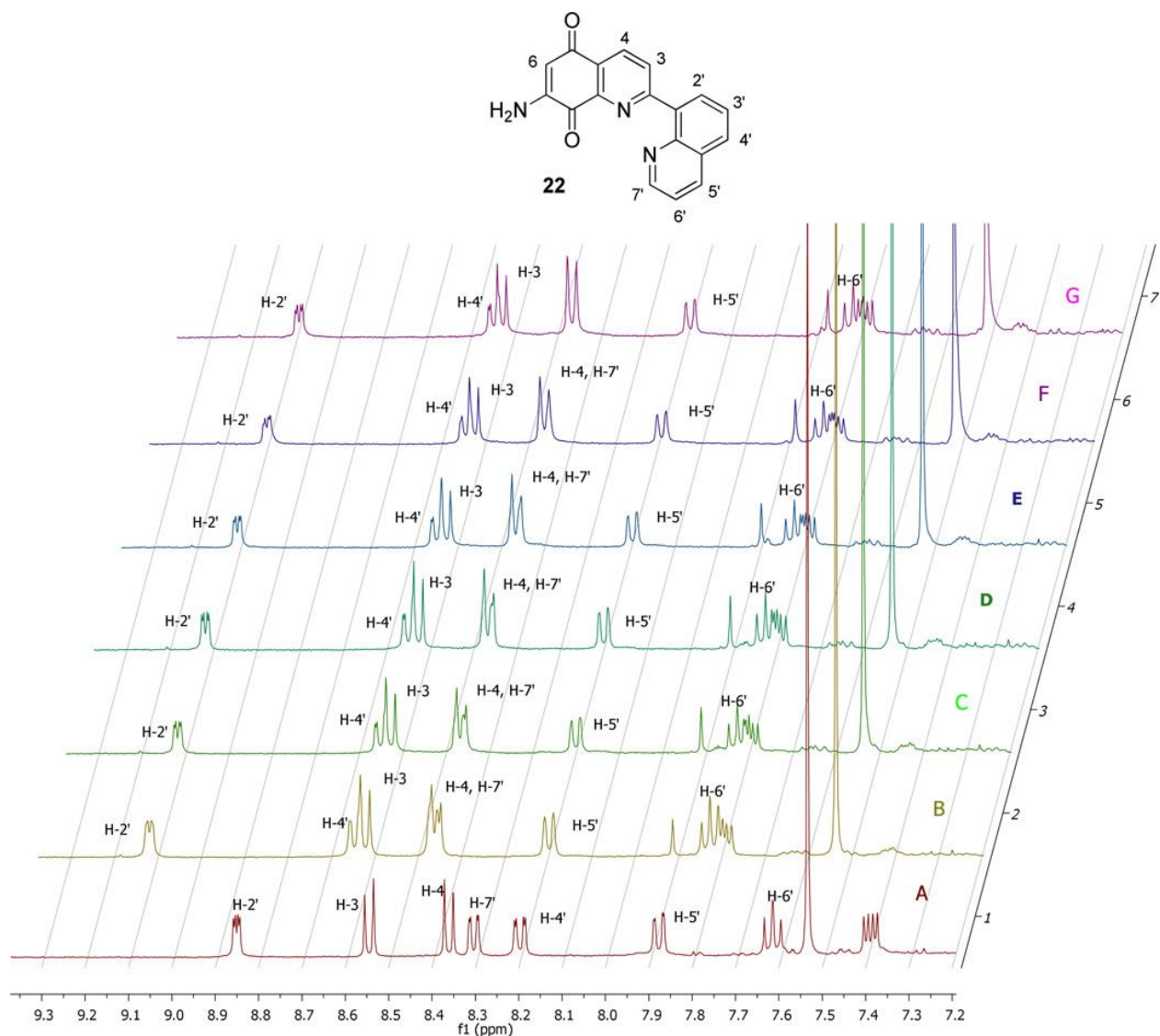
Figure 2-3. Aromatic protons region NMR spectra of 22 upon addition of increasing equivalents of Zn(SO3CF3)2 in THF-d8. Equivalents of Zn2+: A = 0, B = 1, C = 2, D = 3, E = 4, F = 5, and G = 10.

Increasing the amount of Zn2+ (2−10 equiv) added to compound 22 made little or no difference in δ afterward (>0.01 ppm). This means that the quinoline derivative binds the Zn2+ more efficiently than compound 19 and only 1 equiv of Zn2+ is enough to cause chemical shift variations.
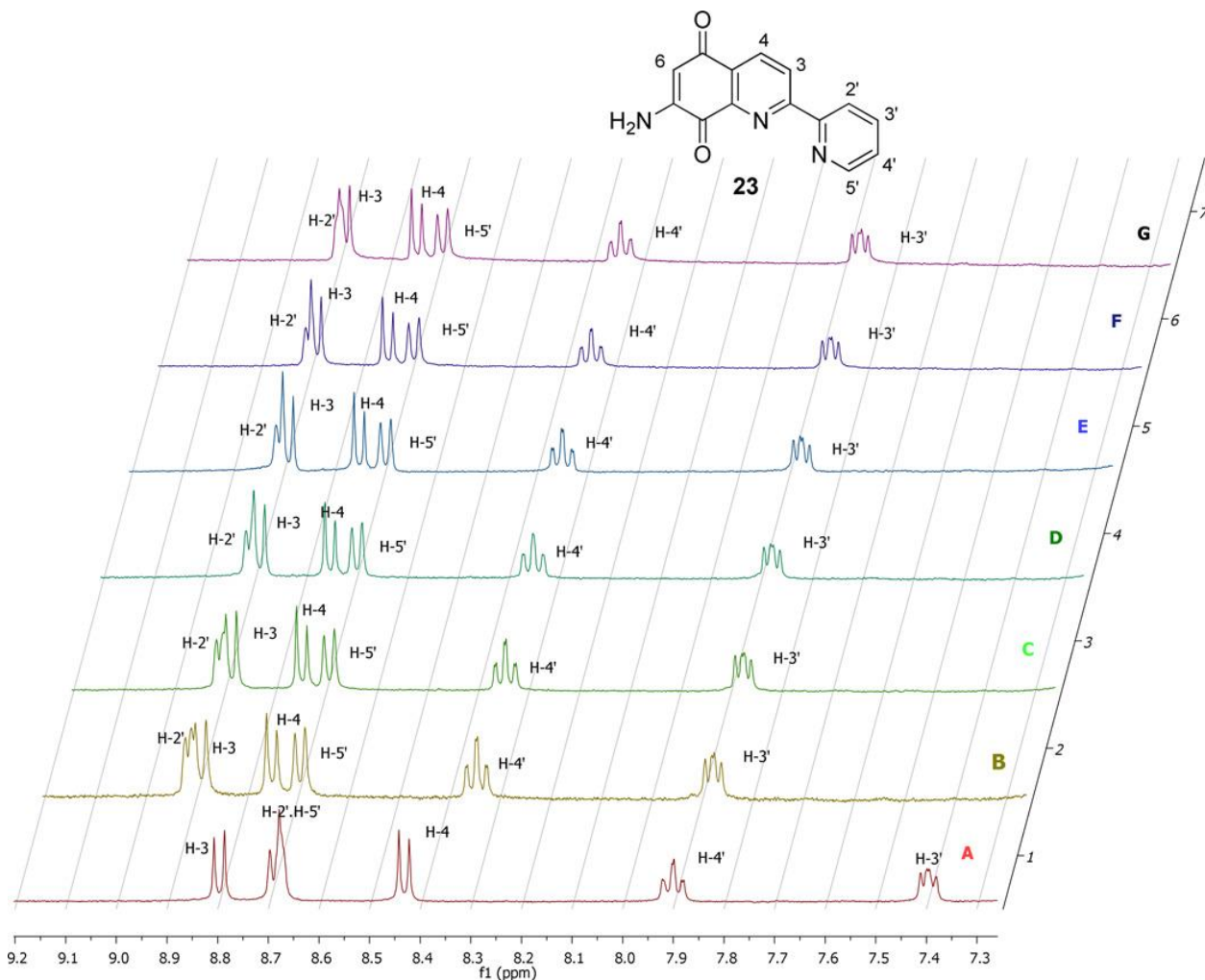
Figure 2-4. Aromatic proton region NMR spectra of 23 upon addition of increasing equivalents of Zn(SO3CF3)2 in THF-d8. Equivalents of Zn2+: A = 0, B = 1, C = 2, D = 3, E = 4, F = 5, and G = 10.

Similar observations were made with compounds 23 (Table S3, Supporting Information, and Figure 2-4) and 13 (Table S4, Supporting Information). This is consistent with the results reported by Long and Harding,[25] where they demonstrated that the 1:1 bipyridyl complex of streptonigrin was the major complex formed at room temperature by performing an NMR study in THF-d8 with addition of Zn2+. Titration of compound 23 with Zn2+ in a mixture of dimethyl sulfoxide/methanol (1:3) was monitored by a spectrophotometer as reported in literature.[26] A plot

of $\Delta\lambda 355$ against Zn2+ concentration gave a moderate affinity constant of $1.41 \times 104M-1$ for compound 23 binding with Zn2+.

2.5 Results and Discussion

Quinolinequinone metabolism by recombinant human NQO1 was examined via a spectrophotometric assay that employs cytochrome c as the terminal electron acceptor. Initial rates of reduction (micromoles of cytochrome c reduced per minute per milligram of NQO1) were calculated from the linear portion (0−30 s) of the reaction graphs. The 7-acetamido-2-(2-pyridinyl) compound 13 displayed the highest reduction rate by NQO1 (Table 2-2), although it was the only acetylated analogue with a high reduction rate. In all other cases, 7-amino compounds had much higher reduction rates than corresponding 7-acetamido compounds with identical substituents at the quinolone 2-position. Although unusual, higher rates for acetylated analogues have been observed in other series.[6,11] With regard to the aromatic substituents at the quinoline 2-position, no clear trend in reduction rates was observed except that bulkier groups generally decreased reduction rates. Oxygen consumption is a measure of the ability of the reduced quinone (hydroquinone) to redox-cycle following reduction by NQO1. This could lead to production of toxic reactive oxygen species and ultimately to cell death. Oxygen consumption was measured for select quinolinequinones, and the trend, if not the magnitude, mirrored the reduction rates (Table 2-2).

Cell survival wasmeasured by the [3-(4,5-dimethylthiazol-2-yl)-2,5-diphenyltetrazolium bromide (MTT) colorimetric assay. In previous work, we demonstrated that IC50 values generated from standard clonogenic assays and MTT assays were positively correlated, suggesting that the MTT assay is a reliable indicator of cytotoxicity.[6] We utilized MDA-MB-468 human breast cancer cells stably transfected with human NQO1 cDNA
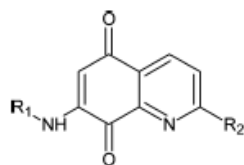
No.	R1	R2	IC$_{50}$ (µM) MDA468-WT	IC$_{50}$ (µM) MDA468-NQ16	Selectivity Ratio IC$_{50}$ (WT)/ IC$_{50}$ NQ16
9	CH$_3$CO	[4-CF$_3$-phenyl]	1.7 +/- 0.8	2.4 +/- 1.9	0.73
10	CH$_3$CO	[3-pyridyl]	3.3 +/- 0.1	6.3 +/- 0.2	0.52
11	CH$_3$CO	[8-methylquinolinyl]	0.80 +/- 0.33	0.64 +/- 0.41	1.2
13	CH$_3$CO	[2-methylpyridyl]	0.53 +/- 0.27	2.2 +/- 0.5	0.24
17	CH$_3$CO	[2-indolyl]	7.4 +/- 5.0	19.1 +/- 5.9	0.39
19	H	[4-CF$_3$-phenyl]	5.3 +/- 0.8	17 +/- 5	0.31
20	H	[3-pyridyl]	5.6 +/- 1.3	15 +/- 2	0.37
21	H	[2-indolyl]	4.8 +/- 0.9	10 +/- 1	0.47
22	H	[8-methylquinolinyl]	0.14 +/- 0.02	0.19 +/- 0.04	0.75
23	H	[2-methylpyridyl]	19 +/- 12	5.3 +/- 2.1	3.5
24	H	[2-methylpyrrolyl]	4.5 +/- 1.9	17 +/- 2	0.26

Table 2-3. Cytotoxicity of Quinoline-5,8-diones toward MDA468-WT (NQO1-deficient) and MDA468-NQ16 (NQO1-rich) Human Breast Cancer Cell Lines.

(MDA468-NQ16) along with the nontransfected wild-type cells (MDA468) to compare the

cytotoxicity of the quinolinequinones (Table 2-3).[27]

Quinolinequinone cytotoxicity (IC50) to MDA468 cells was generally in the single-digit micromolar range following 2-h exposures, with some in the high nanomolar range (11, 13, and 22). Surprisingly, selectivity ratios [IC50 (MDA468)/IC50 (MDA468-NQ16)] were generally <1, meaning that the quinolinequinones were less cytotoxic to the NQO1-rich MDA468-NQ16 cells rather than more cytotoxic. This suggests that NQO1 was protective to the cells rather than functioning as an activating enzyme.[27] Only two compounds (11 and 23) were selectively cytotoxic to the MDA468-NQ16 cells. The reason for the general absence of selective cytotoxicity with this particular series of compounds is unclear, but it is consistent with NQO1's primary role as a detoxification enzyme.[27]

Molecular docking of the quinolinequinones in the NQO1 active site was performed by use of Sybyl 8.1.1 and GOLD 5.1 for scoring. Three good NQO1 substrates (13, 20, and 24) and three poor NQO1 substrates (9, 11, and 17) were docked and scored with ChemPLP and ChemScore (Table 2-4). The highest scores representing a good fit for the model were found for 20 and 24, consistent with the metabolism data. The exception again was 13, which scored the lowest but was the best substrate. Interatomic distances between quinolinequinone carbonyl groups and flavin adenine dinucleotide (FAD) atom N5 and His161 were shortest for 20, but all were within a reasonable distance for hydride transfer from FAD when the dynamic effects of the quinone−enzyme interaction are considered. Figure 2-5 shows possible docking conformations for 20 and 11 with NQO1. All quinolinequinones orient with the quinone ring above the FAD isoalloxazine ring as needed for hydride transfer.

The mechanism of action of lavendamycin and streptonigrin is not clearly understood. However, previous studies demonstrated that quinone moieties are reduced by NQO1 to the

corresponding hydroquinones, which undergo autoxidation to produce activated oxygen species
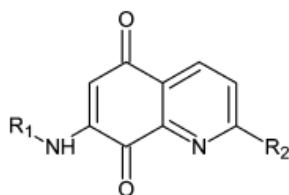
No.	R^1	R^2	ChemPLP	ChemScore	C=O8...NH5 (Å)	C=O5...His161NE2 (Å)
9	CH₃CO		63.2	22.6	3.9	3.6
11	CH₃CO		63.8	22.6	4.7	3.3
13	CH₃CO		57.6	21.4	4.3	3.5
17	CH₃CO		63.8	22.1	4.2	3.3
20	H		72.8	26.0	3.6	3.2
24	H		67.3	22.7	4.1	3.3

Table 2-4. Computational Parameters for Selected Quinoline-5,8-diones.

including not only semiquinone derivatives but also superoxide and hydroxyl radicals.[28] In addition, both streptonigrin and lavendamycin chelate divalent cationic metal ions. This property might confer to streptonigrin and lavendamycin the ability to shuttle iron cations into the cells, which in turn can catalyze production of reactive oxygen species through a Fenton reaction. On the other hand, this chelation can result in depletion of intracellular cationic metals, which might result in cell death.[29] Generation of the semiquinone radical, after reduction of the quinone to the hydroquinone followed by autoxidation, results in a decrease of activity in nine compounds. The

best NQO1 substrates are less active compounds (13, 20, and 24) in NQO1 expressing cells. In contrast, poor NQO1 substrates such as compound 22 or 11, exhibit the best activity in both
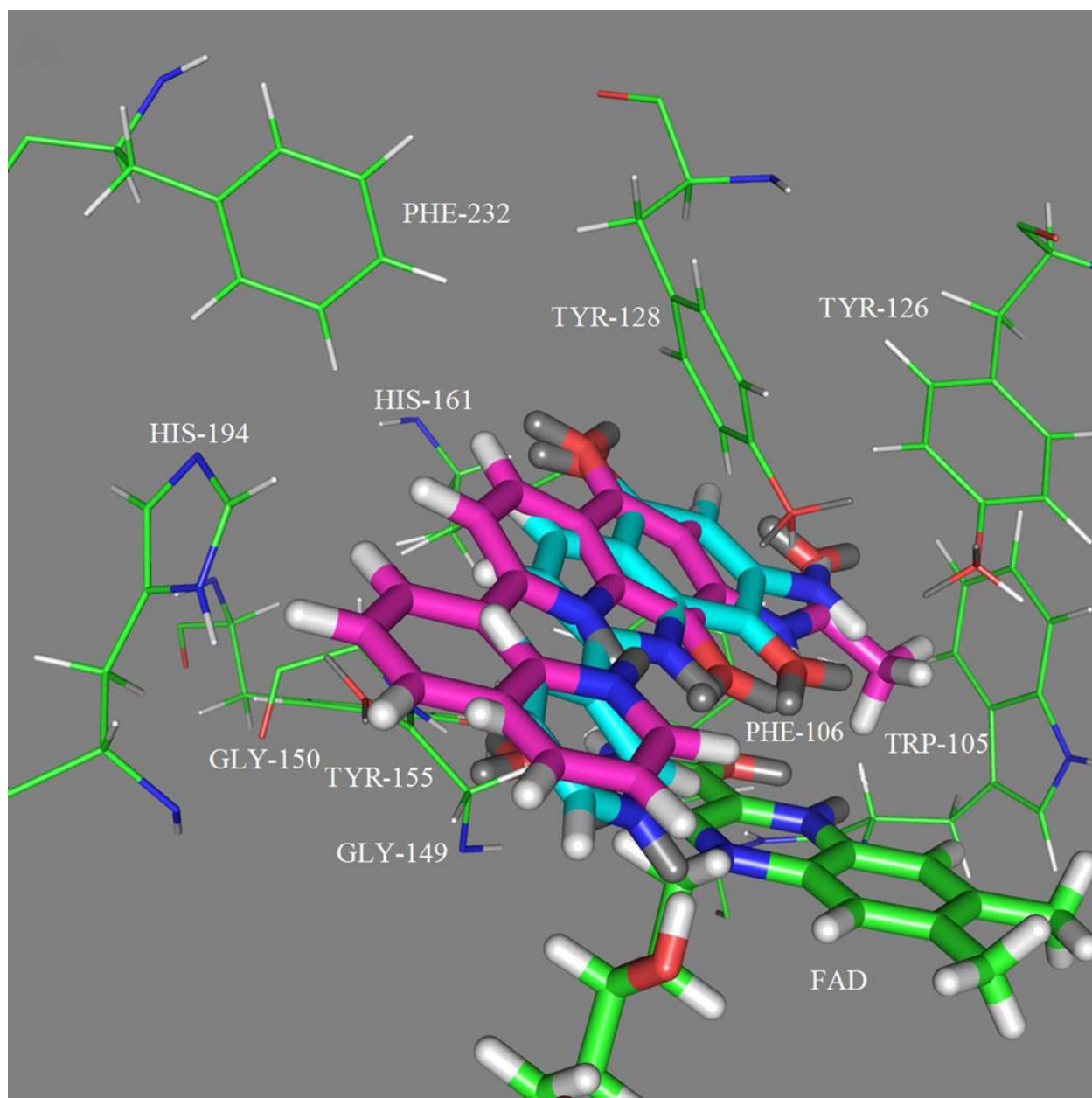
Figure 2-5. Quinolinequinones docked in NQO1 active site: 20, cyan; 11, magenta; FAD, green.

cancer cells expressing NQO1 and those not expressing NQO1. According to the NMR experiments, quinoline derivative 22 and compound 13 bind the Zn2+ more efficiently than

compound 19, and only 1 equiv of Zn2+ is enough to cause important chemical shift variations. Similar observations were made with compound 23, which was less cytotoxic than compound 22. Even though metal chelation by these compounds is still a plausible mechanism to explain their activity against breast cancer cells, another mode of action cannot be discarded. Most active compounds (11, 13, and 22) are potential tridentate ligands for metals. Compound 23 exhibits lower activity than the corresponding acetylated amino analogue 13. It was proposed that metals can assist tautomeric shift from the active quinone analogues to the quinoid analogue, which has a structure isoelectronic with the biologically inactive azastreptonigrin.[24] This tautomeric shift can explain the decrease of activity of the amino derivative compared to the amido derivative. In our series of aryl-substituted quinonequinolines, the active molecules are the quinone derivatives and not the semiquinone derivatives. A similar mode of action to the bidentate metal ligand derivative 8-hydroxyquinoline is currently under investigation.[30,31]

2.6 Conclusions

A ten-step synthetic scheme led to good yields for quinolinequinone analogues of lavendamycin projected as NQO1-directed antitumor agents. Unexpectedly, 10 of 11 analogues demonstrated excellent cytotoxicity (IC50 values of single-digit micromolar or better) toward MDA468 breast cancer cells, but only two were selectively cytotoxic to NQO1-expressing MDA468-NQ16 cells. Compounds 22 and 11 are poor NQO1 substrates and exhibit the best activity against breast cancer cells. In our novel series of aryl-substituted quinonequinolines, the active molecules appears to be the quinone derivatives and not the semiquinone derivatives resulting from NQO1 reduction, suggesting that the mode of action of this novel series differs from that of lavendamycin and involves an unidentified target. Quinolinequinone derivatives 11, 13, and 22 cytotoxicities (IC50) to MDA468 cells were in the high nanomolar range. Our results

seem to indicate that compounds 11, 13, and 22 effects could be also, at least partially, mediated by metal chelation. These aryl quinonequinoline derivatives represent a promising class of cytotoxic agents with potential novel therapeutic value.

2.7 Experiments Section

2.7.1 Cell Culture.

MDA-MB-468 (MDA468) human breast cancer cells and stably NQO1-transfected MDA468-NQ16[32] were a gift from Dr. David Ross (University of Colorado-Denver, Denver, CO). MDA468 cells had no measurable NQO1 activity whereas activity in MDA468-NQ16 cells was 1070 nmol·min−1 (mg of total cell protein) −1, with dichlorophenolindophenol (DCPIP) as the standard electron acceptor. Cells were grown in RPMI 1640 medium with L-glutamine and penicillin/streptomycin, supplemented with 10% fetal bovine serum (FBS). Cell culture medium and supplements were obtained from Invitrogen (Carlsbad, CA). The cells were incubated at 37 °C under a humidified atmosphere containing 5% CO_2.

2.7.2 Spectrophotometric Cytochrome c Assay.

Quinolinequinone reduction was monitored by a spectrophotometric assay in which the rate of reduction of cytochrome c was quantified at 550 nm. Briefly, the assay mixture contained cytochrome c (70 μM), reduced nicotinamide adenine dinucleotide (NADH; 1 mM), recombinant human NQO1 (0.1−10 μg) (gift from Dr. David Ross, University of Colorado-Denver, Denver, CO), and quinonlinequinones (25 μM) in a final volume of 1 mL of Tris-HCl (25 mM, pH 7.4) containing 0.7 mg/mL bovine serumalbumin (BSA) and 0.1%Tween-20. Reactions were carried out at room temperature and started by the addition of NADH. Rates of reduction were calculated from the initial linear part of the reaction curve (0−30 s), and results were expressed in terms of micromoles of cytochrome c reduced per minute per milligram of NQO1 by use of a

molar extinction coefficient of 21.1 mM−1·cm−1 for cytochrome c. All reactions were carried out at least in triplicate.

2.7.3 Oxygen Consumption.

Oxygen concentration was monitored with a MI-730 micro-oxygen electrode (Microelectrodes, Bedford, NH) with concentrations adjusted for temperature (25 °C). Assay mixtures contained 25 μM quinonlinequinones, 200 μM NADH, and 1 μg/mL NQO1 in a 2 mL Tris-HCl/BSA/Tween (0.1%) buffer system. Reactions were started with NADH and measured over 3-min intervals at room temperature. All reactions were carried out in triplicate.

2.7.4 Electrochemistry.

Cyclic voltammograms (CV) were collected for 10 analogues on a BAS CV-50W electrochemical analyzer using a standard three-electrode cell. Experiments were performed with an Ag/AgCl reference electrode, a glassy carbon working electrode, and a to the ferrocene (0/+) couple in the solvent used, primarily THF, which occurs at +0.60 V versus Ag/AgCl. The compounds were run at concentrations of 1 mMin THF, except compound 15 which was run in DMSO, with 0.1 M tetrabutylammonium hexafluorophosphate as supporting electrolyte. All samples were purged and run under an Ar atmosphere during the course of the experiment, and the electrodes were washed and wiped down between each sample. Each CV was collected at a sweep rate of 50 mV/s in the potential range of 0 to −2Vat room temperature of 21 °C.

2.7.5 NMR Spectroscopy.

One-dimensional 1H NMR spectra were recorded at room temperature on a Bruker Avance IIITM spectrometer (The Woodlands, Texas) at 400 MHz using a 5-mm probe and a simple pulse-acquire sequence. Acquisition parameters consisted of spectral width of 4000 Hz

with an acquisition time of 3.98 s, number of scans 128, and relaxation delay 1 s. Complexes were prepared in a mixture of CDCl3 and THF-d8.

2.7.6 Cell Viability Assay.

Growth inhibition was determined by the MTT colorimetric assay. Cells were plated in 96-well plates at a density of 10 000 cells/mL and allowed to attach overnight (16 h). Quinolinequinone solutions were applied in medium for 2 h, removed, and replaced with fresh medium, and the plates were incubated at 37 °C under a humidified atmosphere containing 5% CO_2 for 3−5 days. MTT (50 μg) was added and the cells were incubated for another 4 h. Medium/MTT solutions were removed carefully by aspiration, the MTT formazan crystals were dissolved in 100 μL of DMSO, and absorbance was determined on a plate reader at 560 nm. IC50 values (concentration at which cell survival equals 50% of control) were determined from semilog plots of percent of control versus concentration. Selectivity ratios were defined as IC50 value for the MDA468 cell line divided by IC50 value for the MDA468-NQ16 cell line.

2.7.7 Molecular Modeling.

For docking purposes, the crystallographic coordinates of the human NQO1 complex with

3-(hydroxymethyl)-5-(2-methylaziridin-1-yl)-1-methyl-2-phenylindole-4,7-dione (25) were obtained from the Brookhaven Database (PDB code 1H69[33] and resolution 1.86 Å) and the structure was edited accordingly to provide a monomer of the protein. The protein complex was then minimized within Sybyl 7.3 (Tripos Ltd., St. Louis, MO) while all heavy atoms were held stationary. The ligand was then removed to leave the receptor complex, which was used for the subsequent docking studies. For preparation of ligand structures, fragments from Sybyl 8.1.1 were used to construct the compounds and all symmetric compounds were prepared as

monoanionic ligands. Ligands were subject to 1000 iterations of energy minimization by the Powell method with MMFF94s force field. For computational docking, GOLD 5.1 software was used in combination with the ChemPLP[34] scoring function (rescoring with ChemScore).[35]

The active site was defined as being any volume within 8 Å of the quinone scaffold of 25 in its crystal pose in 1H69. Each GA run used the default parameters of 100 000 genetic operations on an initial population of 100 members divided into five subpopulations, with weights for crossover, mutation, and migration being set to 95, 95, and 10, respectively. GOLD allows a user-definable number of GA runs per ligand, each of which starts from a different orientation. For these experiments, the number of GA runs was set to 10, and scoring of the docked poses was performed with the ChemPLP scoring function with ChemScore rescore. Each GOLD run was saved and the strongest scoring binding pose of each ligand (subject to a rmsd default distance threshold of 1.5 Å) was compared to that of the reference ligand position observed in the crystal structure. The best output poses (orientations) of the ligands generated were analyzed on the basis of ChemPLP/ChemScore score, feasibility of hydride transfer process, and H-bonding to the enzyme. The best pose(s) were visualized with PyMOL Molecular Graphics System version 1.3.

2.7.8 Chemistry

All moisture sensitive reactions were performed in an inert, dry atmosphere of argon in flame dried glassware. Air sensitive liquids were transferred via syringe or cannula through rubber septa. Reagent grade solvents were used for extraction and flash chromatography. THF was distilled from Na/benzophenone under argon; dichloromethane (CH_2Cl_2) and chloroform ($CHCl_3$) were distilled from CaH_2 under argon. All other reagents and solvents which were purchased from commercial sources, were used directly without further purification. The

progress of reactions was checked by analytical thin-layer chromatography (Sorbent Technologies, Silica G TLC plates w/UV 254). The plates were visualized first with UV illumination followed by charring with ninhydrin (0.3% ninhydrin (w/v), 97:3 EtOH-AcOH). Flash column chromatography was performed using prepacked Biotage SNAP cartridges on a Biotage Isolera One instrument. Microwave reactions were performed using a Biotage Initiator instrument. The solvent compositions reported for all chromatographic separations are on a volume/volume (v/v) basis. ^{1}HNMR spectra were recorded at 400 or 500 MHz and are reported in parts per million (ppm) on the δ scale relative to tetramethylsilane as an internal standard. ^{13}CNMR spectra were recorded at 100 or 125 MHz and are reported in parts per million (ppm) on the δ scale relative to CDCl3 (δ 77.00). Melting points were determined on a Stuart melting point apparatus from Bibby Scientific Limited and are uncorrected. High Resolution mass spectrometry (HRMS) was performed on a Waters/Micromass LCT-TOF instrument. All compounds were more than 95% pure.

5-chloro-8-hydroxy-7-nitroquinoline (1). This compound was prepared according to the literature [12] procedure to yield a yellow solid, 4.40 g (79%). M.p. 198-200°C, [lit.[12], m.p. 192-194°C]; ^{1}H NMR (500 MHz, DMSO) δ 9.09 (dd, $J = 4.2$, 0.5 Hz, 1H), 8.58 (dd, $J = 8.5$, 0.8 Hz, 1H), 8.18 (s, 1H), 7.94 (dd, $J = 8.5$, 4.3 Hz, 1H). ^{13}C NMR (126 MHz, DMSO) δ 150.5, 150.1, 139.9, 133.6, 132.3, 128.5, 125.9, 122.0, 117.9. HRMS (TOF MS ES+) for $C_9H_6ClN_2O_3^+$ (MH+) calcd. 225.0067, found 225.0055.

7-Amino-8-hydroxyquinoline (2). Compound **1** (2.4 g, 10.69 mmol) was placed in a hydrogenation apparatus equipped with a magnetic stir bar and methanol added. Pd/C (150 mg) in a small amount of MeOH (60 mL) was added and stirring commenced. H_2 gas was introduced at a pressure of 40-50 psi and reacted at rt overnight. TLC showed full conversion. The black

solution was filtered using a celite pad and concentrated under reduced pressure to yield **2** as a black oil, 99% yield. ^{1}H NMR (500 MHz, CDCl$_3$) δ 8.66 (dd, J = 4.4, 1.6 Hz, 1H), 8.03 (dd, J = 8.2, 1.6 Hz, 1H), 7.24 (d, J = 8.7 Hz, 1H), 7.17 (dd, J = 8.2, 4.4 Hz, 1H), 7.10 (d, J = 8.7 Hz, 1H). ^{13}C NMR (126 MHz, CDCl$_3$) δ 148.0, 137.9, 136.6, 136.1, 132.1, 122.4, 119.3, 118.5, 117.7. HRMS (TOF MS ES+) for C$_9$H$_9$N$_2$O$^+$ (MH+) calcd. 161.0715, found 161.0707.

7-acetamido-8-acetyloxyquinoline (3). Compound **2** (330 mg, 2.06 mmol) was dissolved in dried THF (10 mL) and DIEA added with stirring. AcCl (176 μL) in 1mL THF was added drop wise while stirring and reacted at rt for 2 hrs. Then concentrated under reduced pressure followed by redissolving in CH$_2$Cl$_2$ (20 mL) and water (10 mL). The two layers were allowed to partition and extracted 2x 20 mL CH$_2$Cl$_2$. The combined organic layers were dried over MgSO$_4$, filtered and concentrated under reduced pressure. Then purified on a Biotage SNAP cartridge (25 g) at a flow rate of 25 mL/min to yield an orange solid, 382 mg (76%); m.p. 151-153°C; ^{1}H NMR (500 MHz, CDCl$_3$) δ 8.85 (dd, J = 4.1, 1.3 Hz, 1H), 8.49 (d, J = 9.1 Hz, 1H), 8.13 (dd, J = 8.3, 1.5 Hz, 1H), 7.70 (d, J = 9.1 Hz, 1H), 7.67 (s, 1H), 7.36 (dd, J = 8.2, 4.2 Hz, 1H), 2.56 (s, 1H), 2.04 (s, 1H); ^{13}C NMR (126 MHz, CDCl$_3$) δ 169.7, 168.5, 150.6, 140.7, 135.8, 134.9, 130.8, 125.8, 125.6, 121.3, 120.6, 24.5, 21.0; HRMS (TOF MS ES+) for C$_{13}$H$_{13}$N$_2$O$_3$$^+$ (MH+) calcd. 245.0926, found 245.0923.

7-acetamido-8-benzyloxyquinoline (4). To a solution of **3** (1.2 g, 4.91 mmol) in MeOH (100 mL) was added water (10 mL) and the reaction stirred under reflux for 1 hr. The black solution was concentrated and in vacuo and flash chromatographed on a KP-Sil 100 g Biotage SNAP cartridge using MeOH: DCM as the solvent (0-5% MeOH). A white solid (0.9 g) obtained and used for the next step directly. R$_f$= 0.11 (5% MeOH:CH$_2$Cl$_2$).

To a solution of 7-acetamido-8-hydroxyquinoline (2.27 g, 11.23 mmol) in 40 mL DMF was added K_2CO_3 (2.33 g, 16.80 mmol) and BnBr (2 mL, 16.80 mmol) respectively. The reaction was stirred at 50°C for 24 hrs after which TLC showed almost all the starting material was consumed. The reaction mixture was diluted with 30 mL CH_2Cl_2, filtered with a pad of celite and concentrated under reduced pressure. The residue was loaded onto a 100 g Biotage SNAP cartridge by dissolving in a small amount of CH_2Cl_2 and eluted with EtOAc:heptane gradient (0-50%). Yield 2.95 g (90%) of a yellow oil was obtained. R_f= 0.50 (60% EtOAc:heptane). ^{1}H NMR (500 MHz, CDCl$_3$) δ 8.95 (dd, J = 4.2, 1.7 Hz, 1H), 8.58 (d, J = 9.0 Hz, 1H), 8.14 (dd, J = 8.3, 1.7 Hz, 1H), 7.77 (s, 1H), 7.57 (d, J = 9.0 Hz, 1H), 7.40 – 7.35 (m, 6H), 5.49 (s, 2H), 1.93 (s, 4H). ^{13}C NMR (126 MHz, CDCl$_3$) δ 168.3, 150.0, 142.0, 141.0, 137.4, 136.2, 132.0, 128.9, 128.8, 128.8, 126.0, 124.0, 120.0, 120.0, 77.3, 24.6. HRMS (TOF MS ES+) for $C_{18}H_{17}N_2O_2^+$ (MH+) calcd. 293.1290, found 293.1264.

*7-acetamido-8-(benzyloxy)quinoline-1-oxide (**5**).* The starting material (**4**) (428 mg, 1.46 mmol) was dissolved in 4.3 mL 1,2-dichloroethane with stirring. The *m*CPBA (340 mg, 1.76 mmol) was added (0.5 M) and the reaction stirred at rt for 48 hrs. TLC showed almost all the starting material was consumed. The precipitated *m*CPBA was filtered and washed with 5 mL 1, 2-dichloroethane. The filtrate was concentrated under reduced pressure and flash chromatographed on a KP-sil 100 g Biotage SNAP cartridge using a 5% MeOH: DCM gradient at a flow rate of 25 mL/min to yield a yellow solid, 373 mg (82%). M.p. 145-147°C; R_f 0.24 (5%MeOH:DCM). ^{1}H NMR (500 MHz, DMSO) δ 9.45 (s, 1H), 8.46 (d, J = 6.1 Hz, 1H), 8.20 (d, J = 8.9 Hz, 1H), 7.81 (d, J = 8.3 Hz, 1H), 7.77 (d, J = 9.0 Hz, 1H), 7.58 – 7.50 (2H), 7.40 – 7.30 (aromatic, 4H). ^{13}C NMR (126 MHz, DMSO) δ 168.9, 139.8, 138.1, 137.1, 136.4, 133.3, 129.8, 129.1, 128.1, 128.0,

124.7, 124.4, 120.8, 77.7, 23.8. HRMS (TOF MS ES+) for $C_{18}H_{17}N_2O_3^+$ (MH+) calcd. 309.1239, found 309.1227.

*7-acetamido-8-benzyloxy-2-chloroquinoline (**6**).* Phosphoryl chloride (280 μL, 3.0 mmol) in CHCl$_3$ (1.0 mL) was added to a stirred solution of the oxide **5** (770 mg, 2.50 mmol) in 21 mL CHCl$_3$ and stirred for 15 min. The mixture was then refluxed for 2 hrs, cooled and poured into ice (50 g) and the pH adjusted to 12 with NaOH (aq.). The aq. layer was extracted with 2 x 50 mL CH$_2$Cl$_2$, washed with 2 x 20 mL H$_2$O, dried over MgSO$_4$, filtered and concentrated under reduced pressure to yield a brown oil. Then purified on a HP-Sil 25 g Biotage SNAP cartridge using EtOAc:heptane gradient (0-50%) as the solvent. Yield 504 mg (62%) of an off-white solid was obtained. R_f= 0.58 (60% EtOAc:heptane); M.P. 92-94°C; ^{1}H NMR (500 MHz, CDCl$_3$) δ 8.60 (d, *J* = 9.0 Hz, 1H), 8.06 (d, *J* = 8.5 Hz, 1H), 7.81 (s, 1H), 7.54 (d, *J* = 9.0 Hz, 1H), 7.45 – 7.35 (m, 1H), 7.32 (d, *J* = 8.5 Hz, 1H), 5.48 (s, 1H), 1.96 (s, 1H). ^{13}C NMR (126 MHz, CDCl$_3$) δ 168.4, 150.5, 141.4, 140.3, 139.0, 137.2, 133.0, 128.9, 128.8, 128.8, 124.3, 123.3, 121.1, 120.1, 77.4, 24.7. HRMS (TOF MS ES+) for $C_{18}H_{16}ClN_2O_2^+$ (MH+) calcd. 327.0900, found 327.0936.

*7-acetamido-2-chloro-8-hydroxyquinoline (**7**).* To a solution of **6** (330 mg, 1.01 mmol) in CH$_2$Cl$_2$ (10.1 mL) under an Ar atmosphere was added BCl$_3$•SMe$_2$ (10.1 mL) via a syringe and stirred at rt overnight. TLC showed the reaction was complete. The reaction was then quenched with saturated NaHCO$_3$(aq.) and extracted with 2x20 mL CH$_2$Cl$_2$. The organic layers were combined, dried over MgSO$_4$, filtered and concentrated under reduced pressure. The residue was purified on 50 g KP-Sil Biotage SNAP cartridge using a MeOH: CH$_2$Cl$_2$ gradient (0-5% MeOH) at a flow rate of 25 mL/minute to give a yellow solid, 198 mg (82%). M.P. 176-178°C; R_f= 0.50 (5% MeOH:CH$_2$Cl$_2$). ^{1}H NMR (400 MHz, CDCl$_3$) δ 8.60 (d, *J* = 9.0 Hz, 1H), 8.05 (d, *J* = 8.5 Hz, 1H), 7.82 (brs, 1H), 7.72 (s, 1H), 7.35 (d, *J* = 9.0 Hz, 1H), 7.30 (d, *J* = 8.5 Hz, 1H), 2.29 (s,

3H). ^{13}C NMR (101 MHz, CDCl$_3$) δ 168.6, 149.7, 138.9, 138.2, 137.1, 124.4, 123.3, 121.5, 121.3, 118.0, 24.9. HRMS (TOF MS ES+) for $C_{11}H_{10}ClN_2O_2^+$ (MH+) calcd. 237.0431, found 237.0424.

7-Acetamido-2-chloroquinoline-5,8-dione (8). To a solution of **7** (300 mg, 1.27 mmol) in acetone (30 mL) was added a solution of Fremy's salt in NaH$_2$PO$_4$ buffer (0.3 M, 30 mL) and the mixture stirred at rt for 1 hr. A further solution of Fremy's salt in the buffer (0.3M, 30 mL) was added and stirring continued for 2 hrs. The acetone was removed under reduced pressure and the residue extracted with 2 x 50 mL CH$_2$Cl$_2$. The CH$_2$Cl$_2$ phases were combined, dried over MgSO$_4$ and concentrated under reduced pressure. The residue was purified on a 25 g HP-Sil Biotage SNAp cartridge using EtOAc:heptanes gradient (0-60%) to obtain a yellow solid, 225 mg (71% over 2 steps); m.p. 224-226°C (decomposes into a black mass), R$_f$= 0.49 (60% EtOAc:heptane). ^{1}H NMR (500 MHz, CDCl$_3$) δ 8.41 (s, 1H), 8.39 (d, J = 8.2 Hz, 1H), 7.97 (s, 1H), 7.74 (d, J = 8.2 Hz, 1H), 2.34 (s, 3H). ^{13}C NMR (126 MHz, CDCl$_3$) δ 183.4, 178.1, 169.5, 156.7, 145.9, 140.4, 137.2, 129.9, 128.0, 116.3, 25.1. HRMS (TOF MS ES+) for $C_{11}H_8ClN_2O_3^+$ (MH+) calcd. 251.0223, found 250.0203.

General procedure for Suzuki coupling under microwave conditions. The 7-acetamido-2-chloroquinoline-5,8-dione **8** (21 mg, 0.08 mmol) was dissolved in 4 mL dimethoxyethane (DME) and degassed under reduced pressure. The palladium (0) catalyst, Pd(PPh$_3$)$_4$ (10 mg, 0084 mmol) was added and the solution degassed further. The mixture was stirred under Ar atmosphere for 10 minutes. Na$_2$CO$_3$ solution (0.2 mL, 2.0 M) was added followed by the boronic acid (0.126 mmol). The mixture was then heated using a Biotage microwave initiator at 110-140°C for 20 minutes. After cooling, TLC showed all the starting material was consumed. The reaction mixture was poured into DCM and washed with 2 x 10 mL water. Then dried over

MgSO$_4$, filtered and concentrated under reduced pressure. The residue was purified on HP-Sil 25

g Biotage SNAP cartridge using EtOAc:heptane gradient (0-50%) at a flow rate of 20 mL/min.

For very polar products, MeOH:CH$_2$Cl$_2$ (0-10%MeOH) was used as solvent for purification.

7-acetamido-2-(4-(trifluoromethyl)phenyl)quinoline-5,8-dione (9). Yield 21 mg (70%) of a

yellow solid was obtained. R$_f$= 0.47 (50% EtOAc:heptane); m.p. 250°C(decomposes); ^{1}H NMR

(500 MHz, CDCl$_3$) δ 8.53 (d, *J* = 8.2 Hz, 1H), 8.45 (s, 1H), 8.27 (d, *J* = 8.1 Hz, 2H), 8.17 (d, *J* =

8.2 Hz, 1H), 7.99 (s, 1H), 7.80 (d, *J* = 8.2 Hz, 2H), 2.35 (s, 4H).^{13}C NMR (126 MHz, CDCl$_3$) δ

184.1, 179.1, 169.5, 160.1, 146.1, 140.6, 135.7, 128.3, 128.0, 126.0, 126.0, 126.0, 125.3, 116.5,

25.2; HRMS (TOF MS ES+) for C$_{18}$H$_{12}$F$_3$N$_2$O$_3$$^+$(MH+) calcd. 361.0800, found 361.0834.

7-acetamido-2-(3-pyridinyl))quinoline-5,8-dione (10). Yield 21 mg (41%) of a yellow solid

obtained, R$_f$= 0.19 (5% MeOH:DCM); m.p. >300°C(decomposes); ^{1}H NMR (500 MHz, CDCl$_3$)

δ 9.29 (s, 1H), 8.72 (d, *J* = 3.9 Hz, 1H), 8.56 (d, *J* = 8.2 Hz, 1H),8.55 (m, 1H), 8.21 (d, *J* = 8.2

Hz, 1H), 8.00 (s, 1H), 7.56 (dd, *J* = 8.0, 4.9 Hz, 1H), 2.35 (s, 3H). ^{13}C NMR (126 MHz, CDCl$_3$)

δ 184.2, 179.0, 170.4, 158.9, 150.7, 148.1, 146.1, 140.9, 135.7, 135.7, 128.1, 125.3, 116.6, 24.6 ;

HRMS (TOF MS ES+) for C$_{16}$H$_{12}$N$_3$O$_3$$^+$MH+) calcd. 294.0879, found 294.0914. 7-amino-2-(3-

pyridinyl)quinoline-5,8-dione: 6 mg (12%) of a red solid was obtained. R$_f$= 0.13 (5%

MeOH:DCM); m.p. 195-197°C (decomposes, turns black); ^{1}H NMR (500 MHz, CDCl$_3$) δ 9.29

(d, *J* = 1.7 Hz, 1H), 8.67 (dd, *J* = 4.9, 1.4 Hz, 1H), 8.58 (ddd, *J* = 8.0, 2.2, 1.7 Hz, 1H), 8.52 (d, *J*

= 8.2 Hz, 1H), 8.22 (d, *J* = 8.2 Hz, 1H), 7.59 (ddd, *J* = 8.0, 4.9, 0.7 Hz, 1H), 6.07 (s, 1H). [13]C

NMR (126 MHz, CDCl$_3$) δ 181.9, 179.8, 157.0, 150.4, 149.6, 147.6, 146.3, 135.4, 135.0, 133.5,

129.4, 124.7, 123.8, 102.1. HRMS (TOF MS ES+) for C$_{14}$H$_{10}$N$_3$O$_2$$^+$MH+) calcd. 252.0773,

found 252.0795.

7-acetamido-2-(8'-quinolinyl)quinoline-5,8-dione (11). Yield 31 mg (51%) of a yellow solid was obtained. R_f= 0.25 (70% EtOAc:heptane), crystallized from MeOH/CH_2Cl_2; m.p. 295°C (decomposes); ^{1}H NMR (500 MHz, $CDCl_3$) δ 8.93 (dd, *J* = 4.2, 1.8 Hz, 1H), 8.53 (d, *J* = 8.1 Hz, 1H), 8.48 (d, *J* = 8.1 Hz, 1H), 8.34 (dd, *J* = 8.3, 1.8 Hz, 1H), 8.22 (dd, *J* = 7.2, 1.4 Hz, 1H), 8.04 (dd, *J* = 8.2, 1.4 Hz, 1H), 8.00 (s, 1H), 7.76 (dd, *J* = 8.1, 7.3 Hz, 1H), 7.54 (dd, *J* = 8.3, 4.2 Hz, 1H), 2.34 (s, 3H). ^{13}C NMR (126 MHz, $CDCl_3$) δ 184.8, 179.1, 170.9, 161.9, 150.5, 145.7, 145.1, 140.9, 136.7, 136.5, 133.3, 131.9, 131.7, 130.2, 128.4, 127.6, 126.3, 121.4, 116.5, 24.2. HRMS (TOF MS ES+) $C_{20}H_{14}N_3O_3^+$ (MH+) calcd. 344.1035, found 344.1022.

7-acetamido-2-(2-(1-tert-butoxycarbonylindolyl))quinoline-5,8-dione (12). Yield 63mg (67%) of an orange was obtained. R_f= 0.40 (50% EtOAc:heptane); m.p. 191-193°C (decomposes); ^{1}H NMR (500 MHz, $CDCl_3$) δ 8.47 (s, 1H), 8.45 (d, *J* = 8.1 Hz, 1H), 8.15 (d, *J* = 8.4 Hz, 1H), 7.97 (s, 1H), 7.89 (d, *J* = 8.1 Hz, 1H), 7.60 (d, *J* = 7.8 Hz, 1H), 7.40 (t, *J* = 7.8 Hz, 1H), 7.27 (dd, *J* = 9.1, 5.9 Hz, 1H), 6.98 (s, 1H), 2.33 (s, 3H), 1.41 (s, 9H). ^{13}C NMR (126 MHz, $CDCl_3$) δ 184.2, 179.0, 169.6, 157.4, 149.7, 145.3, 140.4, 138.1, 137.5, 134.2, 128.6, 127.9, 127.6, 126.0, 123.3, 121.5, 116.5, 115.2, 114.0, 84.2, 27.8, 25.1. HRMS (TOF MS ES+) $C_{24}H_{22}N_3O_5^+$(MH+) calcd. 432.1559, found 432.1568.

7-acetamido-2-(2-pyridinyl)quinoline-5,8-dione (13). Yield 37 mg (71%) of a yellow solid was obtained. R_f= 0.19 (5% MeOH:CH2Cl2), crystallized from MeOH/CH_2Cl_2; m.p. 255-258°C (decomposes); ^{1}H NMR (500 MHz, DMSO) δ 10.08 (s, 1H), 8.78 (ddd, *J* = 4.8, 1.6, 0.8 Hz, 1H), 8.53 (d, *J* = 7.9 Hz, 1H), 8.46 (d, *J* = 8.2 Hz, 1H), 8.08 (td, *J* = 7.7, 1.8 Hz, 1H), 7.77 (s, 1H), 7.58 (ddd, *J* = 7.5, 4.7, 1.1 Hz, 1H), 2.28 (s, 3H). ^{13}C NMR (126 MHz, DMSO) δ 184.6, 178.4, 171.5, 158.6, 153.6, 149.8, 146.4, 142.5, 137.8, 135.0, 128.5, 125.5, 124.6, 121.7, 115.3, 24.7. HRMS (TOF MS ES+) $C_{16}H_{12}N_3O_3^+$ (MH+) calcd. 294.0879, found 294.0914.

*7-acetamido-2-(2-(1-tert-butoxycarbonylpyrrolyl))quinoline-5,8-dione (**14**).* Yield 36 mg (53%) of a yellow solid was obtained. R_f= 0.30 (50% EtOAc:heptane); m.p. 191-193°C (decomposes), recrystallized from methanol; ^{1}H NMR (500 MHz, CDCl$_3$) δ 8.42 (s, 1H), 8.39 (d, J = 8.2 Hz, 1H), 7.95 (s, 1H), 7.79 (d, J = 8.2 Hz, 1H), 7.42 (dd, J = 3.2, 1.7 Hz, 1H), 6.64 (dd, J = 3.4, 1.7 Hz, 1H), 6.29 (t, J = 3.3 Hz, 1H), 2.32 (s, 3H), 1.43 (s, 9H). ^{13}C NMR (126 MHz, CDCl$_3$) δ 184.3, 179.2, 169.5, 156.9, 148.8, 145.3, 140.3, 134.0, 132.5, 128.0, 127.3, 125.5, 118.6, 116.4, 111.2, 84.4, 27.7, 25.1. HRMS (TOF MS ES+) C$_{20}$H$_{20}$N$_3$O$_5$$^+$ (MH+) calcd. 382.1403, found 382.1381.

*7-acetamido-2-(4-pyrazolyl))quinoline-5,8-dione (**15**).* Yield 31 mg (42%) of a brown solid was obtained. R_f= 0.33 (5% MeOH:CH$_2$Cl$_2$); m.p. 270°C (decomposes), recrystallized from methanol; ^{1}H NMR (500 MHz, DMSO) δ 13.34 (s, 1H), 9.97 (s, 1H), 8.55 (s, 1H), 8.25 (d, J = 8.2 Hz, 1H), 8.21 (s, 1H), 8.11 (d, J = 8.2 Hz, 1H), 7.69 (s, 1H), 2.26 (s, 3H). ^{13}C NMR (126 MHz, DMSO) δ 184.6, 178.6, 171.4, 156.1, 146.6, 142.1, 134.2, 126.1, 123.8, 121.2, 115.1, 24.6. HRMS (TOF MS ES+) C$_{14}$H$_{11}$N$_4$O$_3$$^+$ (MH+) calcd. 283.0831, found 283.0846.

*7-acetamido-2-(3-(2-acetamido-pyridinyl))quinoline-5,8-dione (**16**).* The quinone **8** (71 mg, 0.28 mmol) was dissolved in 2 mL 1,4-dioxane and degassed under reduced pressure. PdCl$_2$(dppf) (20 mg), K$_3$PO$_4$ (238 mg) and the boronate were added and the solution degassed further. The mixture was stirred under Ar atmosphere for 10 minutes. The mixture was then heated heated using a Biotage microwave initiator at 120°C for 30 minutes. After cooling, the reaction mixture was poured into CH$_2$Cl$_2$ and washed with 2 x 10 mL water and extracted 2x 30 mL DCM. The combined organic phases were dried over MgSO$_4$, filtered and concentrated under reduced pressure. The residue was purified on a HP-Sil 25 g Biotage SNAP cartridge using MeOH:CH$_2$Cl$_2$ gradient (0-5%) at a flow rate of 20 mL/min. Yield 23mg (23%) of a brown solid

was obtained. R_f= 0.32 (5% MeOH:CH$_2$Cl$_2$); m.p. 249°C (decomposes); ^{1}H NMR (500 MHz, DMSO) δ 10.82 (s, 1H), 10.04 (s, 1H), 9.17 (d, J = 2.5 Hz, 1H), 8.60 (dd, J = 8.8, 2.5 Hz, 1H), 8.45 (d, J = 8.3 Hz, 1H), 8.38 (d, J = 8.2 Hz, 1H), 8.27 (d, J = 8.8 Hz, 1H), 7.75 (s, 1H), 2.28 (s, 3H), 2.14 (s, 3H). ^{13}C NMR (126 MHz, DMSO) δ 184.6, 178.5, 171.5, 169.7, 157.4, 153.6, 147.3, 146.6, 142.4, 137.0, 134.8, 128.0, 127.2, 124.1, 115.3, 113.0, 24.7, 24.0. HRMS (TOF MS ES+) C$_{18}$H$_{15}$N$_4$O$_4{}^+$ (MH+) calcd. 351.1093, found 351.1064.

7-acetamido-2-(2-indolyl)quinoline-5,8-dione (17). The starting material **12** (39 mg, 0.09 mmol) was dissolved in 2.5 mL CH$_2$Cl$_2$ and cooled to 0°C using an ice bath. Trifluoroacetic acid (140 µL) was the added dropwise and reacted at rt for 2 hrs. TLC showed full conversion. Then quenched with sat. NaHCO$_3$ (10 mL) and extracted 2x20 mL CH$_2$Cl$_2$. The organic layers were combined, dried over MgSO$_4$, filtered and concentrated under reduced pressure. The residue was purified on a HP-Sil 25 g Biotage SNAP cartridge using EtOAc:heptane gradient (0-70%) at a flow rate of 20 mL/min. Yield 17 mg (59%) of a red solid was obtained after recrystallization from MeOH. M.p. 185°C, decomposes; R_f= 0.38 (70% EtOAc:heptane). ^{1}H NMR (500 MHz, CDCl$_3$) δ 8.35 (d, J = 8.3 Hz, 1H), 8.14 (d, J = 8.3 Hz, 1H), 7.92 (s, 1H), 7.67 (d, J = 8.0 Hz, 1H), 7.49 (d, J = 8.3 Hz, 1H), 7.29 (t, J = 7.6 Hz, 1H), 7.23 (s, 1H), 7.13 (t, J = 7.4 Hz, 1H), 2.34 (s, 3H). ^{13}C NMR (126 MHz, CDCl$_3$) δ 184.2, 180.4, 170.5, 154.7, 145.4, 140.3, 137.8, 134.7, 134.4, 128.3, 126.6, 124.4, 124.4, 121.5, 120.2, 117.0, 111.7, 104.4, 24.4. HRMS (TOF MS ES+) C$_{19}$H$_{14}$N$_3$O$_3{}^+$ (MH+) calcd. 332.1035, found 332.1030.

7-acetamido-2-(2-(pyrrolyl))quinoline-5,8-dione (18). The starting material **14** (30 mg, 0.08 mmol) was dissolved in 3 mL CH$_2$Cl$_2$ and cooled to 0°C using an ice bath. Trifluoroacetic acid (150 µL) was the added dropwise and reacted at rt for 2 hrs. TLC showed full conversion. Then quenched with sat. NaHCO$_3$ (10 mL) and extracted 2x20 mL CH$_2$Cl$_2$. The organic layers were

combined, dried over MgSO$_4$, filtered and concentrated under reduced pressure. The residue was purified on a HP-Sil 25 g Biotage SNAP cartridge using EtOAc:heptane gradient (0-50%) at a flow rate of 20 mL/min. Yield 21 mg (93%) of a red solid was obtained after recrystallization from MeOH. M.P. 255°C, decomposes. R$_f$= 0.11 (50% EtOAc:heptane). ^{1}H NMR (500 MHz, DMSO) δ 11.65 (s, 1H), 9.95 (s, 1H), 8.20 (d, J = 8.4 Hz, 1H), 8.05 (d, J = 8.4 Hz, 1H), 7.69 (s, 1H), 7.07 − 7.04 (m, 2H), 6.28 − 6.22 (m, 1H), 2.27 (s, 3H). ^{13}C NMR (126 MHz, DMSO) δ 184.6, 178.7, 171.4, 154.0, 146.6, 141.9, 133.9, 130.1, 125.3, 123.8, 121.8, 115.2, 111.9, 110.4, 24.7. HRMS (TOF MS ES+) C$_{15}$H$_{12}$N$_3$O$_3^+$ (MH+) calcd. 282.0879, found 282.0909.

General procedure for removal of the acetate group with MeOH-H$_2$SO$_4$. To the starting material (0.1 mmol) in a 20 mL vial was added 175μL of H$_2$SO$_4$ in 3.0 mL MeOH and stirred at rt for 3 hrs. The red solution was then neutralized with 5 mL 5% NaHCO$_3$ (aq.) and extracted with 5 X 10 mL CH$_2$Cl$_2$. The combined organic extracts were dried over MgSO$_4$, filtered and concentrated under reduced pressure. Then purified on a HP-Sil 25 g Biotage SNAP cartridge using EtOAc:heptanes (0-70%) or MeOH:CH$_2$Cl$_2$ gradient (0-5%) at a flow rate of 20 mL/min.

*7-Amino-2-(4-(trifluoromethyl)phenyl)quinoline-5,8-dione (**19**).* The general procedure was used to obtain 6.0 mg (67%) of a red solid; R$_f$= 0.38 (60% EtOAc:heptane); m.p. 151-153°C (decomposes, turns black); ^{1}H NMR (500 MHz, CDCl$_3$) δ 8.28 (d, J = 8.2 Hz, 1H), 8.05 (d, J = 8.2 Hz, 2H), 7.95 (d, J = 8.2 Hz, 1H), 7.58 (d, J = 8.3 Hz, 2H), 5.84 (s, 1H). ^{13}C NMR (126 MHz, CDCl$_3$) δ 182.2, 180.1, 158.7, 150.3, 146.3, 140.6, 135.1, 129.4, 127.7, 125.5, 125.5, 125.1, 105.8, 102.4. HRMS (TOF MS ES+) C$_{16}$H$_{10}$F$_3$N$_2$O$_2^+$ (MH+) calcd. 319.0694, found 319.0666.

*7-amino-2-(3-pyridinyl)quinoline-5,8-dione (**20**).* The general procedure was used to obtain 10 mg (83%) of a red solid. R$_f$= 0.16 (5% MeOH:CH$_2$Cl$_2$); m.p. 195-197°C (decomposes, turns

black). ^{1}H NMR (500 MHz, CDCl$_3$) δ 9.29 (d, J = 1.7 Hz, 1H), 8.67 (dd, J = 4.9, 1.4 Hz, 1H), 8.58 (ddd, J = 8.0, 2.2, 1.7 Hz, 1H), 8.52 (d, J = 8.2 Hz, 1H), 8.22 (d, J = 8.2 Hz, 1H), 7.59 (ddd, J = 8.0, 4.9, 0.7 Hz, 1H), 6.07 (s, 1H). ^{13}C NMR (126 MHz, CDCl$_3$) δ 181.9, 179.8, 157.0, 150.4, 149.6, 147.6, 146.3, 135.4, 135.0, 133.5, 129.4, 124.7, 123.8, 102.1. HRMS (TOF MS ES+) for C$_{14}$H$_{10}$N$_3$O$_2^+$MH+) calcd. 252.0773, found 252.0795.

7-amino-2-(2-indolyl)quinoline-5,8-dione (21). The general procedure was used to obtain 19 mg (63%) of a dark-brown solid. R$_f$= 0.22 (70% EtOAc:heptane); m.p. 235°C decomposes. ^{1}H NMR (500 MHz, CDCl$_3$) δ 8.33 (d, J = 8.3 Hz, 1H), 8.10 (d, J = 8.3 Hz, 1H), 7.67 (d, J = 8.0 Hz, 1H), 7.49 (d, J = 8.2 Hz, 1H), 7.39 (s, 1H), 7.27 (ddd, J = 8.1, 7.1, 1.1 Hz, 1H), 7.19 (s, 1H), 7.12 (td, J = 7.5, 0.8 Hz, 1H), 6.01 (s, 1H). ^{13}C NMR (126 MHz, CDCl$_3$) δ 182.6, 181.6, 153.6, 149.5, 145.9, 137.6, 135.0, 134.2, 128.3, 128.0, 124.1, 124.0, 121.3, 120.0, 111.7, 103.5, 102.9. HRMS (TOF MS ES+) for C$_{17}$H$_{12}$N$_3$O$_2^+$ (MH+) calcd. 290.0930, found 290.0900.

7-amino-2-(8-quinolinyl)quinoline-5,8-dione (22). The general procedure was used to obtain 55 mg (71%) of a brown solid. R$_f$= 0.29 (5% MeOH:CH$_2$Cl$_2$); m.p. 243-245°C, recrystallized from MeOH. ^{1}H NMR (500 MHz, CD$_3$OD) δ 8.92 (dd, J = 4.2, 1.8 Hz, 1H), 8.49 (d, J = 8.1 Hz, 1H), 8.40 (d, J = 8.1 Hz, 1H), 8.33 (dd, J = 8.3, 1.8 Hz, 1H), 8.21 (dd, J = 7.2, 1.5 Hz, 1H), 8.02 (dd, J = 8.2, 1.4 Hz, 1H), 7.75 (dd, J = 8.1, 7.3 Hz, 1H), 7.53 (dd, J = 8.3, 4.2 Hz, 1H), 6.06 (s, 1H). ^{13}C NMR (126 MHz, CDCl$_3$) δ 182.8, 180.1, 160.5, 150.3, 150.2, 146.2, 145.2, 136.7, 136.7, 133.2, 131.6, 131.5, 129.8, 129.1, 128.4, 126.3, 121.2, 102.4. HRMS (TOF MS ES+) for C$_{18}$H$_{12}$N$_3$O$_2^+$ (MH+) calcd. 302.0930, found 302.0939.

7-amino-2-(2-pyridinyl)quinoline-5,8-dione (23). The general procedure was used to obtain 16 mg (76%) of a red solid. R$_f$= 0.25 (20% MeOH:CH$_2$Cl$_2$), recrystallized from MeOH. ^{1}H NMR (500 MHz, DMSO) δ 8.75 (d, J = 4.1 Hz, 1H), 8.72 (d, J = 8.2 Hz, 1H), 8.50 (d, J = 7.9 Hz, 1H),

8.40 (d, $J = 8.1$ Hz, 1H), 8.05 (t, $J = 7.7$ Hz, 1H), 7.58 – 7.53 (m, 1H), 5.89 (s, 1H). HRMS (TOF MS ES+) for $C_{14}H_{10}N_3O_2^+$ (MH+) calcd. 252.0773 found 252.0749.

*7-Amino-2-(2-pyrrolyl)quinoline-5,8-dione (**24**).* The general procedure was used to obtain 11 mg (78%) of a red solid. R_f= 0.37 (5% MeOH:CH_2Cl_2); m.p. 230°C (decomposes), recrystallized from MeOH. ^{1}H NMR (500 MHz, $CDCl_3$) δ 8.23 (d, $J = 8.4$ Hz, 1H), 7.84 (d, $J = 8.4$ Hz, 1H), 7.06 (dd, $J = 2.5$, 1.3 Hz, 1H), 6.91 (dd, $J = 3.7$, 1.3 Hz, 1H), 6.32 (dd, $J = 3.7$, 2.6 Hz, 1H), 5.97 (s, 1H). ^{13}C NMR (126 MHz, $CDCl_3$) δ 183.0, 181.7, 153.5, 149.4, 145.7, 133.9, 129.9, 126.6, 122.7, 122.3, 110.8, 110.3, 102.5. HRMS (TOF MS ES+) for $C_{13}H_{10}N_3O_2^+$ (MH+) calc. 240.0773, found 240.0779.

References

(1)   Balitz, D. M.; Bush, J. A.; Bradner, W. T.; Doyle, T. W.; O'Herron, F. A.; Nettleton, D. E.

        Isolation of Lavendamycin, a New Antibiotic from Streptomyces Lavendulae. *J. Antibiot.*

        (Tokyo) **1982**, *35* (3), 259–265.

(2)   Doyle, T. W.; Balitz, D. M.; Grulich, R. E.; Nettleton, D. E.; Gould, S. J.; Tann, C.;

Moews, A. E. Structure Determination of Lavendamycin- a New Antitumor Antibiotic from

Streptomyces Lavendulae. *Tetrahedron Lett.* **1981**, *22* (46), 4595–4598.

(3)   Rao, K. V.; Cullen, W. P. Streptonigrin, an Antitumor Substance. I. Isolation and

Characterization. *Antibiot. Annu.* **1959**, *7*, 950–953.

(4)   Rao, K. V.; Biemann, K.; Woodward, R. B. The Structure of Streptonigrin. *J. Am. Chem.*

Soc. **1963**, *85* (16), 2532–2533.

(5)   Podeszwa, B.; Niedbala, H.; Polanski, J.; Musiol, R.; Tabak, D.; Finster, J.; Serafin, K.;

Milczarek, M.; Wietrzyk, J.; Boryczka, S.; Mol, W.; Jampilek, J.; Dohnal, J.; Kalinowski, D. S.;

Richardson, D. R. Investigating the Antiproliferative Activity of Quinoline-5,8-Diones and

Styrylquinolinecarboxylic Acids on Tumor Cell Lines. *Bioorg. Med. Chem. Lett.* **2007**, *17* (22),

6138–6141.

(6)   Hassani, M.; Cai, W.; Holley, D. C.; Lineswala, J. P.; Maharjan, B. R.; Ebrahimian, G.

R.; Seradj, H.; Stocksdale, M. G.; Mohammadi, F.; Marvin, C. C.; Gerdes, J. M.; Beall, H. D.;

Behforouz, M. Novel Lavendamycin Analogues as Antitumor Agents: Synthesis, in Vitro

Cytotoxicity, Structure−Metabolism, and Computational Molecular Modeling Studies with

NAD(P)H:Quinone Oxidoreductase 1. *J. Med. Chem.* **2005**, *48* (24), 7733–7749.

(7)   Fryatt, T.; Pettersson, H. I.; Gardipee, W. T.; Bray, K. C.; Green, S. J.; Slawin, A. M. Z.;

Beall, H. D.; Moody, C. J. Novel Quinolinequinone Antitumor Agents: Structure-Metabolism

Studies with NAD(P)H:quinone Oxidoreductase (NQO1). *Bioorg. Med. Chem.* **2004**, *12* (7), 1667–1687.

(8)   Beall, H. D.; Winski, S.; Swann, E.; Hudnott, A. R.; Cotterill, A. S.; O'Sullivan, N.; Green, S. J.; Bien, R.; Siegel, D.; Ross, D.; Moody, C. J. Indolequinone Antitumor Agents: Correlation between Quinone Structure, Rate of Metabolism by Recombinant Human NAD(P)H:Quinone Oxidoreductase, and in Vitro Cytotoxicity. *J. Med. Chem.* **1998**, *41* (24), 4755–4766.

(9)   Swann, E.; Barraja, P.; Oberlander, A. M.; Gardipee, W. T.; Hudnott, A. R.; Beall, H. D.; Moody, C. J. Indolequinone Antitumor Agents: Correlation between Quinone Structure and Rate of Metabolism by Recombinant Human NAD(P)H:Quinone Oxidoreductase. Part 21. *J. Med. Chem.* **2001**, *44* (20), 3311–3319.

(10)   Hassani, M.; Cai, W.; Koelsch, K. H.; Holley, D. C.; Rose, A. S.; Olang, F.; Lineswala, J. P.; Holloway, W. G.; Gerdes, J. M.; Behforouz, M.; Beall, H. D. Lavendamycin Antitumor Agents: Structure-Based Design, Synthesis, and NAD(P)H:Quinone Oxidoreductase 1 (NQO1) Model Validation with Molecular Docking and Biological Studies. *J. Med. Chem.* **2008**, *51* (11), 3104–3115.

(11)   Cai, W.; Hassani, M.; Karki, R.; Walter, E. D.; Koelsch, K. H.; Seradj, H.; Lineswala, J. P.; Mirzaei, H.; York, J. S.; Olang, F.; Sedighi, M.; Lucas, J. S.; Eads, T. J.; Rose, A. S.; Charkhzarrin, S.; Hermann, N. G.; Beall, H. D.; Behforouz, M. Synthesis, Metabolism and in Vitro Cytotoxicity Studies on Novel Lavendamycin Antitumor Agents. *Bioorg. Med. Chem.* **2010**, *18* (5), 1899–1909.

(12)   Colucci, M. A.; Moody, C. J.; Couch, G. D. Natural and Synthetic Quinones and Their Reduction by the Quinone Reductase Enzyme NQO1: From Synthetic Organic Chemistry to Compounds with Anticancer Potential. *Org. Biomol. Chem.* **2008**, *6* (4), 637–656.

(13)   Behforouz, M.; Haddad, J.; Cai, W.; Arnold, M. B.; Mohammadi, F.; Sousa, A. C.; Horn, M. A. Highly Efficient and Practical Syntheses of Lavendamycin Methyl Ester and Related Novel Quinolindiones. *J. Org. Chem.* **1996**, *61* (19), 6552–6555.

(14)   Prieto, M.; Zurita, E.; Rosa, E.; Muñoz, L.; Lloyd-Williams, P.; Giralt, E. Arylboronic Acids and Arylpinacolboronate Esters in Suzuki Coupling Reactions Involving Indoles. Partner Role Swapping and Heterocycle Protection. *J. Org. Chem.* **2004**, *69* (20), 6812–6820.

(15)   Collot, V.; Dallemagne, P.; Bovy, P. R.; Rault, S. Suzuki-Type Cross-Coupling Reaction of 3-Iodoindazoles with Aryl Boronic Acids: A General and Flexible Route to 3-Arylindazoles. *Tetrahedron* **1999**, *55* (22), 6917–6922.

(16)   Musser, J. H.; Jones, H.; Sciortino, S.; Bailey, K.; Coutts, S. M.; Khandwala, A.; Sonnino-Goldman, P.; Leibowitz, M.; Wolf, P.; Neiss, E. S. Synthesis and Antiallergic Activities of 1,3-oxazolo[4,5-H]quinolines. *J. Med. Chem.* **1985**, *28* (9), 1255–1259.

(17)   Tang, Q.; Zhang, C.; Luo, M. A New Method for N−N Bond Cleavage of N,N-Disubstituted Hydrazines to Secondary Amines and Direct Ortho Amination of Naphthol and Its Analogues. *J. Am. Chem. Soc.* **2008**, *130* (18), 5840–5841.

(18)   Campeau, L.-C.; Stuart, D. R.; Leclerc, J.-P.; Bertrand-Laperle, M.; Villemure, E.; Sun, H.-Y.; Lasserre, S.; Guimond, N.; Lecavallier, M.; Fagnou, K. Palladium-Catalyzed Direct Arylation of Azine and Azole N-Oxides: Reaction Development, Scope and Applications in Synthesis. *J. Am. Chem. Soc.* **2009**, *131* (9), 3291–3306.

(19)   LaMontagne, M. P.; Blumbergs, P.; Smith, D. C. Antimalarials. 16. Synthesis of 2-Substituted Analogs of 8-[(4-Amino-1-Methylbutyl)amino]-6-Methoxy-4-Methyl-5-[3-(trifluoromethyl)phenoxy]quinoline as Candidate Antimalarials. *J. Med. Chem.* **1989**, *32* (8), 1728–1732.

(20)   Rodríguez, J. G.; de los Rios, C.; Lafuente, A. Synthesis of N-Chloroquinolines and N-Ethynylquinolines (n=2, 4, 8): Homo and Heterocoupling Reactions. *Tetrahedron* **2005**, *61* (38), 9042–9051.

(21)   Miyaura, N.; Suzuki, A. Palladium-Catalyzed Cross-Coupling Reactions of Organoboron Compounds. *Chem. Rev.* **1995**, *95* (7), 2457–2483.

(22)   Boger, D. L.; Duff, S. R.; Panek, J. S.; Yasuda, M. Inverse Electron Demand Diels-Alder Reactions of Heterocyclic Azadienes. Studies on the Total Synthesis of Lavendamycin: Investigative Studies on the Preparation of the CDE .beta.-Carboline Ring System and AB Quinoline-5,8-Quinone Ring System. *J. Org. Chem.* **1985**, *50* (26), 5782–5789.

(23)   Buffinton, G. D.; Ollinger, K.; Brunmark, A.; Cadenas, E. DT-Diaphorase-Catalysed Reduction of 1,4-Naphthoquinone Derivatives and Glutathionyl-Quinone Conjugates. Effect of Substituents on Autoxidation Rates. *Biochem. J.* **1989**, *257* (2), 561–571.

(24)   Gibson, N. W.; Hartley, J. A.; Butler, J.; Siegel, D.; Ross, D. Relationship between DT-Diaphorase-Mediated Metabolism of a Series of Aziridinylbenzoquinones and DNA Damage and Cytotoxicity. *Mol. Pharmacol.* **1992**, *42* (3), 531–536.

(25)   Long, G. V.; Harding, M. M. A Proton Nuclear Magnetic Resonance Study of the Interaction of zinc(II) with the Antitumour Drug Streptonigrin. *J. Chem. Soc. Dalton Trans.* **1996**, No. 4, 549–552.

(26)   Wei, X.; Ming, L.-J. Comprehensive 2D 1H NMR Studies of Paramagnetic Lanthanide(III) Complexes of Anthracycline Antitumor Antibiotics. *Inorg. Chem.* **1998**, *37* (9), 2255–2262.

(27)   Ross, D.; Kepa, J. K.; Winski, S. L.; Beall, H. D.; Anwar, A.; Siegel, D. NAD(P)H:quinone Oxidoreductase 1 (NQO1): Chemoprotection, Bioactivation, Gene Regulation and Genetic Polymorphisms. *Chem. Biol. Interact.* **2000**, *129* (1–2), 77–97.

(28)   Margaret Harding; Georgina Long. Interaction of the Antitumor Antibiotic Streptonigrin with Metal Ions and DNA. *Curr. Med. Chem.* **1997**, *4*, 405–420.

(29)   Budimir, A. Metal Ions, Alzheimer's Disease and Chelation Therapy. *Acta Pharm. Zagreb Croat.* **2011**, *61* (1), 1–14.

(30)   Kraus, J.-L.; Conti, F.; Madonna, S.; Tchoghandjian, A.; Beclin, C. Alternative Responses of Primary Tumor Cells and Glioblastoma Cell Lines to N,N-Bis-(8-Hydroxyquinoline-5-Yl Methyl)-Benzyl Substituted Amines: Cell Death versus P53-Independent Senescence. *Int. J. Oncol.* **2010**, *37* (6), 1463–1470.

(31)   King, O. N. F.; Li, X. S.; Sakurai, M.; Kawamura, A.; Rose, N. R.; Ng, S. S.; Quinn, A. M.; Rai, G.; Mott, B. T.; Beswick, P.; Klose, R. J.; Oppermann, U.; Jadhav, A.; Heightman, T. D.; Maloney, D. J.; Schofield, C. J.; Simeonov, A. Quantitative High-Throughput Screening Identifies 8-Hydroxyquinolines as Cell-Active Histone Demethylase Inhibitors. *PLoS ONE* **2010**, *5* (11), e15535.

(32)   Yan, C.; Kepa, J. K.; Siegel, D.; Stratford, I. J.; Ross, D. Dissecting the Role of Multiple Reductases in Bioactivation and Cytotoxicity of the Antitumor Agent RH1. *Mol. Pharmacol.* **2008**, *74* (6), 1657–1665.

(33)   Faig, M.; Bianchet, M. A.; Winski, S.; Hargreaves, R.; Moody, C. J.; Hudnott, A. R.;

Ross, D.; Amzel, L. M. Structure-Based Development of Anticancer Drugs: Complexes of

NAD(P)H:Quinone Oxidoreductase 1 with Chemotherapeutic Quinones. *Structure* **2001**, *9*

(8), 659–667.

(34)   Verdonk, M. L.; Giangreco, I.; Hall, R. J.; Korb, O.; Mortenson, P. N.; Murray, C. W.

Docking Performance of Fragments and Druglike Compounds. *J. Med. Chem.* **2011**, *54* (15),

5422–5431.

(35)   Verdonk, M. L.; Cole, J. C.; Hartshorn, M. J.; Murray, C. W.; Taylor, R. D. Improved

Protein-Ligand Docking Using GOLD. *Proteins* **2003**, *52* (4), 609–623.

Chapter 3

Improved design and biological activity of 10-alkoxy-anthracenyl-isoxazole

derivatives for G-quadruplex antitumor agents

3.1 Introduction

G-quadruplex DNA (Figure 3-1) structures have been of serious interest as targets for cancer

chemotherapeutics due to their novel structures, when compared to genomic DNA, and their
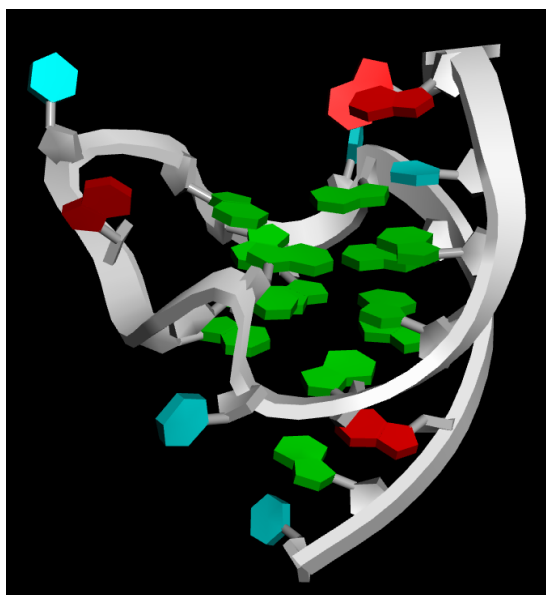
Figure 3-1. c-MYC G-quadruplex Pu22 sequence (PDB: 2L7V)

isolated locations in human genes.[1–3] Additionally, inhibition of the c-MYC proto-oncogene,

which is over expressed in up to 80% of tumor cells,[1] has been correlated to quadruplex

stabilization in the promoter region where these structures form.[4,5] Molecules that stabilize these

quadruplexes of DNA (G4-DNA) are typically medium sized planar aromatics often showing

selectivity for G4-DNA over B-DNA.[6–8]

Given the conserved elements of the various G4-DNA[1] structures as they occur *in vitro*

and *in vivo* we designed a novel class of combilexin molecules based on two moieties known to

interact with genomic DNA, an intercalator and minor-groove binder; yet pre-organized such

that intercalation and/or minor-groove binding with B-DNA would be highly disfavored. Though, ideally suited for π-stacking and hydrogen bond donor-acceptor interactions with G4-DNA.

3.2 Structural Features of a Q-quadruplex binder

G4-DNA binding molecules have been the subject of much study in the past decade with many examples showing a high degree of selectivity and binding stability.[1,9–13] Parkinson has demonstrated that a competition dialysis study of many known DNA binding compounds reveals some striking and significant G4-DNA interactions.[13] Most importantly, the Parkinson dialysis
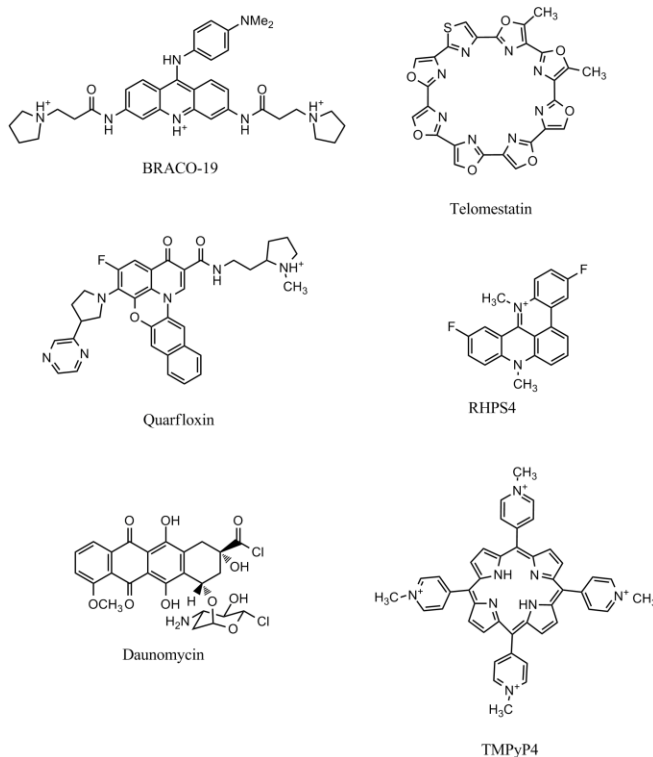
Figure 3-2. Quadruplex-DNA binding molecules

study shows a very distinct structure to activity relationship where the molecules with the highest affinity for G4-DNA share similar properties. These compounds all contain a large planar moiety

that is responsible for pi stacking interactions and side groups consisting of hydrogen bond donors and/or acceptors (Figure 3-2).

The anthracene isoxazole ester system (AIM) (Figure 3-3) was designed to stabilize g-quadruplex DNA because of the orthogonal properties between the isoxazole and anthracene moieties to enhance π-π stacking, and possible intercalation, with G-DNA structures. Hurley had previously shown that there were several possible binding modes for quindoline derivatives to
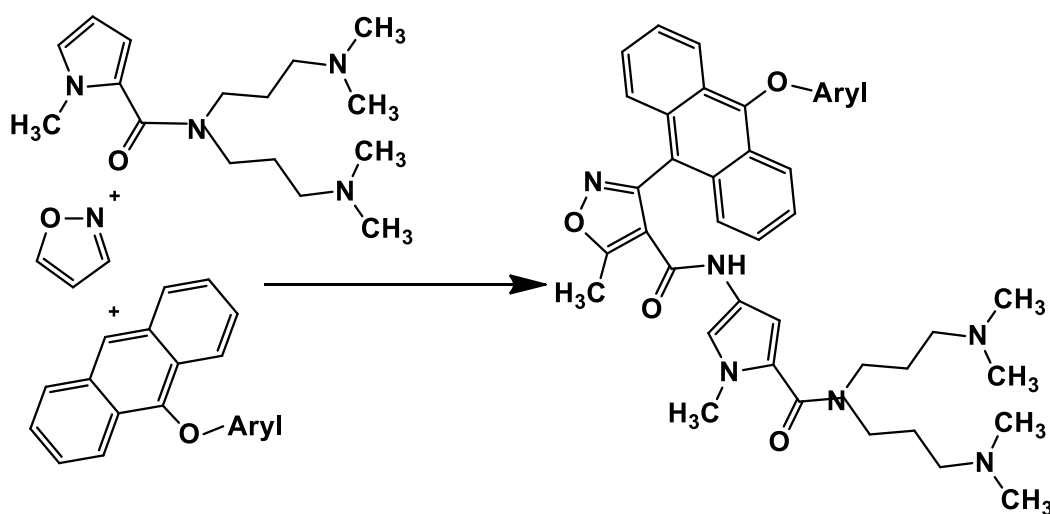
Figure 3-3. Combining functionalities to form a selective G4-DNA ligand

quadruplex DNA based on substitution patterns using molecular modeling,[14] H NMR and X-ray crystalography.[12] Hurley showed that the porphyrns 5,10,15,20-tetra-(N-methyl-2-pyridyl)pophine (TMPyP2) and 5,10,15,20-tetra-(N-methyl-2-pyridyl)pophine (TMPyP4), bind G-quadruplex structures externally atop the G-tetrad.[15] Given these findings we felt the next step was to use computer based molecular modeling to determine which mode of binding best suited the AIM-2 system.

It is proposed that designing the optimal G4-DNA binder must also contain some mimic of a bio-molecule (e.g. peptide bonds) so as to minimize recognition as an antigen, quick metabolism (See Chapter 5), and excretion from the body before it can exert its function.

Because of the compact nature of duplex DNA a G4-DNA binding ligand would need to be pre-organized so that unfavorable steric interactions would keep the required large planar group from intercalating between the base pairs. Figure 3-3 shows how an isoxazole system, containing an anthracene and peptide linked hydrogen bond acceptor, methyl pyrrole, could serve the purpose addressing all of the important factors (i.e. preorganization, hydrogen bond acceptor/donor, and small size). Variation of the peptide length and number of methyl pyrrole (0-2) units served to define a simple SAR as it relates to tumor growth inhibition[16]. Full description of the synthesis of G4-DNA binding isoxazoles is detailed below in this chapter.

3.3 Molecular Modeling of alkoxy series with Quadruplex DNA

A training set of AIMs was constructed and prepared using Accelrys Discovery Studio 4.0. The minimization during ligand preparation took into account both amide and imidate tautomers at the C-4 amide of the isoxazole. The coordinates for the Pu22 sequence of the human c-myc oncogene used were the NMR structure reported by Hurley and Yang, pdb accession number 2L7V. The ligand docking was conducted using the CHARMm forcefield, at physiological pH, and docking at both binding sites, the top15 poses were obtained for each tautomer of the training set. Consensus scoring was evaluated using CDocker Interaction energy, comparing versions of the PLP, Jain, PMF and Ludi scoring protocols (10 total scoring functions), and compared to the Hurley and Wang quindoline as control. The best pose for the most active compound **8c** in the present study is shown above (Figure 3.4), allowing the ligand to minimize within a 14Å binding sphere. The larger binding sphere enabled the AIM to tumble during the minimization process, to achieve substantially higher binding energies for the final poses.

In the best binding pose each functional group of the AIM interacts with the G-4, the dimethyl amino double tail lies along the sugar-phosphate backbone, the 10-biphenyl moiety
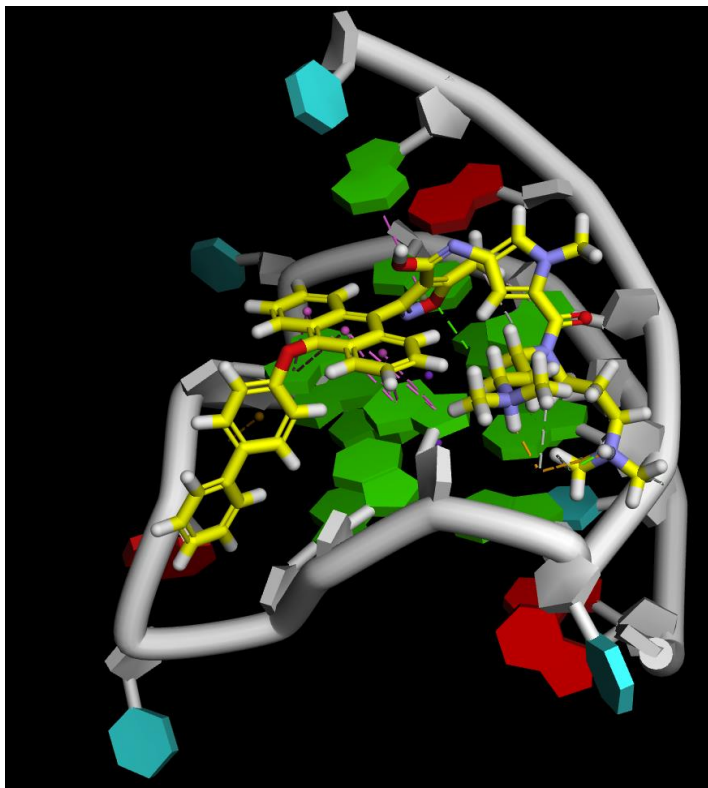
Figure 3-4. Discovery Studio 4.0 best energy pose for **8c**, docked at site 1 of the human Pu22 sequence of the c-myc oncogene.

occupies the groove. The CDocker Interaction Energy prediction of 80.5 kcal/mol was substantially higher than that calculated for the literature quindoline (range of 46-49 kcal/mol at sites 1 and 2), and also provides interactions which bridge between the G tetrad and adjacent functional groups, and therefore could potentially provide enhanced sequence selectivity. The best site 2 pose was within an approximate strong hydrogen bond energy of site 1 (ca. 5 kcal/mol).

3.4 Synthesis to alkoxy anthracene pyrrole doubletails

3.4.1 Preparation of Anthryl-10-oxy-isoxazole-DTs (AAIMs)

The anthracenyl isoxazole DTs can be made by starting with commercially available 9-anthraldehyde using bromine in dichloromethane achieved the 10-bromo substituted anthraldehyde $\mathbf{1}$[17] in 80% yield (Scheme 3-1). Using a modified S_NAr (addition-elimination mechanism) procedure from Bair[18], the nucleophilic aromatic substitution reaction using
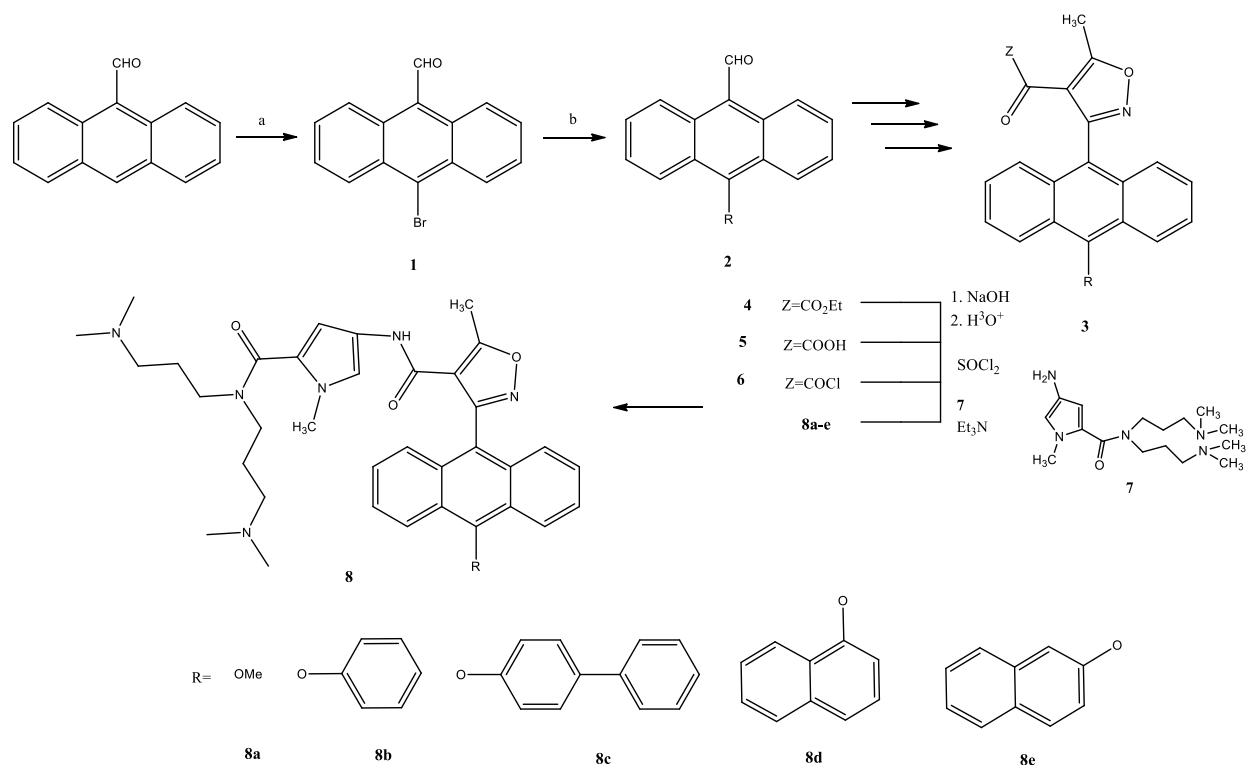
Scheme 3-1. Synthesis of anthryl-oxy-DT conjugate **8a-e**.

alkoxides as the nucleophile gave us **2** with yields greater than 90%. Oxime formation of 10-oxy substituted aldehyde was achieved using hydroxylamine HCl. The oxime then reacted with N-chlorosuccinimide (NCS) to give the oximinoyl chloride. The formation of the isoxazole was accomplished via a 1,3-dipolar cycloaddition to give the anthracene isoxazole ester $\mathbf{3}$[19]. The double tail moiety was achieved through the acetylation of N-methyl pyrrole using trichloroacetyl chloride previously described[16]. Subsequent nitration gave product in 75% yield

when performed on a molar scale. Next, the nitro pyrrole could be coupled with 3-dimethylaminopropylamine and hydrogenated. Once the ester was characterized, it was hydrolyzed to the carboxylic acid **5**. Then using thionyl chloride gave acid chloride **6** which were then reacted with the amine-pyrrole double tail **7** using a modified Schotten-Baumann reaction to give the final product **8a-e**.

3.4.2 Crystal Structure of 8a

Our previous report of CD melting point increase and selective NMR anisotropy indicates that certain structural features of the AIMs correspond to increased anti-tumor activity[20], namely, a dihedral angle between the mean plane of the isoxazole (all atoms) and the mean plane of the anthracene (all atoms) shown to be 70.47°, while the ester carbonyl and ether atom is virtually co-planar with the isoxazole mean plane having a dihedral angle of 4.51°. The anthracene ring is virtually planar as evident by the sum of the eighteen intra-ring torsion angle of 5.40°. These values are similar to other sc-xrd of isoxazole-3-anthracenes[21–26] and isoxazole-3-anthroquinones[27]. Furthermore, pairs of weak C—H---O hydrogen bonds link the molecules into dimers, and weak C—H---π interactions further link these molecules. Full sc-xrd data and parameters are given in the Supplementary Data.
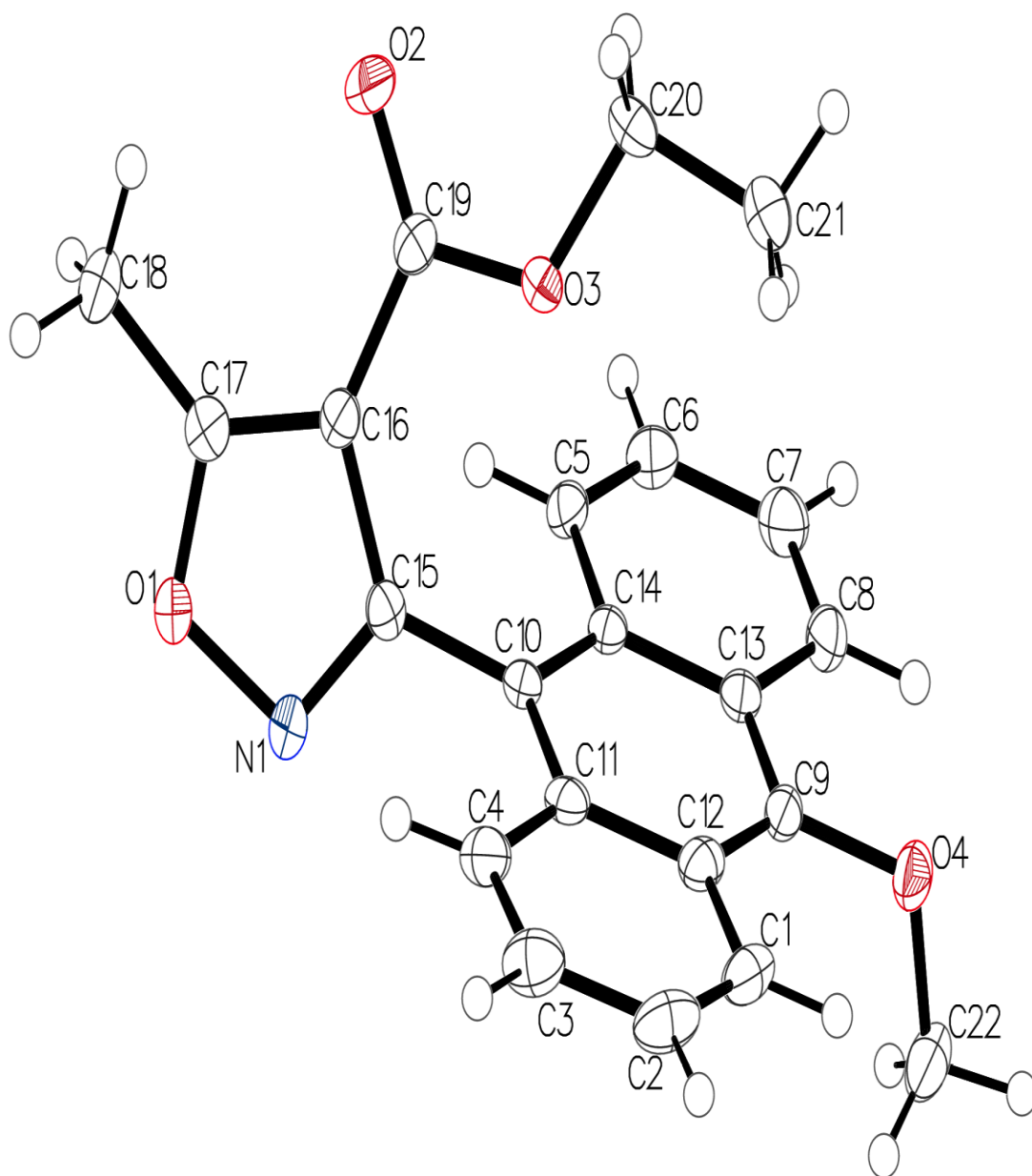
Figure 3-5. Single crystal x-ray diffractometry of **4a**.

3.5 MTT Cell Viability Assay

Growth inhibition was determined by the MTT colorimetric assay. Cells were plated in 96-well plates at a density of 10,000 cells/mL and allowed to attach overnight (16-18h). AAIM solutions were applied in medium for 24 h, removed, and replaced with fresh medium, and the plates were incubated at 37 °C under a humidified atmosphere containing 5% CO_2 for 3−5 days.
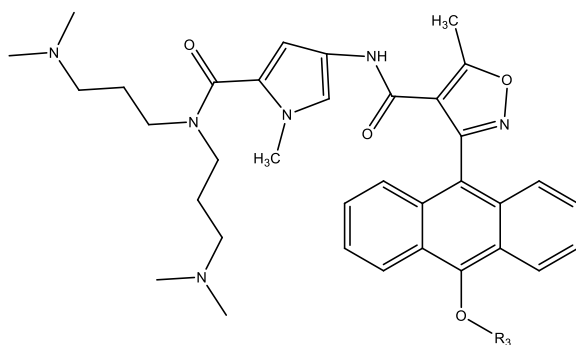
	IC$_{50}$	R$_3$
8a	7.77 μM ± 1.11	—CH$_3$
8b	1.03 μM ± 0.07	
8c	0.58 μM ± 0.03	
8d	1.07 μM ± 0.03	
8e	3.10 μM ± 0.11	

Table 3-1. Cytotoxicity activity of **8a-e** against human glioma SNB-19 cells

MTT (50 μg) was added and the cells were incubated for another 4 h. Medium/MTT solutions were removed carefully by aspiration, the MTT formazan crystals were dissolved in 100 μL of DMSO, and absorbance was determined on a plate reader at 560 nm. IC$_{50}$ values (concentration

at which cell survival equals 50% of control) were determined from semilog plots of percent of control versus concentration. The results are shown in Table 3-1.

Compounds shown in Table 3-1 have low micromolar binding affinities, which some are much better than the previously reported analogues.[20] The phosphate backbone chain in the NMR structure is solvent exposed (Figure 3-1) and can be accessed with lipophilic groups to increase binding affinity. For example, Compound **8a** lacking any corresponding ring system in the 10-position greatly decrease the cytotoxicity of the group, reinforcing the importance of the π - π stacking and π -face interactions between the phenyl group and the phosphate backbone. Substitution of this phenoxy by a naphthyl (compound **8d** and **8e**), phenyl (compound **8b**) or biphenyl (compound **8c**) was well tolerated and in general decreased the IC50 values with the addition on each phenyl ring. These alkoxy derivatives are all good hydrogen bond acceptors and gave increasing potencies.

Summary: Anthryl-10-alkoxy-isoxazole-pyrrole-doubletails can be readily made and easily substituted to enlarge the oxy-ether library series. Current studies are focused on whether the AAIMs may represent useful tools for the study of quadruplex DNA, and ultimately lead to clinically useful inhibitors.

REFERENCES

(1)   Balasubramanian, S.; Hurley, L. H.; Neidle, S. Targeting G-Quadruplexes in Gene Promoters: A Novel Anticancer Strategy? *Nat. Rev. Drug Discov.* **2011**, *10* (4), 261–275.

(2)   Ohnmacht, S. A.; Neidle, S. Small-Molecule Quadruplex-Targeted Drug Discovery. *Bioorg. Med. Chem. Lett.* **2014**, *24* (12), 2602–2612.

(3)   Siddiqui-Jain, A.; Hurley, L. H. DNA Structure: Visualizing the Quadruplex. *Nat. Chem.* **2013**, *5* (3), 153–155.

(4)   Siddiqui-Jain, A.; Grand, C. L.; Bearss, D. J.; Hurley, L. H. Direct Evidence for a G-Quadruplex in a Promoter Region and Its Targeting with a Small Molecule to Repress c-MYC Transcription. *Proc. Natl. Acad. Sci.* **2002**, *99* (18), 11593–11598.

(5)   Brooks, T. A.; Hurley, L. H. Targeting MYC Expression through G-Quadruplexes. *Genes Cancer* **2010**, *1* (6), 641–649.

(6)   Vy Thi Le, T.; Han, S.; Chae, J.; Park, H.-J. G-Quadruplex Binding Ligands: From Naturally Occurring to Rationally Designed Molecules. *Curr. Pharm. Des.* **2012**, *18* (14), 1948–1972.

(7)   Ren, J.; Chaires, J. B. Sequence and Structural Selectivity of Nucleic Acid Binding Ligands. *Biochemistry (Mosc.)* **1999**, *38* (49), 16067–16075.

(8)   Yang, D.; Okamoto, K. Structural Insights into G-Quadruplexes: Towards New Anticancer Drugs. *Future Med. Chem.* **2010**, *2* (4), 619–646.

(9)   Monchaud, D.; Teulade-Fichou, M.-P. A Hitchhiker's Guide to G-Quadruplex Ligands. *Org. Biomol. Chem.* **2008**, *6* (4), 627–636.

(10)   Bidzinska, J.; Cimino-Reale, G.; Zaffaroni, N.; Folini, M. G-Quadruplex Structures in the Human Genome as Novel Therapeutic Targets. *Molecules* **2013**, *18* (10), 12368–12395.

(11)   Collie, G. W.; Sparapani, S.; Parkinson, G. N.; Neidle, S. Structural Basis of Telomeric RNA Quadruplex−Acridine Ligand Recognition. *J. Am. Chem. Soc.* **2011**, *133* (8), 2721–2728.

(12)   Dai, J.; Carver, M.; Hurley, L. H.; Yang, D. Solution Structure of a 2:1 Quindoline–c-MYC G-Quadruplex: Insights into G-Quadruplex-Interactive Small Molecule Drug Design. *J. Am. Chem. Soc.* **2011**, *133* (44), 17673–17680.

(13)   Haider, S. M.; Neidle, S.; Parkinson, G. N. A Structural Analysis of G-Quadruplex/ligand Interactions. *Biochimie* **2011**, *93* (8), 1239–1251.

(14)   Ou, T.-M.; Lu, Y.-J.; Zhang, C.; Huang, Z.-S.; Wang, X.-D.; Tan, J.-H.; Chen, Y.; Ma, D.-L.; Wong, K.-Y.; Tang, J. C.-O.; Chan, A. S.-C.; Gu, L.-Q. Stabilization of G-Quadruplex DNA and Down-Regulation of Oncogene c-Myc by Quindoline Derivatives. *J. Med. Chem.* **2007**, *50* (7), 1465–1474.

(15)   Han, F. X.; Wheelhouse, R. T.; Hurley, L. H. Interactions of TMPyP4 and TMPyP2 with Quadruplex DNA. Structural Basis for the Differential Effects on Telomerase Inhibition. *J. Am. Chem. Soc.* **1999**, *121* (15), 3561–3570.

(16)   Han, X.; Li, C.; Mosher, M. D.; Rider, K. C.; Zhou, P.; Crawford, R. L.; Fusco, W.; Paszczynski, A.; Natale, N. R. Design, Synthesis and Biological Evaluation of a Novel Class of Anticancer Agents: Anthracenylisoxazole Lexitropsin Conjugates. *Bioorg. Med. Chem.* **2009**, *17* (4), 1671–1680.

(17)   Cakmak, O.; Aydogan, L.; Berkil, K.; Gulcin, I.; Buyukgungor, O. Highly Brominated Anthracenes as Precursors for the Convenient Synthesis of 2,9,10-Trisubstituted Anthracene Derivatives. *Beilstein J. Org. Chem.* **2008**, *4*, 50.

(18)   Bair, K. W. Anthracene Derivatives. US4719049 A, January 12, 1988.

(19)   Mirzaei, Y. R.; Weaver, M. J.; Steiger, S. A.; Kearns, A. K.; Gajewski, M. P.; Rider, K. C.; Beall, H. D.; Natale, N. R. Improved Synthesis of 3-Aryl Isoxazoles Containing Fused Aromatic Rings. *Tetrahedron* **2012**, *68* (50), 10360–10364.

(20)   Weaver, M. J.; Kearns, A. K.; Stump, S.; Li, C.; Gajewski, M. P.; Rider, K. C.; Backos, D. S.; Reigan, P. R.; Beall, H. D.; Natale, N. R. AIMing towards Improved Antitumor Efficacy. *Bioorg. Med. Chem. Lett.*

(21)   Mosher, M. D.; Natale, N. R.; Vij, A. An Intercalating Isoxazole. *Acta Crystallogr. C* **1996**, *52* (10), 2513–2515.

(22)   Li, C.; Campbell, M. J.; Weaver, M. J.; Duncan, N. S.; Hunting, J. L.; Natale, N. R. Ethyl 3-(10-Bromoanthracen-9-Yl)-5-Methyl-1,2-Oxazole-4-Carboxylate. *Acta Crystallogr. Sect. E Struct. Rep. Online* **2013**, *69* (12), o1804–o1805.

(23)   Li, C.; Twamley, B.; Natale, N. R. Ethyl 3-(10-Chloroanthracenyl)-5-(1-Phenyl-2-Hydroxyethenyl)isoxazole-4-Carboxylate: An Enol Produced by Dess–Martin Oxidation. *Acta Crystallogr. Sect. E Struct. Rep. Online* **2006**, *62* (2), o854–o856.

(24)   Li, C.; Twamley, B.; Natale, N. R. Preparation and Crystal Structures of Two 3-Anthracenyl Isoxazolyl Sulfonamides. *J. Heterocycl. Chem.* **2008**, *45* (1), 259–264.

(25)   Han, X.; Twamley, B.; Natale, N. R. Preparation of 3-(10′-Halo-9′-Anthracenyl) Isoxazolecarboxylic Esters. *J. Heterocycl. Chem.* **2003**, *40* (3), 539–545.

(26)   Han, X.; Li, C.; Rider, K. C.; Blumenfeld, A.; Twamley, B.; Natale, N. R. The Isoxazole as a Linchpin for Molecules That Target Folded DNA Conformations: Selective Lateral Lithiation and Palladation. *Tetrahedron Lett.* **2002**, *43* (43), 7673–7677.

(27)   Duncan, N. S.; Beall, H. D.; Kearns, A. K.; Li, C.; Natale, N. R. Ethyl 3-(9-Chloro-10-Oxo-9,10-Dihydroanthracen-9-Yl)-5-Methylisoxazole-4-Carboxylate. *Acta Crystallogr. Sect. E Struct. Rep. Online* **2014**, *70* (3), o315–o316.

Supplementary Material

Experimental Section. *General.* All chemicals were purchased from commercial vendors and were used without any further purification unless otherwise indicated. Solvents were reagents grade and dried just prior to use by standard methods. All reactions were performed under inert atmosphere. Tetrahydrofuran (THF) was dried over sodium/benzophenone and distilled prior to use. Triethylamine (EtN$_3$) was dried with calcium hydride (CaH$_2$). Melting points were determined in open capillary tubes on a Melt-Temp apparatus and are uncorrected. High resolution mass spectra (HRMS) were obtained using a Micromass electrospray ionization (ES)/time-of-flight mass spectrometry (LCTOF). Mass spectrometer samples were introduced using a Waters model 2690 separations module HPLC fitted with a C-18 reversed phase column (2.1 mm i.d., 5 cm). Flash chromatography was performed using Sorbent Technologies standard silica gel (60 Å) with reagent grade solvents using in house compressed air.

Cell Viability Assay. Growth inhibition was determined by the MTT colorimetric assay. Cells were plated in 96-well plates at a density of 10 000 cells/mL and allowed to attach overnight (16 h). Anthryl-10-oxy-isoxazole-DT solutions were applied in medium for 2 h, removed, and replaced with fresh medium, and the plates were incubated at 37 °C under a humidified atmosphere containing 5% CO2 for 3−5 days. MTT (50 μg) was added and the cells were incubated for another 4 h. Medium/MTT solutions were removed carefully by aspiration, the MTT formazan crystals were dissolved in 100 μL of DMSO, and absorbance was determined on a plate reader at 560 nm. IC50 values (concentration at which cell survival equals 50% of control) were determined from semilog plots of percent of control versus concentration.

NMR. The 1H and 13C NMR high-resolution spectra were obtained with a Bruker AC200 (UltraShield™ 400MHz) using X-Win NMR (3.1) at ambient temperature in CDCl$_3$ unless otherwise specified. The signal assignments were performed on the basis of a series of 2D experiments with *z*-gradient selection: 1H-1H COSY (Correlation Spectroscopy), 1H-13C HMQC ((Heteronuclear Multiple Quantum Coherence) and 1H-13C HMBC (Heteronuclear Multiple Bond Correlation).
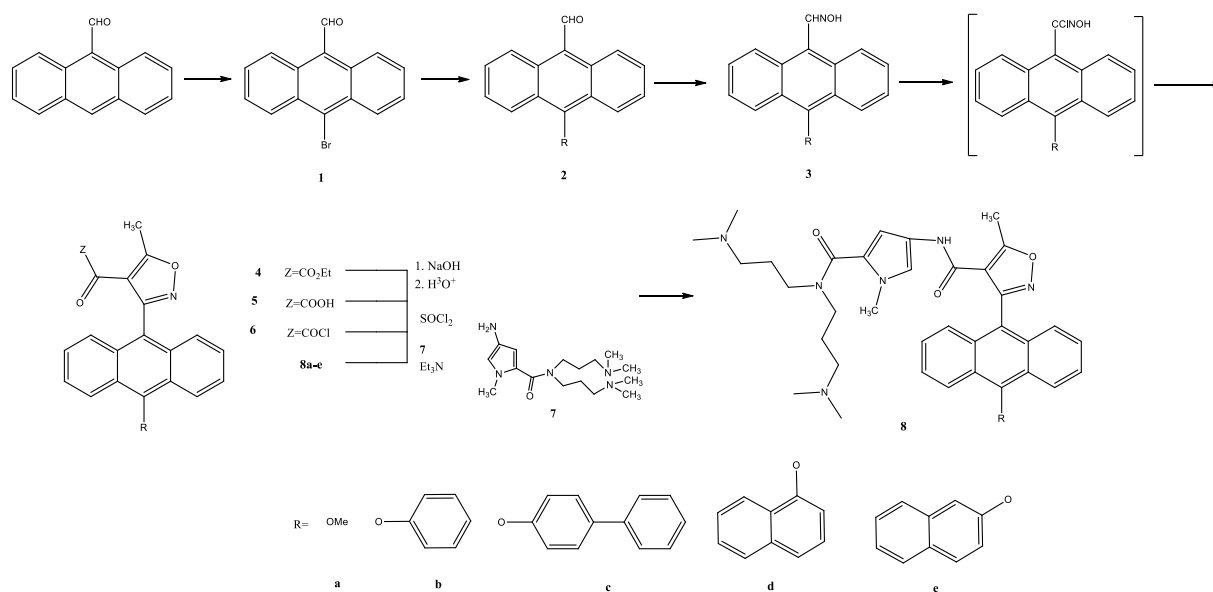
Scheme 3-1. Synthesis of anthryl-oxy-DT conjugate **8a-e**.

.

Method of 10-methoxy anthryl isoxazole ester formation

To a suspension of anthraldehyde (4.175g, 20.244mmol; Sigma-Aldrich, 97%) in methylene chloride (120mL) was added Br_2 (1.1 eq., 1.2mL, 23.428mmol) diluted in methylene chloride (5mL) drop wise over 5 minutes. The reaction was covered with septa and guard column (charged with $CaCl_2$ and NaOH(s)) and allowed to stir at 63°C until TLC showed no starting material remained (ca. 5 hours). Once the solution reached room temperature, 25g Na_2SO_3 in 200mL H_2O was added to neutralize excess Br_2. The solution was then transferred to a separatory funnel, washed with 50mL metheylene chloride and the organic layer extracted and dried with sodium sulfate and concentrated under reduced pressure to yield **1** (Rf=0.34, 10:1 Hex/EtOAc). Recrystallized from chloroform/hexanes.

10-Bromoanthracene-9-carbaldehyde (1). (83%) ^{1}H NMR ($CDCl_3$) δ 11.52 (s, 1H), 8.90-8.93 (m, 2H), 8.69-8.71 (m, 2H), 7.64-7.74 (m, 4H). ^{13}C NMR ($CDCl_3$) δ 193.28, 131.94, 131.82, 130.29, 129.02, 128.91, 128.29, 128.29, 127.47, 127.40, 125.70, 123.84. mp 205-208°C. Spectral data are in accord with those reported previously.[28,29]

General Procedure for 10-alkoxy aldehyde.

The bromo-aldehyde **1** (0.150g, 0.5261mmol) was taken up in 2mL of DMF (dried over sieves) under a nitrogen atmosphere. Freshly distilled methanol (1.2 eq., 0.03mL) was added via syringe. Sodium hydride (1.2 eq., 0.0253g) was added with a water condenser. The solution was allowed to stir at 60°C for 3.5 hours under an argon atmosphere. Once the solution cooled to room temperature, 50mL DI H_2O and 50mL diethyl ether was added and allowed to stir for 15 minutes. The solution was transferred to a separatory funnel and washed with 50mL diethyl ether. The combined organic layers were washed with 50mL Brine, dried over sodium sulfate

and concentrated under reduced pressure. The solid was taken up in minimal methylene chloride and ran on a prepared hexanes silica column in 12:1 (Hexanes:EtOAc) until all desired product **2** was collected.

10-Methoxyanthracene-9-carbaldehyde (2a). (85%) ^{1}H NMR (CDCl$_3$) δ 11.49 (s, 1H), 9.09 (d, J=9.03 Hz, 2H), 8.42 (d, J=8.66 Hz, 2H), 7.70-7.74 (m, 2H), 7.58-7.62 (m, 2H), 4.22 (s, 3H). ^{13}C NMR (CDCl$_3$) δ 191.93, 159.18, 134.12, 133.89, 129.34, 127.23, 125.60, 124.21, 123.96, 123.11, 121.17, 63.96. MS (ESI) *m/z* 236 (22.37, M+), 237(100, M+1), 238 (18.80, M+2). (Rf=0.46 4:1:1 Hex/EtOAc/DCM).

10-phenoxyanthracene-9-carbaldehyde (2b). In 250 mL round-bottom, add 50 mL dry Benzene, phenol (0.2748 g, 2.920 mmol) , sodium (0.048 g, 2.088 mmol), and 18-crown-6 (0.4632 g, 1.752 mmol) with 25 mL DMF. The reaction was heated to 150°C for 1 hr until all sodium as dissolved. Brominated (405.4 mg, 1.432 mmol) in 15 mL dry Benzene was added to the hot alkoxide solution and stirred under heat for 1.5 hours. Once cool, 50 mL EtOAc and 50 mL diH$_2$O was added to a sepratory funnel containing the reaction mixture. The contents were extracted with 3x40mL EtOAc, 2x15mL 10% NaOH and finally 3x100mL H$_2$O until a neutral pH. Dried over Na$_2$SO$_4$ and concentrated to obtain **2b** (0.4216 g, 98.7%) ^{1}H NMR (Acetone-d$_6$) δ 11.58 (s, 1H), 9.17 (d, J=9.16 Hz, 2H), 8.22 (d, J=8.66 Hz, 2H), 7.79 (t, J=7.65, 7.78, 15.43 Hz, 2H), 7.61 (t, J=8.28, 6.65, 14.93 Hz, 2H), 7.32 (m, 2H), 7.07 (t, J=7.28, 6.40, 13.68 Hz, 1H), 6.86 (d, J=7.78 Hz, 2H). ^{13}C NMR (Acetone-d$_6$) δ 193.37, 161.00, 152.38, 134.19, 131.04, 130.27, 127.37, 125.47, 125.11, 124.20, 123.92, 123.43, 116.20. MS (ESI) *m/z* 299.1162 (100, M+1), 300.1200(23.40, M+2). HRMS (ESI) accurate mass calcd. for C$_{21}$H$_{15}$O$_2$ (M+1) requires 299.1071, found 299.1072. (Rf=0.34 1:1 Hex/DCM).

10-([1,1'-biphenyl]-4-yloxy)anthracene-9-carbaldehyde (2c). By the same procedure as that described for **2b**, from 20 mL dry THF, [1,1'-biphenyl]-4-ol (2.6325 g, 15.16 mmol), sodium (0.3386 g, 14.73 mmol), 18-crown-6 (3.8928 g, 14.73 mmol) refluxed for 2.75 hour. Add bromo-aldehyde solid (3.3524 g, 11.757 mmol) to reaction round bottom, cool to room temperature and stir overnight (ca. 18.5 hours). 50 mL EtOAc and 50 mL diH$_2$O was added to a sepratory funnel containing the reaction mixture. The contents were extracted with 3x40mL DCM, 2x25mL 10% NaOH and finally 3x100mL H$_2$O until a neutral pH. Dried over Na$_2$SO$_4$ and concentrated to obtain **2c** (3.5861 g, 90.71%). (Rf=0.19 1:1 Hex/DCM). ^{1}H NMR (Acetone-d$_6$) δ 11.59 (s, 1H), 9.16 (d, J=9.03 Hz, 2H), 8.26 (d, J=8.66 Hz, 2H), 7.79 (m, 2H), 7.61 (m, 6H), 7.42 (t, J=7.40, 7.91, 15.31 Hz, 2H), 7.31 (t, J=7.40, 14.81 Hz, 1H), 6.95 (m, 2H). ^{13}C NMR (Acetone-d$_6$) δ 193.39, 160.61, 152.31, 141.09, 136.41, 135.27, 134.18, 130.30, 129.81, 129.52, 128.00, 127.80, 127.55, 127.47, 125.46, 125.13, 124.32, 123.91, 116.55. MS (ESI) *m/z* 379.1668 (100, M+1), 380.1725(38, M+2). HRMS (ESI) accurate mass calcd. for C$_{27}$H$_{19}$O$_2$ (M+1) requires 375.1385, found 375.1385.

10-(naphthalen-1-yloxy)anthracene-9-carbaldehyde (2d). By the same procedure as that described for **2b**, from 22 mL dry THF, naphthalen-1-ol (2.2085 g, 15.319 mmol), sodium (0.3784 g, 16.459 mmol), 18-crown-6 (4.6613 g, 17.635 mmol) refluxed for 4.5 hours. Add bromo-aldehyde (3.3524 g, 11.757 mmol) solid to reaction round bottom, cool to room temperature and stir overnight (ca. 17 hours). 50 mL EtOAc and 50 mL diH$_2$O was added to a sepratory funnel containing the reaction mixture. The contents were extracted with 3x50mL DCM, 2x25mL 10% NaOH and finally 3x100mL H$_2$O until a neutral pH. Dried over Na$_2$SO$_4$ and concentrated to obtain **2d** (3.3524 g, 81.84%). (Rf=0.54 1:1 Hex/DCM). ^{1}H NMR (CDCl$_3$) δ 11.58 (s, 1H), 9.10 (d, J=8.91 Hz, 2H), 8.84 (d, J=8.03 Hz, 1H), 8.21 (d, J=8.66 Hz, 2H), 7.97 (d,

J=7.91 Hz, 1H), 7.71 (m, 4H), 7.53 (d, J=8.03 Hz, 1H), 7.46 (m, 2H), 7.09 (t, J=7.78, 8.03, 15.81 Hz, 1H), 6.08 (d, J=7.65 Hz, 1H). ^{13}C NMR (CDCl$_3$) δ 192.18, 155.83, 152.47, 134.89, 133.53, 129.47, 127.89, 127.05, 126.30, 126.23, 125.72, 124.65, 124.54, 123.89, 123.29, 122.73, 122.07, 121.68. HRMS (ESI) accurate mass calcd. for C$_{25}$H$_{17}$O$_2$ (M+1) requires 349.1229, found 349.1232.

10-(naphthalen-2-yloxy)anthracene-9-carbaldehyde (2e). By the same procedure as that described for **2b**, from 20 mL dry THF, naphthalen-2-ol (2.2751 g), sodium (0.3386 g), 18-crown-6 (3.8928 g) refluxed for 4.5 hours. Add bromo-aldehyde (3.0089 g, 10.55 mmol) solid to reaction round bottom, cool to room temperature and stir overnight (ca. 15.5 hours). 50 mL EtOAc and 50 mL diH$_2$O was added to a sepratory funnel containing the reaction mixture. The contents were extracted with 3x50mL DCM, 2x25mL 10% NaOH and finally 3x100mL H$_2$O until a neutral pH. Dried over Na$_2$SO$_4$ and concentrated to obtain **2e** (2.2676 g, 62%). (Rf=0.90 DCM). ^{1}H NMR (400 MHz, CHLOROFORM-*d*) δ ppm 11.55 (s, 1 H), 9.09 (d, *J*=9.03 Hz, 2 H), 8.27 (d, *J*=8.78 Hz, 2 H), 7.88 (m, 1 H), 7.71 (m, 3 H), 7.48 (m, 4 H), 7.37 (m, 2 H), 6.78 (d, *J*=2.51 Hz, 1 H) ^{13}C NMR (101 MHz, CHLOROFORM-*d*) δ ppm 193.44, 193.45, 192.25, 157.85, 152.05, 134.20, 134.10, 133.56, 131.85, 131.72, 130.82, 130.29, 129.78, 129.59, 129.44, 129.10, 128.88, 127.73, 127.68, 127.22, 127.10, 126.95, 126.76, 126.71, 126.61, 126.47, 126.32, 126.19, 125.98, 125.85, 124.90, 124.49, 123.94, 123.86, 123.77, 123.53, 123.40, 122.73, 117.75, 117.35, 109.98, 109.44.

General Procedure of 10-alkoxy oxime

To a suspension of **2a** (0.6066g, 2.567mmol) in EtOH:THF:H$_2$O (50:25:25 mL) was dissolved hydroxylamine hydrochloride (0.4002g, 6.206mmol) and pyridine (1.11eq, 0.23mL) The reaction was covered with a septa under an argon atmosphere let stir at room temperature for

1 hour. The solution was first concentrated under reduced pressure then transferred to a separatory funnel and washed 1 x 10mL 1N HCl (cold) and the combined aqueous layers washed 2 x 50mL H_2O, 2 x 50mL Brine, 2 x 50mL CH_2Cl_2, dried over sodium sulfate, filtered, and the solvent removed under vacuum.

10-Methoxyanthracene-9-carbaldehyde oxime (3a): (92% yield). (Rf=0.35 4:1:1 Hex/EtOAc/DCM). ^{1}H NMR (CDCl$_3$) δ 9.20 (s, 1H), 8.45-8.46 (m, 2H), 8.36-8.38 (m, 2H), 7.53-7.60 (m, 4H), 4.17 (s, 3H). ^{13}C NMR (CDCl$_3$) δ 154.22, 148.95, 131.20, 126.90, 125.36, 125.29, 124.29, 122.72, 119.83, 63.45. MS (ESI) *m/z* 234 (100, M-H$_2$O), 235 (28.54, M-H$_2$O)[+], 252 (38.87, M+1). (Rf=0.34, 4:1:1 Hex/EtOAc/DCM).

10-phenoxyanthracene-9-carbaldehyde oxime (3b). By the same procedure as that described for **3a**, from aldehyde (0.4216g, 1.413mmol) in EtOH:THF:H$_2$O (40:12:12 mL) was dissolved hydroxylamine hydrochloride (0.5324g) and pyridine (3mL) The reaction was covered with a septa under an argon atmosphere and condenser and heated to 40°C for 8 hours, then stirred room temperature overnight. Washed 2 x 60mL 1N HCl (cold) and the combined aqueous layers washed 3 x 125mL H$_2$O, 3 x 125mL Brine, 3 x 40mL CH$_2$Cl$_2$. Obtained (0.4380 g, 98.92%). (Rf=0.62 4:1:1 Hex/EtOAc/DCM). ^{1}H NMR (Acetone-d$_6$) δ 10.91 (s, 1H), 9.25 (s, 1H), 8.60 (d, J=8.91 Hz, 2H), 8.12 (d, J=8.53 Hz, 2H), 7.63 (m, 2H), 7.54 (m, 2H), 7.30 (t, J=8.53, 7.53, 16.06 Hz, 1H), 7.03 (t, J=7.40, 14.81 Hz, 1H), 6.83 (d, J=7.91 Hz, 2H). ^{13}C NMR (Acetone-d$_6$) δ 161.09, 147.62, 147.55, 131.93, 130.91, 127.80, 127.06, 126.78, 125.54, 124.05, 123.41, 123.05, 116.08. MS (ESI) *m/z* 314 (100, M+1), 315 (25, M+2). HRMS (EI) accurate mass calcd. for C$_{21}$H$_{16}$N$_1$O$_1$ (M+1) requires 314.1181, found 314.1148.

10-([1,1'-biphenyl]-4-yloxy)anthracene-9-carbaldehyde oxime (3c).By the same procedure as that described for **3a**, from aldehyde (1.8039g, 4.814mmol) in EtOH:THF:H$_2$O (100:35:35 mL)

was dissolved hydroxylamine hydrochloride (1.8369g) and pyridine (10mL) The reaction was covered with a septa under an argon atmosphere and condenser and heated to 40°C for 6 hours, then stirred room temperature overnight. Washed 1 x 100mL 1N HCl (cold) and the combined aqueous layers washed 4 x 125mL H_2O, 2 x 100mL Brine, 2 x 25mL CH_2Cl_2. Obtained (1.6234 g, 86.59%). (Rf=0.36 4:1:1 Hex/EtOAc/Et_2O). ^{1}H NMR (Acetone-d_6) δ 10.90 (s, 1H), 9.26 (s, 1H), 8.60 (d, J=8.91 Hz, 2H), 8.17 (d, J=8.53 Hz, 2H), 7.63 (m, 10H), 7.41 (t, J=7.53, 7.91, 15.43 Hz, 2H), 7.30 (t, J=7.40, 7.28, 14.68 Hz, 1H), 6.92 (d, J=8.78 Hz, 2H). ^{13}C NMR (Acetone-d_6) δ 161.22, 148.13, 148.05, 141.47, 136.58, 135.78, 132.46, 130.28, 129.92, 128.41, 128.35, 128.02, 127.67, 127.33, 126.06, 124.70, 123.91, 117.05. MS (ESI) m/z 390 (100, M+1), 391 (23, M+2). HRMS (ESI) accurate mass calcd. for $C_{27}H_{20}N_1O_2$ (M+1) requires 390.1494, found 390.1446.

10-(naphthalen-1-yloxy)anthracene-9-carbaldehyde oxime (3d). By the same procedure as that described for **3a**, from aldehyde (0.2289g, 0.657mmol) in EtOH:THF:H_2O (20:20:15 mL) was dissolved hydroxylamine hydrochloride (1.0440g) and pyridine (8mL) The reaction was covered with a septa under an argon atmosphere and condenser and heated to 40°C for 1 hours, then stirred room temperature overnight. Washed 2 x 50mL 1N HCl (cold) and the combined aqueous layers washed 4 x 50mL H_2O, 3 x 50mL Brine, 2 x 20mL CH_2Cl_2. Obtained (0.2376 g, 99.5%). (Rf=0.46 4:1:1 Hex/EtOAc/Et_2O). ^{1}H NMR (CDCl$_3$) δ 9.27 (s, 1H), 8.87 (d, J=8.03 Hz, 1H), 8.50 (d, J=8.91 Hz, 2H), 8.14 (d, J=8.53 Hz, 2H), 7.95 (d, J=7.91 Hz, 1H), 7.70 (m, 2H), 7.57 (t, J=7.28, 7.91, 15.18 Hz, 2H), 7.51 (d, J=8.03 Hz, 1H), 7.41 (t, J=7.53, 15.06 Hz, 2H), 7.08 (t, J=7.78, 8.03, 15.81 Hz, 1H), 6.11 (d, J=7.65 Hz, 1H). ^{13}C NMR (CDCl$_3$) δ 155.80, 148.77, 147.80, 134.85, 131.12, 127.81, 127.13, 126.87, 126.81, 12606, 125.97, 125.80, 125.71,

125.29, 124.79, 124.60, 122.94, 122.87, 121.85, 121.64, 121.43. HRMS (ESI) accurate mass calcd. for $C_{25}H_{17}N_1O_2$ (M+1) requires 364.1338, found 364.1374.

10-(naphthalen-2-yloxy)anthracene-9-carbaldehyde oxime (3e). By the same procedure as that described for **3a**, from aldehyde (2.2676g, 6.509mmol) in EtOH:THF:H_2O (135:50:50 mL) was dissolved hydroxylamine hydrochloride (2.48370g) and pyridine (13.5mL) The reaction was covered with a septa under an argon atmosphere and stirred at room temperature overnight (19 hours). Concentrated, then washed 1 x 100mL 1N HCl (cold) and the combined aqueous layers washed 3 x 150mL H_2O, 1 x 150mL Brine, 2 x 25mL CH_2Cl_2. Obtained (2.3636 g, 99.93%). (Rf=0.33 4:1:1 Hex/EtOAc/Et_2O). MS (ESI) 364.1190 (100).

The starting oxime **3a** (0.6450g, 2.5669mmol) was taken up in 35mL of chloroform at room temperature, to which the solution was added 10mol% pyridine (0.490mL of 5M) and recrystallized NCS (1.2 eq, 0.3903g, 2.92mmol) over 5 minutes. The solution was allowed to stir at 40°C under argon for 3 hours. The organic layer was washed with 3 x 30mL DI H_2O, 4 x 25mL Brine, then the aqueous layer washed 2 x 20mL $CHCl_3$, dried with sodium sulfate, filtered, and the solvent removed under reduced pressure. The intermediate was purified only through extractive isolation using water and $CHCl_3$ and taken on to the next reaction as is. To a solution of the intermediate in absolute ethanol (40mL) was added 2.4 equivalents of ethyl acetoacetate (0.7701g, 5.85mmol) dissolved in 10 mL EtOH and sodium (2eq, 0.1133g, 4.29mmol) slowly. The mixture was allowed to stir at room temperature under argon for 2 hours until TLC in 4:1:1 Hex/EtOAc/DCM revealed all nitrile oxide had been consumed. Finally, the ethanol was removed via rotary evaporation and the solid dissolved in $CHCl_3$, washed 2 x 50mL DI H_2O, 2 x 50mL Brine, and the aqueous layer washed 1 x 20mL $CHCl_3$, dried sodium sulfate, and

concentrated under reduced pressure. The solid was then chromatographed using 1:1 Hex/EtOAc, then 1:2 and flushed with EtOAc until all desired product **4** was collected.

N-hydroxy-10-methoxyanthracene-9-carbimidoyl chloride: Was not purified, carried on through *in situ* procedure only. ^{1}H NMR(400 MHz, CDCl$_3$) δ 8.36 (d, J=8.78 Hz, 2H), 8.31 (d, J=8.78, 2H), 7.70 (t, J=15.06, 7.40 Hz, 2H), 7.60 (t, J=15.31, 8.28 Hz, 2H), 4.20 (s, 3H).

Ethyl 3-(10-methoxyanthracen-9-yl)-5-methylisoxazole-4-carboxylate (4a). Yield from two steps 77%. (Rf=0.49 1:2 Hex/DCM. ^{1}H NMR (CDCl$_3$) δ ppm 8.39 (d, *J*=8.53 Hz, 2 H), 7.70 (d, *J*=8.66 Hz, 2 H), 7.48 - 7.54 (m, 2 H), 7.42 - 7.47 (m, 2 H), 4.20 (s, 3 H), 3.73 (q, *J*=7.07 Hz, 2 H), 2.93 (s, 3 H), 0.37 (t, *J*=7.09 Hz, 3 H). ^{13}C NMR (CDCl$_3$) δ 176.10, 161.40, 160.34, 153.91, 131.64, 126.29, 125.71, 125.01, 123.90, 122.30, 118.62, 111.32, 63.55, 59.90, 14.01, 13.30, 12.74. HRMS (ESI) accurate mass calcd. for $C_{22}H_{20}N_1O_4$ (M+1) requires 362.1392, found 362.1392.

Ethyl 5-methyl-3-(10-phenoxyanthracen-9-yl)isoxazole-4-carboxylate (4b).

By the same procedure as that described for **4a**, from oxime (0.2080g, 0.6638mmol) in chloroform (20mL) was added 10mol% pyridine (1.33mL from 5M) and NCS (1.15eq, 0.1023g. The reaction was warmed to 40°C for 3hr under an argon atmosphere. Washed 3 x 20mL H$_2$O, 4 x 15mL Brine, 2 x 10mL CH$_2$Cl$_2$, dried and taken onto next reaction. To a solution of the intermediate in absolute ethanol (15mL) was added 1.46 equivalents of ethyl acetoacetate (0.1260g) dissolved in 5mL EtOH and sodium (1.22eq, 0.0186g) slowly. The mixture was allowed to stir at room temperature under argon for 1.5 hours until TLC in 4:1:1 Hex/EtOAc/DCM revealed all nitrile oxide had been consumed. Finally, the ethanol was removed via rotary evaporation and the solid dissolved in CHCl$_3$, washed 2 x 50mL DI H$_2$O, 2 x 50mL Brine, and the aqueous layer washed 1 x 20mL CHCl$_3$, dried sodium sulfate, and

concentrated under reduced pressure. The solid was then chromatographed using dichloromethane until all desired product **4** was collected. Obtained (Yield from two steps 0.2177 g, 77%). (Rf=0.42 DCM).^{1}H NMR (Acetone-d_6) δ 8.15 (m, 2H), 7.75 (m, 2H), 7.51 (m, 4H), 7.31 (t, J=7.65, 8.28, 15.94 Hz, 2H), 7.05 (t, J=7.28, 7.40, 14.68 Hz, 1H), 6.88 (d, J=8.03 Hz, 2H), 3.76 (q, J=7.15, 14.31 Hz, 2H), 2.93 (s, 3H), 0.50 (t, J=7.03, 7.15, 14.18 Hz, 3H). ^{13}C NMR (Acetone-d_6) δ 177.62, 161.86, 161.11, 160.91, 147.86, 132.60, 130.89, 127.66, 127.01, 126.88, 125.26, 123.23, 123.08, 122.14, 116.08, 112.15, 60.72, 13.57. MS (ESI) *m/z* 236 (22.37, M+), 237(100, M+1), 238 (18.80, M+2). HRMS (ESI) accurate mass calcd. for $C_{27}H_{22}N_1O_4$ (M+1) requires 424.1549, found 424.1578.

Ethyl 3-(10-([1,1'-biphenyl]-4-yloxy)anthracen-9-yl)-5-methylisoxazole-4-carboxylate (4c). By the same procedure as that described for **4a**, from oxime (1.6234g, 4.1685mmol) in chloroform (140mL) was added 10mol% pyridine (8.33mL from 5M) and NCS (1.2eq, 0.6914g. The reaction was warmed to 40°C for 5hr under an argon atmosphere. Washed 4 x 125mL H_2O, 2 x 125mL Brine, 2 x 25mL CH_2Cl_2, dried and taken onto next reaction. To a solution of the intermediate in absolute ethanol (100mL) was added 2.42 equivalents of ethyl acetoacetate (1.3mL) dissolved in 35mL EtOH and sodium (2.15eq, 0.2060g) slowly. The mixture was allowed to stir at room temperature under argon for 17 hours until TLC in 4:1:1 Hex/EtOAc/DCM revealed all nitrile oxide had been consumed. Finally, the ethanol was removed via rotary evaporation and the solid dissolved in $CHCl_3$, washed 2 x 100mL DI H_2O, 2 x 100mL Brine, and the aqueous layer washed 2 x 20mL $CHCl_3$, dried sodium sulfate, and concentrated under reduced pressure. The solid was then chromatographed using 4:1 Hex/EtOAc until all desired product **4** was collected. Obtained (0.2177 g, 77%). Obtained (Yield from two steps 1.3741g, 66%). (Rf=0.38 2:1 Hex/DCM). ^{1}H NMR (CDCl$_3$) δ 8.21(m, 2H), 7.72 (m, 2H),

7.47 (m, 10H), 7.31 (m, 1H), 6.95 (m, 2H), 3.79 (q, J=7.15 Hz, 14.31, 2H), 2.96 (s, 3H), 0.45 (t, J=7.03, 7.15 Hz, 14.18).^{13}C NMR (CDCl$_3$) δ 176.41, 161.50, 160.23, 159.64, 147.14, 140.48, 135.10, 131.86, 128.72, 128.46, 126.87, 126.78, 126.62, 125.82, 125.76, 124.34, 122.62, 120.41, 115.60, 111.43, 60.18, 13.46, 12.97. HRMS (ESI) accurate mass calcd. for C$_{33}$H$_{26}$N$_1$O$_4$ (M+1) requires 500.1862, found 500.1863.

Ethyl 5-methyl-3-(10-(naphthalen-1-yloxy)anthracen-9-yl)isoxazole-4-carboxylate (4d).

By the same procedure as that described for **4a**, from oxime (0.2217g, 0.6100mmol) in chloroform (20mL) was added 10mol% pyridine (1.22mL from 5M) and NCS (1.2eq, 0.1038g. The reaction was warmed to 40°C for 4hr under an argon atmosphere. Washed 4 x 50mL H$_2$O, 3 x 50mL Brine, 2 x 25mL CH$_2$Cl$_2$, dried and taken onto next reaction. To a solution of the intermediate in absolute ethanol (15mL) was added 2.2 equivalents of ethyl acetoacetate (0.17mL) dissolved in 5mL EtOH and sodium (2.1eq, 0.0295g) slowly. The mixture was allowed to stir at room temperature under argon for 1 hour until TLC in 4:1:1 Hex/EtOAc/DCM revealed all nitrile oxide had been consumed. Finally, the ethanol was removed via rotary evaporation and the solid dissolved in CHCl$_3$, washed 2 x 100mL DI H$_2$O, 2 x 100mL Brine, and the aqueous layer washed 2 x 20mL CHCl$_3$, dried sodium sulfate, and concentrated under reduced pressure. The solid was then chromatographed using dichloromethane until all desired product **4** was collected. Obtained (Yield from two steps 0.2411 g, 83%). (Rf=0.41 DCM). ^{1}H NMR (CDCl$_3$) δ 8.92 (d, J=8.26 Hz, 1H), 8.18 (d, J=8.66 Hz, 2H), 7.98 (d, J=8.16 Hz, 1H), 7.78 (m, 3H), 7.69 (m, 1H), 7.54, (d, J=8.28 Hz , 1H), 7.48 (m, 2H), 7.39 (m, 2H), 7.12 (bs, 1H), 6.21 (bd, J=7.28 Hz, 1H), 3.85 (bs, 2H), 3.00 (s, 3H), 0.52 (bs, 3H). ^{13}C NMR (CDCl$_3$) δ 176.30, 161.43, 160.26, 155.82, 147.54, 134.79, 131.65, 128.00, 127.76, 126.79, 126.66, 126.60, 126.47, 125.98, 125.78, 125.71, 125.58, 124.77, 124.62, 124.59, 124.27, 124.10, 122.49, 122.31, 122.20, 121.82, 121.56,

120.33, 111.41, 108.16, 107.77, 60.14, 13.42, 13.01. HRMS (ESI) accurate mass calcd. for $C_{31}H_{24}N_1O_4$ (M+1) requires 474.1705, found 474.1700.

Ethyl 5-methyl-3-(10-(naphthalen-2-yloxy)anthracen-9-yl)isoxazole-4-carboxylate (4e).

By the same procedure as that described for **4a**, from oxime (2.3653g, 6.509mmol) in chloroform (220mL) was added 10mol% pyridine (6.5mL from 5M) and NCS (1.2eq, 1.0752g. The reaction was warmed to 40°C for 6.5hr under an argon atmosphere. Washed 4 x 150mL H_2O, 2 x 125mL Brine, 2 x 25mL CH_2Cl_2, dried and taken onto next reaction. To a solution of the intermediate in absolute ethanol (150mL) was added 2.4 equivalents of ethyl acetoacetate (2mL) dissolved in 55mL EtOH and sodium (2eq, 0.2993g) slowly. The mixture was allowed to stir at room temperature under argon for 15.5 hours until TLC in 4:1:1 Hex/EtOAc/DCM revealed all nitrile oxide had been consumed. Finally, the ethanol was removed via rotary evaporation and the solid dissolved in $CHCl_3$, washed 2 x 100mL DI H_2O, 2 x 100mL Brine, and the aqueous layer washed 2 x 20mL $CHCl_3$, dried sodium sulfate, and concentrated under reduced pressure. The solid was then chromatographed using dichloromethane until all desired product **4** was collected. Obtained (Yield from two steps 2.605 g, 85%). (Rf=0.33 4:1:1Hex/EtOAc/Et$_2$O). ^{1}H NMR (CDCl$_3$) δ 8.05 (m, 2H), 7.72 (d, J=8.91 Hz, 1H), 7.65 (m, 1H), 7.58 (d, J=8.28 Hz, 2H), 7.25 (m, 8H), 6.68, (d, J=2.38 Hz, 1H), 3.64 (q, J=7.15 Hz, 14.31, 2H), 2.81 (s, 3H), 0.45 (t, J=7.03, 7.15 Hz, 14.18). ^{13}C NMR (CDCl$_3$) δ 176.4, 161.5, 160.3, 158.0, 147.2, 134.3, 134.1, 131.7, 130.1, 129.5, 127.7, 127.2, 126.9, 126.7, 126.6, 126.6, 126.2, 125.8, 125.8, 124.3, 124.2, 122.6, 120.4, 117.6, 111.5, 109.7, 60.2, 13.4, 13.0. HRMS (ESI) accurate mass calcd. for $C_{31}H_{24}N_1O_4$ (M+1) requires 474.1705, found 474.1705.

General Procedure from ester to double tail.

Ester **8a-e** (0.5 mmol) was dissolved in THF (5 mL). To the solution was then added methanol (5 mL) and aqueous KOH (5 eq. in 10 mL H_2O). The solution was then brought to reflux for three hours until completion of the reaction as indicated by TLC. The reaction was then cooled to room temperature and the organic solvents were removed under reduced pressure. The aqueous mixture was diluted with then diluted with water (10 mL). The aqueous solution was cooled to 0 °C and acidified to pH 2 with 1M HCl. The resulting precipitate was filtered and washed with water (3 x 5 mL). The solid was then dissolved in ethyl acetate and dried over sodium sulfate. The solid was removed by filtration and the solution was concentrated under reduced pressure to yield the carboxylic acid.

To the carboxylic acid was added excess thionyl chloride (10 mL). The solution was stirred at room temperature for 18 hr under a drying tube equipped with CaCl2 and NaOH. The reaction mixture was concentrated under reduced pressure. The chlorinating agent was chased with chloroform and hexanes to yield to acid chloride.

The acid chloride was dissolved in dry methylene chloride (5 mL) and to the solution was added triethyl amine (2 eq.). To a stirring solution of the acid chloride, at 0 °C, was slowly added the amino pyrrole **7** in methylene chloride (5 mL). The mixture was allowed to warm to room temperature while stirring for 24 hr. The reaction mixture was diluted with chloroform (40 mL) and washed with water (20 mL). The aqueous fraction was then extracted with methylene chloride (3 x 10 mL). The combined organic fractions were dried over sodium sulfate, filtered, and concentrated. The product was then purified by column chromatography eluting 10% ammonium hydroxide in methanol.

N-(5-(bis(3-(dimethylamino)propyl)carbamoyl)-1-methyl-1H-pyrrol-3-yl)-3-(10-methoxyanthracen-9-yl)-5-methylisoxazole-4-carboxamide, 8a.

Yield from two steps 62%. 1H NMR (CDCl$_3$) δ 8.43 (d, 2H**,** J=8.41 Hz anthracene-H), 7.72 (d, 2H, J= 8.78 Hz, anthracene-H), 7.54 (m, 4H, anthracene-H), 6.59 (s, 1H, pyrrole-H), 6.49 (s, 1H, pyrrole-H), 5.06 (s, 1H, amide-H), 4.24 (s, 3H, methoxy), 3.45 (s, 3H, pyrrole methyl), 3.30 (bs, 4H, double tail), 3.01 (s, 3H, isoxazole methyl), 2.18 (bs, 16H, double tail), 1.63 (bs, 4H, double tail). 13C NMR (CDCl$_3$) δ 176.03, 163.55, 157.70, 157.41, 155.42, 131.90, 127.94, 125.92, 125.22, 124.27, 123.96, 122.77, 119.85, 116.05, 115.69, 112.80, 101.89, 63.72, 56.75, 45.32, 35.15, 13.62. HRMS (EI) accurate mass calcd. for C$_{36}$H$_{45}$O$_4$N$_6$ (M+1) requires 625.3502, found 625.3215.

N-(5-(bis(3-(dimethylamino)propyl)carbamoyl)-1-methyl-1H-pyrrol-3-yl)-5-methyl-3-(10-phenoxyanthracen-9-yl)isoxazole-4-carboxamide, 8b.

Yield from two steps 86%. 1H NMR (CDCl$_3$) δ 8.24 (d, 2H**,** J=8.41 Hz anthracene-H), 7.77 (d, 2H, J= 8.41 Hz, anthracene-H), 7.52 (m, 4H, anthracene-H), 7.25 (d, 2H, J=8.41 Hz, aryl-H), 7.04 (t, 1H, J=7.28, 14.56 Hz, aryl-H), 6.85 (d, 2H, J=8.16 Hz, aryl-H), 6.62 (s, 1H, pyrrole-H), 6.49 (s, 1H, pyrrole-H), 5.10 (s, 1H, amide-H), 3.47 (s, 3H, pyrrole methyl), 3.30 (bs, 4H, double tail), 3.03 (s, 3H, isoxazole methyl), 2.15 (bs, 16H, double tail), 1.61 (bs, 4H, double tail). 13C NMR (CDCl$_3$) δ 176.11, 163.55, 159.88, 157.62, 157.27, 148.64, 131.79, 129.94, 128.14, 126.55, 125.15, 124.66, 124.07, 123.10, 122.32, 119.90, 117.80, 115.67, 115.24, 112.93, 101.82, 56.75, 45.28, 35.21, 35.21, 13.62. HRMS (ESI) accurate mass calcd. for C$_{41}$H$_{47}$O$_4$N$_6$ (M+1) requires 687.3659, found 687.3629.

3-(10-([1,1'-biphenyl]-4-yloxy)anthracen-9-yl)-N-(5-(bis(3-(dimethylamino)propyl)carbamoyl)-1-methyl-1H-pyrrol-3-yl)-5-methylisoxazole-4-carboxamide, 8c.

Yield from two steps 73%. 1H NMR (CDCl$_3$) δ 8.27 (bd, 2H, J=8.91 Hz anthracene-H), 7.78 (bd, 2H, J= 7.91 Hz, anthracene-H), 7.52 (m, 8H, anthracene-H, aryl-H), 7.41 (t, 2H, J=7.53, 15.18 Hz, aryl-H), 7.30 (t, 1H, J=7.40, 14.68 Hz, aryl-H), 6.91 (d, 2H, J=8.53 Hz, aryl-H), 6.64 (s, 1H, pyrrole-H), 6.53 (s, 1H, pyrrole-H), 5.12 (s, 1H, amide-H), 3.47 (s, 3H, pyrrole methyl), 3.26 (t, 4H, J=7.28, 14.56, double tail), 3.03 (s, 3H, isoxazole methyl), 2.15 (bs, 16H, double tail), 1.59 (bs, 4H, double tail). 13C NMR (CDCl$_3$) δ 176.04, 163.51, 159.40, 157.56, 157.25, 148.54, 140.16, 135.42, 131.75, 128.74, 128.53, 128.14, 126.96, 126.73, 126.60, 125.14, 124.60, 124.04, 123.02, 119.88, 117.89, 115.65, 115.50, 112.92, 101.74, 56.65, 45.16, 35.18, 13.58. HRMS (ESI) accurate mass calcd. for C$_{47}$H$_{51}$O$_4$N$_6$ (M+1) requires 763.3948, found 763.3972.

N-(5-(bis(3-(dimethylamino)propyl)carbamoyl)-1-methyl-1H-pyrrol-3-yl)-5-methyl-3-(10-(naphthalen-1-yloxy)anthracen-9-yl)isoxazole-4-carboxamide, 8d.

Yield from two steps 48%. ^{1}H NMR (CDCl$_3$) δ ppm 8.98 (m, 1 H), 8.44 (m, 1 H), 8.22 (dd, *J*=18.51, 8.72 Hz, 2 H), 8.06 (m, 1 H), 7.81 (m, 5 H), 7.54 (m, 5 H), 6.64 (m, 2 H), 5.18 (m, 1 H), 3.50 (m, 3 H), 3.36 (br. s., 4 H), 3.06 (m, 4 H), 2.18 (br. s., 16 H), 1.68 (br. s., 4 H). ^{13}C NMR (CDCl$_3$) δ 176.21, 163.64, 158.75, 157.10, 157.27, 157.19, 140.09, 148.52, 147.95, 134.88, 132.93, 131.82, 130.89, 128.57, 128.25, 128.19, 127.89, 127.03, 126.84, 126.63, 126.17, 125.64, 125.36, 125.25, 125.17, 124.78, 124.63, 124.45, 124.18, 122.97, 122.70, 122.47, 122.14, 121.73, 119.79, 118.68, 115.89, 112.99, 108.28, 107.60, 107.19, 102.04, 60.95, 56.79, 45.32,

35.20, 15.52, 13.65. HRMS (ESI) accurate mass calcd. for $C_{45}H_{49}O_4N_6$ (M+1) requires 737.3815, found 737.3833.

N-(5-(bis(3-(dimethylamino)propyl)carbamoyl)-1-methyl-1H-pyrrol-3-yl)-5-methyl-3-(10-(naphthalen-2-yloxy)anthracen-9-yl)isoxazole-4-carboxamide, 8e.

Yield from two steps 42% ^{1}H NMR (CDCl$_3$) δ ppm 8.26 (d, *J*=8.53 Hz, 2 H), 7.72 - 7.93 (m, 4 H), 7.31 - 7.58 (m, 8 H), 6.77 (d, *J*=1.88 Hz, 1 H), 6.49 - 6.68 (m, 2 H), 5.20 (d, *J*=1.13 Hz, 1 H), 3.42 - 3.58 (m, 3 H), 3.29 (br. s., 4 H), 3.04 (s, 3 H), 2.00 - 2.34 (m, 16 H), 1.58 (br. s., 4 H). ^{13}C NMR (101 MHz, CHLOROFORM-*d*) δ ppm 176.08, 163.52, 163.43, 157.76, 157.61, 157.53, 157.24, 157.14, 152.59, 148.58, 148.43, 134.17, 131.90, 131.80, 131.67, 130.25, 130.18, 129.53, 128.23, 128.13, 127.90, 127.57, 126.95, 126.87, 126.79, 126.55, 125.12, 124.57, 124.54, 124.42, 124.10, 123.64, 123.03, 122.68, 119.82, 119.76, 117.89, 117.24, 115.68, 112.98, 112.93, 109.69, 101.93, 56.69, 45.22, 35.20, 35.15, 13.58. HRMS (ESI) accurate mass calcd. for $C_{45}H_{49}O_4N_6$ (M+1) requires 737.3815, found 737.3809.

Results and Discussion.

These novel compounds were purified and characterized by EI-MS and a sequence of NMR techniques, such as: 1H, 13C, 1H-1H COSY, HSQC and HMBC. Of the ID-dansyl analogs that were examined by NMR, all were found to display more signals than expected, even after careful chromatography, which we rationalized by their ability to adopt multiple conformations (Fig SM-1).
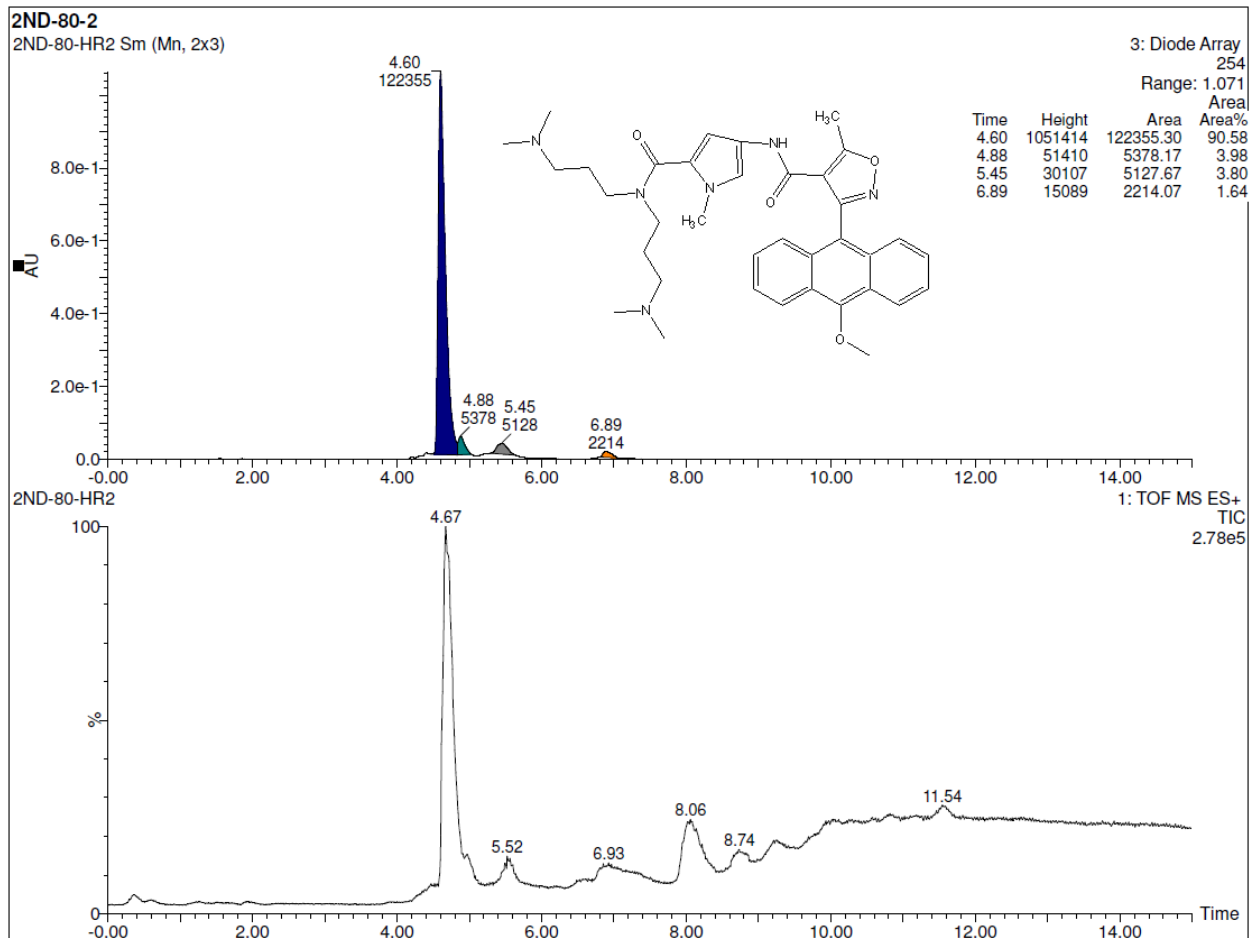
2ND-80-2
2ND-80-HR2 Sm (Mn, 2x3)

3: Diode Array
254
Range: 1.071

Time	Height	Area	Area%
4.60	1051414	122355.30	90.58
4.88	51410	5378.17	3.98
5.45	30107	5127.67	3.80
6.89	15089	2214.07	1.64

2ND-80-HR2

1: TOF MS ES+
TIC
2.78e5

Elemental Composition Report

Page 1

Single Mass Analysis
Tolerance = 5.0 mDa / DBE: min = -1.5, max = 50.0
Element prediction: Off
Number of isotope peaks used for i-FIT = 3

Monoisotopic Mass, Even Electron Ions
29 formula(e) evaluated with 1 results within limits (up to 50 closest results for each mass)
Elements Used:
C: 0-36   H: 0-45   N: 0-6   O: 0-4
2ND-80-2
2ND-80-HR2 466 (4.679)

1: TOF MS ES+
5.13e+004
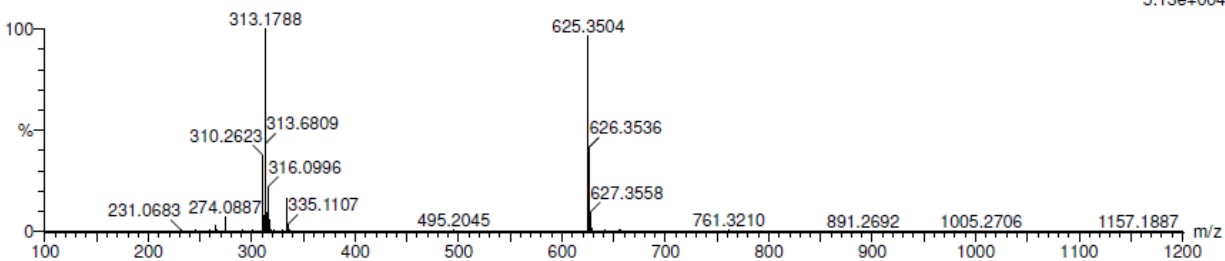
Minimum:				-1.5			
Maximum:		5.0	10.0	50.0			
Mass	Calc. Mass	mDa	PPM	DBE	i-FIT	i-FIT (Norm)	Formula
625.3504	625.3502	0.2	0.3	17.5	187.3	0.0	C36 H45 N6 O4
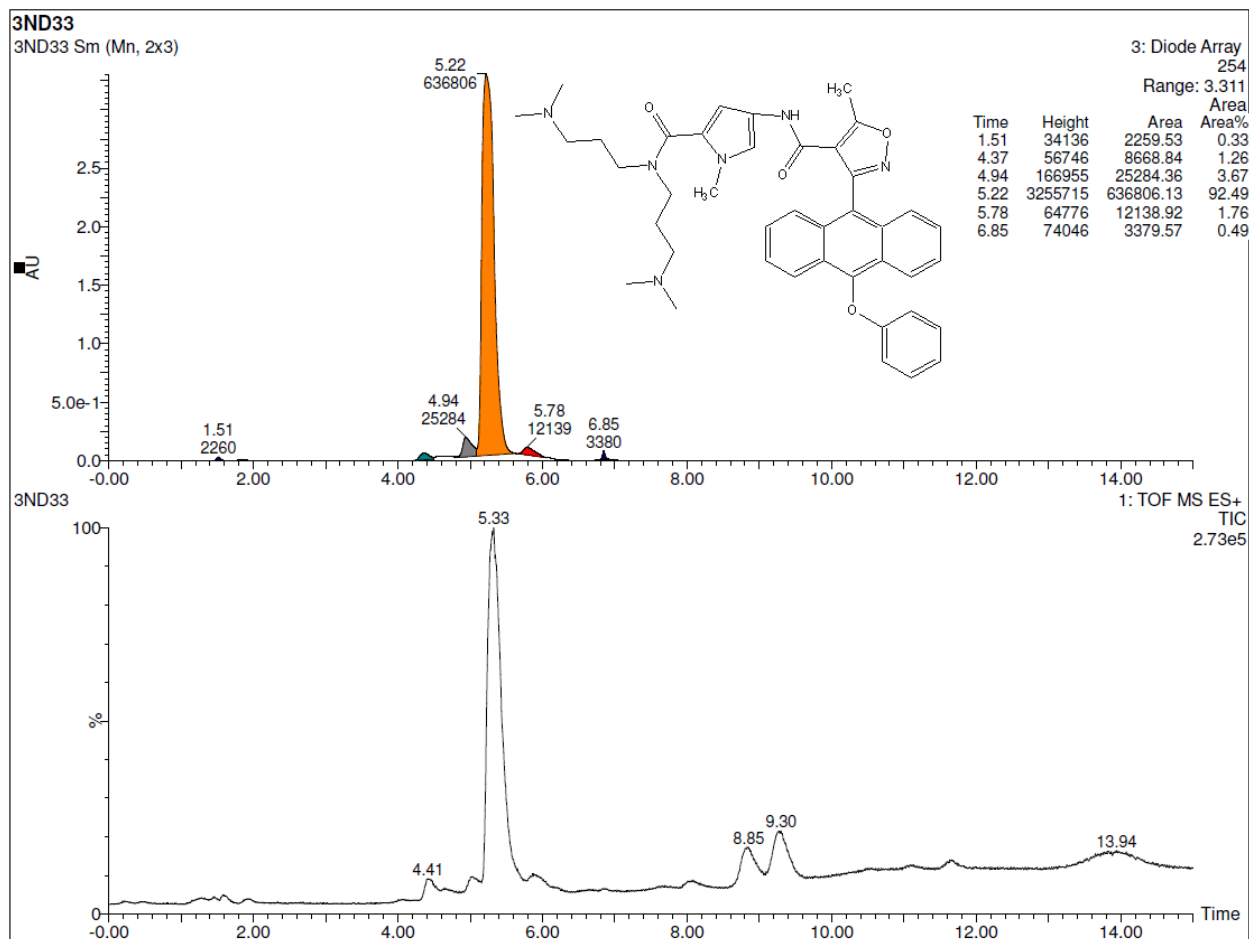
107

3ND33
3ND33 Sm (Mn, 2x3)

3: Diode Array
254
Range: 3.311

Time	Height	Area	Area%
1.51	34136	2259.53	0.33
4.37	56746	8668.84	1.26
4.94	166955	25284.36	3.67
5.22	3255715	636806.13	92.49
5.78	64776	12138.92	1.76
6.85	74046	3379.57	0.49

3ND33

1: TOF MS ES+
TIC
2.73e5

Elemental Composition Report

Single Mass Analysis

Tolerance = 5.0 mDa   /   DBE: min = -1.5, max = 50.0
Element prediction: Off
Number of isotope peaks used for i-FIT = 3

Monoisotopic Mass, Even Electron Ions
26 formula(e) evaluated with 1 results within limits (up to 50 closest results for each mass)
Elements Used:
C: 0-41   H: 0-47   N: 0-6   O: 0-4
3ND33hr
3ND33hr 537 (5.393)

1: TOF MS ES+
4.08e+004
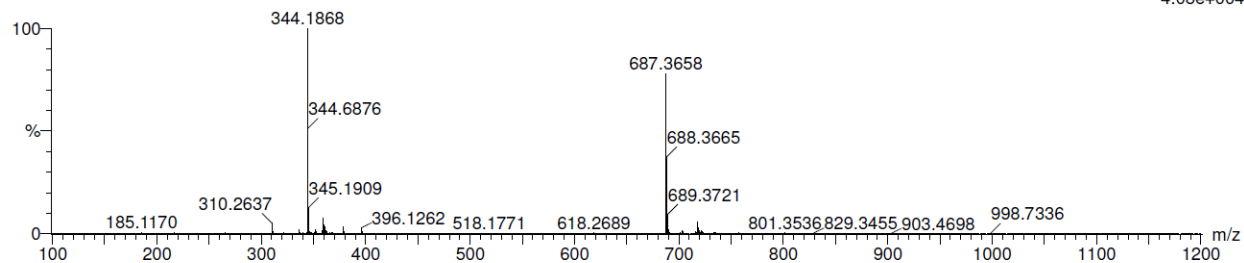
Minimum:				-1.5			
Maximum:		5.0	10.0	50.0			
Mass	Calc. Mass	mDa	PPM	DBE	i-FIT	i-FIT (Norm)	Formula
687.3658	687.3659	-0.1	-0.1	21.5	172.3	0.0	C41 H47 N6 O4
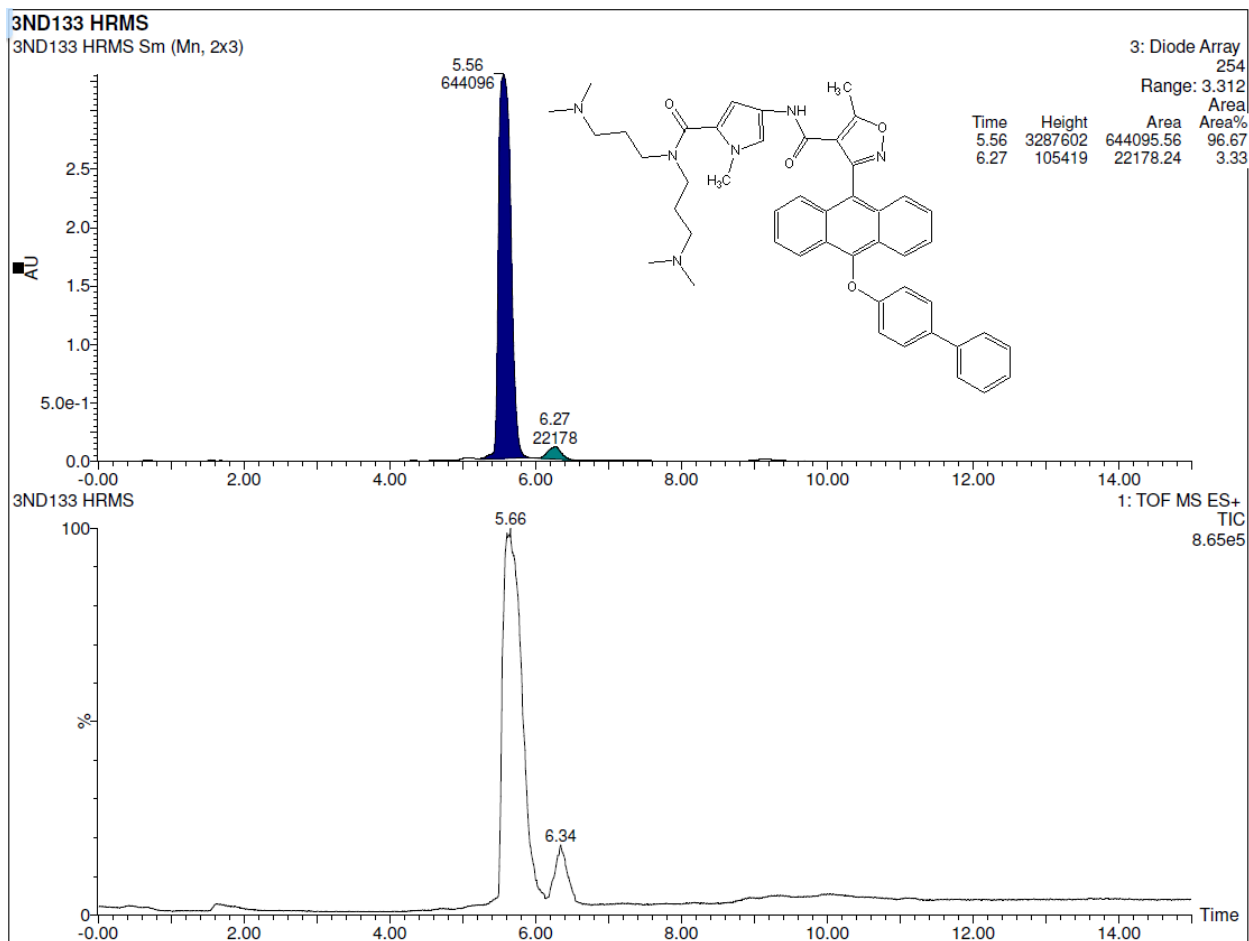
Page 1

108

3ND133 HRMS
3ND133 HRMS Sm (Mn, 2x3)

3: Diode Array
254
Range: 3.312
Area

Time	Height	Area	Area%
5.56	3287602	644095.56	96.67
6.27	105419	22178.24	3.33

3ND133 HRMS

1: TOF MS ES+
TIC
8.65e5

Elemental Composition Report

Page 1

Single Mass Analysis

Tolerance = 5.0 mDa / DBE: min = -1.5, max = 50.0
Element prediction: Off
Number of isotope peaks used for i-FIT = 3

Monoisotopic Mass, Even Electron Ions
24 formula(e) evaluated with 1 results within limits (up to 50 closest results for each mass)
Elements Used:
C: 0-47   H: 0-51   N: 0-6   O: 0-4
3ND133 HRMS
3ND133 HRMS 600 (6.023)

1: TOF MS ES+
1.23e+004
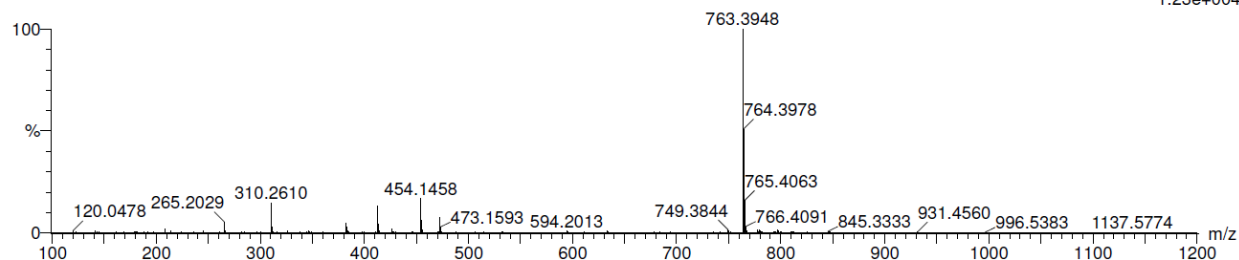
Minimum:				-1.5			
Maximum:		5.0	10.0	50.0			

Mass	Calc. Mass	mDa	PPM	DBE	i-FIT	i-FIT (Norm)	Formula
763.3948	763.3972	-2.4	-3.1	25.5	156.4	0.0	C47 H51 N6 O4
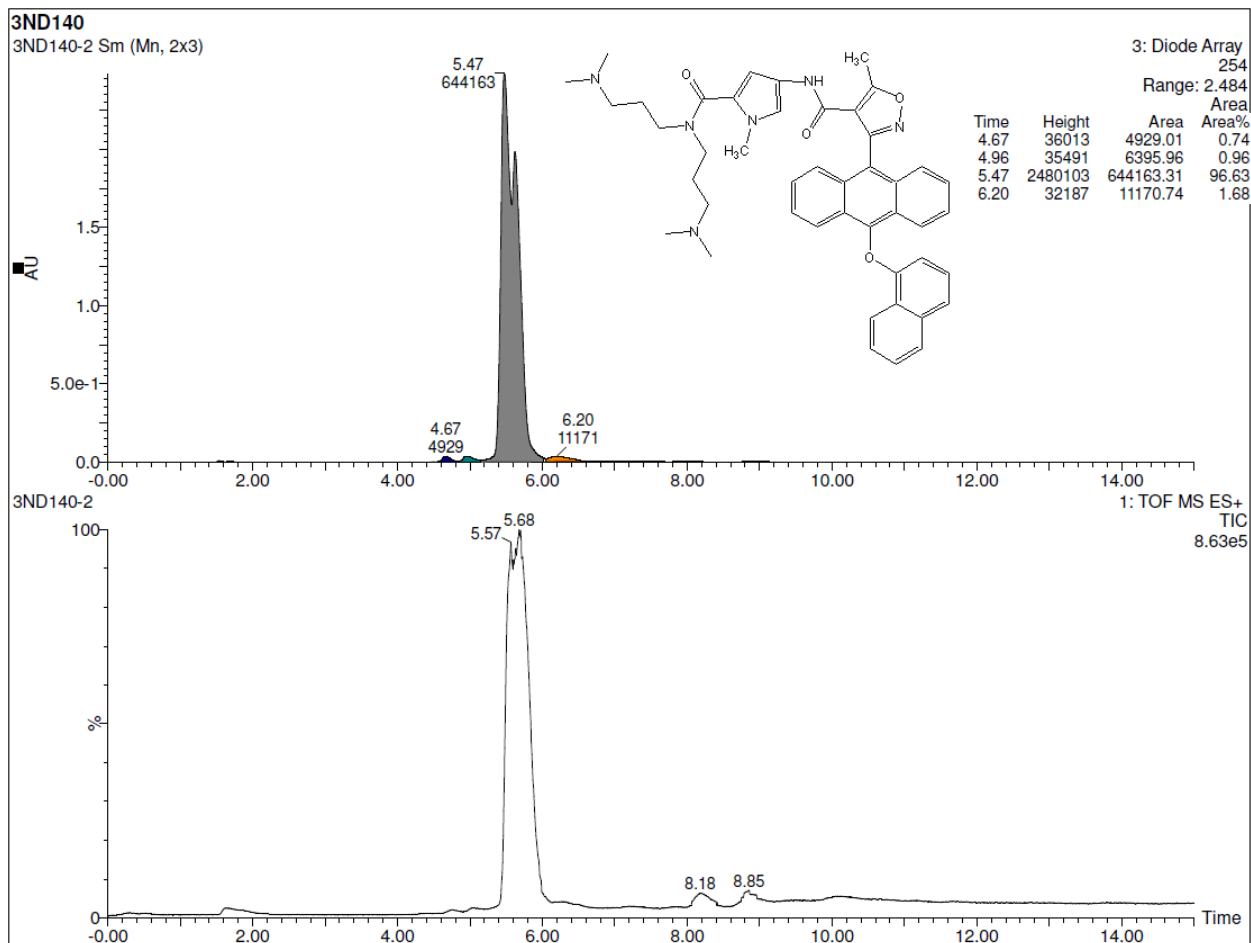
109

3ND140
3ND140-2 Sm (Mn, 2x3)

Time	Height	Area	Area%
4.67	36013	4929.01	0.74
4.96	35491	6395.96	0.96
5.47	2480103	644163.31	96.63
6.20	32187	11170.74	1.68

5.47
644163

4.67
4929

6.20
11171

3ND140-2

1: TOF MS ES+
TIC
8.63e5

5.57   5.68

8.18   8.85

Elemental Composition Report

Page 1

Single Mass Analysis

Tolerance = 5.0 mDa   /   DBE: min = -1.5, max = 50.0
Element prediction: Off
Number of isotope peaks used for i-FIT = 3

Monoisotopic Mass, Even Electron Ions
26 formula(e) evaluated with 1 results within limits (up to 50 closest results for each mass)
Elements Used:
C: 0-45   H: 0-49   N: 0-6   O: 0-4

3ND140
3ND140 637 (6.394)

1: TOF MS ES+
5.25e+004

310.2565

771.3340   829.3684

737.3782

830.3851

265.2044

420.0814 462.0925

311.2663

480.1028

831.3872

141.0660 214.1912

482.1008

832.3880

653.1870

907.3774   997.4719
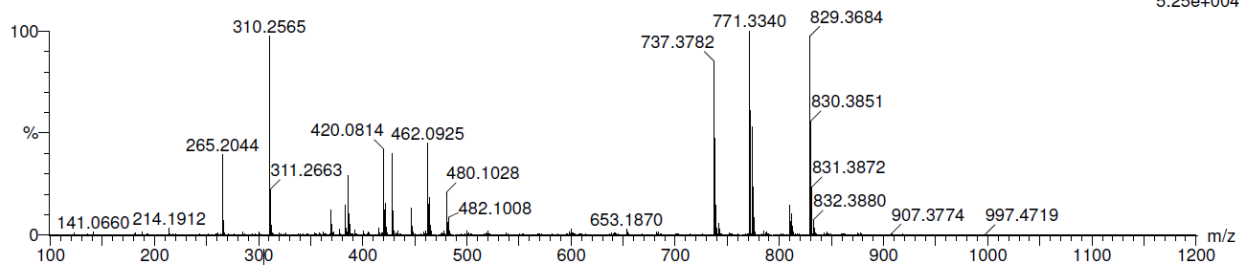
Minimum:				-1.5			
Maximum:		5.0	10.0	50.0			

Mass	Calc. Mass	mDa	PPM	DBE	i-FIT	i-FIT (Norm)	Formula
737.3782	737.3815	-3.3	-4.5	24.5	221.9	0.0	C45 H49 N6 O4
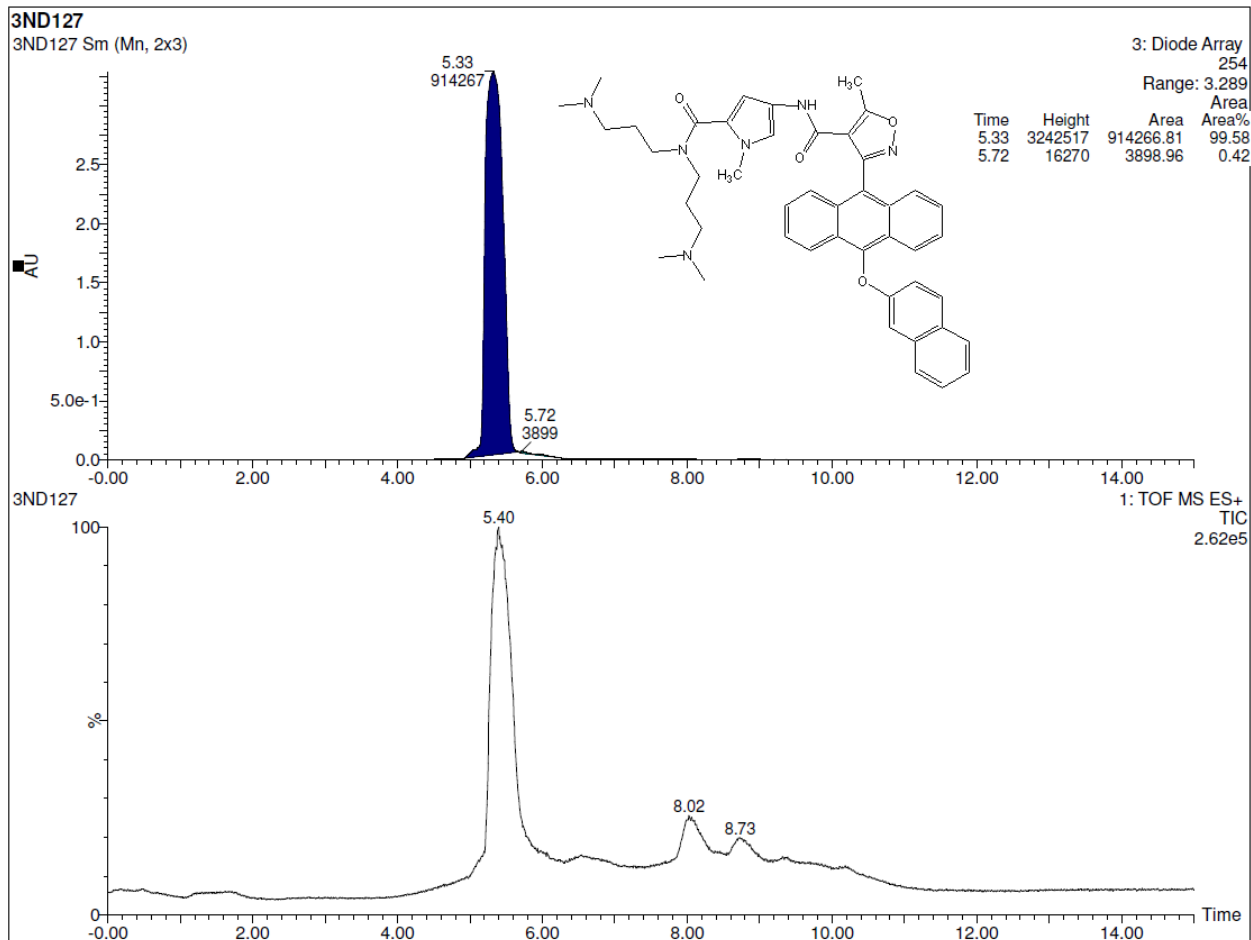
110

3ND127
3ND127 Sm (Mn, 2x3)

	Time	Height	Area	Area%
	5.33	3242517	914266.81	99.58
	5.72	16270	3898.96	0.42

3ND127

1: TOF MS ES+
TIC
2.62e5

Elemental Composition Report

Page 1

Single Mass Analysis

Tolerance = 5.0 mDa / DBE: min = -1.5, max = 50.0
Element prediction: Off
Number of isotope peaks used for i-FIT = 3

Monoisotopic Mass, Even Electron Ions
26 formula(e) evaluated with 1 results within limits (up to 50 closest results for each mass)
Elements Used:
C: 0-45   H: 0-49   N: 0-6   O: 0-4
3ND127
3ND127 536 (5.380)

1: TOF MS ES+
5.55e+004
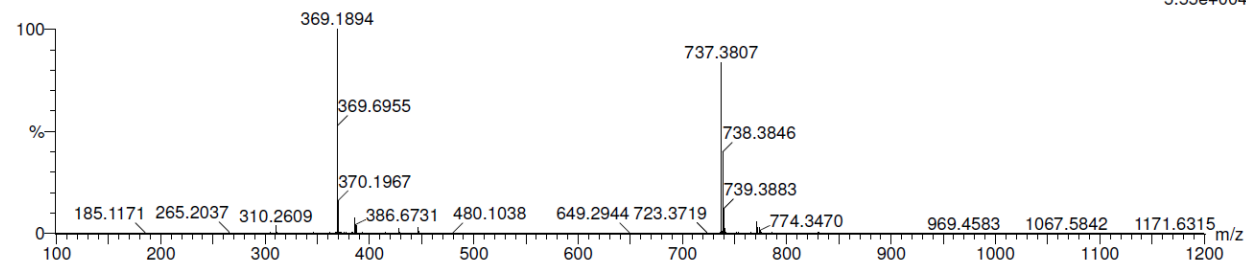
Minimum:				-1.5			
Maximum:		5.0	10.0	50.0			

Mass	Calc. Mass	mDa	PPM	DBE	i-FIT	i-FIT (Norm)	Formula
737.3807	737.3815	-0.8	-1.1	24.5	152.6	0.0	C45 H49 N6 O4

111

112
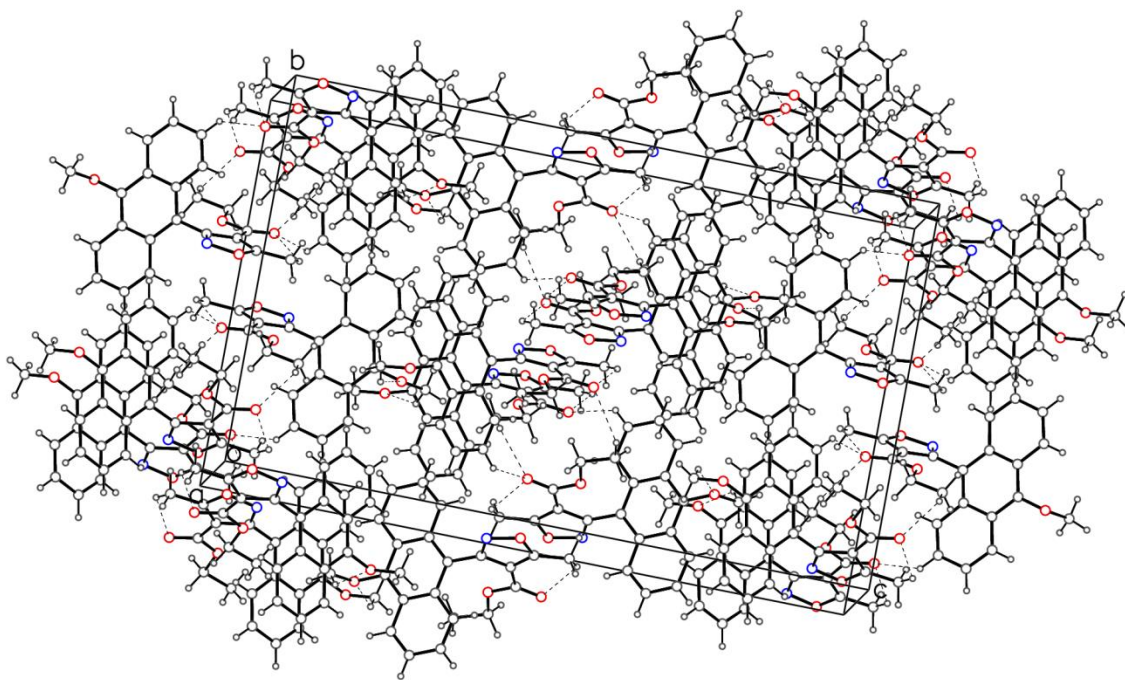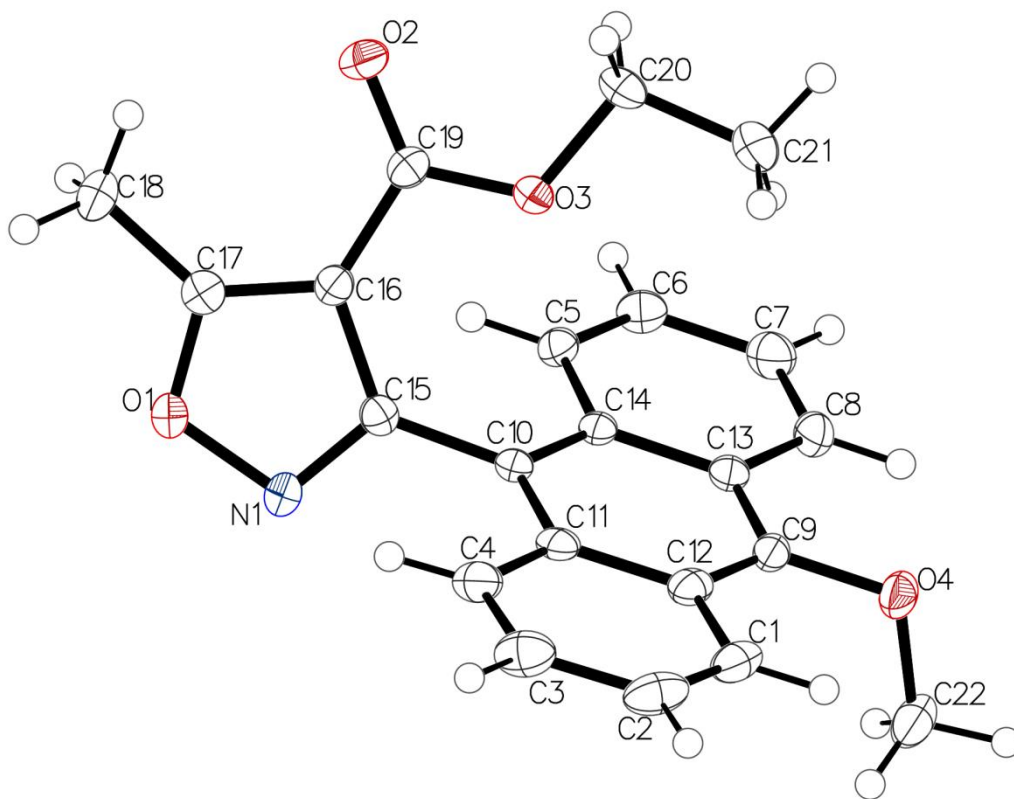
Computer programs:

SAINT V8.27B (Bruker AXS Inc., 2012), *SHELXS97* (Sheldrick, 2008), *SHELXL97* (Sheldrick, 2008).

Computing details

Data collection: *APEX2 (Bruker, 2012)*; cell refinement: *APEX2 (Bruker, 2012)*; data reduction: *SAINT (Bruker, 2012)*; program(s) used to solve structure: *SHELXS (Sheldrick, 2008)*; program(s) used to refine structure: *SHELXL (Sheldrick, 2008)*; molecular graphics: Olex2 (Dolomanov *et al.*, 2009); software used to prepare material for publication: Olex2 (Dolomanov *et al.*, 2009).

Crystal data

$C_{22}H_{19}NO_4$	?
$M_r = 361.38$	$D_x = 1.328$ Mg m^{-3}
Orthorhombic, *Pbca*	Melting point: ? K
Hall symbol: ?	Mo $K\alpha$ radiation, $\lambda = 0.71073$ Å
$a = 7.9091\ (3)$ Å	Cell parameters from 9912 reflections
$b = 16.5970\ (7)$ Å	$\theta = 2.6$–$27.4°$
$c = 27.5365\ (12)$ Å	$\mu = 0.09$ mm^{-1}
$V = 3614.6\ (3)$ Å^3	$T = 100$ K

$Z = \underline{8}$	Prism, yellow
$F(000) = \underline{1520}$	$\underline{0.29} \times \underline{0.28} \times \underline{0.21}$ mm

Data collection

Bruker SMART BREEZE CCD diffractometer	$\underline{4109}$ independent reflections
Radiation source: $\underline{2\ kW\ sealed\ X\text{-}ray\ tube}$	$\underline{2911}$ reflections with $I > 2\sigma(I)$
? monochromator	$R_{int} = \underline{0.042}$
Detector resolution: ? pixels mm^{-1}	$\theta_{max} = \underline{27.4}°$, $\theta_{min} = \underline{2.5}°$
φ and ω scans	$h = \underline{-10} \quad \underline{10}$
Absorption correction: multi-scan SADABS-2012/1 (Bruker, 2012)	$k = \underline{-21} \quad \underline{20}$
$T_{min} = \underline{0.912}$, $T_{max} = \underline{1.000}$	$l = \underline{-35} \quad \underline{35}$
$\underline{24975}$ measured reflections	

Refinement

Refinement on F^2	Secondary atom site location: ?
Least-squares matrix: full	Hydrogen site location: inferred from

114

	neighbouring sites
$R[F^2 > 2\sigma(F^2)] = 0.045$	H-atom parameters constrained
$wR(F^2) = 0.112$	$w = 1/[\sigma^2(F_o^2) + (0.0453P)^2 + 1.5524P]$ where $P = (F_o^2 + 2F_c^2)/3$
$S = 1.03$	$(\Delta/\sigma)_{max} = 0.001$
4109 reflections	$\Delta\rho_{max} = 0.29$ e Å^{-3}
247 parameters	$\Delta\rho_{min} = -0.29$ e Å^{-3}
0 restraints	Extinction correction: none
? constraints	Extinction coefficient: ?
Primary atom site location: structure-invariant direct methods	

Fractional atomic coordinates and isotropic or equivalent isotropic displacement parameters (Å^2)

	X	y	Z	$U_{iso}*/U_{eq}$
O1	−0.35989 (14)	0.96574 (7)	0.03187 (4)	0.0244 (3)
O2	0.08525 (15)	0.86256 (8)	−0.02913 (4)	0.0326 (3)
O3	0.15087 (14)	0.85246 (7)	0.04993 (4)	0.0221 (3)
O4	0.15548 (14)	0.81274 (7)	0.25306 (4)	0.0268 (3)

N1	−0.31613 (18)	0.95133 (8)	0.08136 (5)	0.0242 (3)
C1	0.1407 (2)	0.97991 (11)	0.23304 (6)	0.0262 (4)
H1	0.1984	0.9627	0.2615	0.031*
C2	0.1298 (2)	1.05948 (11)	0.22282 (6)	0.0314 (4)
H2	0.1805	1.0977	0.2440	0.038*
C3	0.0434 (2)	1.08603 (11)	0.18080 (7)	0.0312 (4)
H3	0.0354	1.1421	0.1743	0.037*
C4	−0.0282 (2)	1.03283 (10)	0.14967 (6)	0.0248 (4)
H4	−0.0854	1.0522	0.1217	0.030*
C5	−0.13449 (19)	0.74685 (9)	0.10343 (6)	0.0195 (4)
H5	−0.1910	0.7627	0.0745	0.023*
C6	−0.1161 (2)	0.66719 (10)	0.11336 (6)	0.0237 (4)
H6	−0.1590	0.6282	0.0913	0.028*
C7	−0.0337 (2)	0.64178 (10)	0.15626 (6)	0.0277 (4)
H7	−0.0208	0.5859	0.1627	0.033*
C8	0.0271 (2)	0.69681 (10)	0.18821 (6)	0.0250 (4)
H8	0.0809	0.6790	0.2171	0.030*

C9	0.0755 (2)	0.83883 (10)	0.21113 (6)	0.0211 (4)
C10	−0.08595 (19)	0.89041 (9)	0.12594 (5)	0.0172 (3)
C11	−0.01913 (19)	0.94783 (10)	0.15827 (6)	0.0193 (4)
C12	0.0659 (2)	0.92129 (10)	0.20144 (6)	0.0206 (4)
C13	0.01135 (19)	0.78115 (10)	0.17903 (6)	0.0190 (4)
C14	−0.07079 (19)	0.80738 (9)	0.13549 (5)	0.0170 (3)
C15	−0.1677 (2)	0.91653 (9)	0.08000 (6)	0.0181 (3)
C16	−0.1090 (2)	0.90742 (9)	0.03098 (6)	0.0177 (3)
C17	−0.2353 (2)	0.93860 (9)	0.00304 (6)	0.0201 (4)
C18	−0.2625 (2)	0.94596 (11)	−0.05010 6)	0.0263 (4)
H18A	−0.3440	0.9051	−0.0607	0.039*
H18B	−0.1549	0.9379	−0.0671	0.039*
H18C	−0.3066	0.9997	−0.0576	0.039*
C19	0.0495 (2)	0.87249 (9)	0.01309 (6)	0.0193 (4)
C20	0.3063 (2)	0.80968 (11)	0.03884 (6)	0.0269 (4)
H20A	0.3835	0.8442	0.0197	0.032*
H20B	0.2820	0.7602	0.0200	0.032*

C21	0.3843 (2)	0.78877 (12)	0.08684 (7)	0.0346 (5)
H21A	0.4879	0.7576	0.0815	0.052*
H21B	0.3043	0.7566	0.1059	0.052*
H21C	0.4115	0.8384	0.1045	0.052*
C22	0.0470 (2)	0.81194 (12)	0.29442 (6)	0.0304 (4)
H22A	−0.0540	0.7799	0.2872	0.046*
H22B	0.0136	0.8672	0.3024	0.046*
H22C	0.1069	0.7881	0.3221	0.046*

Atomic displacement parameters (Å^2)

	U^{11}	U^{22}	U^{33}	U^{12}	U^{13}	U^{23}
O1	0.0228 (6)	0.0306 (7)	0.0198 (6)	0.0084 (5)	−0.0030 (5)	0.0022 (5)
O2	0.0289 (7)	0.0516 (9)	0.0172 (6)	0.0090 (6)	0.0026 (5)	−0.0030 (6)
O3	0.0176 (6)	0.0305 (7)	0.0183 (6)	0.0067 (5)	0.0008 (5)	−0.0013 (5)
O4	0.0182 (6)	0.0434 (8)	0.0187 (6)	0.0029 (5)	−0.0031 (5)	0.0038 (5)
N1	0.0247 (8)	0.0309 (8)	0.0170 (7)	0.0068 (6)	−0.0025 (6)	0.0020 (6)
C1	0.0219 (9)	0.0393 (11)	0.0174 (8)	−0.0058 (8)	0.0024 (7)	−0.0040 (8)

C2	0.0328 (10)	0.0360 (11)	0.0255 (10)	−0.0112 (8)	0.0061 (8)	−0.0117 (8)
C3	0.0398 (11)	0.0235 (10)	0.0302 (10)	−0.0033 (8)	0.0077 (8)	−0.0041 (8)
C4	0.0272 (9)	0.0244 (9)	0.0227 (9)	0.0018 (7)	0.0044 (7)	−0.0022 (7)
C5	0.0186 (8)	0.0241 (9)	0.0160 (8)	0.0008 (7)	0.0013 (6)	0.0015 (7)
C6	0.0248 (9)	0.0232 (9)	0.0233 (9)	−0.0022 (7)	0.0035 (7)	−0.0017 (7)
C7	0.0343 (10)	0.0207 (9)	0.0282 (10)	0.0049 (8)	0.0056 (8)	0.0048 (8)
C8	0.0254 (9)	0.0284 (10)	0.0213 (9)	0.0066 (8)	0.0024 (7)	0.0074 (7)
C9	0.0133 (8)	0.0350 (10)	0.0150 (8)	0.0034 (7)	0.0012 (6)	0.0031 (7)
C10	0.0146 (8)	0.0225 (9)	0.0147 (8)	0.0035 (7)	0.0022 (6)	−0.0003 (6)
C11	0.0157 (8)	0.0247 (9)	0.0174 (8)	0.0018 (7)	0.0053 (6)	−0.0017 (7)
C12	0.0154 (8)	0.0289 (9)	0.0176 (8)	−0.0016 (7)	0.0030 (6)	−0.0019 (7)
C13	0.0145 (8)	0.0255 (9)	0.0170 (8)	0.0026 (7)	0.0038 (6)	0.0023 (7)
C14	0.0129 (8)	0.0237 (9)	0.0143 (8)	0.0016 (6)	0.0031 (6)	0.0008 (6)
C15	0.0178 (8)	0.0171 (8)	0.0194 (8)	0.0009 (6)	−0.0007 (6)	−0.0001 (6)
C16	0.0199 (8)	0.0167 (8)	0.0165 (8)	−0.0003 (6)	−0.0010 (7)	0.0001 (6)
C17	0.0214 (8)	0.0173 (8)	0.0215 (8)	−0.0021 (7)	0.0002 (7)	0.0003 (7)
C18	0.0285 (10)	0.0305 (10)	0.0199 (9)	0.0001 (8)	−0.0054 (7)	0.0034 (7)

C19	0.0205 (8)	0.0203 (9)	0.0171 (8)	−0.0021 (7)	−0.0007 (7)	−0.0006 (7)
C20	0.0184 (9)	0.0339 (10)	0.0284 (9)	0.0070 (8)	0.0043 (7)	−0.0024 (8)
C21	0.0247 (10)	0.0470 (12)	0.0322 (10)	0.0123 (9)	−0.0033 (8)	−0.0035 (9)
C22	0.0280 (10)	0.0439 (11)	0.0194 (9)	−0.0033 (9)	−0.0035 (8)	0.0066 (8)

Geometric parameters (Å, °)

O1—N1	1.4262 (17)	C8—C13	1.428 (2)
O1—C17	1.3433 (19)	C9—C12	1.396 (2)
O2—C19	1.2075 (18)	C9—C13	1.398 (2)
O3—C19	1.3348 (18)	C10—C11	1.407 (2)
O3—C20	1.4523 (19)	C10—C14	1.408 (2)
O4—C9	1.3860 (19)	C10—C15	1.485 (2)
O4—C22	1.426 (2)	C11—C12	1.435 (2)
N1—C15	1.309 (2)	C13—C14	1.431 (2)
C1—H1	0.9500	C15—C16	1.436 (2)
C1—C2	1.353 (3)	C16—C17	1.363 (2)
C1—C12	1.433 (2)	C16—C19	1.467 (2)
C2—H2	0.9500	C17—C18	1.484 (2)

C2—C3	1.414 (3)	C18—H18A	0.9800
C3—H3	0.9500	C18—H18B	0.9800
C3—C4	1.354 (2)	C18—H18C	0.9800
C4—H4	0.9500	C20—H20A	0.9900
C4—C11	1.432 (2)	C20—H20B	0.9900
C5—H5	0.9500	C20—C21	1.499 (2)
C5—C6	1.358 (2)	C21—H21A	0.9800
C5—C14	1.429 (2)	C21—H21B	0.9800
C6—H6	0.9500	C21—H21C	0.9800
C6—C7	1.414 (2)	C22—H22A	0.9800
C7—H7	0.9500	C22—H22B	0.9800
C7—C8	1.356 (2)	C22—H22C	0.9800
C8—H8	0.9500		
C17—O1—N1	109.30 (11)	C9—C13—C8	121.85 (15)
C19—O3—C20	118.06 (12)	C9—C13—C14	119.07 (14)
C9—O4—C22	113.18 (12)	C5—C14—C13	117.62 (14)
C15—N1—O1	105.33 (12)	C10—C14—C5	122.86 (14)

C2—C1—H1	119.7	C10—C14—C13	119.51 (14)
C2—C1—C12	120.68 (16)	N1—C15—C10	119.67 (14)
C12—C1—H1	119.7	N1—C15—C16	111.30 (14)
C1—C2—H2	119.8	C16—C15—C10	129.01 (14)
C1—C2—C3	120.32 (16)	C15—C16—C19	129.34 (14)
C3—C2—H2	119.8	C17—C16—C15	104.71 (14)
C2—C3—H3	119.4	C17—C16—C19	125.94 (14)
C4—C3—C2	121.11 (17)	O1—C17—C16	109.35 (14)
C4—C3—H3	119.4	O1—C17—C18	116.66 (14)
C3—C4—H4	119.4	C16—C17—C18	133.96 (15)
C3—C4—C11	121.10 (17)	C17—C18—H18A	109.5
C11—C4—H4	119.4	C17—C18—H18B	109.5
C6—C5—H5	119.3	C17—C18—H18C	109.5
C6—C5—C14	121.49 (15)	H18A—C18—H18B	109.5
C14—C5—H5	119.3	H18A—C18—H18C	109.5
C5—C6—H6	119.7	H18B—C18—H18C	109.5
C5—C6—C7	120.53 (16)	O2—C19—O3	123.86 (15)

C7—C6—H6	119.7	O2—C19—C16	125.26 (15)
C6—C7—H7	119.8	O3—C19—C16	110.88 (13)
C8—C7—C6	120.30 (16)	O3—C20—H20A	110.5
C8—C7—H7	119.8	O3—C20—H20B	110.5
C7—C8—H8	119.5	O3—C20—C21	106.02 (13)
C7—C8—C13	120.97 (15)	H20A—C20—H20B	108.7
C13—C8—H8	119.5	C21—C20—H20A	110.5
O4—C9—C12	119.34 (15)	C21—C20—H20B	110.5
O4—C9—C13	118.58 (15)	C20—C21—H21A	109.5
C12—C9—C13	122.05 (15)	C20—C21—H21B	109.5
C11—C10—C14	120.85 (14)	C20—C21—H21C	109.5
C11—C10—C15	120.31 (14)	H21A—C21—H21B	109.5
C14—C10—C15	118.80 (14)	H21A—C21—H21C	109.5
C4—C11—C12	117.56 (15)	H21B—C21—H21C	109.5
C10—C11—C4	122.94 (15)	O4—C22—H22A	109.5
C10—C11—C12	119.48 (14)	O4—C22—H22B	109.5
C1—C12—C11	119.21 (15)	O4—C22—H22C	109.5

C9—C12—C1	121.82 (15)	H22A—C22—H22B	109.5
C9—C12—C11	118.97 (15)	H22A—C22—H22C	109.5
C8—C13—C14	119.07 (15)	H22B—C22—H22C	109.5
O1—N1—C15—C10	−177.98 (13)	C11—C10—C14—C5	−179.10 (14)
O1—N1—C15—C16	0.40 (17)	C11—C10—C14—C13	1.0 (2)
O4—C9—C12—C1	1.7 (2)	C11—C10—C15—N1	−72.2 (2)
O4—C9—C12—C11	−179.18 (13)	C11—C10—C15—C16	109.79 (19)
O4—C9—C13—C8	−0.3 (2)	C12—C1—C2—C3	0.4 (3)
O4—C9—C13—C14	−179.69 (13)	C12—C9—C13—C8	177.59 (15)
N1—O1—C17—C16	−0.65 (17)	C12—C9—C13—C14	−1.8 (2)
N1—O1—C17—C18	177.80 (13)	C13—C9—C12—C1	−176.22 (15)
N1—C15—C16—C17	−0.79 (18)	C13—C9—C12—C11	2.9 (2)
N1—C15—C16—C19	179.49 (15)	C14—C5—C6—C7	0.5 (2)
C1—C2—C3—C4	−0.8 (3)	C14—C10—C11—C4	178.65 (14)
C2—C1—C12—C9	179.94 (16)	C14—C10—C11—C12	0.2 (2)
C2—C1—C12—C11	0.8 (2)	C14—C10—C15—N1	110.33 (17)
C2—C3—C4—C11	0.1 (3)	C14—C10—C15—C16	−67.7 (2)

C3—C4—C11—C10	−177.46 (15)	C15—C10—C11—C4	1.2 (2)
C3—C4—C11—C12	1.1 (2)	C15—C10—C11—C12	−177.29 (14)
C4—C11—C12—C1	−1.5 (2)	C15—C10—C14—C5	−1.6 (2)
C4—C11—C12—C9	179.36 (15)	C15—C10—C14—C13	178.48 (13)
C5—C6—C7—C8	0.4 (3)	C15—C16—C17—O1	0.85 (17)
C6—C5—C14—C10	179.19 (15)	C15—C16—C17—C18	−177.22 (17)
C6—C5—C14—C13	−0.9 (2)	C15—C16—C19—O2	175.21 (16)
C6—C7—C8—C13	−0.8 (3)	C15—C16—C19—O3	−4.6 (2)
C7—C8—C13—C9	−179.00 (15)	C17—O1—N1—C15	0.15 (16)
C7—C8—C13—C14	0.4 (2)	C17—C16—C19—O2	−4.4 (3)
C8—C13—C14—C5	0.5 (2)	C17—C16—C19—O3	175.79 (15)
C8—C13—C14—C10	−179.59 (14)	C19—O3—C20—C21	−174.81 (14)
C9—C13—C14—C5	179.86 (14)	C19—C16—C17—O1	−179.42 (14)
C9—C13—C14—C10	−0.2 (2)	C19—C16—C17—C18	2.5 (3)
C10—C11—C12—C1	177.07 (14)	C20—O3—C19—O2	−5.8 (2)
C10—C11—C12—C9	−2.1 (2)	C20—O3—C19—C16	174.02 (13)
C10—C15—C16—C17	177.39 (15)	C22—O4—C9—C12	85.45 (18)

C10—C15—C16—C19	−2.3 (3)	C22—O4—C9—C13	−96.56 (17)

Hydrogen-bond geometry (Å, °)

D—H⋯A	D—H	H⋯A	D⋯A	D—H⋯A
C18—H18B⋯O2	0.98	2.50	3.133 (2)	122
C21—H21A⋯O2[i]	0.98	2.58	3.371 (2)	138

Symmetry code: (i) $x+1/2, -y+3/2, -z$.

All e.s.d.'s (except the e.s.d. in the dihedral angle between two l.s. planes) are estimated using the full covariance matrix. The cell e.s.d.'s are taken into account individually in the estimation of e.s.d.'s in distances, angles and torsion angles; correlations between e.s.d.'s in cell parameters are only used when they are defined by crystal symmetry. An approximate (isotropic) treatment of cell e.s.d.'s is used for estimating e.s.d.'s involving l.s. planes.

Supplementary References

(28)   Gore, P. H.; Gupta, S. D.; Obaji, G. A. Anomalous Reactions of Cyanide with Two Hindered Aromatic Aldehydes. *J. Für Prakt. Chem.* **1984**, *326* (3), 381–384.

(29)   Vellis, P. D.; Mikroyannidis, J. A.; Bagnis, D.; Valentini, L.; Kenny, J. M. New Anthracene-Containing Phenylene- or Thienylene-Vinylene Copolymers: Synthesis, Characterization, Photophysics, and Photovoltaics. *J. Appl. Polym. Sci.* **2009**, *113* (2), 1173–1181.

Chapter 4

3-Aryl isoxazoles exhibit atropisomerism

4.1 Introduction

3-Aryl isoxazole amides (AIMs) exhibit robust anticancer activity in the *in vitro* NCI Developmental Therapeutics Program's 60 cell line protocol (NCI 60), comparable to several agents currently in general medical practice (such as bleomycin and rubidazone)[1]. It is hypothesized that unsymmetrical AIMs should exhibit enantioselectivity of action at our putative target, G-Quadruplex (G4) DNA. Calculations at the B3LYP/6-31G* level of theory indicated that the barrier to rotation in many examples should be consistent with isolable atropoisomers, that is, in the range of 23.2 - 25.6 kcal/mole[2]. Nitrile oxide cycloaddition using unsymmetrical naphthyl-nitrile oxides gave isoxazoles in modest to good yields. Reaction of acid chlorides with (S)-2-butyl amine gives diastereomeric 3-aryl isoxazolyl amides which were studied by dynamic NMR. The barrier to rotation about the chiral axis in **8g** was determined by line-shape analysis to be approximately 18.4 kcal/mole.

4.2 Atropisomerism

Chapter 3 examined structure-activity relationship (SAR) of AIMs, although the plausibility of restricted rotation at the aryl-isoxazole ring juncture has not yet been examined. Atropisomerism or axial chirality is non-superimposability of an organic compound about a hindered axis. These molecules should result in isolable enantiomers should they meet the so-called Oki criteria of having a barrier of 22.3 kcal/mol at 300°K and a half-life of approximately 1000s (16.7 min).[2]

Scan point 9
+21 kcal/mole

T.S. 24.5 kcal/mole

Scan point 10 +10 kcal/mole

Dihedral angle 102
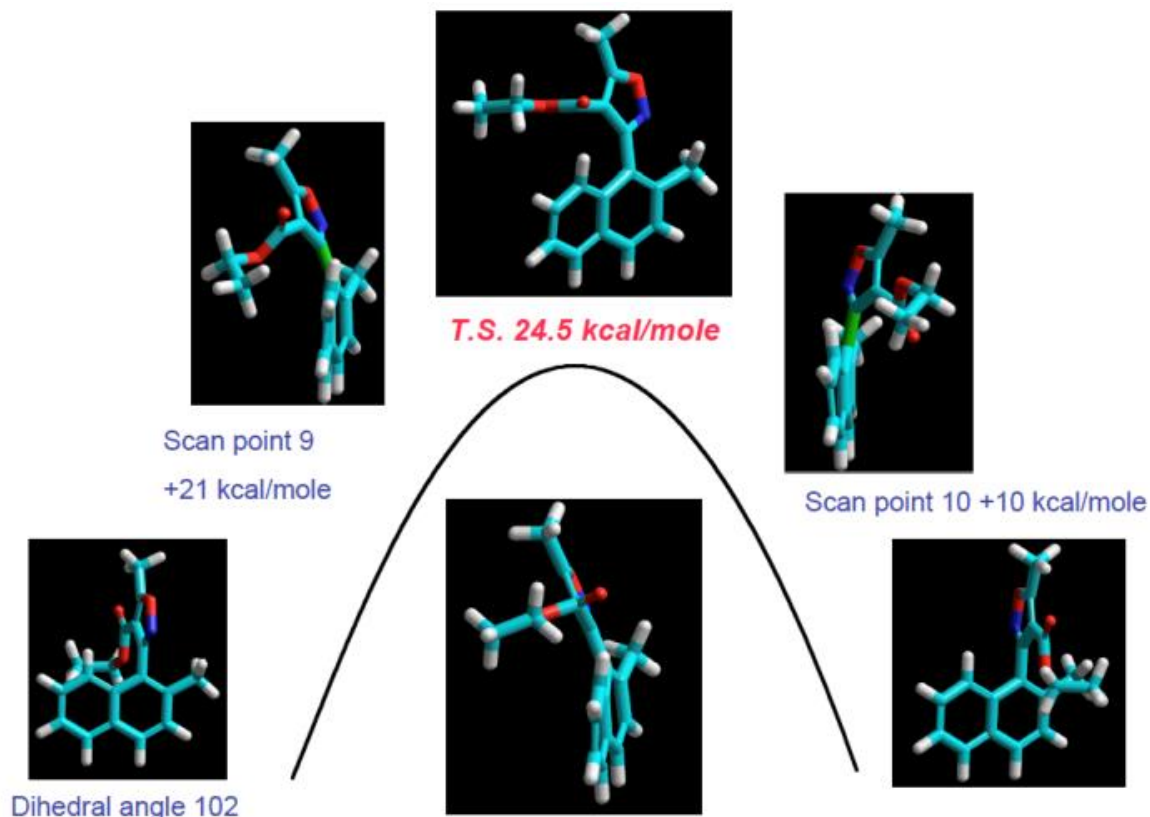
Figure 4-1. Transition state for compound **8g.**

We tested the plausibility of axially chiral isoxazoles employing calculations at the

B3LYP/6-31G* level of theory. The results on number of examples are summarized in Table 4-

1.[3, 4] The structure was rotated through increments of 10°, and again minimized. A transition is

shown in Figure 4-1, where the isoxazolyl 4-moiety must move out of conjugation with the

isoxazole in order to pass by the peri-proton, and represents the usual saddle point significant

deformation at the aromatic ring and lengthening of the isoxazole-3-aryl single bond is observed.

A compensating factor, however, is that the isoxazole at this juncture moves into conjugation

with the 3-aryl functionality. Substituents were varied at the C-4 position (esters **5**, amides **8**) and

C-5 (2-methyl and 2-methoxy naphthyl, 1- and 2,10-dimethoxy-anthracenyl) , and we observed

that were in the range (23.2 to 25.6 kcal/mole) where the isolation of rotomers would be expected to indeed be possible.

4.3 Dynamic NMR

If a molecule exists in two interconvertible conformations, both approximately equally populated, it may show, depending on the frequency of interconversion, either the nuclear magnetic resonance spectra corresponding to the individual conformations or an average spectrum of confirmations A and B. If one has two conformations A and B in equilibrium in a substance and one heats the substance until a given pair of resonance lines due to A and B just coalesces (or if, originally, there was only one set of lines, if one cools the substance until the resonance lines just begin to split), this temperature is called the coalescence temperature T_c.[2, 5] Molecules are in constant motion, and the different conformations which are interconverted by bond rotations and other molecular gymnastics often have different NMR spectra. Variable-temperature NMR, often referred to as dynamic NMR (DNMR), can be used to study the kinetics of these exchanges.[5]

The energy of activations, E_A, for a simple reaction such as the rotation of amides can be accessed from the Arrhenius equation for the reaction rate, k.

$$k = A^{-\frac{EA}{RT}} \tag{1}$$

If in equation 1, R is a gas constant, T the absolute temperature and A roughly corresponds to the fraction of species that reaches the transition state and successfully passes over the product side of the reaction. A is usually referred as the pre-exponential term and represents the frequency of collisions between reactant molecule, is called a 'constant' in spite of the fact that it does vary a little with T.

A different approach gives the Eyring equation

$$k_c = K \text{ k}_\text{B}\text{T/h}^{-\Delta\text{G}\ddagger/\text{RT}} \tag{2}$$

$$\text{or } \Delta G \ddagger = RT \left(\ln\frac{k_B}{h} + lnT - lnk_c\right) \tag{3}$$

In this, k is the rate constant, k_B is the Boltzmann constant, h is the Planck constant and $\Delta\text{G}\ddagger$ is the free energy of activation ($\Delta\text{G}\ddagger = \Delta\text{H}\ddagger - \text{T}\Delta\text{S}\ddagger$). The kinetic constant (*k* value) is obtained at each given temperature and the free energy of activation ($\Delta G\ddagger$) can then be derived by means of Equation (3), above giving the activation energy to reach the transition state.[5]

The 'constant' K is analogous to the 'constant' A in the Arrhenius equation and is likewise subject to variation in non-simple reactions: it relates the 'reaction success rate'. Provided the transition state can easily transfer energy to the surroundings (and this is commonly true in large molecules), the K is near unity. For a *mutual exchange* or *mutual site exchange* (in which the exchange produces indistinguishable molecules) and for first-order cases, H.S. Gutowsky showed that the rate of rotation, k_c, at the temperature of coalescence, T_c, is given by

$$k_c = \pi \Delta v/\sqrt{2} \tag{4}$$

The lifetime, t_c, of the separate isomers at the point of coalescence is the reciprocal of the rate, $1/k_c$.

Using these equations allows $\Delta G\ddagger$ values between about 4.5 and about 23 kcalmol^{-1} to be determined. The temperature ranges over which *k* values can be accurately measured by DNMR technique are usually quite small. A number of books and reviews have previously been devoted to describing the applications of DNMR in conformational analysis [2,5,6]. An example of a variable temperature NMR is shown in Figure 4-2 for compound **9** showing the coalescence point at about 43°C. Table 4-2 shows the experimental DNMR calculations for the set of compounds, which are still in progress and will be reported in due course.

4.4 Bond Rotation

The discovery of bioactive natural products containing chiral axes, as well as, catalysts changed the concept of axial chirality in rotationally hindered systems. The most popular systems used for asymmetric synthesis contain the binaphthyl scaffold, such as BINAP or BINOL[5][7]. The putative diastereomers of the 3-aryl isoxazoles were expected to show non-equivalence in the NMR if the barrier to rotation was sufficiently high to provide for slow exchange of the atropoisomers at any temperature. The 3-(2-methoxyphenyl) derivative **2** indicated no observed non-equivalence, even at reduced temperature in the NMR. This is in reasonable agreement with a calculated low barrier to rotation. The 3-(2-methoxy-naphthlyl) **8** isoxazole indicated broadening of several signals at room temperature.

Examination of the 3-(2-methylnaphthyl) analog **7** showed clear non-equivalence in both deuterochloroform and DMSO. Variable temperature NMR indicated gradual broadening of the signals, and coalescence at about 140°C. Because the signals being examined were coupled, line shape analysis was used to ascertain the experimental rotational barrier, which was found to be approximately 18 kcal/mole. This barrier amply demonstrates the plausibility of axial chirality in this system. The discrepancy between the experimental and theoretical barriers could be from an underestimation of the energy necessary for aromatic ring deformation or bond lengthening along the isoxazole-3-aryl axis at the saddle point, or overestimation of the energy gained from conjugation of the isoxazole and naphthalene ring, since the peri-proton of the latter provides an apparent encumbrance to full conjugation between these rings. Clearly, while further computational and experimental studies are warranted, atropoisomeric isoxazoles can indeed exist and potentially exist long enough allowing to isolate and analytical separation if the half-life of the interconversion is ~1000 s (16.7 min) or longer. [2,7]

8a. R_1 = CH$_3$, R_2 = H
8b. R_1 = OCH$_3$, R_2 = H
8c. R_1 = Cl, R_2 = H
8d. R_1 = CH$_3$, R_2 = Cl
8e. R_1 = Br, R_2 = H

8f. R_1 = H
8g. R_1 = CH$_3$
8h. R_1 = OCH$_3$
8i. R_1 = OCH$_2$C$_6$H$_5$

9a. R_1 = OCH$_3$, R_2 = OCH$_3$, R_3 = H
9b. R_1 = OCH$_3$, R_2 = OCH$_3$, R_3 = Cl
9c. R_1 = Br, R_2 = Br, R_3 = H
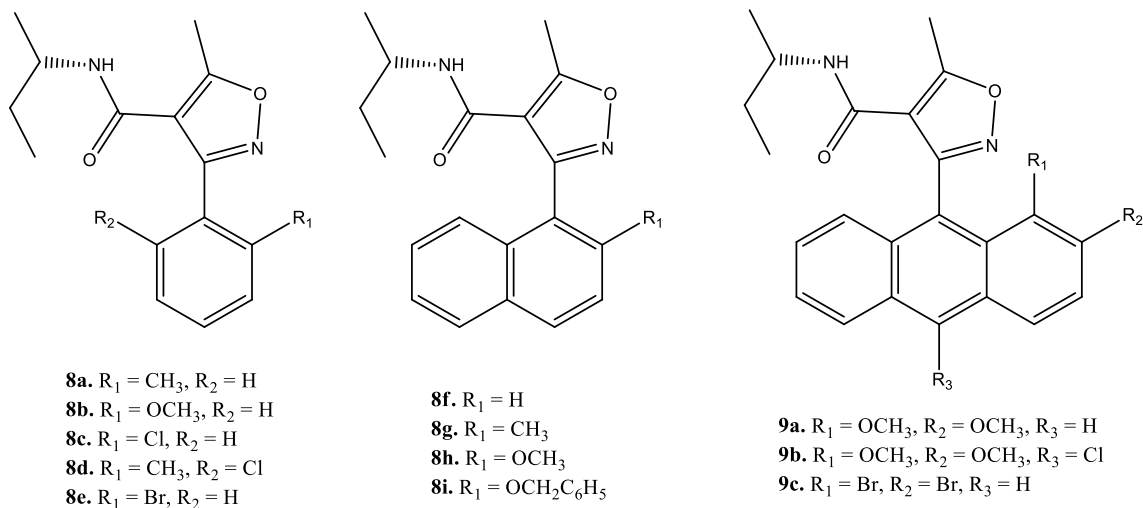
Compound	$\Delta H^{\ddagger}$ (Expt)	$\Delta S^{\ddagger}$ (Expt)	$\Delta G^{\ddagger}$ (Expt)	$\Delta H^{\ddagger}$ (Calc)	$\Delta G^{\ddagger}$ (Calc)
8a	submitted				
8b	-4.1		-6.16*	-7.8	-9.7
8c	submitted				
8d	submitted		NMR-2 diast.		
8e	submitted				
8f	submitted			-14.2	-15.5
8g doublet	-13.8±0.1	-15.3±0.1	-18.4±0.2	-20.7	-24.6
8g triplet	-12.5±0.1	-18.5±0.1	-18.0±0.2		
8h	-10.9±0.05	-8.9±0.1	-13.6±0.1	-22.3	-24.7
8i	-7.84±0.02	-10.1±0.2			
9a	submitted		~18		
9b	submitted		Locked 200°C		
9c	submitted		Locked 85°C		

Activation barriers in cal/mol

Table 4-1. Computational and /or experimental barriers at the 3-aryl-isoxazole junction.

As determined by variable temperature NMR.
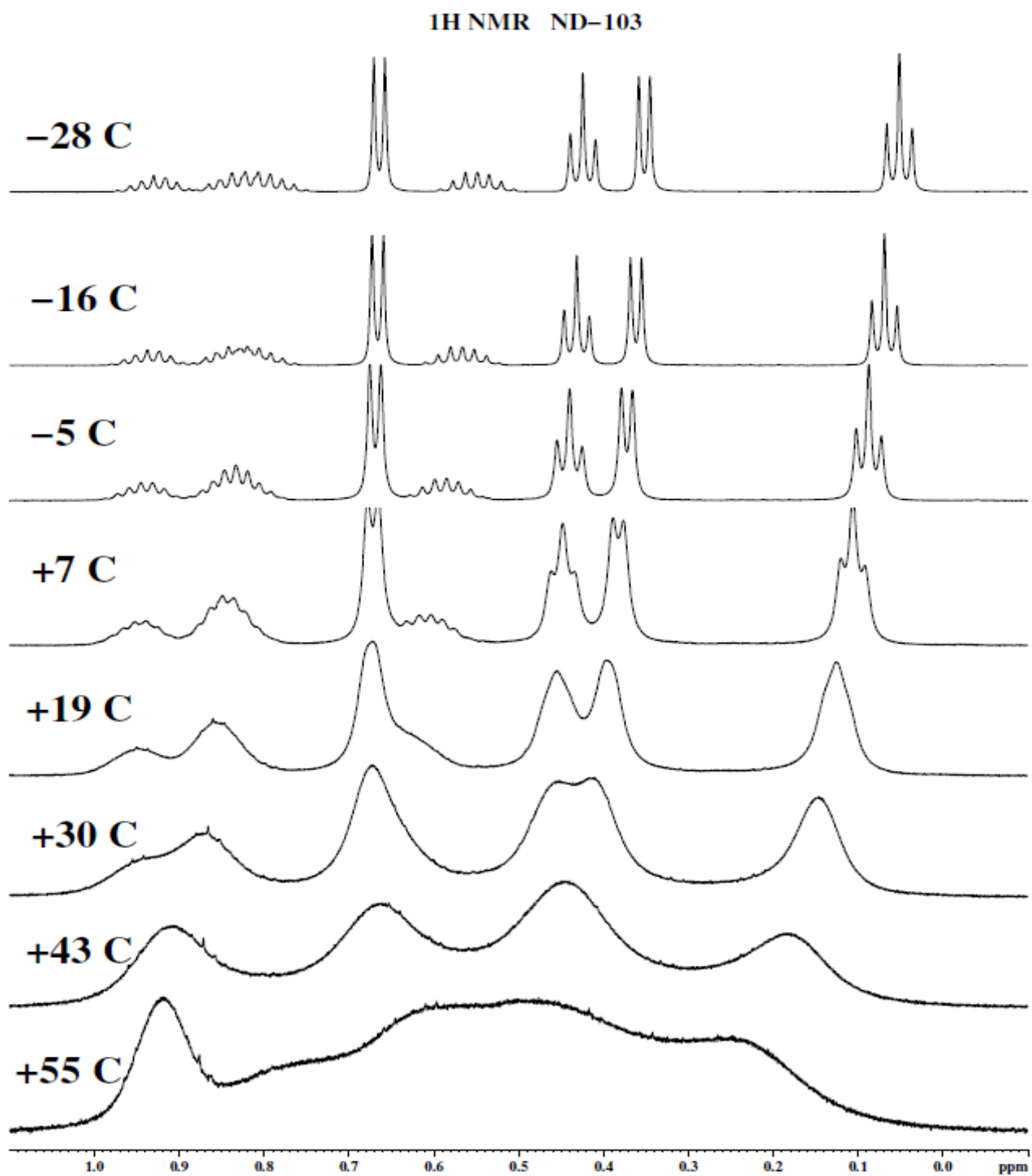
Figure 4-2. Variable temperature NMR of compound **8i**.

4.5 Synthesis of desired Anthryl-isoxazole-secbutyl amides and doubletails

The synthesis for the phenyl and naphthyl series shown in Scheme 4-1 was carried based upon work done by the Natale group.[8] From the ester, the synthesis was carried out in a similar manner to that of Scheme 4-2 with hydrolysis with potassium hydroxide and subsequent acid chloride reaction with thionyl chloride. The final step uses a modified Schotten-Baumann reaction with a one-phase organic solvent system with trimethylamine base.

Biehl and coworkers have described a facile route for the formation of unsymmetrical anthracenes using novel benzyne chemistry.[9] The more modern of the techniques provides a considerably safer and more convenient pathway where the generation of hydrogen cyanide gas, on the molar scale, is not required.[10] Using the Biehl aryne technique it was possible to generate the first potentially axially chiral anthracene isoxazole ester system (Scheme 4-2).

Scheme 4-2 depicts the route used to synthesize **15** using the Biehl aryne technique. As mentioned above, the important 2-acylphenylacetonitrile intermediate **10** was synthesized via a more facile route[10]. The Price method[11] was given up as too dangerous *in lieu* of the recently published route proposed by Canepa and Bravo.[10] The Canepa synthesis utilizes Ethyl o-toluate as a substrate for radical bromination of the ortho methyl group using N-Bromo succinamide (Scheme 4-2) in Carbon Tetrachloride (CCl_4). The expense of CCl_4 is often prohibitive for large scale reactions but with careful collection, washing, and recycling this solvent can be reused many times over. This product **10** can thus be obtained in a safe manner and in higher yield[21] than the Price method. Scheme 5-2 outlines the aryne synthesis combined with the method used by Natale and coworkers[22] to generate unsymmetrical anthracene isoxazole ester **15** with a large degree of selectivity that contradicts the findings of Stevens.[12] Again, with this benzyne reaction, there is a substantial learning curve where optimal yields of the nitrile **11** are only obtained when

the second addition, via cannula, of Lithium Diisopropyl Amine (LDA) is performed very slowly (*ca*. 20 min.). Subsequent methylation of the C-10 hydroxyl group was achieved with the addition of a three-fold excess of dimethylsulfate in refluxing THF until the color turns a deep yellow-green yielding **12**. The structure of the 2,10-dimethoxy-1-cyano **12** was confirmed by single crystal x-ray diffractometry

Attempts were made to reduce the unsymmetrical anthracene nitrile using DIBAL-H in solutions of Hexanes (insoluble nitrile) and THF, but no aldehyde was obtained after hydrolysis using 10% aqueous sulfuric acid. Full reduction of the anthracene nitrile, in <5 hours at 0°C, was obtained when DIBAL-H in toluene was employed. Hydrolysis, using 5% aqueous sulfuric acid, gave the unsymmetrical anthracene aldehyde **13** in ~70% yield. Reaction of **13** with hydroxyl amine hydrochloride in chloroform afforded the oxime **14** in ~95% yield. Formation of the oximinoyl chloride intermediate was performed using recrystallized N-Chlorosuccinamide (from benzene) and dry ethanol at 0°C (yield not calculated). Finally, the intermediate was reacted with the ethyl acetoacetate and sodium alkoxide in absolute ethanol to give the final product **15** in 70% yield (not optimized) after two steps.
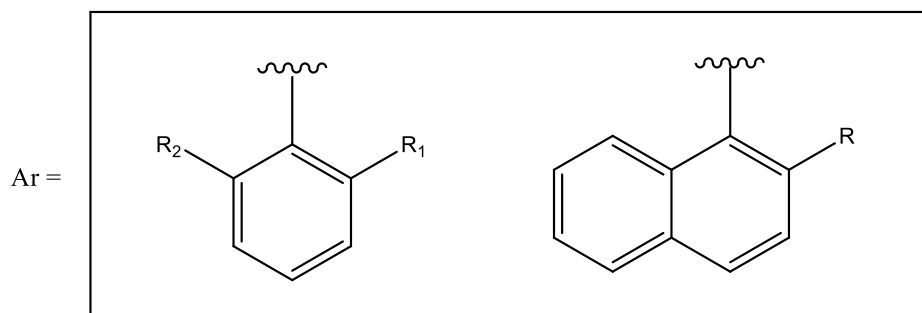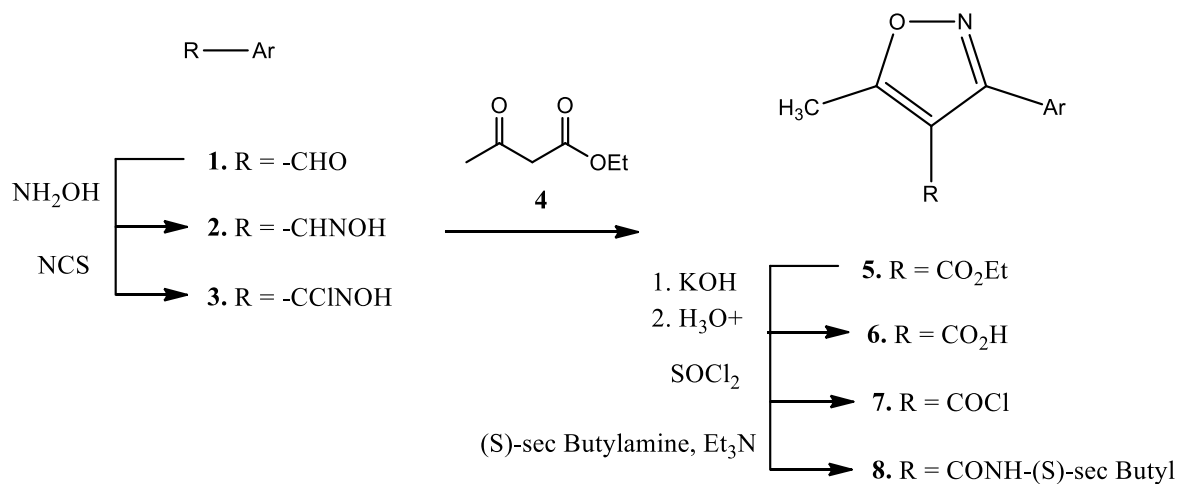
Scheme 4-1. Synthesis of phenyl and naphthyl sec-butyl amides **8a, c-d, f, i**.
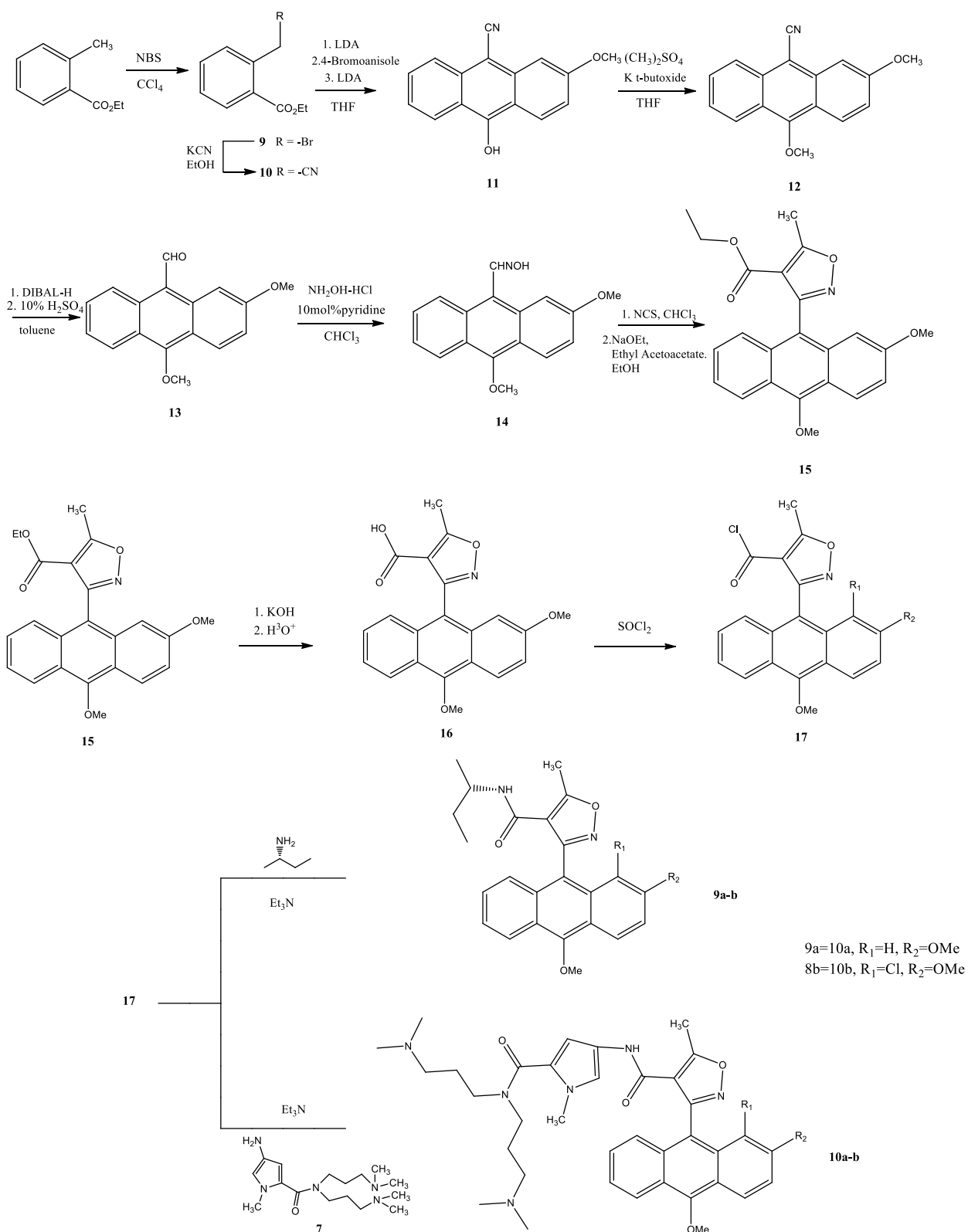
Scheme 4-2. Synthesis of anthryl-sec butyl amides **9a-b** and anthryl-DT conjugate **10a-b.**

9a=10a, R$_1$=H, R$_2$=OMe
8b=10b, R$_1$=Cl, R$_2$=OMe

4.6 Crystal Structure of 12

Within the unit cell, evidence of the 10-methoxy methyl hydrogens show van der Waals interactions to the 10-methoxy oxygen in the molecule directly below. While the 2-methoxy oxygen and 3-H proton on the same molecule both have interactions with the 3-H and 2-methoxy oxygen, respectively, in the molecule directly parallel to it. Thus, the unit cell shows molecule flips both horizontally and vertically for each column structure. Full sc-xrd data and parameters are given in the Supplementary Data.
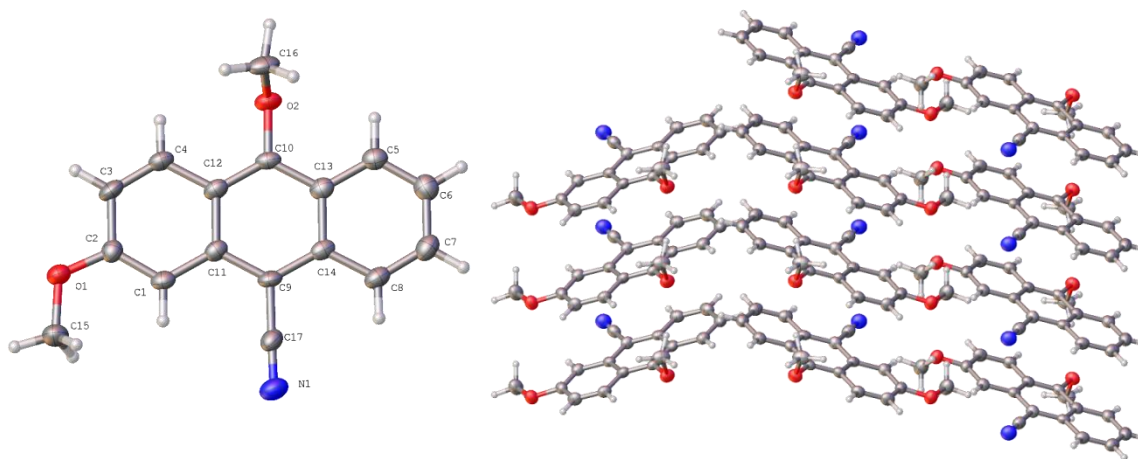
Figure 4-3. Single crystal x-ray structure of **12**.

4.7 MTT Cell Viability Assay

Growth inhibition was determined by the MTT colorimetric assay. Cells were plated in 96-well plates at a density of 10,000 cells/mL and allowed to attach overnight (16-18h). AAIM solutions were applied in medium for 24 h, removed, and replaced with fresh medium, and the plates were incubated at 37 °C under a humidified atmosphere containing 5% CO_2 for 3−5 days. MTT (50 μg) was added and the cells were incubated for another 4 h. Medium/MTT solutions were removed carefully by aspiration, the MTT formazan crystals were dissolved in 100 μL of DMSO, and absorbance was determined on a plate reader at 560 nm. IC_{50} values (concentration

at which cell survival equals 50% of control) were determined from semilog plots of percent of control versus concentration. Two compounds shown in Table 4-2 have low micromolar binding affinities, in which the addition of the methoxy group does correlate to better activity versus a single methoxy group shown in Chapter 3.[13]

	IC_{50}	R_3	R_2	R_1
10a	4.80 μM ± 0.80	—CH$_3$	—OCH$_3$	H
10b	12.57 μM ± 1.51	—CH$_3$	—OCH$_3$	—Cl

Table 4-2. Cytotoxicity activity of **10a-b** against human glioma SNB-19 cells.

4.8 Summary

Anthryl-10-alkoxy-isoxazole-pyrrole-doubletails can be readily made and easily substituted to enlarge the oxy-ether library series. Current studies are focused on whether the AAIMs may represent useful tools for the study of quadruplex DNA, and ultimately lead to clinically useful inhibitors. We have provided experimental verifcation of atropisomerism in 3-aryl isoxazoles, which was suggested from computation. Our original motivation for this study sprang from the concept that anti-cancer activity of the related AIMs might exhibit a eudismic ratio, and hence increased efficacy. We shall report on our progress in this arena in due course.

References

(1)   Han, X.; Li, C.; Mosher, M. D.; Rider, K. C.; Zhou, P.; Crawford, R. L.; Fusco, W.; Paszczynski, A.; Natale, N. R. Design, Synthesis and Biological Evaluation of a Novel Class of Anticancer Agents: Anthracenylisoxazole Lexitropsin Conjugates. *Bioorg. Med. Chem.* **2009**, *17* (4), 1671–1680.

(2)   Ernest L. Eliel; Samuel H. Wilen. *Stereochemistry of Organic Compounds*; Wiley: New York, 1994.

(3)   M. J. Frisch, G. W. Trucks, H. B. Schlegel, G. E. Scuseria, M. A. Robb, J. R. Cheeseman, V. G. Zakrzewski, J. A. Montgomery, R. E. Stratmann, J. C. Burant, S. Dapprich, J. M. Millam, A. D. Daniels, K. N. Kudin, M. C. Strain, O. Farkas, J. Tomasi, V. Barone, M. Cossi, R. Cammi, B. Mennucci, C. Pomelli, C. Adamo, S. Clifford, J. Ochterski, G. A. Petersson, P. Y. Ayala, Q. Cui, K. Morokuma, D. K. Malick, A. D. Rabuck, K. Raghavachari, J. B. Foresman, J. Cioslowski, J. V. Ortiz, B. B. Stefanov, G. Liu, A. Liashenko, P. Piskorz, I. Komaromi, R. Gomperts, R. L. Martin, D. J. Fox, , T. Keith, M. A. Al-Laham, C. Y. Peng, A. Nanayakkara, C. Gonzalez, M. Challacombe, P. M. W. Gill, B. G. Johnson, W. Chen, M. W. Wong, J. L. Andres, M. Head-Gordon, E. S. Replogle, and J. A. Pople. Gaussian 98 (Revision A.9). Gaussian, Inc., Pittsburgh, PA 1998.

(4)   Williams, R. V.; Edwards, W. D.; Mitchell, R. H.; Robinson, S. G. A DFT Study of the Thermal, Orbital Symmetry Forbidden, Cyclophanediene to Dihydropyrene Electrocyclic Reaction. Predictions to Improve the Dimethyldihydropyrene Photoswitches. *J. Am. Chem. Soc.* **2005**, *127* (46), 16207–16214.

(5)   Casarini, D.; Lunazzi, L.; Mazzanti, A. Recent Advances in Stereodynamics and Conformational Analysis by Dynamic NMR and Theoretical Calculations. *Eur. J. Org. Chem.* **2010**, *2010* (11), 2035–2056.

(6)   Stewart, W. E.; Siddall, T. H. Nuclear Magnetic Resonance Studies of Amides. *Chem. Rev.* **1970**, *70* (5), 517–551.

(7)   LaPlante, S. R.; Edwards, P. J.; Fader, L. D.; Jakalian, A.; Hucke, O. Revealing Atropisomer Axial Chirality in Drug Discovery. *ChemMedChem* **2011**, *6* (3), 505–513.

(8)   Mirzaei, Y. R.; Weaver, M. J.; Steiger, S. A.; Kearns, A. K.; Gajewski, M. P.; Rider, K. C.; Beall, H. D.; Natale, N. R. Improved Synthesis of 3-Aryl Isoxazoles Containing Fused Aromatic Rings. *Tetrahedron* **2012**, *68* (50), 10360–10364.

(9)   Bhawal, B. M.; Khanapure, S. P.; Zhang, H.; Biehl, E. R. Preparation of Anthraquinones from 10-Hydroxy-9-Anthracenecarbonitriles Obtained from a Novel Aryne Annulation Reaction. *J. Org. Chem.* **1991**, *56* (8), 2846–2849.

(10)   Cánepa, A. S.; Bravo, R. D. A Convenient Synthesis of 2-Acylphenylacetonitriles. *Synth. Commun.* **2004**, *34* (4), 579–588.

(11)   Price, C. C.; Lewis, F. M.; Meister, M. The Reaction of the Grignard Reagent with Homophthalic Anhydride. *J. Am. Chem. Soc.* **1939**, *61* (10), 2760–2762.

(12)   Stevens, R. V.; Bisacchi, G. S. An Efficient and Remarkably Regioselective Synthesis of Benzocyclobutenones from Benzynes and 1,1-Dimethoxyethylene. *J. Org. Chem.* **1982**, *47* (12), 2393–2396.

(13)   Weaver, M. J.; Kearns, A. K.; Stump, S.; Li, C.; Gajewski, M. P.; Rider, K. C.; Backos, D. S.; Reigan, P. R.; Beall, H. D.; Natale, N. R. AIMing towards Improved Antitumor Efficacy. *Bioorg. Med. Chem. Lett.*

(14)   Zamponi, G. W.; Stotz, S. C.; Staples, R. J.; Andro, T. M.; Nelson, J. K.; Hulubei, V.; Blumenfeld, A.; Natale, N. R. Unique Structure−Activity Relationship for 4-Isoxazolyl-1,4-Dihydropyridines. *J. Med. Chem.* **2003**, *46* (1), 87–96.

(15)   Anzalone, L.; Hirsch, J. A. Substituent Effects on Hydrogenation of Aromatic Rings: Hydrogenation vs. Hydrogenolysis in Cyclic Analogs of Benzyl Ethers. *J. Org. Chem.* **1985**, *50* (12), 2128–2133.

Supplementary Material

General Experimental Section

All chemicals were purchased from commercial vendors and were used without any further purification unless otherwise indicated. Solvents were reagent grade and dried just prior to use by standard methods. All reactions were performed under inert atmosphere. Tetrahydrofuran (THF) was dried over sodium/benzophenone and distilled prior to use. Triethylamine (NEt3) was dried with calcium hydride (CaH2). Melting points were determined in open capillary tubes on a Melt-Temp apparatus and are uncorrected. High resolution mass spectra (HRMS) were obtained using a Micromass electrospray ionization (ES)/time-of-flight mass spectrometry (LCTOF). Mass spectrometer samples were introduced using a Waters model 2690 separations module HPLC fitted with a C-18 reversed phase column (2.1 mm i.d., 5 cm). Flash chromatography was performed using Sorbent Technologies standard silica gel (60 Å) with reagent grade solvents using in house compressed air.

Cell Viability Assay

Growth inhibition was determined by the MTT colorimetric assay. Cells were plated in 96-well plates at a density of 10 000 cells/mL and allowed to attach overnight (16 h). Anthryl-10-oxy-isoxazole-DT solutions were applied in medium for 2 h, removed, and replaced with fresh medium, and the plates were incubated at 37 °C under a humidified atmosphere containing 5% CO_2 for 3−5 days. MTT (50 μg) was added and the cells were incubated for another 4 h. Medium/MTT solutions were removed carefully by aspiration, the MTT formazan crystals were dissolved in 100 μL of DMSO, and absorbance was determined on a plate reader at 560 nm. IC50 values (concentration at which cell survival equals 50% of control) were determined from semilog plots of percent of control versus concentration.

NMR

The 1H and 13C NMR high-resolution spectra were obtained with a Bruker AC200 (UltraShield™ 400MHz) using X-Win NMR (3.1) at ambient temperature in CDCl3 unless otherwise specified. The signal iii assignments were performed on the basis of a series of 2D experiments with *z*-gradient selection: 1H-1H DQF COSY (Correlation Spectroscopy), 1H-13C HMQC ((Heteronuclear Multiple Quantum Coherence) and 1H-13C HMBC (Heteronuclear Multiple Bond Correlation).

Preparation (S)-N-(sec-butyl)-5-methyl-3-(o-tolyl)isoxazole-4-carboxamide, 8a.

o-Tolualdehyde **1a** (4.0247 g, 37.50 mmol), hydroxylamine hydrochloride (5.3847 g), and sodium acetate·3H$_2$0 (20.4119 g) was dissolved in THF/ethanol/water (70 mL: 35 mL: 35 mL). After stirring at rt for 30 minutes, the mixture was concentrated then washed 2 x 125 H$_2$O, 2 x 125 mL Brine and 2 x 50mL EtOAc, dried over anhydrous sodium sulfate, filtered, and concentrated to produce the oxime **2a**, 4.386 g (97%). The oxime **2a** (2.5444 g, 18.825 mmol) was treated with N-Chlorosuccinimide (3.1087 g), 10mol% pyridine (5 drops) in 200mL chloroform and was heated to 40°C for 6 hours. The solution was washed with 4 x 150mL H$_2$O, 2 x 125mL Brine, and 2 x 25mL chloroform, then dried over anhydrous sodium sulfate, filtered, and concentrated to produce the product **3a**. To a solution of the nitrile oxide **3a** in ethanol (30 mL), was added ethyl acetoacetate (5.8mL) and sodium (0.8655g) in ethanol (100mL), dropwise, and the reaction mixture allowed to stir at room temperature overnight. The solution was concentrated, washed with 2 x 75mL H$_2$O, 2 x 50mL brine, then dried over anhydrous sodium sulfate, filtered, and concentrated. The crude product was purified on a flash column starting 10:1 Hex/EtOAc, 8:1 Hex/EtOAc, and 6:1 Hex/EtOAx until all product **5a** was collected, 4.3526 g, 94%. Ester **5a** (0.3315 g, 1.352 mmol) in methanol/THF (25mL:16.5mL) was refluxed in 2.1 M KOH for 2.5 h, acidified with 1N aqueous HCl, to give the carboxylic acid **6a** (0.2878g,

98%). The carboxylic acid **6a** was stir in an ice bath and allowed to warm up overnight in neat SOCl$_2$ (8mL), the mixture was then concentrated using hexanes, then dichloromethane three times and the residue was used without further purification in the next step. To acid chloride **7a** in 7mL of DCM was added (S)-sec-Butyl amine (0.1192 g) and 2 mL TEA, the mixture was stirrred at rt for 2.5 hours, after which time it was concentrated and purified by flash chromotagraphy (4:1:1 Hex/EtOAc) to give the product **8a** (0.1254 g, 34%). ^{1}H NMR (400 MHz, d-CHCl$_3$) δ ppm 7.46 (m, 1H), 7.35 (m, 3H), 4.99 (bd, J=8 Hz, 1H), 3.84 (m, 1H), 2.80 (s, 3H), 2.23 (s, 3H), 1.17 (m, 1H), 1.08 (m, 1H), 0.84 (d, J=8 Hz, 3H); 0.63 (t, J=8, 16 Hz, 3H). ^{13}C NMR (100 MHz, d-CHCl$_3$) δ ppm 174.63, 160.45, 159.64, 137.73, 130.85, 130.61, 129.70, 128.11, 126.57, 111.13, 45.97, 29.07, 19.72, 19.57, 13.20, 9.63. Accurate Mass Calculated for C$_{16}$H$_{21}$N$_2$O$_2$: 273.1603, Found: 273.1594.

Preparation of (S)-N-(sec-butyl)-3-(2-chlorophenyl)-5-methylisoxazole-4-carboxamide, 8c. Ester **5c** matched previously reported literature.[14] Ester **5c** (0.4789 g, 1.802 mmol) in methanol/THF (22mL:33mL) was refluxed in 2.1M KOH for 48 h, acidified with 1N aqueous HCl, to give the carboxylic acid **6c** (0.4301g, 96%). The carboxylic acid **6c** was stir in an ice bath and allowed to warm up overnight in neat SOCl$_2$ (10mL), the mixture was then concentrated using hexanes, then dichloromethane three times and the residue was used without further purification in the next step. The acid chloride **7c** and (S)-sec-Butyl amine (0.1581g, 1.18 eq) were dissolved in 10 mL of dry dichloromethane (dried over CaCl$_2$) with 2 mL of triethyl amine (TEA), after stirring 2.5 hours at room temperature, the product was purified by silica column (4:1 Hex:EtOAc) to give the amide **8c** (0.4797g, 96%). ^{1}H NMR (400 MHz, d-CHCl$_3$) δ ppm 7.49 (m, 4H), 4.95 (bd, J=8 Hz, 1H), 3.89 (m, 1H), 2.77 (s, 3H), 1.20 (m, 2H), 0.91 (d, J=8 Hz, 3H); 0.68 (t, J=8, 16 Hz, 3H). ^{13}C NMR (100 MHz, d-CHCl$_3$) □ ppm 174.08, 160.33, 158.11,

134.26, 131.85, 131.52, 130.21, 128.06, 127.47, 112.04, 46.26, 29.18, 19.75, 12.98, 9.70. Accurate Mass Calculated for $C_{15}H_{18}N_2O_2$: 293.1057, Found: 293.1059.

Preparation of N-((S)-sec-butyl)-3-(2-chloro-6-methylphenyl)-5-methylisoxazole-4-carboxamide, 8d.

2-chloro-6-methylbenzaldehyde **1d** (1.000 g, 6.469 mmol), hydroxylamine hydrochloride (3.5212 g), and sodium acetate·3H$_2$0 (3.5212 g) was dissolved in THF/ethanol/water (12 mL: 6 mL: 6 mL). After stirring at rt for 2.5 hours, the mixture was concentrated then washed 2 x 100 H$_2$O, 2 x 75 mL Brine and 2 x 25mL EtOAc, dried over anhydrous sodium sulfate, filtered, and concentrated to produce the oxime **2d**, 1.0965 g (99%). The oxime **2d** (1.0965 g, 6.465 mmol) was treated with N-Chlorosuccinimide (1.0679 g), 10mol% pyridine (6.5mL of 1mM stock solution) in 100mL chloroform was heated to 40°C for 5.5 hours. The solution was washed with 4 x 150mL H$_2$O, 2 x 125mL Brine, and 2 x 25mL chloroform, then dried over anhydrous sodium sulfate, filtered, and concentrated to produce the product **3d**. To a solution of the nitrile oxide **3d** in ethanol (120 mL), was added ethyl acetoacetate (2mL) and sodium (0.2973g) in ethanol (45mL), dropwise, and the reaction mixture allowed to stir at room temperature overnight. The solution was concentrated, washed with 2 x 75mL H$_2$O, 2 x 50mL brine, then dried over anhydrous sodium sulfate, filtered, and concentrated. The crude product was purified on a flash column starting 10:1 Hex/EtOAc (~220mL), then 8:1 Hex/EtOAc until all product **5d** was collected, 1.6472 g, 91%. Ester **5c** (0.4118 g, 1.472 mmol) in methanol/THF (18mL:27mL) was refluxed in 2.08 M KOH for 1 h, acidified with 1N aqueous HCl, to give the carboxylic acid **6d** (0.3322g, 90%). The carboxylic acid **6d** was stir in an ice bath and allowed to warm up overnight in neat SOCl$_2$ (8mL), the mixture was then concentrated using hexanes, then dichloromethane three times and the residue was used without further purification in the next step. To acid

chloride **7d** in 7mL of DCM was added (S)-sec-Butyl amine (0.1158 g) and 2 mL TEA, the mixture was stirrred at rt for 2.5 hours, after which time it was concentrated and purified by flash chromotagraphy (8:1:1 Hex/EtOAc/DCM, then 6:1:1) to give the product **8d** (0.247 g, 61%). ^{1}H NMR (400 MHz, d-CHCl$_3$) δ ppm 7.40 (m, 4H), 7.29 (m, 2H), 4.96 (bt, 1H), 3.87 (m, 2H), 2.82 (d, 3H), 2.19 (s, 3H), 1.24 (m, 2H), 1.08 (m, 2H), 0.91 (d, J=8 Hz, 3H), 0.83 (d, J=8 Hz, 3H), 0.70 (t, J=8, 16 Hz, 3H), 0.60 (t, J=8, 16 Hz, 3H). ^{13}C NMR (100 MHz, d-CHCl$_3$) □ ppm 175.01, 174.96, 160.23, 160.18, 157.18, 140.64, 140.51, 134.62, 134.50, 131.41, 129.06, 126.99, 127.51, 127.44, 111.18, 111.08, 46.01, 45.95, 29.17, 20.23, 20.16, 19.90, 19.84, 13.25, 13.22, 9.60, 9.53. Accurate Mass Calculated for $C_{16}H_{20}N_2O_2Cl_1$: 307.1213, Found: 307.1206.

Preparation of (S)-N-(sec-butyl)-5-methyl-3-(naphthalen-1-yl)isoxazole-4-carboxamide, 8f.

1-naphthaldehyde **1f** (2.000 g, 12.8 mmol), hydroxylamine hydrochloride (1.7789 g), and sodium acetate·3H$_2$0 (3.1499 g) was dissolved in THF/ethanol/water (64 mL: 32mL: 32 mL). After stirring at rt for overnight, the mixture was concentrated then washed 4 x 50 H$_2$O, 2 x 100 mL Brine and 2 x 25mL EtOAc, dried over anhydrous sodium sulfate, filtered, and concentrated to produce the oxime **2f**, 1.979 g (99%). The oxime **2f** (1.000 g, 12.8 mmol) was treated with N-Chlorosuccinimide (1.8801g), pyridine (2 drops) in 130mL chloroform was stirred at 40°C for 4 hours. The solution was washed with 3 x 50mL H$_2$O, 2 x 50mL Brine, and 2 x 25mL chloroform, then dried over anhydrous sodium sulfate, filtered, and concentrated to produce the product **3f**. To a solution of the nitrile oxide **3f** in ethanol (100 mL), was added ethyl acetoacetate (2mL) and sodium (0.2917g) in ethanol (150mL), dropwise, and the reaction mixture allowed to stir at room temperature overnight. The solution was concentrated, washed with 2 x 75mL H$_2$O, 2 x 50mL brine, then dried over anhydrous sodium sulfate, filtered, and concentrated. Product **5f** was collected, 1.5678 g, 79%. Ester **5f** (1.5678 g, 5.5732 mmol) in methanol/THF (22mL:22mL) was

refluxed in 2 M KOH for 3 h then allowed to cool to rt overnight, acidified with 1N aqueous HCl, to give the carboxylic acid **6f** (1.4604g, 99%). The carboxylic acid **6f** was stir in an ice bath and allowed to warm up overnight in neat $SOCl_2$ (40mL), the mixture was then concentrated using hexanes, then dichloromethane three times and the residue was used without further purification in the next step. To acid chloride **7f** in 3mL of DCM was added (S)-sec-Butyl amine (0.0695 g) and 1 mL TEA, the mixture was stirrred at rt overnight, after which time it was concentrated and purified by flash chromotagraphy using 41 Hex/EtOAc to give the product **8f** (0.1366 g, 68%). ^{1}H NMR (400 MHz, d-CHCl$_3$) δ ppm 8.05 (dd, J=8, 12 Hz, 1H), 7.95 (d, J=8 Hz, 1H), 7.58 (m, 5H), 4.79 (bd, J=8 Hz, 1H), 3.67 (m, 1H), 2.86 (s, 3H), 0.86 (m, 1H), 0.71 (m, 1H), 0.49 (d, J=8 Hz, 1H), 0.32 (t, J=8, 16 Hz, 3H). ^{13}C NMR (100 MHz, d-CHCl$_3$) δ ppm 174.63. 160.25. 158.96. 133.50. 131.48. 130.85. 128.49. 128.32. 127.65. 126.98. 125.69. 125.32. 124.94. 112.29. 45.85, 28.75, 19.30, 13.19, 9.24. Accurate Mass Calculated for $C_{19}H_{21}N_2O_2$: 309.1603, Found: 309.1594.

Preparation of 3-(2-(benzyloxy)naphthalen-1-yl)-N-((S)-sec-butyl)-5-methylisoxazole-4-carboxamide, 8i.

2-(Benzyloxy)-1-naphthaldehyde **1i** (1.000 g, 3.8124 mmol), hydroxylamine hydrochloride (0.5298 g), and sodium acetate·3H$_2$0 (1.5564 g) was dissolved in THF/ethanol/water (20 mL: 10mL: 10 mL). After stirring at rt for overnight, the mixture was concentrated then washed 4 x 50 H$_2$O, 2 x 75 mL Brine and 2 x 25mL EtOAc, dried over anhydrous sodium sulfate, filtered, and concentrated to produce the oxime **2i**, 1.057 g (95%). The oxime **2i** (1.0065 g, 3.6294 mmol) was treated with N-Chlorosuccinimide (0.5463g), pyridine (3 drops) in 40mL chloroform was stirred at room temperature for 5 hours. The solution was washed with 3 x 50mL H$_2$O, 2 x 50mL Brine, and 2 x 25mL chloroform, then dried over anhydrous sodium sulfate, filtered, and

concentrated to produce the product **3i**. To a solution of the nitrile oxide **3i** in ethanol (35 mL), was added ethyl acetoacetate (1mL) and sodium (0.150g) in ethanol (100mL), dropwise, and the reaction mixture allowed to stir at room temperature overnight. The solution was concentrated, washed with 2 x 75mL H_2O, 2 x 50mL brine, then dried over anhydrous sodium sulfate, filtered, and concentrated. Product **5i** was collected, 1.3959 g, 99%. Ester **5i** (1.0098 g, 3.629 mmol) in methanol/THF (15mL:15mL) was refluxed in 2 M KOH for 3 h then allowed to cool to rt overnight, acidified with 1N aqueous HCl, to give the carboxylic acid **6i** (1.2781g, 98%). The carboxylic acid **6i** was stir in an ice bath and allowed to warm up overnight in neat $SOCl_2$ (25mL), the mixture was then concentrated using hexanes, then dichloromethane three times and the residue was used without further purification in the next step. To acid chloride **7i** in 4mL of DCM was added (S)-sec-Butyl amine (0.0660 g) and 2 mL TEA, the mixture was stirred at rt for 24 hours, after which time it was concentrated and purified by flash chromatography using DCM to give the product **8i** (0.2478 g, 68%). ^{1}H NMR (400 MHz, d-CHCl$_3$) δ ppm 7.92 (d, J=8 Hz, 1H), 7.78 (d, J=8 Hz, 1H), 7.31 (m, 10H), 5.23 (bs, 1H), 5.19 (s, 2H), 3.65 (m, 1H), 2.82 (d, 3H), 0.87 (bs, 2H), 0.66 (bs, 2H), 0.41 (bs, 3H), 0.13 (bs, 3H). ^{13}C NMR (100 MHz, d-CHCl$_3$) □ ppm 174.22, 160.45, 155.80, 154.54, 136.21, 133.06, 132.28, 128.87, 128.48, 127.98, 127.95, 127.91, 126.83, 124.69, 123.91, 114.63, 112.64, 111.56, 71.39, 45.64, 28.78, 19.71, 19.21, 13.03, 9.22, 8.96. Accurate Mass Calculated for $C_{26}H_{27}N_2O_3$: 415.2022, Found: 415.2010.

Preparation of Ethyl 3-(2,10-dimethoxy-9-anthracenyl)-5-methyl-4-isoxazole carboxylate, 15.

To 500mL of CCl_4 was added 25.41 g (151.65 mmol) of Ethyl o-toluate (Alfa Aesar). Next, 33.470 g (20% molar excess) of N-Bromosuccinamide (NBS, recrystalized from Benzene) was added to the ester solution. The solution was brought to reflux (85°C), after five minutes the solution turned orange then changed back to clear with two layers noticeable. The solution stirred at refluxing temperature for 25 hours, cooled to room temperature and the solution was filtered off, washing with CCl_4.

The resulting pale yellow oil was column chromatographed using 20:1 Hex/EtOAc to yield the product **9**, Ethyl o-(bromomethyl)benzoate: b.p. 90-95°C spectra in agreement with literature values.[15]

The brominated phenyl ester **9** (37.6172, 154.7mmol) was taken up in 200mL of absolute ethanol at room temperature, to which solution was added an aqueous solution (25mL H_2O) of KCN (10.4938g: 154.70mmol) and the solution brought to reflux for 6 hours then cooled to room temperature. The ethanol was evaporated under vacuum then 200mL of distilled H_2O was added to the resulting solution. Chloroform (200mL) was used to extract the aqueous layer. The organic layer was then washed with 5% $HNaCO_3$ (200mL) and then with H_2O (200mL). The organic phase was dried with anhydrous sodium sulfate, filtered, and the solvent removed under reduced pressure. A very clear oil Ethyl 2-(cyanomethyl)benzoate, **10**, resulted, spectra in agreement with literature values.[10]

To a solution of freshly distilled THF (20 mL), containing 3.0196g (15.856 mmol) of **10** and stirring at -78°C under an argon atmosphere, was added 1eq. of LDA (generated at -78°C in freshly distilled THF using a 1:1 equivalence of freshly distilled diisopropyl amine and n-BuLi).

The bright orange-red solution was allowed to reaction for 15 minutes whereupon 1.02 eq (2.02 mL) of 4-bromoanisole was added via syringe. A solution containing 2 eq. of lithium diisopropyl amine (LDA) was cannulated slowly, over 1 hour, into the lithiated ester solution now at a temperature of -42°C. The resulting dark purple-black solution was allowed to stir at -42°C for an additional 30 minutes. The reaction mixture was warmed to room temperature (c.a. 2 hr) and quenched with an excess of aqueous ammonium chloride and allowed to stir 10 min. The THF was removed via rotary evaporator and the dark orange solution taken up in 150mL of CH_2Cl_2. This was washed with 200mL of 0.5M HCl whereupon the solution turned bright yellow. The organic layers were washed with 500mL of brine solution and then 500mL of deionized water. The organic phase was dried using anhydrous sodium sulfate, filtered, and the solvent removed under reduced pressure to give a dark orange solid. The solid (3.8791 g, 15.856 mmol) was taken up in freshly distilled THF (150 mL) and placed under an argon atmosphere. To this solution was added (2.341 g, 1.25 eq) of potassium tert-butoxide whereupon the solution turned orange. To this mixture was added, via syringe, $(Me)_2SO_4$ (6.015mL, 4 eq) and the solution brought to reflux (95°C). This was allowed to stir refluxing until the solution color was dark yellow-green (ca. 3.5 hrs.) and TLC revealed all of the starting material was consumed.

The resulting dark orange solid was taken up in just enough CH_2Cl_2 where it was completely soluble then ~70g of silica gel was added and solvent removed under vacuum. The resulting powder was placed on a wet (10:1 Hex/EtOAc) prepared column, covered in sea sand, and eluted with 8:1 Hexanes/Ethyl Acetate (R_f=0.50). Once the front running 4-bromoanisole was eluted from the column the solvent polarity was increased using stepwise elution of ~300ml each of 6:1, 4:1, and finally 2:1 Hex/EtOAc until the all of the product **12** was collected. 2,10-dimethoxy-9-anthracenecarbonitrile, **12**. Yield 75%, ^{1}H NMR(CDCl$_3$) δ 8.37 (d, J=8.66 Hz, 1H),

8.33 (d, J=8.66 Hz, 1H), 8.27 (d, J=9.41 Hz, 1H), 7.71 (m, 1H), 7.57 (m, 2H), 7.26 (dd, 1H), 4.19 (s, 3H), 4.06 (s, 3H); ^{13}C-NMR (CDCl$_3$) δ ^{13}C NMR (101 MHz, CHLOROFORM-*d*) δ ppm 160.45, 157.88, 137.01, 135.19, 129.15, 125.25, 125.06, 123.21, 122.93, 121.35, 120.43, 117.99, 101.63, 98.83, 77.31, 77.20, 76.68, 64.12, 55.70. MS (ESI) *m/z* 264(100, M+1), 265(21, M+1$^+$),.

Under an argon atmosphere DIBAL-H (in toluene) was added via syringe (2 mL) to a solution of **12** (0.400g: 1.5192mmol) in freshly distilled toluene (20mL) at 0°C and allowed to stir for 2 hour. H$_2$SO$_4$ (5%) was added to the toluene solution and stirred vigorously for 1 hour. The bright yellow-green solution was separated and washed with 3x100mL portions of cold H$_2$O. The toluene was not dried but rather removed by rotary evaporation. The resulting solid was chromatographed on silica starting 12:1 Hex/EtOAc followed by increasing solvent polarity stepwise using 10:1, 8:1, 6:1 yielding **13** (0.3964g, 98%). The aldehyde **13** (0.2690 g, 1.01 mmol) was then taken up in THF:EtOH:H$_2$O (25:25:18mL) to which was added NH$_2$OH·HCl (1.1671) and pyridine (10 mL) and the mixture stirred at room temperature for 1 hour. The solvent was removed by rotary evaporation and the solid taken up in CH$_2$Cl$_2$ (100mL) and washed with 2x100mL of H$_2$O and 2x50 Brine. The CH$_2$Cl$_2$ was dried with anhydrous sodium sulfate, filtered, and the solvent removed under vacuum to yield a dark green solid of **14** (99%, 0.2840g).

2,10-dimethoxy-9-anthracenecarboxaldehyde, **13**. ^{1}H NMR(CDCl$_3$) δ ^{1}H NMR (400 MHz, CHLOROFORM-*d*) δ ppm 11.41 (s, 1 H), 8.92 (d, *J*=8.91 Hz, 1 H), 8.68 (d, *J*=2.38 Hz, 1 H), 8.37 (d, *J*=8.53 Hz, 1 H), 8.30 (d, *J*=9.41 Hz, 1 H), 7.69 (m, 1 H), 7.54 (m, 1 H), 7.25 (dd, J=2.38, 9.41 Hz, 1 H), 4.18 (s, 3 H), 4.04 (s, 3 H). ^{13}C NMR (101 MHz, CHLOROFORM-*d*) δ ppm 191.37, 161.23, 159.75, 135.80, 135.61, 129.24, 124.81, 124.61, 123.45, 122.91, 122.46, 120.61, 120.52, 118.72, 101.19, 64.04, 55.50. MS (ESI) *m/z* 267(100, M+1), 268(20, M+1$^+$)

2,10-dimethoxy-9-anthracenecarboxaldehyde oxime, **14.** ^{1}H NMR(CDCl$_3$) δ ^{1}H NMR (400 MHz, CHLOROFORM-*d*) δ ppm 9.13 (s, 1 H), 8.35 (d, *J*=8.78 Hz, 1 H), 8.30 (d, *J*=8.53 Hz, 1 H), 8.24 (d, *J*=9.41 Hz, 1 H), 7.67 (d, *J*=2.01 Hz, 1 H), 7.54 (m, 1 H), 7.47 (m, 1 H), 7.20 (dd, *J*=9.41, 2.26 Hz, 1 H), 4.13 (s, 2 H), 3.98 (s, 2 H); ^{13}C NMR (101 MHz, CHLOROFORM-*d*) δ ppm 158.64, 154.59, 149.10, 132.59, 131.98, 127.10, 124.61, 124.38, 122.95, 122.81, 120.65, 120.21, 117.37, 101.52, 63.55, 55.32). MS (ESI) *m/z* 282(100, M+1), 283 (21, M+1^{+}).

The oxime **14** (0.3400 g, 1.253 mmol) was taken up in chloroform which was added recrystallized N-Chlorosuccinamide (NCS) (0.2084 g) and 10mol% pyridine. The solution was allowed to stir at 40°C for 4.5 hours whereupon the solution was washed with 4x50mL of distilled H$_2$O, 2x100 Brine and extracted with chloroform (2x25mL). The organic solvent was dried with anhydrous sodium sulfate, filtered, and removed via rotary evaporator. The intermediate was purified only through extractive isolation using water and CH$_2$Cl$_2$ and taken on to the next reaction as is. To a solution of the intermediate in absolute ethanol (35mL) was added ethylacetoacetate (0.37mL) in 9mL ethanol and 0.0341g sodium and the mixture allowed to stir at room temperature for 2 hours until TLC in 4:1 Hex/EtOAc revealed all intermediate had been consumed. Finally, the ethanol was removed via rotary evaporation and the solid chromatographed stepwise starting 12:1 Hex/EtOAc, 10:1, 8:1, 6:1, 4:1 to until all final product **15** was collected (4:1 Hex/EtOAc R$_f$=0.29, yield 64%).

Ethyl 3-(2,10-dimethoxy-9-anthracenyl)-5-methyl-4-isoxazole carboxylate, **15.** ^{1}H NMR (400 MHz, CHLOROFORM-*d*) δ ppm 8.32 (dd, *J*=8.34, 0.82 Hz, 1 H), 8.29 (d, *J*=9.41 Hz, 1 H), 7.59 (m, 1 H), 7.43 (td, *J*=8.63, 1.32 Hz, 2 H), 7.20 (dd, *J*=9.41, 2.26 Hz, 1 H), 6.83 (d, *J*=2.26 Hz, 1 H), 4.17 (s, 3 H), 3.81 (s, 3 H), 3.75 (m, 2 H), 2.93 (s, 3 H), 0.38 (t, *J*=7.09 Hz, 3 H); ^{13}C NMR (101 MHz, CHLOROFORM-*d*) δ ppm 176.19, 161.56, 160.54, 157.94, 154.20, 132.99, 132.44,

126.48, 125.20, 124.28, 124.15, 122.67, 122.40, 120.44, 119.96, 116.43, 111.08, 101.65, 63.49, 59.98, 55.15, 13.41, 12.82. HRMS (ESI) accurate mass calcd. for $C_{23}H_{22}O_5N$ $(M)^{+1}$ requires 392.1498, found 391.1480.

Ester **15** (0.1142g, 0.292 mmol) was dissolved in THF (4.5 mL) then added methanol (3.5 mL). Solution was cooled down to 0°C and aqueous KOH (0.6079g in 3.8mL H_2O) was added. The solution was then taken out of the bath allowed to stir at room temperature for 7 hours under argon until completion of the reaction as indicated by TLC. The organic solvents were removed under reduced pressure. The aqueous mixture was diluted with then diluted with water (50 mL) and 25 mL DCM and acidified to pH 2 with 1N HCl. Washed 3 x 20 mL DCM and dried over sodium sulfate, concentrated under reduced pressure to yield the carboxylic acid **16** (yield 0.1082g, 100%).

To the carboxylic acid **16** at 0°C was added cold excess neat thionyl chloride (6 mL). The solution was taken out of the ice bath and allowed to warm up and stir at room temperature for 2.75 hrs under a drying tube equipped with $CaCl_2$ and NaOH. The reaction mixture was concentrated under reduced pressure. The mixture was then concentrated using hexanes, then dichloromethane three times and the residue was used without further purification in the next step. The mixture of **17** was divided in two separate round bottoms for the next step.

To half of the acid chloride **17** in 3 mL of DCM was added (S)-sec-Butyl amine (0.0128 g) and 1 mL TEA, the mixture was stirred at rt for 21 hr, after which time it was concentrated and purified by flash chromatography starting 8:1 Hex/EtOAc then 6:1, 4:1, 2:1, 1:1 until all product was collected **8f** (0.0178 g, 58%) and **8g** (0.0092 g, 29%)

To the other half of acid chloride **17** in 5 mL of DCM was added **7** (0.07250 g) and 1 mL TEA, the mixture was stirrred at rt for 19 hr, after which time it was concentrated and purified by

prep-plate using 10:10:3 DCM:DCM/NH4OH:MeOH until all product was collected **9f** (0.0209 g, 55%) and **9g** (0.0145 g, 29%).

N-((S)-sec-butyl)-3-(2,10-dimethoxyanthracen-9-yl)-5-methylisoxazole-4-carboxamide, 9a.

^{1}H NMR (400 MHz, *d*-CHCl$_3$) δ ppm ^{1}H NMR (400 MHz, CHLOROFORM-*d*) δ ppm 8.34 (m, 1 H), 8.30 (dd, *J*=9.54, 3.01 Hz, 1 H), 7.60 (m, 1 H), 7.50 (m, 2 H), 7.23 (dt, *J*=9.44, 2.49 Hz, 1 H), 6.80 (dd, *J*=4.58, 2.32 Hz, 1 H), 4.72 (t, *J*=6.59 Hz, 1 H), 4.18 (s, 3 H), 3.82 (s, 3 H), 3.53 (m, 1 H), 2.96 (s, 3 H), 0.72 (m, 1 H), 0.42 (m, 1 H), 0.30 (dd, *J*=18.70, 6.53 Hz, 3 H), 0.05 (dt, *J*=19.10, 7.45 Hz, 3 H). ^{13}C NMR (100 MHz, *d*-CHCl$_3$) δ ppm 175.40, 160.11, 158.99, 158.00, 155.39, 133.43, 133.29, 132.59, 132.46, 127.84, 124.93, 124.90, 124.84, 124.74, 124.60, 124.56, 122.97, 122.89, 122.70, 122.67, 120.92, 120.87, 120.65, 120.55, 114.28, 112.69, 100.99, 100.90, 63.75, 55.40, 55.37, 45.45, 28.59, 28.53, 19.30, 19.24, 13.49, 8.76, 8.70. Accurate Mass Calculated for C$_{25}$H$_{27}$N$_2$O$_4$: 419.1971, Found: 417.1959

N-((S)-sec-butyl)-3-(1-chloro-2,10-dimethoxyanthracen-9-yl)-5-methylisoxazole-4-carboxamide, 9b.

^{1}H NMR (400 MHz, Acetone) δ ppm 8.56 (d, *J*=9.54 Hz, 1 H), 8.39 (m, 1 H), 7.74 (dd, *J*=9.66, 1.88 Hz, 1 H), 7.56 (m, 3 H), 5.02 (m, 1 H), 4.22 (s, 3 H), 4.10 (d, *J*=3.01 Hz, 3 H), 3.54 (m, 1 H), 2.84 (s, 3 H), 2.05 (dt, *J*=4.39, 2.20 Hz, 3 H), 0.87 (m, 1 H), 0.51 (m, 1 H), 0.34 (d, *J*=6.53 Hz, 1 H), 0.23 (t, *J*=7.47 Hz, 1 H), 0.01 (t, *J*=7.47 Hz, 1 H) ^{13}C NMR (100 MHz, *d*-CHCl$_3$) δ ppm 173.66, 161.01, 160.98, 160.84, 160.80, 157.12, 157.09, 156.25, 156.23, 135.42, 135.32, 130.72, 130.67, 129.30, 126.55, 126.18, 126.11, 125.09, 123.77, 123.70, 123.51, 122.93, 122.89, 116.29, 116.26, 115.91, 115.05, 114.98, 64.67, 57.62, 46.27, 46.21, 20.18, 20.01, 13.12, 9.51, 9.30. Accurate Mass Calculated for C$_{25}$H$_{26}$N$_2$O$_4$Cl$_1$: 453.1581, Found: 453.1561.

N-(5-(bis(3-(dimethylamino)propyl)carbamoyl)-1-methyl-1H-pyrrol-3-yl)-3-(2,10-dimethoxyanthracen-9-yl)-5-methylisoxazole-4-carboxamide, 10a., ^{1}H NMR (400 MHz, Acetone) δ ppm 8.56 (d, *J*=9.54 Hz, 1 H), 8.39 (m, 1 H), 7.74 (dd, *J*=9.66, 1.88 Hz, 1 H), 7.56 (m, 3 H), 5.02 (m, 1 H), 4.23 (s, 3 H), 4.10 (d, *J*=3.01 Hz, 3 H), 3.54 (m, 1 H), 2.84 (s, 3 H), 0.87 (m, 2 H), 0.41 (dd, J= 6.53, 61.36 Hz, 3H), 0.12 (dt, J=7.47, 14.93 Hz, 3H). ^{13}C NMR (100 MHz, *d*-CHCl$_3$) δ ppm 173.66, 161.01, 160.98, 160.84, 160.80, 157.12, 157.10, 156.25, 156.23, 135.43, 135.32, 130.72, 130.67, 129.30, 126.55, 126.18, 126.11, 125.10, 123.77, 123.52, 122.93, 122.89, 116.29, 15.93, 115.05, 64.67, 57.62, 46.27, 46.21, 20.18, 20.01, 13.12, 9.51, 9.30. Accurate Mass Calculated for C$_{25}$H$_{26}$N$_2$O$_4$Cl$_1$: 453.1581, Found: 453.1561.

N-(5-(bis(3-(dimethylamino)propyl)carbamoyl)-1-methyl-1H-pyrrol-3-yl)-3-(1-chloro-2,10-dimethoxyanthracen-9-yl)-5-methylisoxazole-4-carboxamide, 10b.

^{1}H NMR (400 MHz, Acetone) δ ppm 8.55 (d, *J*=9.66 Hz, 1 H), 8.37 (d, *J*=7.78 Hz, 1 H), 7.71 (d, *J*=9.66 Hz, 1 H), 7.54 (m, 3 H), 6.84 (d, *J*=1.63 Hz, 1 H), 5.61 (d, *J*=1.51 Hz, 1 H), 4.24 (s, 3 H), 4.07 (s, 3 H), 3.48 (s, 3 H), 3.34 (m, 4 H), 2.89 (s, 3 H), 2.15 (t, *J*=6.65 Hz, 4 H), 2.08 (s, 10 H).

^{13}C NMR (100 MHz, Acetone) δ ppm 172.43, 164.16, 161.74, 158.39, 156.84, 156.00, 135.51, 130.94, 128.98, 126.42, 126.39, 125.31, 125.00, 123.71, 123.52, 122.95, 122.04, 121.95, 116.86, 116.16, 115.78, 115.32, 115.25, 102.36, 102.28, 64.57, 57.55, 45.57, 35.31, 27.05, 13.25. Accurate Mass Calculated for C$_{37}$H$_{46}$N$_6$O$_5$C$_1$: 689.3218, Found: 689.3226.
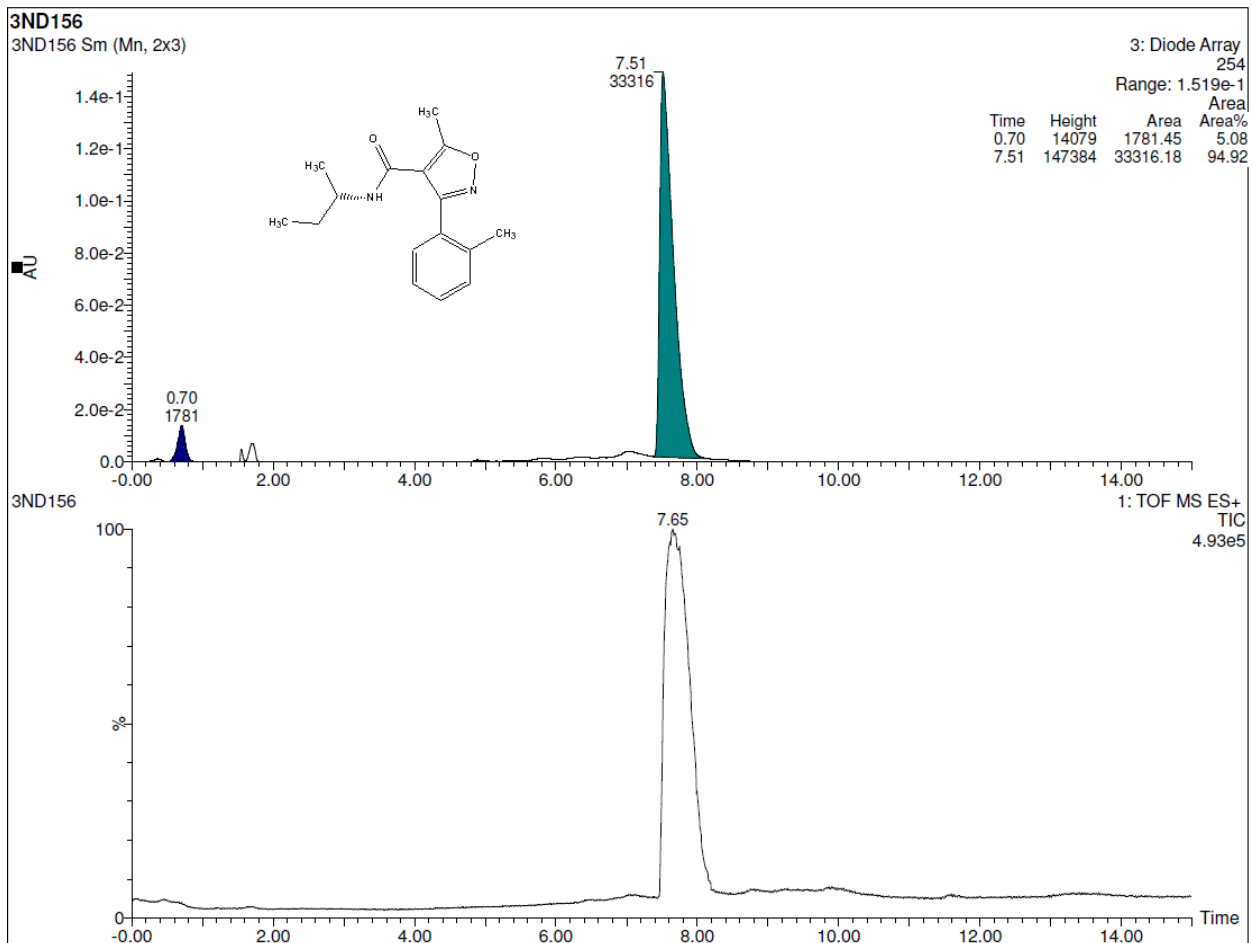
3ND156
3ND156 Sm (Mn, 2x3)

Time	Height	Area	Area%
0.70	14079	1781.45	5.08
7.51	147384	33316.18	94.92

3ND156

1: TOF MS ES+
TIC
4.93e5

Elemental Composition Report   **Page 1**

Single Mass Analysis
Tolerance = 5.0 mDa   /   DBE: min = -1.5, max = 50.0
Element prediction: Off
Number of isotope peaks used for i-FIT = 3

Monoisotopic Mass, Even Electron Ions
1 formula(e) evaluated with 1 results within limits (up to 50 closest results for each mass)
Elements Used:
C: 16-16   H: 21-21   N: 2-2   O: 2-2
3ND156 HRMS
3ND156 HRMS 66 (0.662)

1: TOF MS ES+
2.26e+004

Minimum: -1.5
Maximum: 5.0   10.0   50.0

Mass	Calc. Mass	mDa	PPM	DBE	i-FIT	i-FIT (Norm)	Formula
273.1596	273.1603	-0.7	-2.6	7.5	420.4	0.0	C16 H21 N2 O2

157

3ND145
3ND145 Sm (Mn, 2x3)

3: Diode Array
254
Range: 8.217e-2

Time	Height	Area	Area%
5.52	34618	12289.63	24.45
6.19	8334	2993.53	5.95
7.45	77984	32656.18	64.96
8.90	4215	2334.78	4.64

3ND145

1: TOF MS ES+
TIC
5.19e5

Elemental Composition Report

Page 1

Single Mass Analysis

Tolerance = 5.0 mDa   /   DBE: min = -1.5, max = 50.0
Element prediction: Off
Number of isotope peaks used for i-FIT = 3

Monoisotopic Mass, Even Electron Ions
1 formula(e) evaluated with 1 results within limits (up to 50 closest results for each mass)
Elements Used:
C: 15-15   H: 18-18   N: 2-2   O: 2-2   Cl: 1-1
3ND145
3ND145 788 (7.909)

1: TOF MS ES+
3.20e+004

Minimum:				-1.5				
Maximum:		5.0	10.0	50.0				
Mass	Calc. Mass	mDa	PPM	DBE	i-FIT	i-FIT (Norm)	Formula	
293.1060	293.1057	0.3	1.0	7.5	456.5	0.0	C15 H18 N2 O2 Cl	

158

3ND154 HRMS
3ND154 HRMS Sm (Mn, 2x3)

3: Diode Array
254
Range: 9.73e-1

Time	Height	Area	Area%
4.99	75178	1394.20	0.40
6.68	955437	203258.00	57.62
7.79	436142	104196.23	29.54
9.13	9745	2254.12	0.64
9.57	71124	13941.70	3.95
9.80	123174	27735.81	7.86

3ND154 HRMS

1: TOF MS ES+
TIC
7.08e5

Elemental Composition Report   **Page 1**

Single Mass Analysis
Tolerance = 5.0 mDa   /   DBE: min = -1.5, max = 50.0
Element prediction: Off
Number of isotope peaks used for i-FIT = 3

Monoisotopic Mass, Even Electron Ions
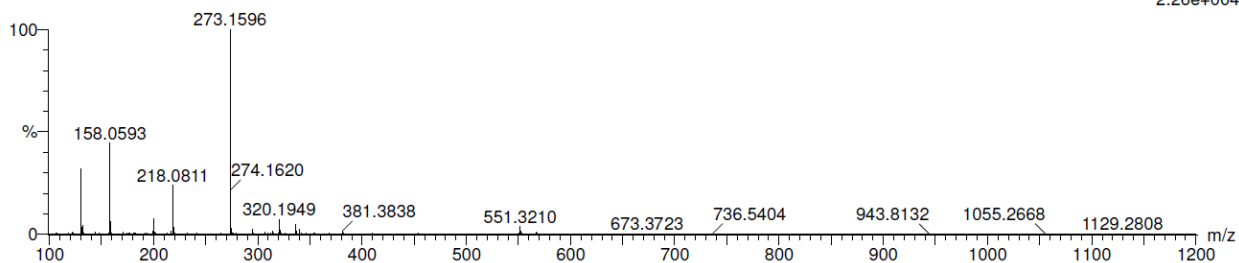1 formula(e) evaluated with 1 results within limits (up to 50 closest results for each mass)
Elements Used:
C: 16-16   H: 20-20   N: 2-2   O: 2-2   Cl: 1-1
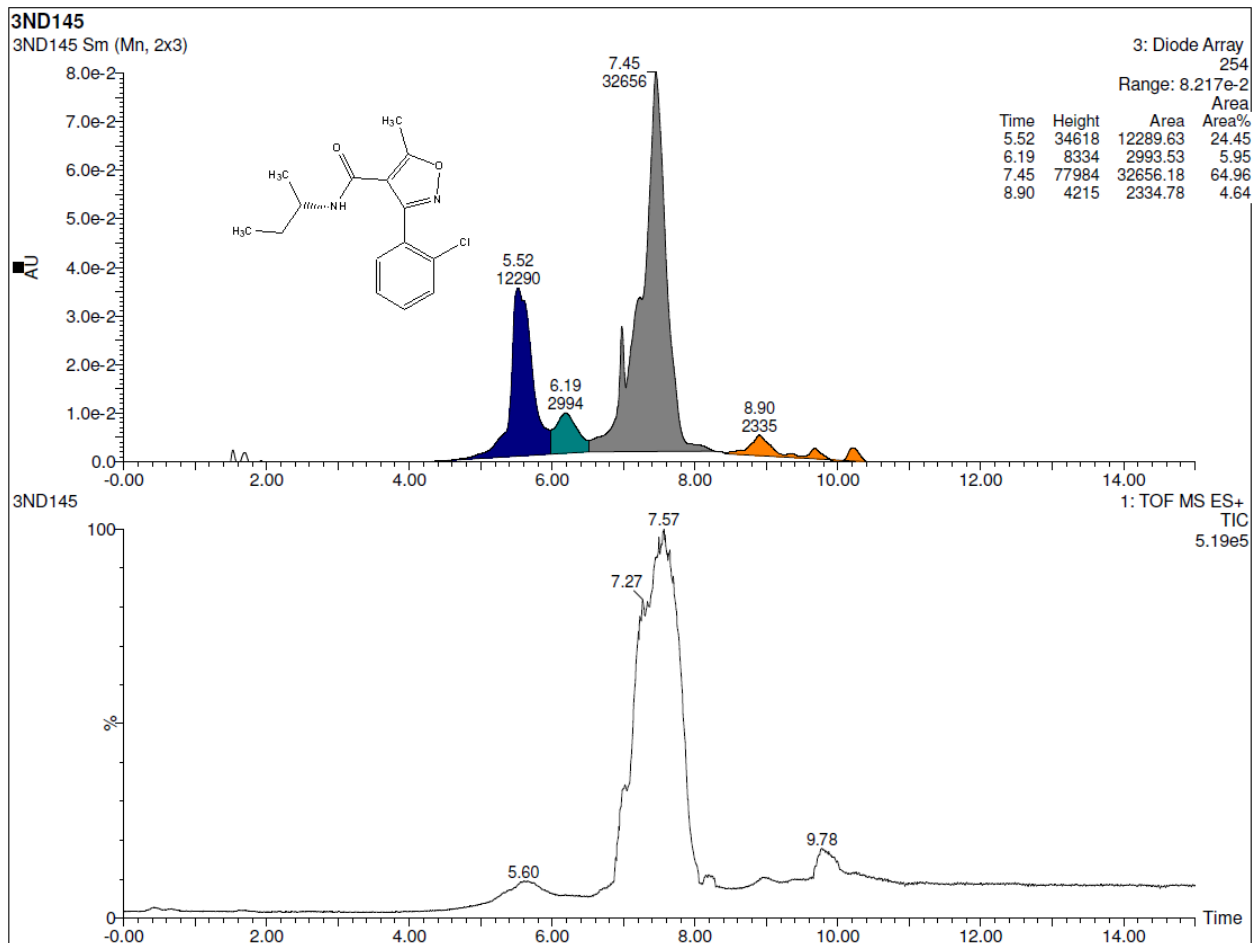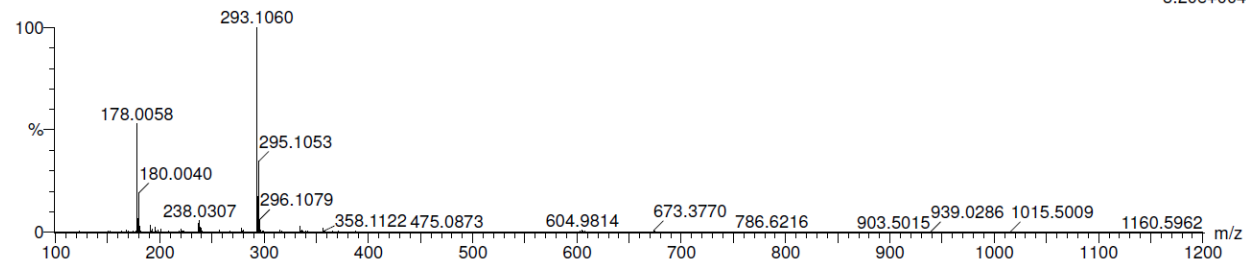3ND154 HRMS 2
3ND154 HRMS 2 105 (1.055)

1: TOF MS ES+
2.73e+004
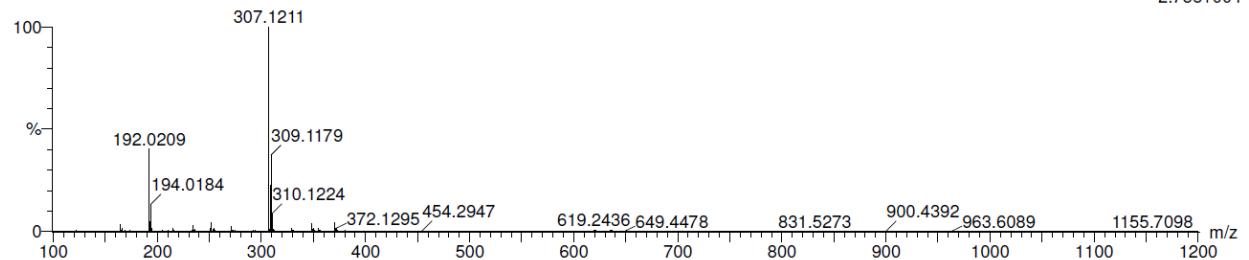
Minimum:				-1.5						
Maximum:		5.0	10.0	50.0						
Mass	Calc. Mass	mDa	PPM	DBE	i-FIT	i-FIT (Norm)	Formula			
307.1211	307.1213	-0.2	-0.7	7.5	397.8	0.0	C16 H20 N2 O2 Cl			

159

LC33
LC33 Sm (Mn, 2x3)

3: Diode Array
254
Range: 2.468
Area

Time	Height	Area	Area%
6.79	487616	48981.14	8.25
7.76	2443211	544963.19	91.75

7.76
544963

6.79
48981

LC33

1: TOF MS ES+
TIC
3.34e5

7.76

8.61

6.88 7.00

5.56

0.01

Time

Elemental Composition Report

Page 1

Single Mass Analysis
Tolerance = 5.0 mDa   /   DBE: min = -1.5, max = 50.0
Element prediction: Off
Number of isotope peaks used for i-FIT = 3

Monoisotopic Mass, Even Electron Ions
1 formula(e) evaluated with 1 results within limits (up to 50 closest results for each mass)
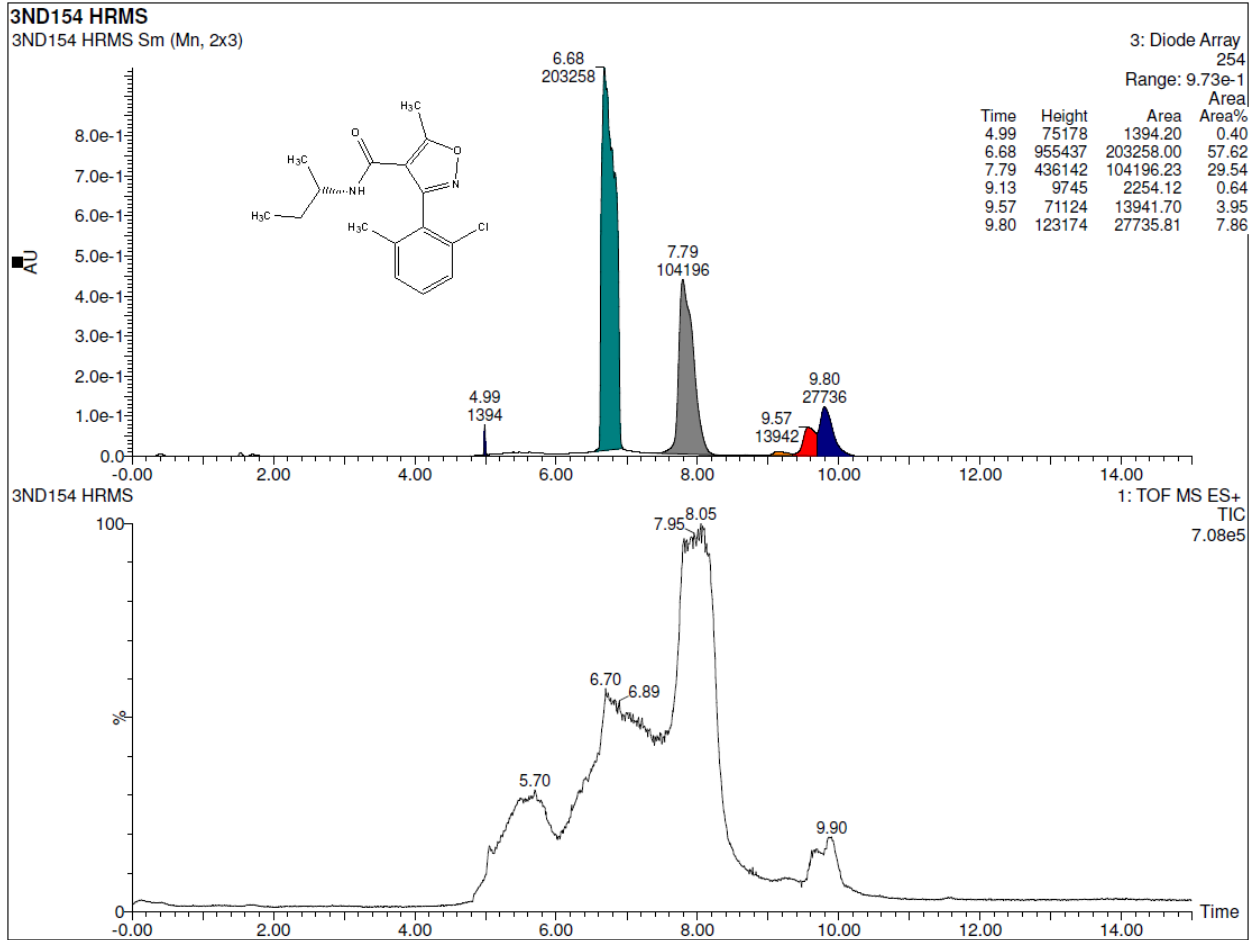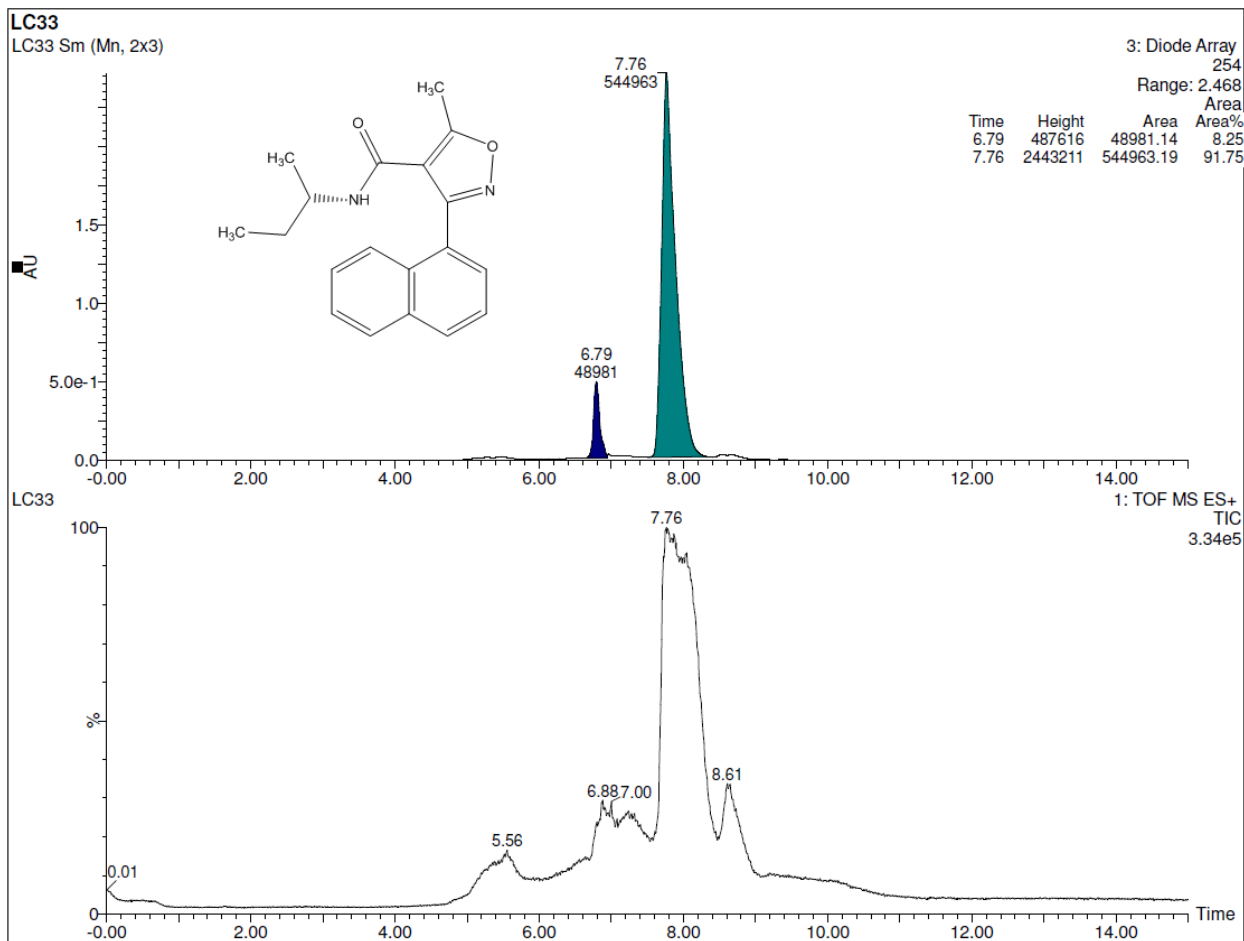Elements Used:
C: 19-19   H: 21-21   N: 2-2   O: 2-2
LC33
LC33 771 (7.739)

1: TOF MS ES+
1.16e+005

309.1602

310.1686

194.0625

324.1759

156.1010

346.1556

497.2159

536.2975

617.3213

669.3252 701.2706

947.4448

1009.4164 1044.4437

m/z

Minimum:			-1.5			
Maximum:	5.0	10.0	50.0			

Mass	Calc. Mass	mDa	PPM	DBE	i-FIT	i-FIT (Norm)	Formula
309.1602	309.1603	-0.1	-0.3	10.5	471.4	0.0	C19 H21 N2 O2

160

3ND103

3ND103 Sm (Mn, 2x3)

3: Diode Array
254
Range: 3.612

Time	Height	Area	Area Area%
6.89	82320	7580.35	0.51
8.62	3607448	1410215.38	95.56
9.37	155964	57880.90	3.92

3ND103

1: TOF MS ES+
TIC
3.36e5

Elemental Composition Report   **Page 1**

Single Mass Analysis
Tolerance = 5.0 mDa   /   DBE: min = -1.5, max = 50.0
Element prediction: Off
Number of isotope peaks used for i-FIT = 3

Monoisotopic Mass, Even Electron Ions
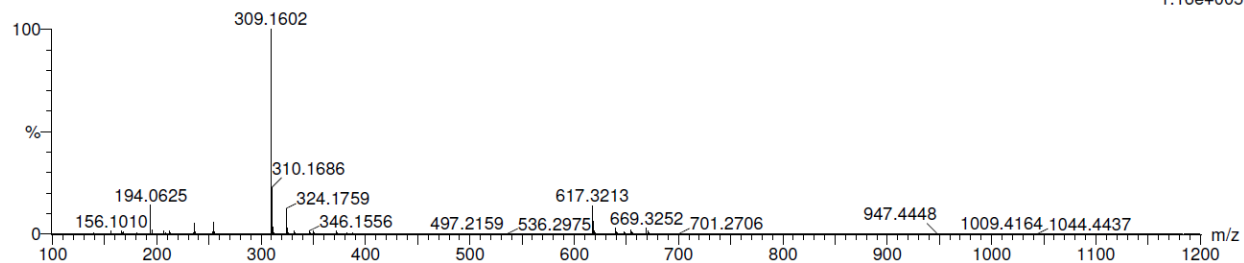1 formula(e) evaluated with 1 results within limits (up to 50 closest results for each mass)
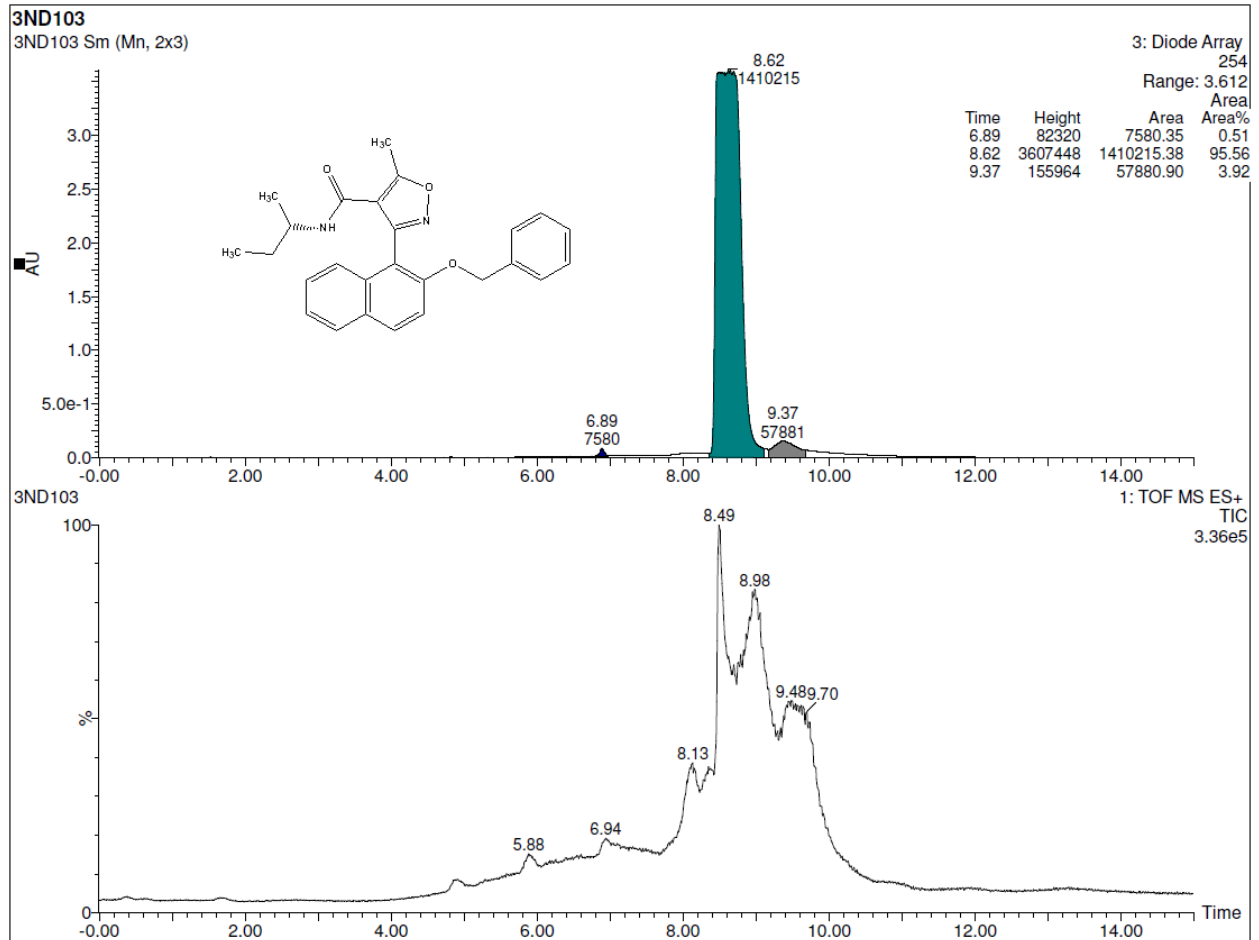Elements Used:
C: 26-26   H: 27-27   N: 2-2   O: 3-3

3ND103
3ND103 838 (8.420)

1: TOF MS ES+
2.22e+004

Minimum:				-1.5			
Maximum:		5.0	10.0	50.0			

Mass	Calc. Mass	mDa	PPM	DBE	i-FIT	i-FIT (Norm)	Formula
415.2025	415.2022	0.3	0.7	14.5	276.1	0.0	C26 H27 N2 O3

161

3ND164 #3-4
3ND164 #3-4 Sm (Mn, 2x3)

3: Diode Array
254
Range: 2.87

Time	Height	Area	Area%
7.93	9922	1723.03	0.26
8.41	125774	20550.59	3.07
8.69	2854457	638791.81	95.44
9.46	31741	8236.33	1.23

8.69
638792

8.41
20551

9.46
8236

3ND164 #3-4

1: TOF MS ES+
TIC
2.23e5

Elemental Composition Report   **Page 1**
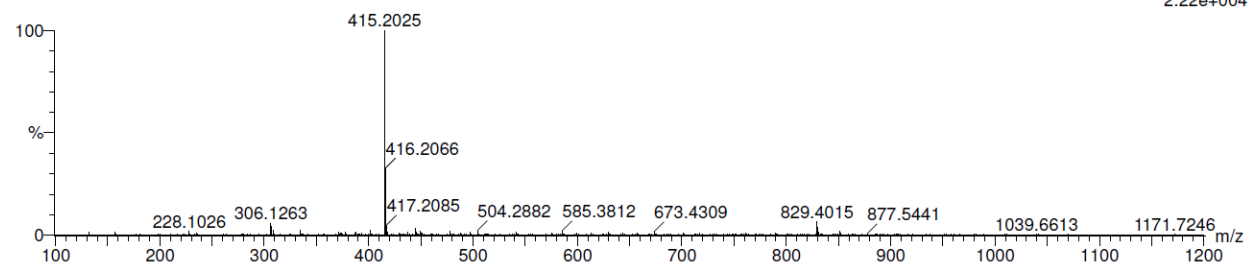
Single Mass Analysis
Tolerance = 5.0 mDa   /   DBE: min = -1.5, max = 50.0
Element prediction: Off
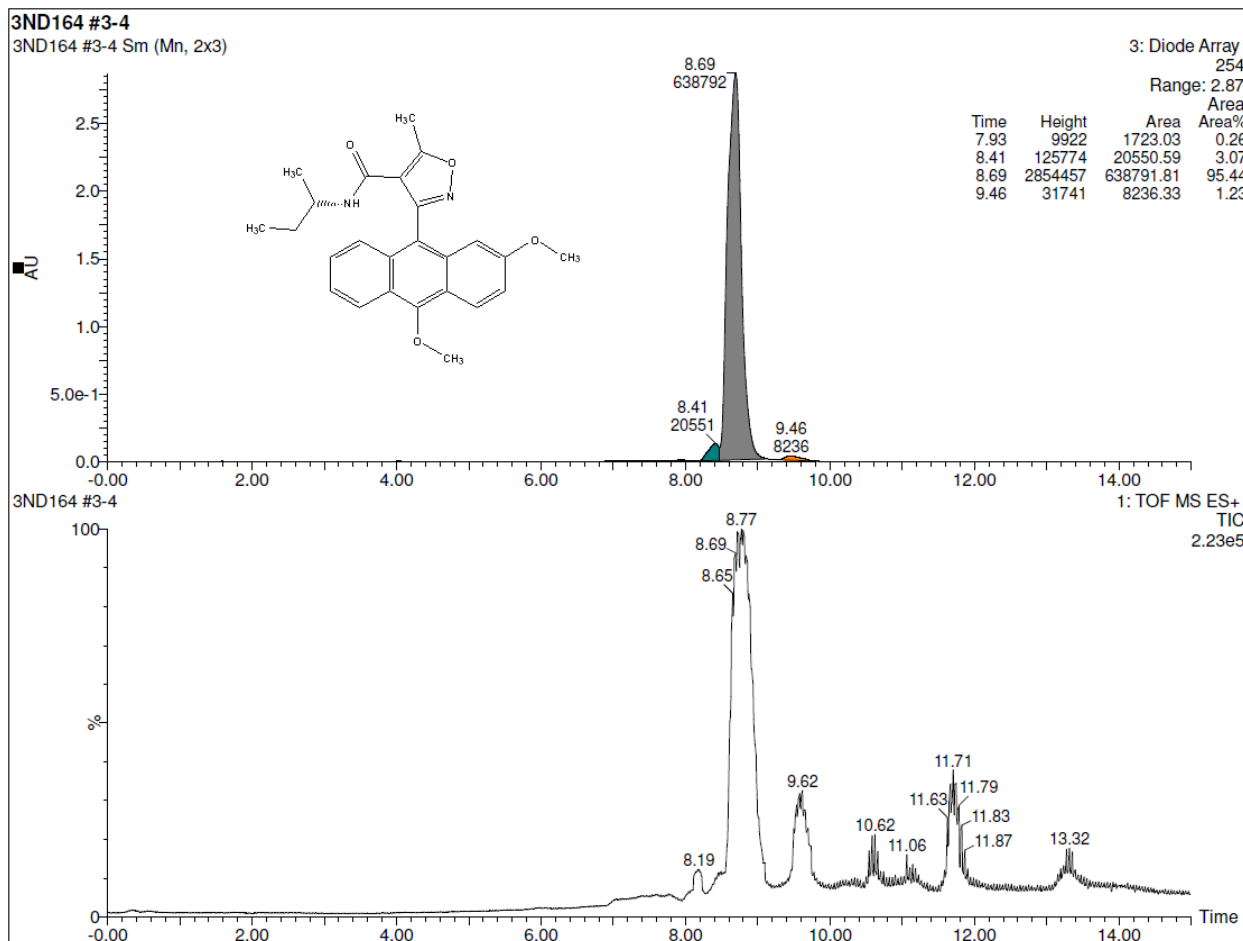Number of isotope peaks used for i-FIT = 3

Monoisotopic Mass, Even Electron Ions
1 formula(e) evaluated with 1 results within limits (up to 50 closest results for each mass)
Elements Used:
C: 25-25   H: 27-27   N: 2-2   O: 4-4
3ND164 #3-4 hrms
3ND164 #3-4 hrms 109 (1.098)

1: TOF MS ES+
2.82e+004
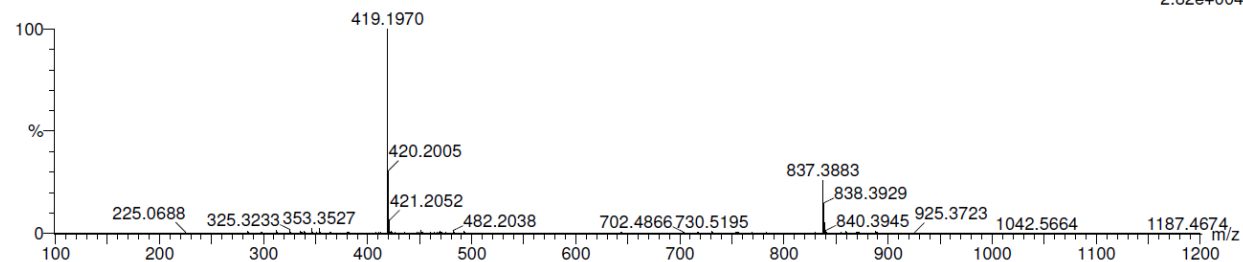
Minimum:			-1.5			
Maximum:	5.0	10.0	50.0			

Mass	Calc. Mass	mDa	PPM	DBE	i-FIT	i-FIT (Norm)	Formula
419.1970	419.1971	-0.1	-0.2	13.5	314.2	0.0	C25 H27 N2 O4

162

3ND164 #7-8
3ND164 #7-8 Sm (Mn, 2x3)

Time	Height	Area	Area%
2.13	57122	8362.74	8.25
6.98	6792	1468.16	1.45
7.16	5172	1062.54	1.05
7.48	4601	1335.81	1.32
7.94	5134	1793.68	1.77
8.46	323981	82156.96	81.02
9.05	19150	5225.57	5.15

3ND164 #7-8

1: TOF MS ES+
TIC
9.30e4

Elemental Composition Report   **Page 1**

Single Mass Analysis
Tolerance = 5.0 mDa   /   DBE: min = -1.5, max = 50.0
Element prediction: Off
Number of isotope peaks used for i-FIT = 3

Monoisotopic Mass, Even Electron Ions
1 formula(e) evaluated with 1 results within limits (up to 50 closest results for each mass)
Elements Used:
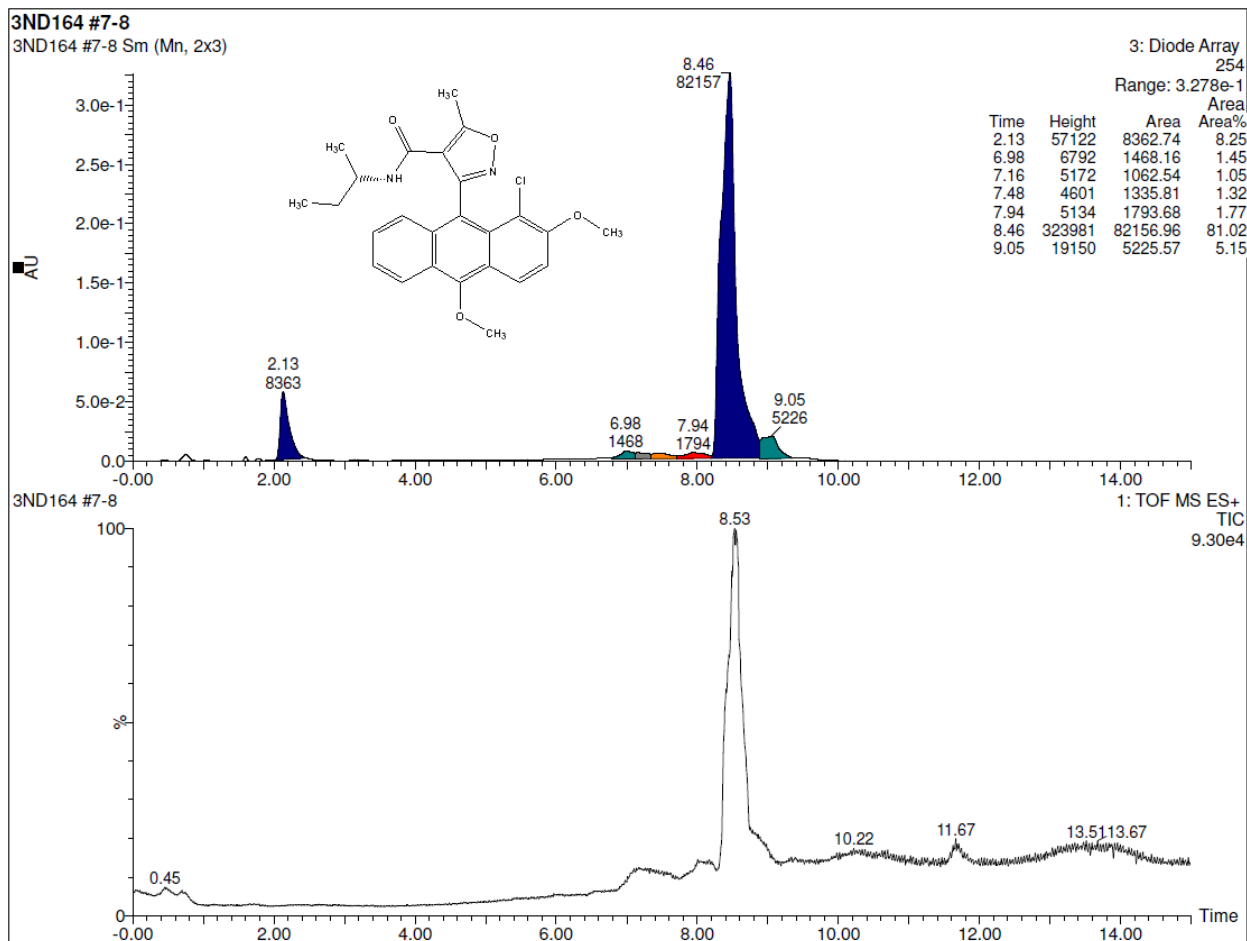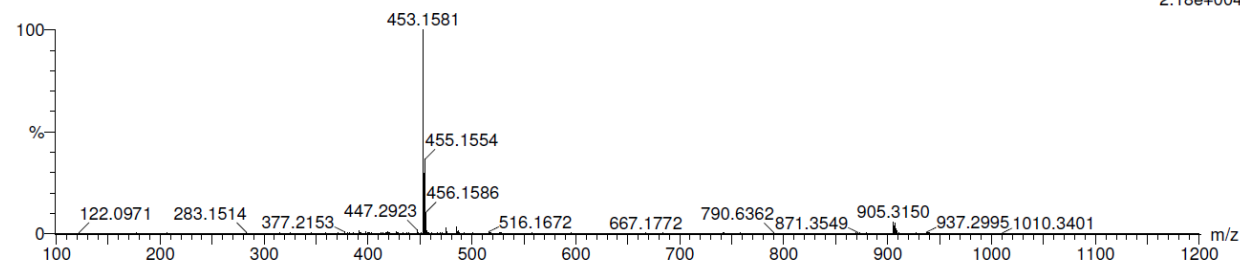C: 25-25   H: 26-26   N: 2-2   O: 4-4   Cl: 1-1
3ND164 #7-8 hrms
3ND164 #7-8 hrms 47 (0.469)

1: TOF MS ES+
2.18e+004

Minimum:			-1.5			
Maximum:	5.0	10.0	50.0			

Mass	Calc. Mass	mDa	PPM	DBE	i-FIT	i-FIT (Norm)	Formula
453.1581	453.1581	0.0	0.0	13.5	268.8	0.0	C25 H26 N2 O4 Cl
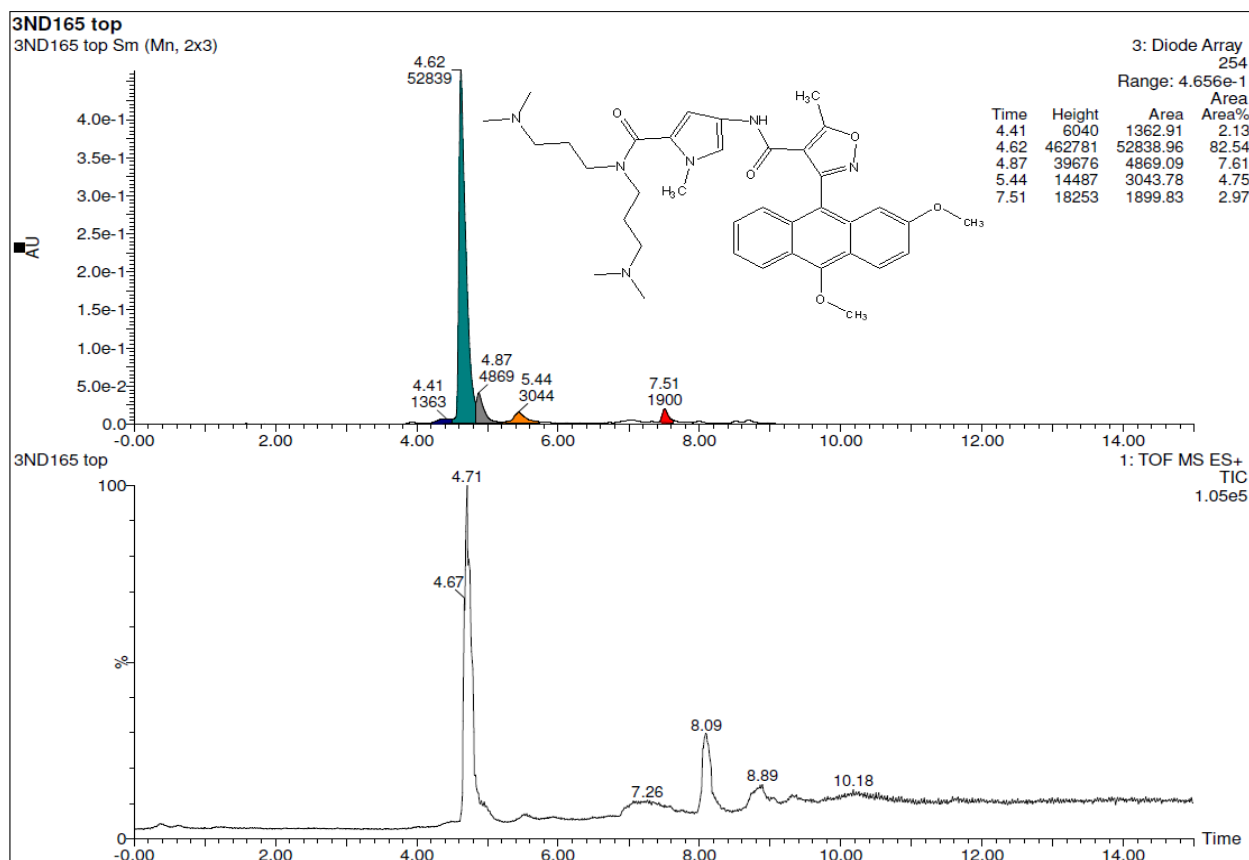
163

3ND165 top
3ND165 top Sm (Mn, 2x3)

3: Diode Array
254
Range: 4.656e-1

Time	Height	Area	Area%
4.41	6040	1362.91	2.13
4.62	462781	52838.96	82.54
4.87	39676	4869.09	7.61
5.44	14487	3043.78	4.75
7.51	18253	1899.83	2.97

3ND165 top

1: TOF MS ES+
TIC
1.05e5

Elemental Composition Report

Page 1

Single Mass Analysis
Tolerance = 5.0 mDa   /   DBE: min = -1.5, max = 50.0
Element prediction: Off
Number of isotope peaks used for i-FIT = 3

Monoisotopic Mass, Even Electron Ions
1 formula(e) evaluated with 1 results within limits (up to 50 best isotopic matches for each mass)
Elements Used:
C: 37-37   H: 47-47   N: 6-6   O: 5-5
3ND165 top hrms
3ND165 top hrms 28 (0.278)
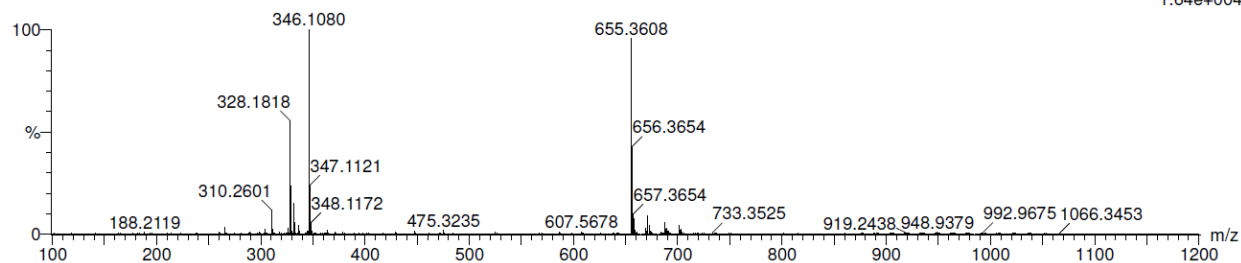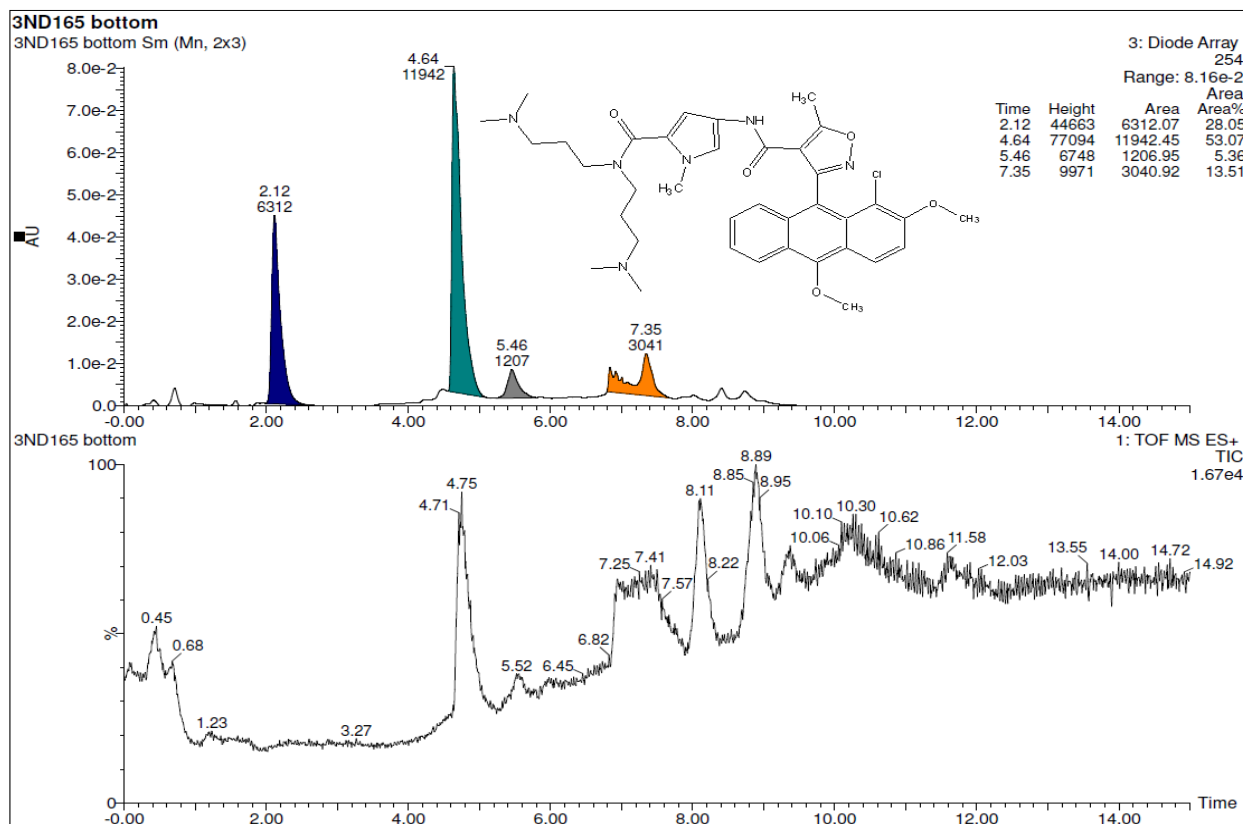
1: TOF MS ES+
1.64e+004

Minimum:				-1.5			
Maximum:		5.0	10.0	50.0			

Mass	Calc. Mass	mDa	PPM	DBE	i-FIT	i-FIT (Norm)	Formula
655.3608	655.3608	0.0	0.0	17.5	174.8	0.0	C37 H47 N6 O5

164

3ND165 bottom
3ND165 bottom Sm (Mn, 2x3)

3: Diode Array
254
Range: 8.16e-2

Time	Height	Area	Area%
2.12	44663	6312.07	28.05
4.64	77094	11942.45	53.07
5.46	6748	1206.95	5.36
7.35	9971	3040.92	13.51

3ND165 bottom

1: TOF MS ES+
TIC
1.67e4

Elemental Composition Report

Single Mass Analysis
Tolerance = 5.0 mDa   /   DBE: min = -1.5, max = 50.0
Element prediction: Off
Number of isotope peaks used for i-FIT = 3

Monoisotopic Mass, Even Electron Ions
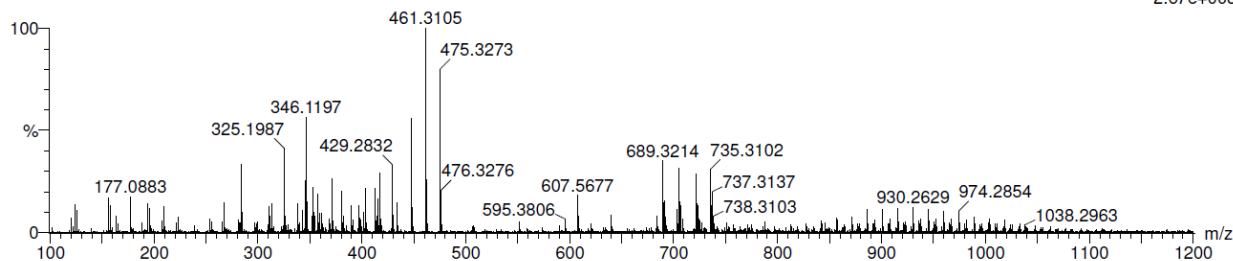1 formula(e) evaluated with 1 results within limits (up to 50 best isotopic matches for each mass)
Elements Used:
C: 37-37   H: 46-46   N: 6-6   O: 5-5   Cl: 1-1

3ND165 bottom hrms
3ND165 bottom hrms 38 (0.381)

1: TOF MS ES+
2.67e+003

| | | | | Minimum: | | | -1.5 | | | |
| | | | | Maximum: | 5.0 | 10.0 | 50.0 | | | |

| Mass	Calc. Mass	mDa	PPM	DBE	i-FIT	i-FIT (Norm)	Formula
689.3214	689.3218	-0.4	-0.6	17.5	69.8	0.0	C37 H46 N6 O5 Cl

**NMR assignments of 2,10-dimethoxy-9-anthracenecarboxaldehyde**, **13**

NMR assignments of the regiochemsitry of our system was establish using ^{1}H, ^{13}C, DEPT, ^{1}H-^{1}H COSEY, HSQC (H-C 1-bond), and HMBC (H-C 2,3-bonds) experiments on the aldehyde **1d**. The aldehyde proton (Figure 3, H_1), being the easiest to assign due to its large downfield shift, carbon coupling was first established using HSQC. HMBC was used to determine the relationship between C_2 and H_4 (Figure 4). Heteronuclear Multiple Bond Coherence (HMBC) showed the coupling between C_5 and H_4, in addition, HMBC showed a crosspeak for C_5 and H_{17}. Were the anthracene substituted at C_6 no C_5-H_{17} crosspeak would be observed.
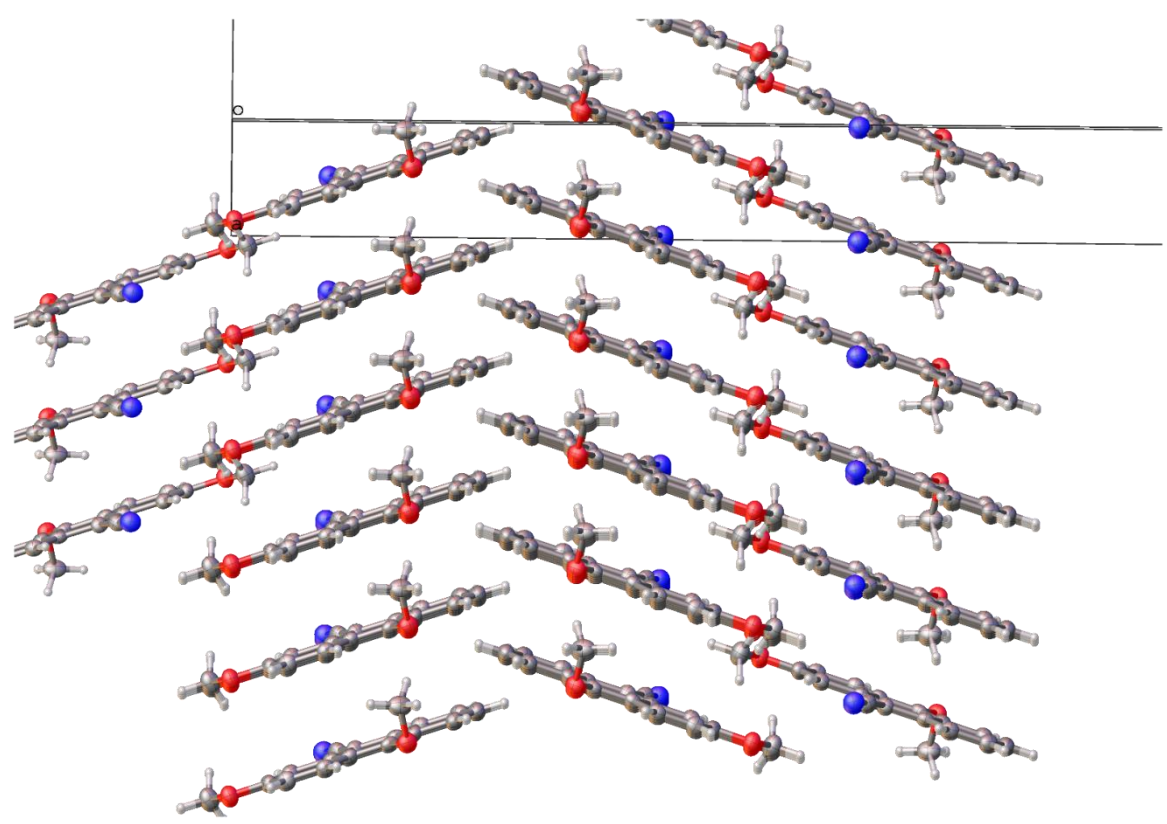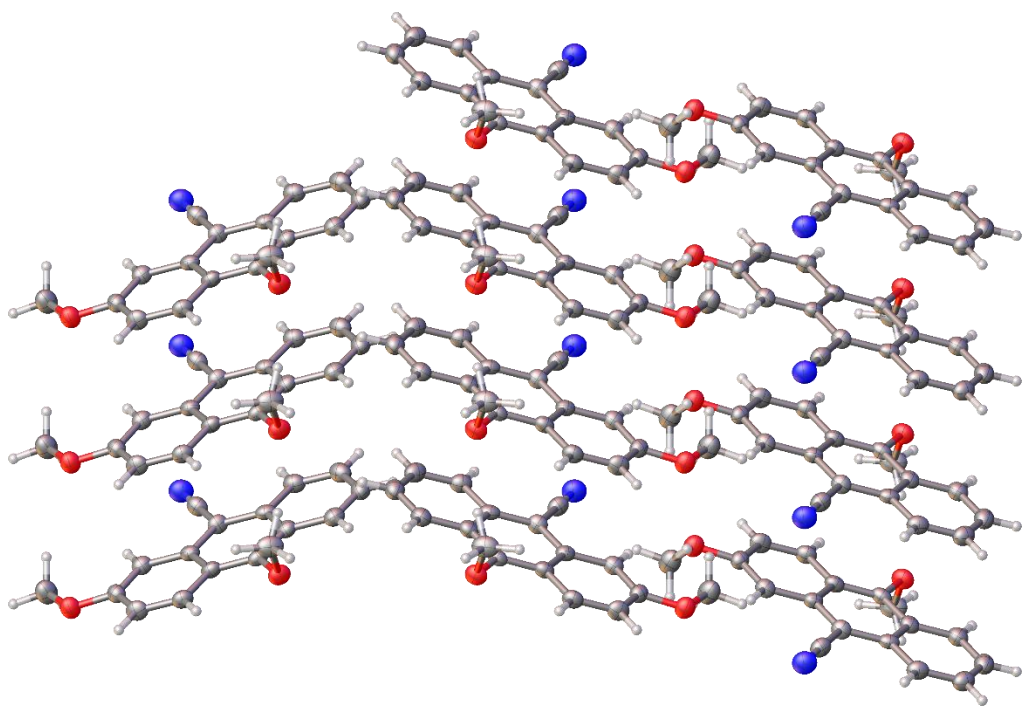
Supplementary Material Figure 3. Numbering for Carbon/Proton for NMR assignments.
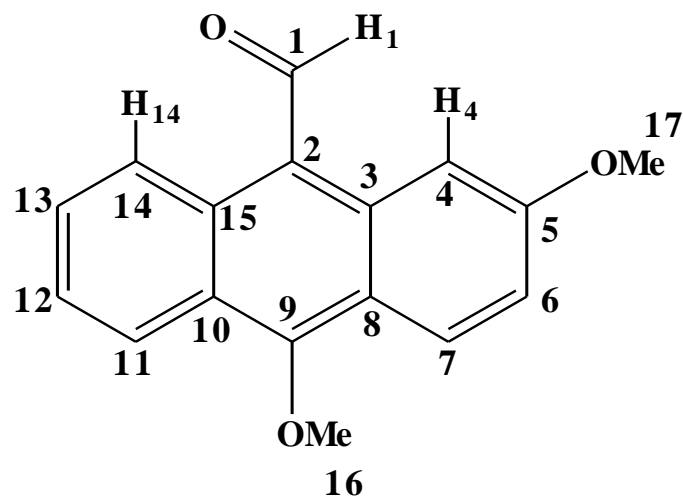
Supplementary Material Figure 4. HMBC (2,3 carbon couplings) full spectrum
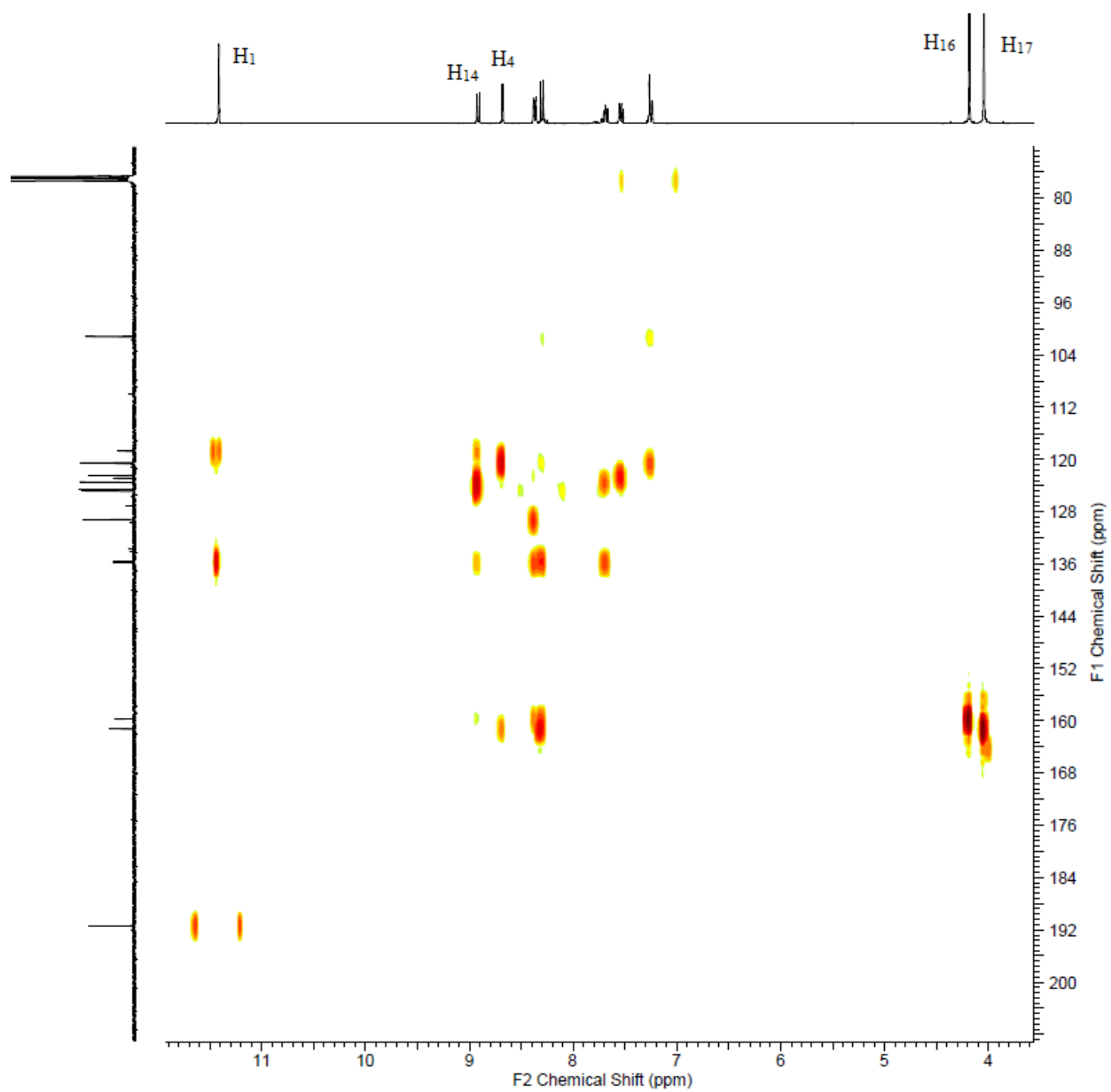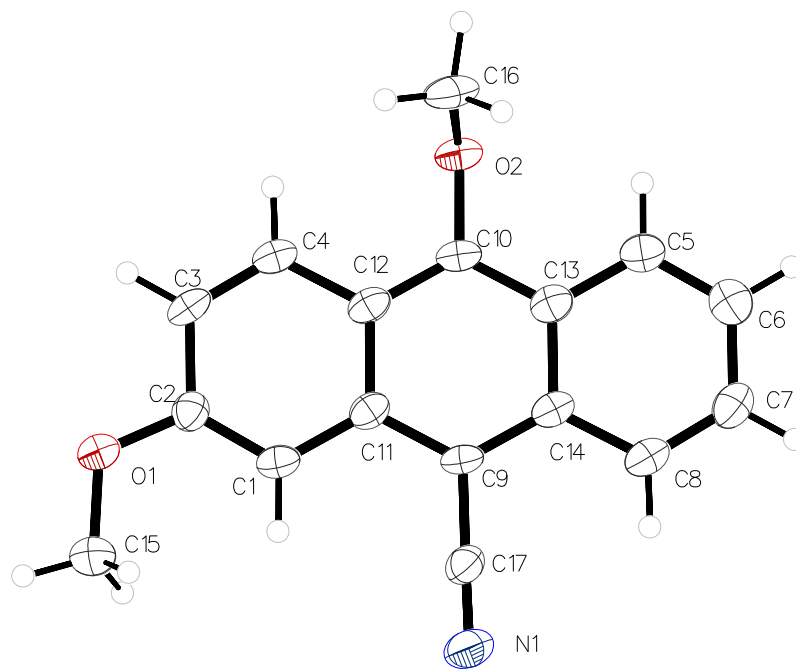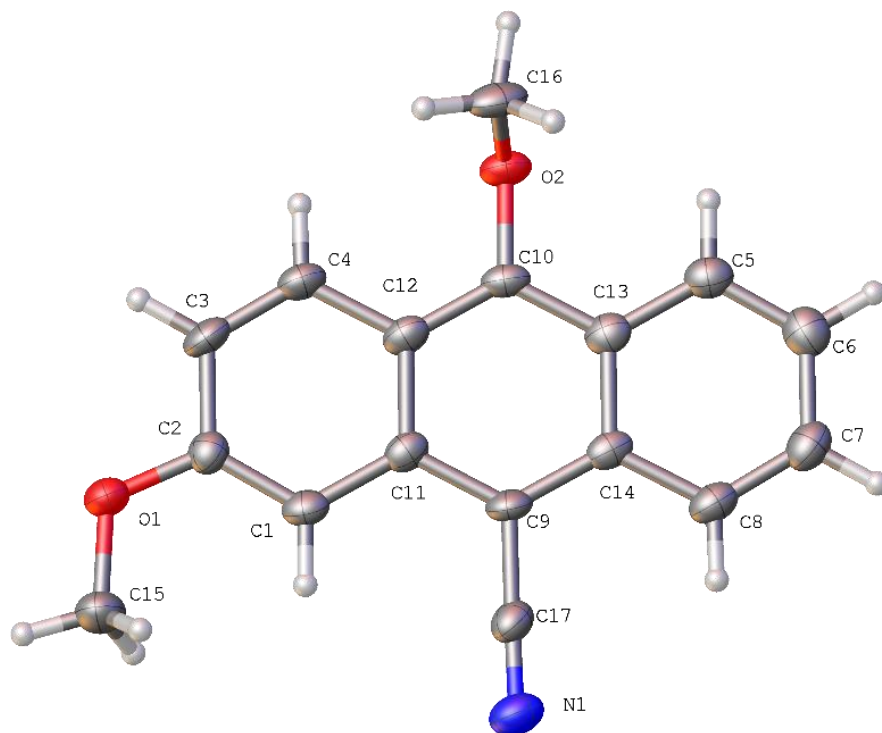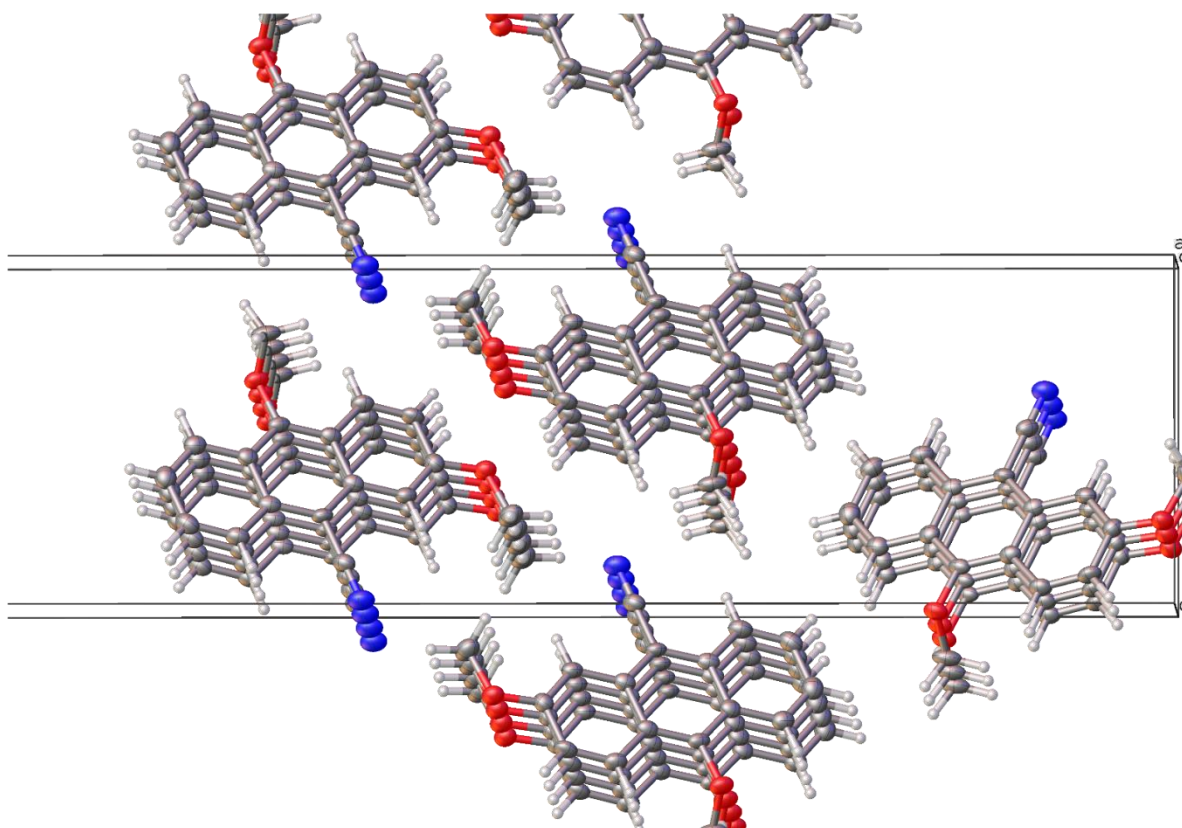
X-ray diffraction data for **12** were collected at 150K on a Bruker D8 Venture using CuKα (λ = 1.54178) radiation. Data have been corrected for absorption using SADABS[1] area detector absorption correction program. Using Olex2[2], the structure was solved with the ShelXT structure solution program using Direct Methods and refined with the ShelXL refinement package using least squares minimization. All non-hydrogen atoms were refined with anisotropic thermal parameters. Hydrogen atoms were refined in calculated positions in a ridged group model with isotropic thermal parameters U(H) = 1.2Ueq (C) for C(H) groups and U(H)=1.5Ueq (C) for all C(H,H,H) groups. Calculations and refinement of structures were carried out using APEX[3], SHELXTL[4], Olex2.

Crystallographic Data for **3ND-77**: C17H13NO2, M =263.28, monoclinic, space group P21/c, a

= 4.0681(3), b = 34.841(3), c = 8.9400(6), β = 93.317(4), V = 1265.02(16), Z = 4, T = 150 K,

μ(CuKα) = 0.733 mm^{-1}, ρ_{calcd} = 1.382 g ml^{-1}, $2\Theta_{max}$ = 114.108, 25793 reflections collected, 1713

unique (R_{int} = 0.1007, R_{sigma} = 0.0536) R1 = 0.0532 (I > 2σ(I)), wR2 = 0.1357 (all data).

Acknowledge

Table 1 Crystal data and structure refinement for 3ND-77.

Identification code	3ND-77
Empirical formula	$C_{17}H_{13}NO_2$
Formula weight	263.28
Temperature/K	150
Crystal system	monoclinic
Space group	$P2_1/c$
a/Å	4.0681(3)

b/Å	34.841(3)
c/Å	8.9400(6)
$\alpha/°$	90
$\beta/°$	93.317(4)
$\gamma/°$	90
Volume/Å^3	1265.02(16)
Z	4
ρ_{calc}g/cm^3	1.382
μ/mm^{-1}	0.733
F(000)	552.0
Crystal size/mm^3	$0.3 \times 0.05 \times 0.05$
Radiation	CuKα ($\lambda = 1.54178$)
2Θ range for data collection/°	5.072 to 114.108
Index ranges	$-4 \leq h \leq 4$, $-37 \leq k \leq 37$, $-9 \leq l \leq 9$
Reflections collected	25793
Independent reflections	1713 [$R_{int} = 0.1007$, $R_{sigma} = 0.0536$]
Data/restraints/parameters	1713/0/183
Goodness-of-fit on F^2	1.060
Final R indexes [I>=2σ (I)]	$R_1 = 0.0532$, $wR_2 = 0.1196$
Final R indexes [all data]	$R_1 = 0.0964$, $wR_2 = 0.1356$
Largest diff. peak/hole / e Å^{-3}	0.23/-0.20

Table 2 Fractional Atomic Coordinates (×10⁴) and Equivalent Isotropic Displacement Parameters ($\mathring{A}^2 \times 10^3$) for 3ND-77. U_{eq} is defined as 1/3 of of the trace of the orthogonalised U_{IJ} tensor.

Atom	x	y	z	U(eq)
O1	7123(5)	4965.0(6)	3316(2)	34.9(6)
O2	4858(5)	3288.7(6)	5818(2)	33.9(6)
N1	-910(7)	4076.4(8)	-726(3)	42.0(8)
C1	4217(7)	4390.6(9)	2480(3)	28.6(8)
C2	6155(7)	4595.4(9)	3487(3)	28.9(8)
C3	7318(8)	4429.4(10)	4874(3)	32.6(9)
C4	6538(7)	4064.6(9)	5202(3)	30.5(8)
C5	874(7)	2848.3(9)	3799(3)	31.8(9)
C6	-999(8)	2636.9(9)	2794(4)	36.4(9)
C7	-2177(8)	2800.5(10)	1421(4)	36.1(9)
C8	-1425(7)	3168.1(10)	1081(3)	32.7(9)
C9	1378(7)	3782.5(9)	1786(3)	27.7(8)
C10	3665(7)	3459.3(9)	4490(3)	26.7(8)
C11	3372(7)	4006.3(9)	2791(3)	26.5(8)
C12	4514(7)	3835.8(9)	4189(3)	27.9(8)
C13	1713(7)	3232.5(9)	3487(3)	28.6(8)
C14	551(7)	3399.3(9)	2085(3)	26.3(8)
C15	6051(9)	5156.4(10)	1963(4)	43.5(10)

C16	2921(8)	3364.8(10)			7082(3)	41.3(10)
C17	144(8)	3947.1(9)			387(4)	31.6(9)

Table 3 Anisotropic Displacement Parameters ($Å^2 \times 10^3$) for 3ND-77. The Anisotropic displacement factor exponent takes the form: $-2\pi^2[h^2a^{*2}U_{11}+2hka^*b^*U_{12}+...]$.

Atom	U_{11}	U_{22}	U_{33}	U_{23}	U_{13}	U_{12}
O1	40.8(14)	36.6(15)	26.2(13)	2.2(11)	-6.3(11)	-3.4(11)
O2	36.0(13)	41.9(14)	23.1(13)	5.1(11)	-4.6(11)	4.2(11)
N1	44.3(18)	52(2)	28.5(18)	1.3(16)	-5.3(15)	-0.6(15)
C1	31.8(19)	35(2)	19.4(18)	0.5(16)	1.6(15)	3.6(16)
C2	30.1(19)	29(2)	27(2)	-3.7(17)	2.3(16)	-1.4(16)
C3	35(2)	42(2)	21(2)	-5.6(16)	-6.4(16)	0.5(17)
C4	29.3(19)	39(2)	22.2(18)	1.0(17)	-3.7(15)	3.6(17)
C5	31(2)	37(2)	27.4(19)	0.8(17)	2.2(16)	4.6(17)
C6	37(2)	34(2)	39(2)	-1.2(18)	7.2(18)	1.3(17)
C7	34(2)	42(2)	32(2)	-9.3(18)	1.6(17)	-3.3(17)
C8	30.5(19)	43(2)	23.9(19)	-3.3(17)	-1.6(16)	1.1(17)
C9	32.7(19)	35(2)	15.6(18)	2.1(15)	0.0(15)	2.3(17)
C10	26.2(18)	35(2)	18.4(19)	2.4(16)	0.8(15)	8.5(16)
C11	21.8(17)	34(2)	23.9(19)	-3.2(16)	-0.1(15)	2.9(15)
C12	25.1(18)	34(2)	23.6(19)	-2.4(16)	-2.6(15)	5.6(16)

174

C13	28.2(18)	32(2)	25(2)	-3.3(16)	2.7(16)	5.5(16)
C14	19.8(17)	38(2)	21.0(19)	-2.3(16)	1.3(15)	3.7(15)
C15	50(2)	44(2)	36(2)	8.7(18)	-9.2(18)	-5.3(18)
C16	40(2)	65(3)	19.2(19)	6.3(18)	0.7(17)	2.6(18)
C17	33(2)	37(2)	24(2)	-4.1(17)	0.9(17)	-5.7(16)

Table 4 Bond Lengths for 3ND-77.

Atom	Atom	Length/Å	Atom	Atom	Length/Å
O1	C2	1.358(4)	C5	C13	1.413(4)
O1	C15	1.428(4)	C6	C7	1.411(4)
O2	C10	1.390(3)	C7	C8	1.355(4)
O2	C16	1.439(4)	C8	C14	1.420(4)
N1	C17	1.153(4)	C9	C11	1.410(4)
C1	C2	1.363(4)	C9	C14	1.406(4)
C1	C11	1.414(4)	C9	C17	1.440(5)
C2	C3	1.424(4)	C10	C12	1.387(4)
C3	C4	1.346(4)	C10	C13	1.405(4)
C4	C12	1.431(4)	C11	C12	1.436(4)
C5	C6	1.361(4)	C13	C14	1.437(4)

Table 5 Bond Angles for 3ND-77.

Atom	Atom	Atom	Angle/°	Atom	Atom	Atom	Angle/°

175

C2	O1	C15	117.5(2)	C12	C10	O2	119.4(3)
C10	O2	C16	114.3(2)	C12	C10	C13	123.1(3)
C2	C1	C11	120.3(3)	C1	C11	C12	119.5(3)
O1	C2	C1	125.6(3)	C9	C11	C1	122.4(3)
O1	C2	C3	113.5(3)	C9	C11	C12	118.1(3)
C1	C2	C3	120.8(3)	C4	C12	C11	117.7(3)
C4	C3	C2	120.1(3)	C10	C12	C4	123.0(3)
C3	C4	C12	121.5(3)	C10	C12	C11	119.2(3)
C6	C5	C13	121.0(3)	C5	C13	C14	118.9(3)
C5	C6	C7	120.3(3)	C10	C13	C5	122.7(3)
C8	C7	C6	120.5(3)	C10	C13	C14	118.3(3)
C7	C8	C14	121.4(3)	C8	C14	C13	117.9(3)
C11	C9	C17	119.5(3)	C9	C14	C8	123.5(3)
C14	C9	C11	122.6(3)	C9	C14	C13	118.6(3)
C14	C9	C17	117.9(3)	N1	C17	C9	178.6(4)
O2	C10	C13	117.4(3)				

Table 6 Hydrogen Atom Coordinates ($\text{Å}\times10^4$) and Isotropic Displacement Parameters ($\text{Å}^2\times10^3$) for 3ND-77.

Atom	x	y	z	U(eq)
H1	3431	4507	1567	34

H3	8648	4576	5570	39
H4	7350	3957	6126	37
H5	1630	2736	4724	38
H6	-1517	2378	3017	44
H7	-3506	2652	731	43
H8	-2238	3273	152	39
H15A	6910	5022	1106	65
H15B	6867	5421	1988	65
H15C	3639	5158	1865	65
H16A	609	3303	6819	62
H16B	3114	3637	7354	62
H16C	3720	3206	7932	62

Chapter 5

Future Direction

5.1 ADME-Tox Considerations

With the initial SAR (Chapter 3) and conformational dynamics (Chapter 4) established for the AIM system, future focus could then be made on the biological issues that are important when designing a medicine: Absorption, Distribution, Metabolism, Excretion, and Toxicity (ADME-Tox). Accurately predicting the fate of a drug and its metabolites is currently becoming mandatory when a potential drug is under development. It has been a challenge to recognize all the factors that contribute to pharmacokinetic and pharmacodynamic unpredictability within and between individuals. This issue will continue to remain a challenge of particular importance for drugs and a particular interest for many years to come. That is why it is a good idea to look for an early understanding of the key metabolites for a new chemical entity in drug development and discovery. In contrast, far fewer drugs fail in clinical development due to pharmacokinetic problems in humans in comparison to the situation ~25 years ago.

There are several pathways by which a small molecule can be metabolized in the body with the most common being enzymatic.[1,2] There are four main fractions that are involved in metabolic reactions of drugs and chemicals: cytochrome P-450 (CYP-450) plays the dominating role of metabolism at ~75%, uridine diphosphate glucuronyl transferase (UGT) around ~12%, esterases at ~8%, while the oxidoreductase enzymes flavin-containing monooxygenase (FMO), aldo-keto reductase (AKR), and monoamine oxidase (MAO) collectively participate in the metabolism of all chemicals to the extent of ~5%.[1–3] It has been shown that the most common metabolism pathways for drugs containing secondary and tertiary amines is N-dealkylation, while, oxygenation of compounds constitutes the second most common process.[4] The isoxazole

was incorporated because of the known metabolic pathway by CYP-450 3A4 as is well described and documented with the antibiotic oxacillin[5,6] and valdecoxib[6–8].

Natale and coworkers have developed a lateral metalation technique useful for a wide variety of isoxazole systems that can place a hydroxyl group at the C5-methyl of the isoxazole on the alpha, beta, and gamma positions that should mimic potential CYP-450 metabolites.[9–12] The synthesis of compounds that mimic potential CYP-450 metabolites should be undertaken with a dual purpose; 1) Future studies in CYP-450 assays to prepare authentic materials to determine the primary metabolites of a series of 3-(9-anthracenyl)-5-methyl 4-isoxazolecarboxylic esters; 2) Addition of a point of chirality to study the structure to activity relationship (SAR) of anthracene isoxazole amides in quadruplex binding studies. Additionally, absorption, distribution, and excretion of a C5-hydroxylated isoxazole should be more favorable as the hydrophobicity of the system, because of the highly lipophilic anthracene, should be reduced allowing for better blood solubility and providing a handle by which transport enzymes can grab onto the molecule and distribute it to cells. Though the P450 family is large, only a handful (Figure 5-1) are involved in the majority of drug metabolism.[1,2,13]
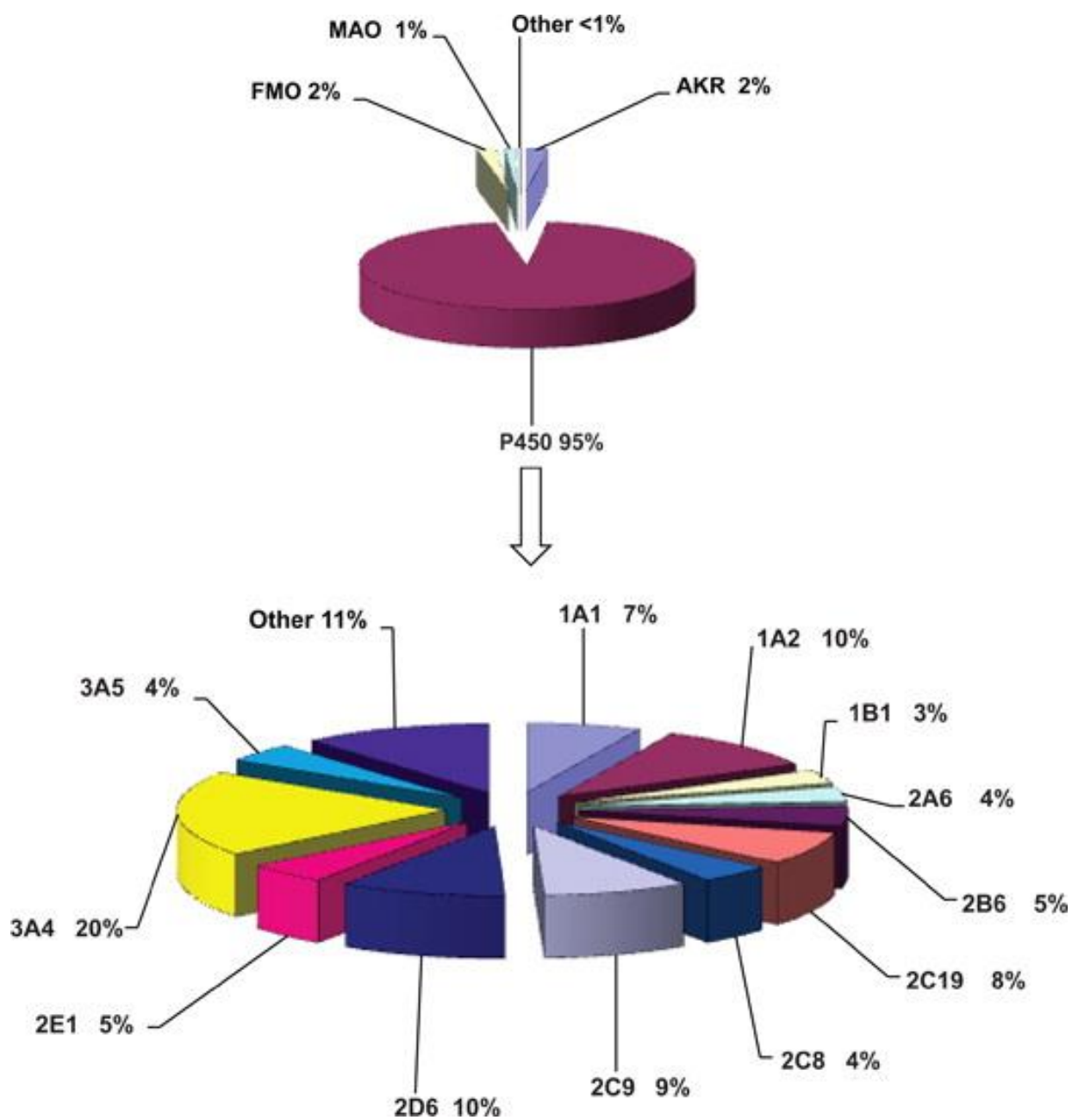
Figure 5-1. Fraction of clinically used drugs metabolized by P450 isoforms. Reprinted with permission from Rendic, Slobodan and Guengerich, F. Peter. *Chem. Res. Toxicol.* 2015, 28, 38−42. Copyright 2015 American Chemical Society[2].

5.2 Lipinaki's Rule

Lipinski has established a "rule of 5" that helps to predict a compound's absorption and distribution properties based on four criteria: calculated log-P (cLogP (octanol water partition coefficient)), number of hydrogen bond donors, number of hydrogen bond acceptors, and molecular weight.[14] The "rule of five" comes from the factor's values being five or multiples of five for optimal absorptivity and distribution. Table 5-1 shows how to assess a molecule's properties to obtain a prediction. Lipinski's guidelines apply to passive transport for the purposes of oral bioavailability.

Property	All parameters are:	Any parameter is:
LogP	≤ 5	> 5
H-Bond Donors	≤ 5	> 5
H-Bond Acceptors	≤ 10	> 10
Molecular Weight	≤ 500	> 500
Lipinski Prediction	Good absorption and/or permeation	Poor absorption and/or permeation

Table 5-1. Lipinski Values for absorption/permeation prediction.

To help assess the 'drug likeness' of the AIM series, ChemAxon Marvin Calculator Plugin Demo[15] was used (Table 5-2). This free-to-use tool can help researchers to calculate both the octanol-water partition coefficients for single protonation state (logP) of a compound and the pH-dependent logD values. Both calculated logP and logD (clogP and clogD) predictions are based on a modified version of the method of Viswanadhan[16], where the predicted partition coefficients are composed of the molecules' atomic values and physicochemical properties. The calculator applies modifications that include the redefinition of some atom types (sulfur, carbon, nitrogen and metal ions) to include electron delocalization and contributions of ionic forms. Within the parameters, three constant calculations are present: first, since logD vales are pH-dependent, the logD calculation relies on pKa prediction; second, the logP value of zwitterions is

calculated from the logD at the isoelectric point; and third, the effect of hydrogen bonds on logP

is considered if the formation of a six membered ring between the suitable donor and acceptor

atoms can take place. The AIM series compounds (Table 5-2) is the best fit of the AIM series

with a cLogD ranging from 0.38-3.68, one hydrogen bond donors, ten hydrogen bond acceptors,

and the molecular weights being high from 624.77 to 762.94 g/mole.
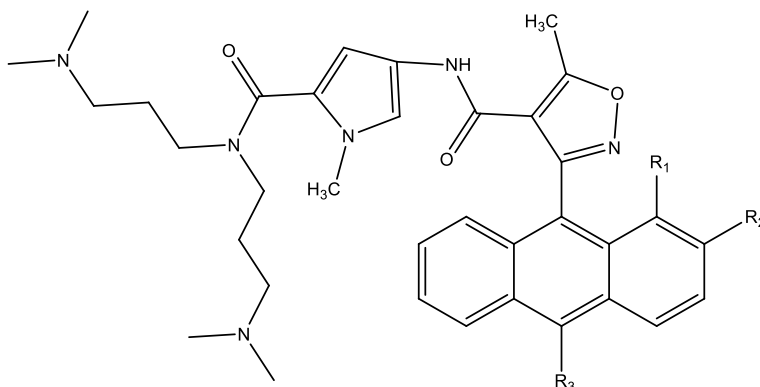
Compound	R1	R2	R3	cLogD @ pH=7.4	Molecular weight
8a	H	H	Methoxy	0.38	624.77
8b	H	H	Phenoxy	2.04	686.84
8c	H	H	Biphenyloxy	3.68	762.94
8d	H	H	1-naphthyloxy	3.03	736.90
8e	H	H	2-naphthyloxy	3.03	736.90
8f	H	Methoxy	Methoxy	0.22	654.35
8g	Cl	Methoxy	Methoxy	0.82	689.24

Table 5-2. Lipinski values for the AIM compounds.

5.3 Anthracene and Isoxazole Metabolism

The primary *in vivo* metabolite of anthracene is 1,2 dihydrodiol (Figure 5-2) and its

glucoronide conjugates.[17] An AIM molecule where the symmetry of the anthracene moiety was

disrupted by the substitution at the C2 position similar to the main anthracene metabolite. With

the addition of a planar C4-ethyl ester C5-methyl functionalized isoxazole ring in the anthracene-

C9 position the system now possesses a chiral axis so long as there is not free rotation about the

anthracene-C9 isoxazole-C3 bond* (Figure 5-4). Furthermore, the C2-anthracene substitution can potentially mimic the primary metabolite and change the properties of the electron rich anthracene which could aid electrostatic interactions with the electron-deficient nucleotides of a G-quadruplex structure. The anthracene-C10 group is a product of the synthesis and should also play a potential role in changing the electronic properties of the anthracene much like the C2 substitution.
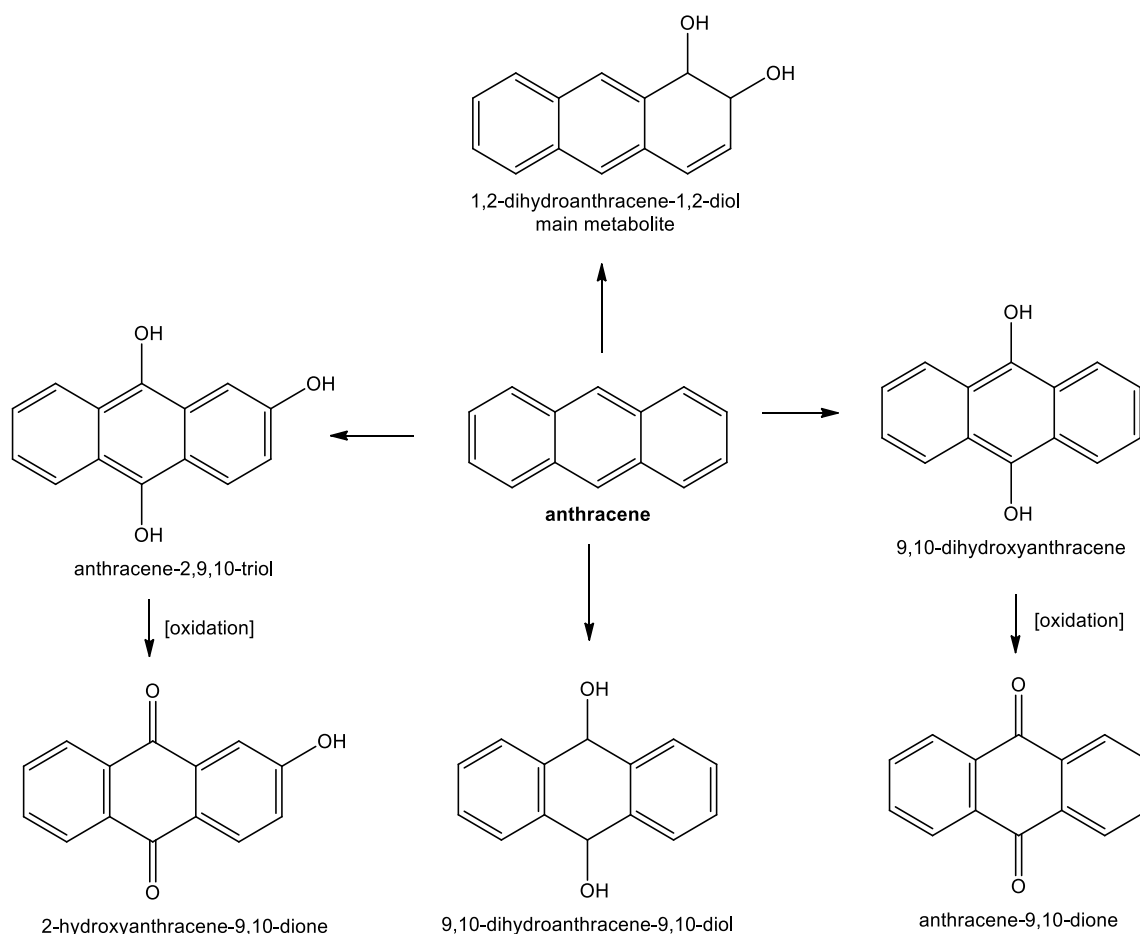

1,2-dihydroanthracene-1,2-diol
main metabolite

anthracene

anthracene-2,9,10-triol

9,10-dihydroxyanthracene

[oxidation]

[oxidation]

2-hydroxyanthracene-9,10-dione

9,10-dihydroanthracene-9,10-diol

anthracene-9,10-dione

Figure 5-2. Anthracene metabolism

It is clear from the above that we would prefer to avoid the anthracene metabolism. Here its worthwhile introducing the role of the isoxazole, which is *Sollbruchstellen*, which translates in English roughly to predetermined breaking point that is built to break on demand. This

concept was popularized by Schollkopf in his asymmetric amino acid synthesis *via* diketopiperazides.[18] In the present study, the isoxazole is the Trojan horse for a safer metabolic route. For a select few medicines containing an isoxazole ring system CYP-450 metabolism is well known and characterized.[6,19–22] The most common pathway for CYP-450 metabolism of isoxazoles is hydroxylation at the C5 position of the ring when an aliphatic carbon is present, such as a methyl or methylene, the earliest example being the oxacillins, including cloxacillin (discussed in Chapter 1).[5,6,21,23] In the oxacillin series the C-5 hydroxymethylene metabolites retain biological activity. This event is frequently followed by the addition of glucose and then
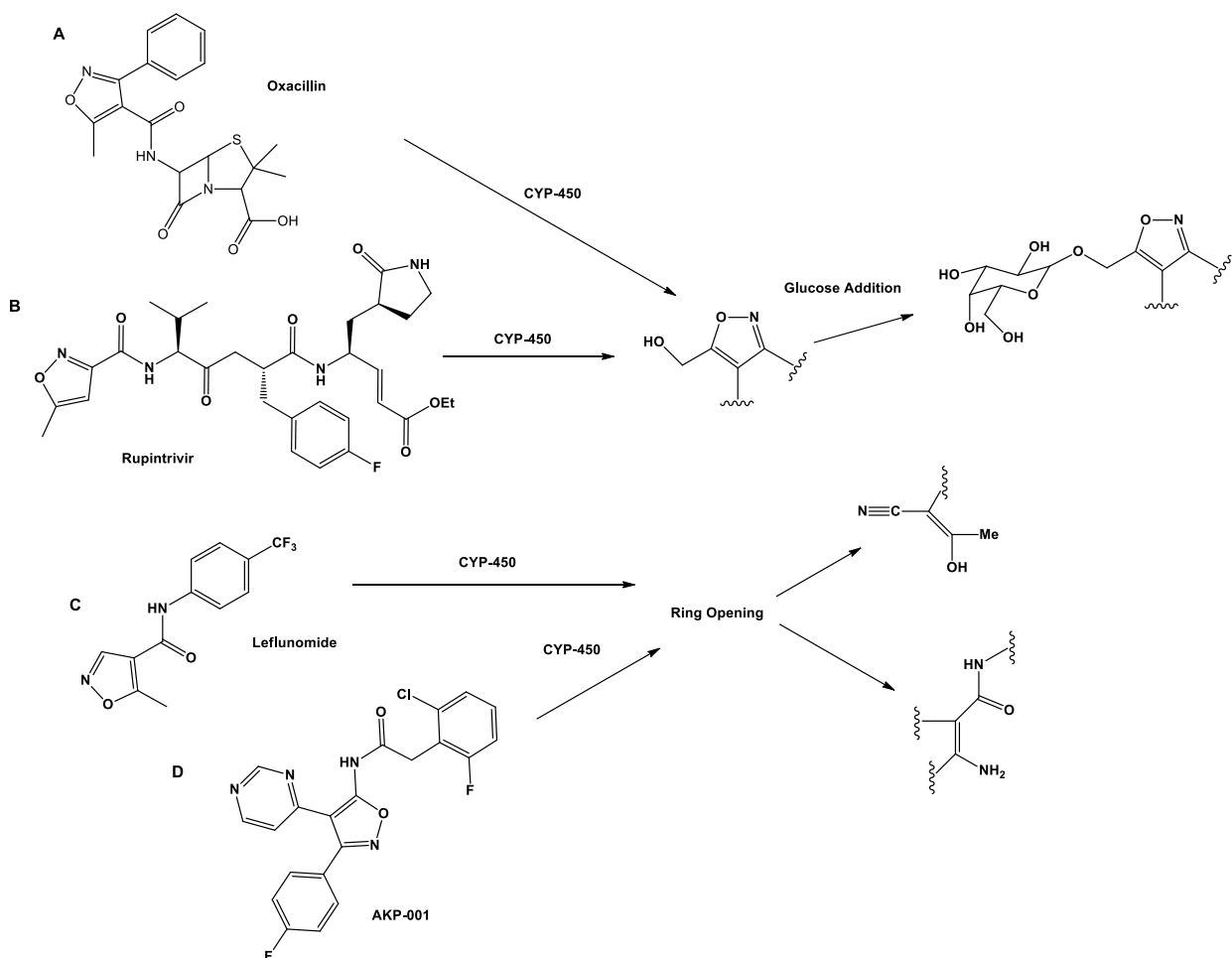
Figure 5-3. Reported fates of isoxazole CYP-450 metabolism

subsequent excretion (Figure 5-3 A and B), an early example being oxacillin.[5,6] Other pathways, such as isoxazole ring-opening of the O-N (Figure 5-3 C, D) bond (Figure 5-3 C and D), [19,22] are also know and characterized.

Collaborations are just in the beginning stages with our colleague Mike Wempe at the University of Colorado Anshutz Medical campus. With his knowledge and expertise in Drug Metabolism and Pharmacokinetics (DMPK) studies, we are confident and excited to start our journey to better understand PK parameters of our AIM compounds. Mike will begin pre-clinical studies by examining Cyp3A4 metabolism of isoxazoles. Initial studies would be evaluated in rat liver microsomes (RLM) using an LC-MS-MS technique, which has been shown to be very sensitive with detection limits as low as 1 ng.[24,25] Authentic C-5 hydroxyl products have been prepared previously by our group.[12,26]

5.4 Computational Modeling

Computational and comparative molecular modeling studies were performed on all seven compounds in Table 5-2 and three of the drugs shown in Figure 5-3 (Oxacillin, Leflunomide and Rupintrivir). For docking purposes, the crystallographic coordinates of the crystal structure of human cytochrome P4503A4 bound to an inhibitor ritonavir[27] were obtained from the Brookhaven Database (PDB code 3NXU and resolution 2.00 Å). The protein complex was then loaded within AutoDock Tools 1.5.6 (The Scripps Research Institute) and the ligand was then removed to leave the binding site unoccupied, which was used for the subsequent docking studies without any further modification. For preparation of ligand structures, fragments from ChemBioDraw Ultra 2010 were used to construct the compounds and loaded each in AutoDock Tools to confirm number of rotatable bonds, charge, and hybridization, and then the ligands were subject to iterations of MM2 energy minimization within ChemBio3D Draw 2010 (v.12.0). For

computational docking, AutoDock Vina 1.1.2 software was used in combination with the built-in scoring function.[28] The active site was defined as being any volume within center_x = 36.834, center_y = -15.442, center_z = 28.77, size_x = 34, size_y = 60, size_z = 40. AutoDock Vina defaults a number of up to 10 runs per ligand, each of which starts from a different orientation. Each AutoDock Vina run was saved and the strongest scoring binding pose of each ligand (subject to a rmsd default distance threshold of 2.0 Å) was compared to that of the reference ligand position observed in the crystal structure. The best pose(s) were visualized with PyMOL Molecular Graphics System version 1.3.

The computational studies were consistent with reported metabolism studies showing C-5 methyl hydroxylation being predominant for Oxacillin[5] (Figure 5-5) and Rupintrivir[21] (Figure 5-6) and isoxazole ring opening between the nitrogen and oxygen in Leflunomide[19] (Figure 5-7). All seven compounds did show anthracene ring oxidation as the primary mechanism of oxidation rather than C-5 methyl oxidation as previously thought. An example showing the ring oxidation is shown in Figure 5-8 in the phenoxy example. Furthermore, both the unsymmetrical derivatives (**8f-g**) only showed possible anthracene ring hydroxylation on either the 3 or 4 position for the 2,10-dimethoxy compound **8f** (Figure 5-9) or the 7/8 position for the 1-Chloro-2,10-methoxy compound **8g** (Figure 5-10). Comparisons can be made between the ligands from the AutoDock Vina[28] docking knowing that a hydrogen bond can vary in strength depending on the temperature, pressure, bond angle and the environment (dielectric constant), but a common rule of thumb is 1-2 kcal/mol. Leflunomide (Figure 5-7) scored the lowest at -8.6 kcal/mol, followed by Rupintrivir (Figure 5-6) at -10.0 kcal/mol and Oxacillin (Figure 5-5) at -10.3 kcal/mol. While not surprising as both Rupintrivir and Oxacillin both have C-5 hydroxylation metabolism, this requires more of a stronger bond to the CYP for hydroxylation to occur, as for Leflunomide

doesn't require as much energy for the one-electron transfer ring opening to occur. On the other side, the 1-Chloro-2,10-dimethoxy AIM DT **8g** (Figure 5-10) only scored at -8.5 kcal/mol and the 2,10-dimethoxy AIM DT **8f** (Figure 5-9) scored in at -8.8 kcal/mol with the phenoxy AIM DT **8b** (Figure 5-8) scored way above the rest at -11.6 kcal/mol. The excessively high scoring of **8b** could be attributed to how well it fits into the CYP pocket above the heme. Comparing the phenoxy group versus the dimethoxy, the extra lipophilic ring helps gets added interactions with the residues without twisting too many residues outside of the pocket.
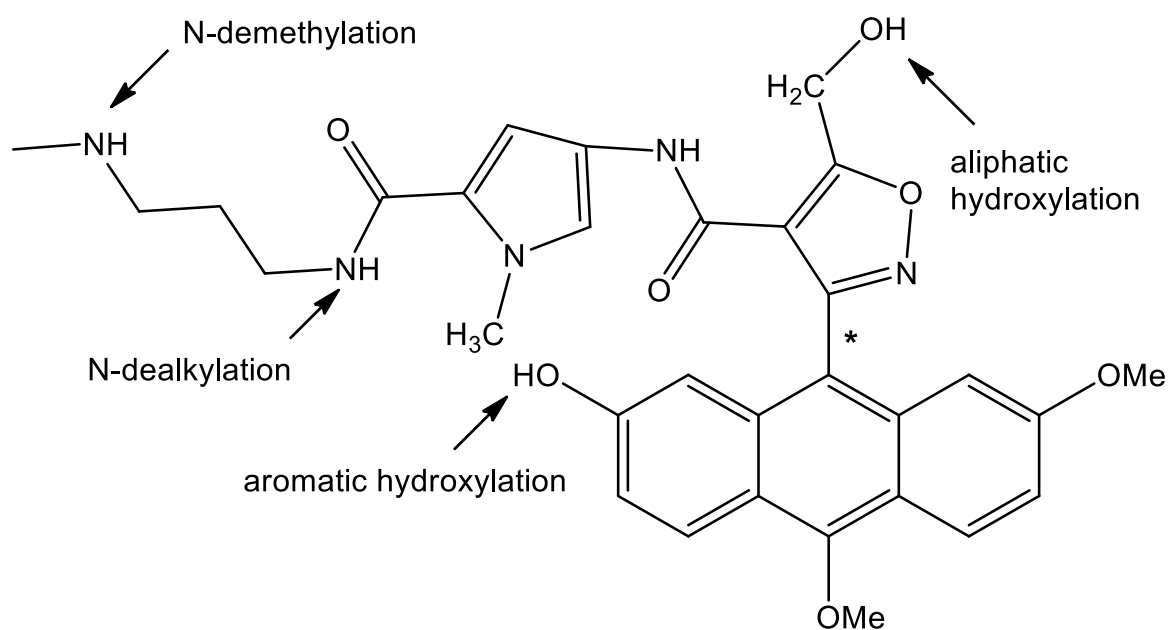
Figure 5-4. Predicted axial chiral AIM **8c** anthracene major metabolite mimic

While not shown, all seven compounds also had poses with the dimethylamine doubletails over the heme group. Thus, the predicted metabolism for the axial chiral compounds and oxy series compounds are not consistent with our previous idea (Figure 5-4). Since anthracene metabolism and its resulting toxicity is a concern, our initial metabolism studies can (1) assess whether the computational model is valid and then either (2) future work should

determine   if substitution at the C-5, and/or anthracene 2,3, or 10 positions populate the

conformation of conformers docking at CYP 3A4 with the isoxazole C-5 proximal to the heme,

or (3) blocking the putative anthracenyl ring metabolism sites with halogens. The question to be

determined in the future is whether selectivity will be observed for the safer isoxazole
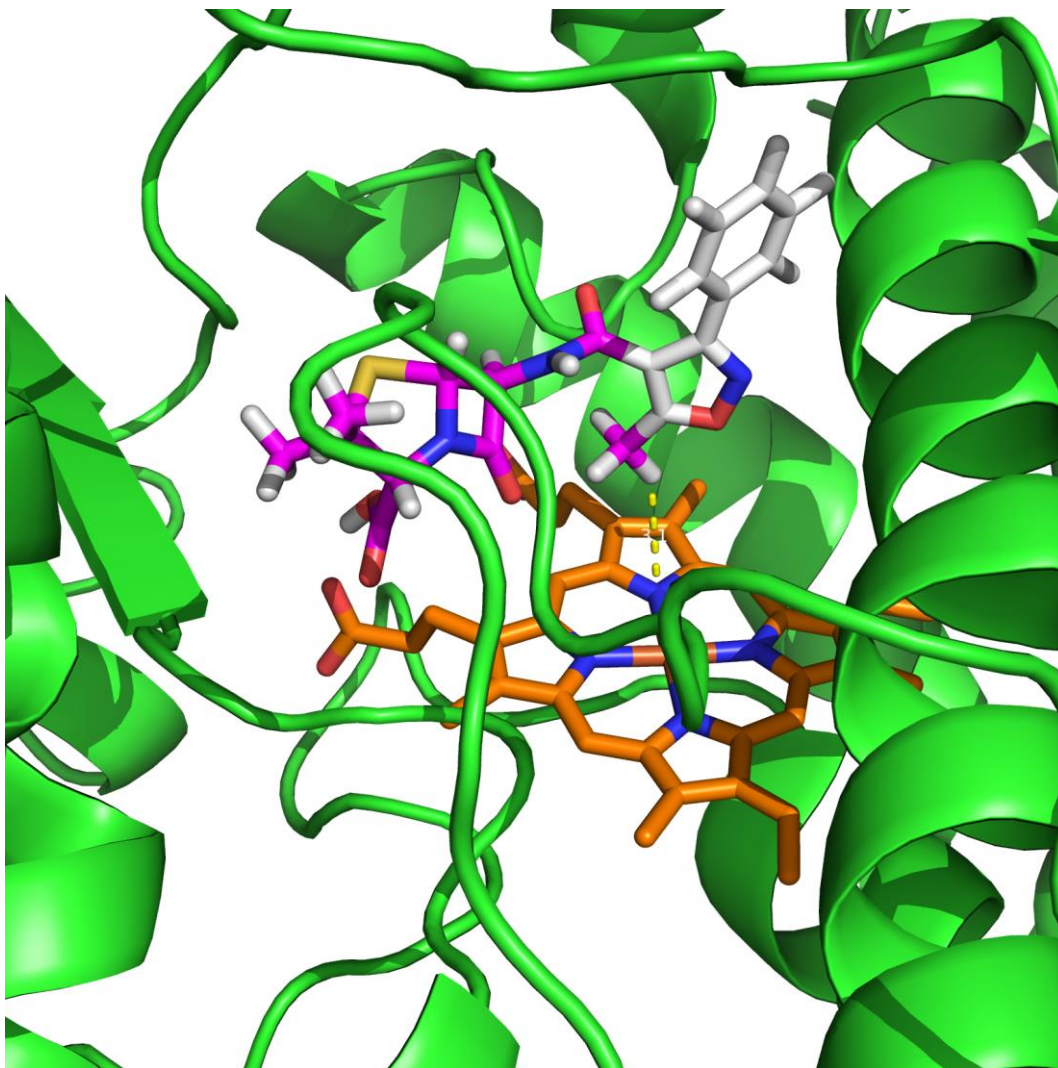
metabolism routes.

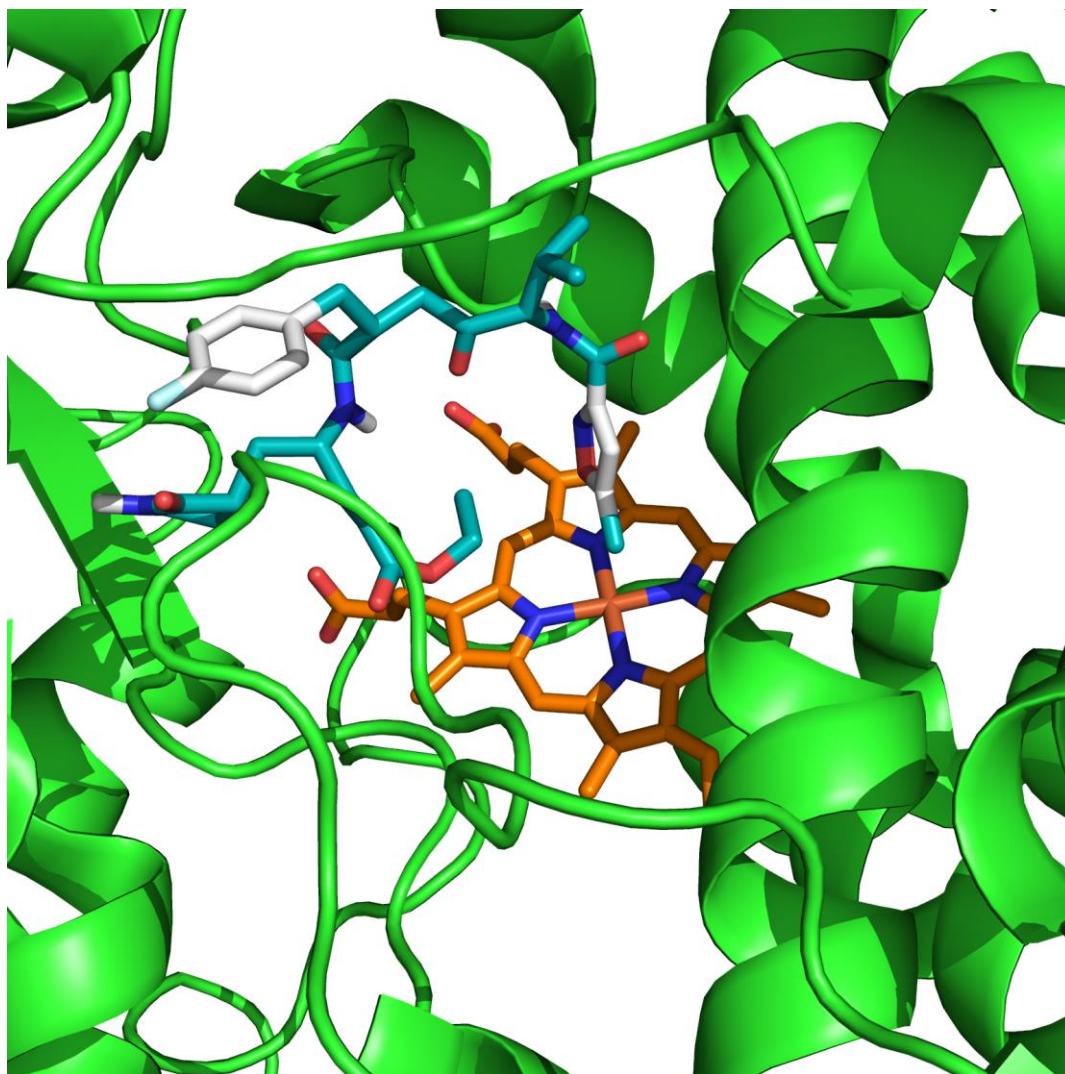**Figure 5-5**. Oxacillin, magenta, docked in CYP450 3A4 active site, green; HEME, orange.

Figure 5-6. Rupintrivir, cyan, docked in CYP450 3A4 active site, green; HEME, orange.
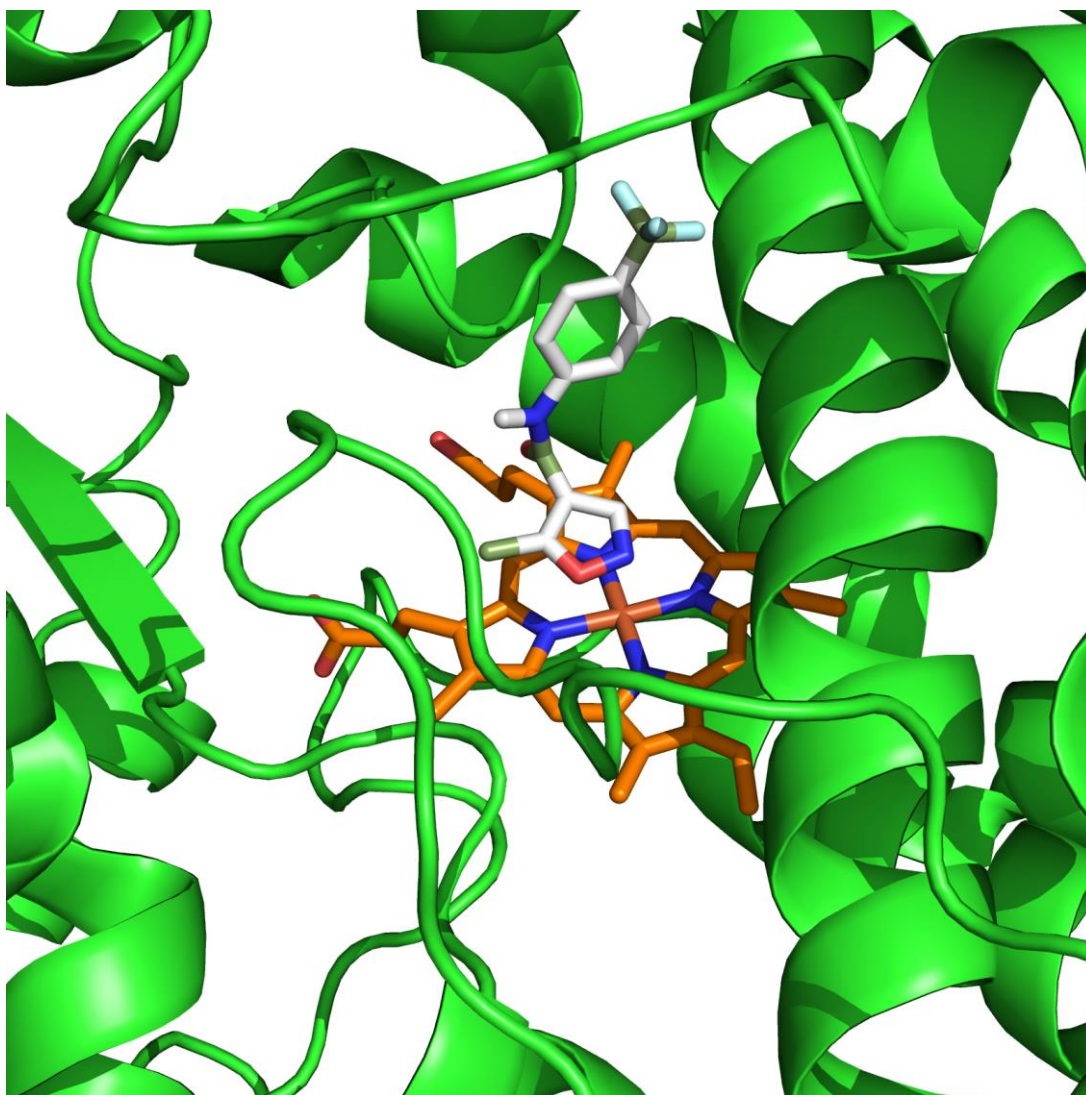
Figure 5-7. Leflunomide, white, docked in CYP450 3A4 active site, green; HEME, orange.
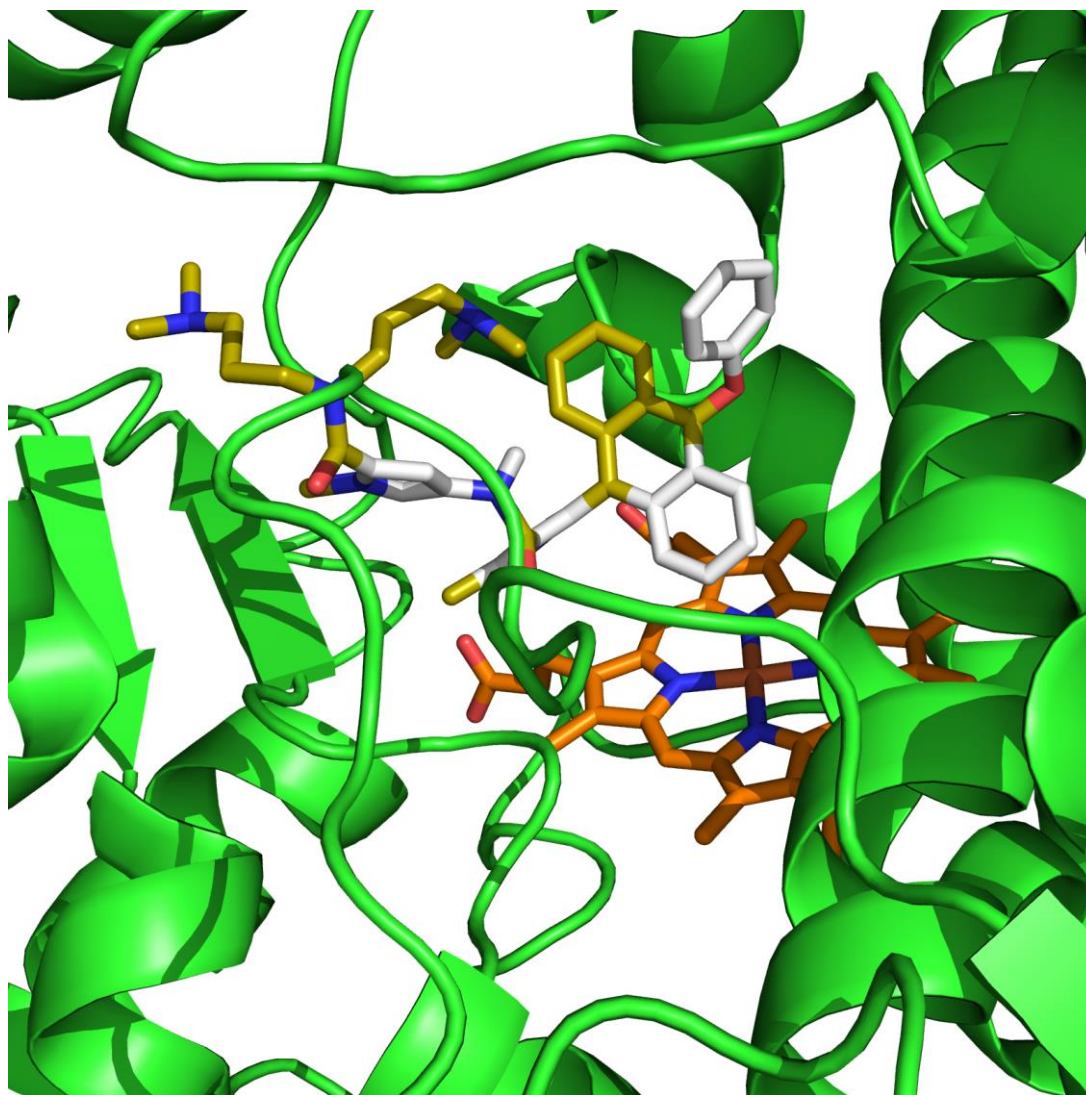
Figure 5-8. Compound **8b**, yellow, docked in CYP450 3A4 active site, green; HEME, orange.
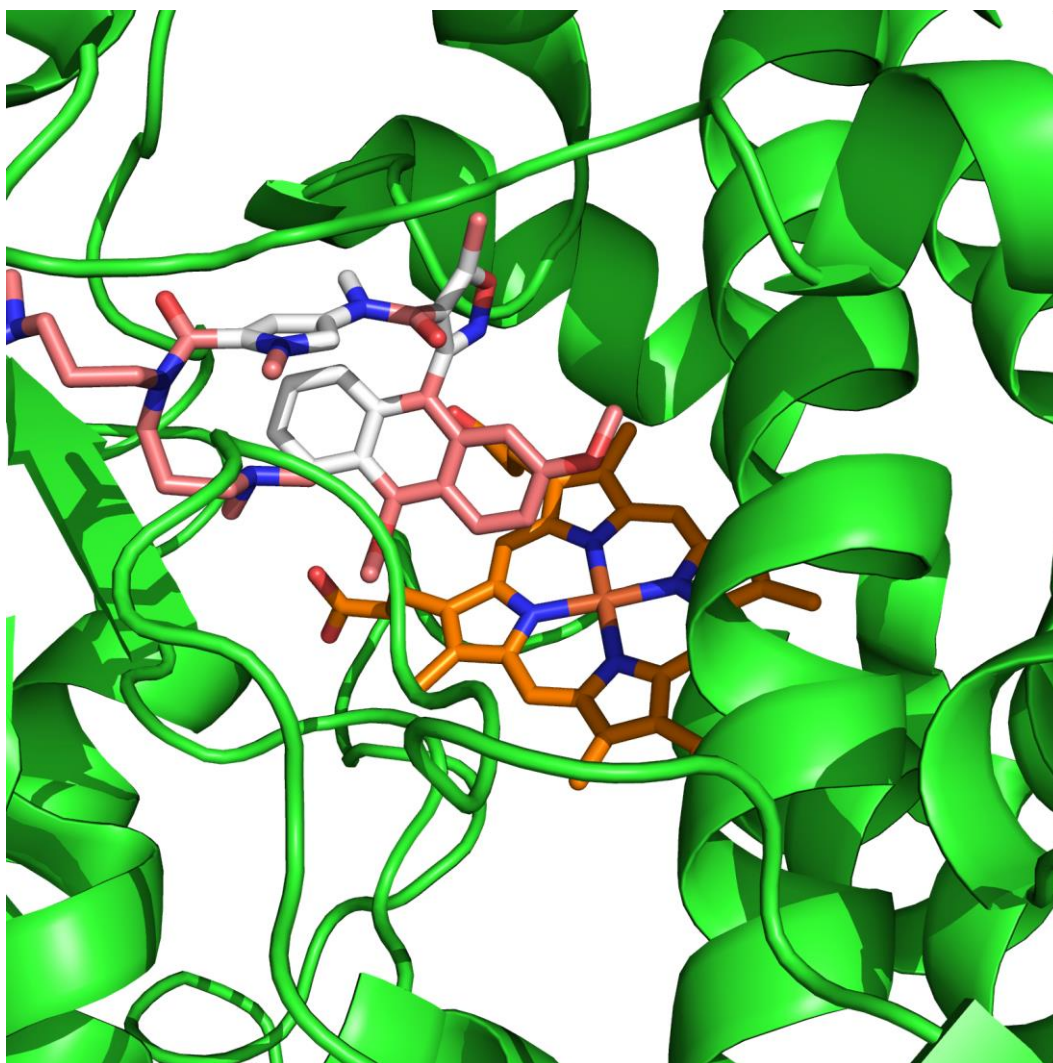
Figure 5-9. Compound **8f**, red, docked in CYP450 3A4 active site, green; HEME, orange.
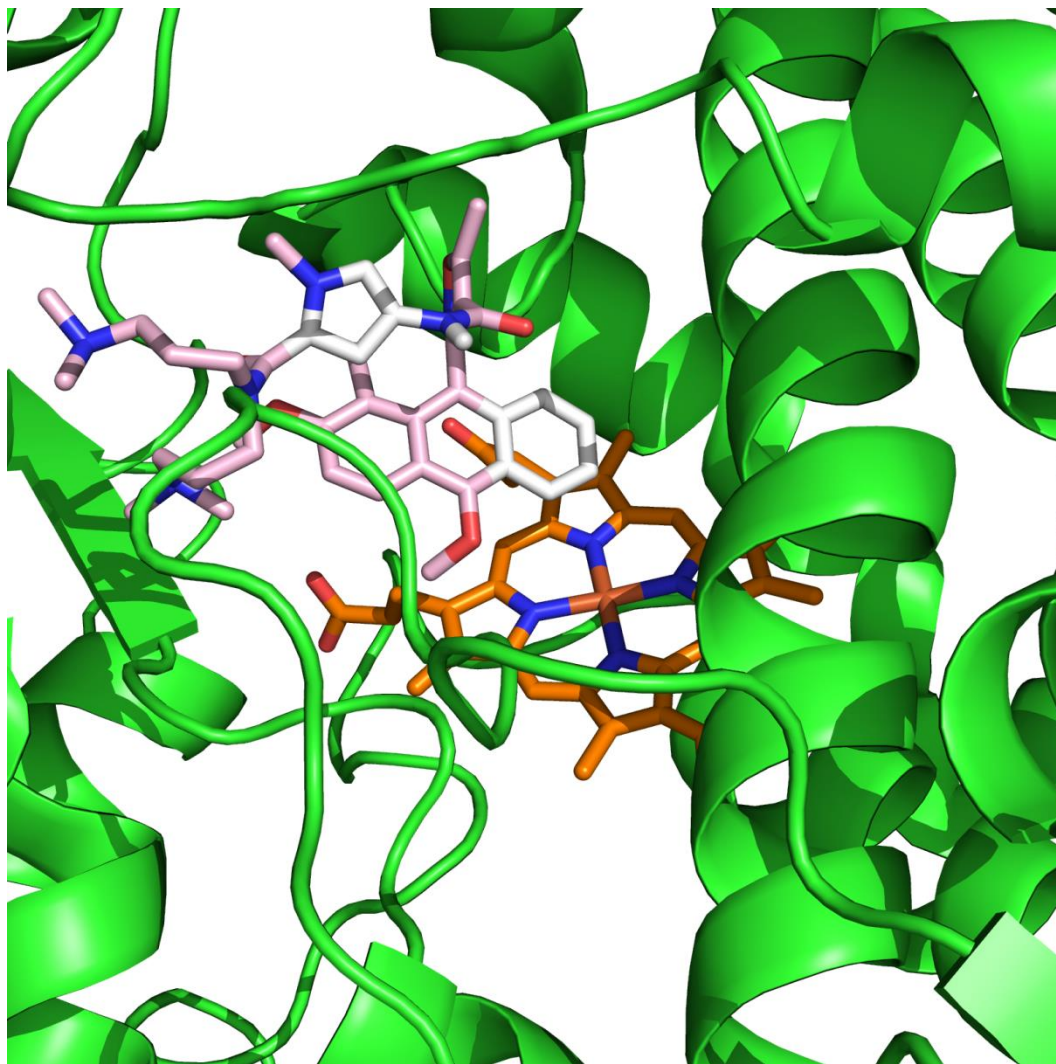
Figure 5-10. Compound **8g**, pink, docked in CYP450 3A4 active site, green; HEME, orange.

References

(1)   Guengerich, F. P. Cytochrome P450 and Chemical Toxicology. *Chem. Res. Toxicol.* **2008**, *21* (1), 70–83.

(2)   Rendic, S.; Guengerich, F. P. Survey of Human Oxidoreductases and Cytochrome P450 Enzymes Involved in the Metabolism of Xenobiotic and Natural Chemicals. *Chem. Res. Toxicol.* **2015**, *28* (1), 38–42.

(3)   Wienkers, L. C.; Heath, T. G. Predicting in Vivo Drug Interactions from in Vitro Drug Discovery Data. *Nat. Rev. Drug Discov.* **2005**, *4* (10), 825–833.

(4)   Loi, C.-M.; Smith, D. A.; Dalvie, D. Which Metabolites Circulate? *Drug Metab. Dispos.* **2013**, *41* (5), 933–951.

(5)   Murai, Y.; Nakagawa, T.; Yamaoka, K.; Uno, T. High Performance Liquid Chromatographic Analysis and Pharmacokinetic Investigation of Oxacillin and Its Metabolites in Man. *Chem. Pharm. Bull. (Tokyo)* **1981**, *29* (11), 3290–3297.

(6)   Bylund, J.; Macsari, I.; Besidski, Y.; Olofsson, S.; Petersson, C.; Arvidsson, P. I.; Bueters, T. Novel Bioactivation Mechanism of Reactive Metabolite Formation from Phenyl Methyl-Isoxazoles. *Drug Metab. Dispos.* **2012**, *40* (11), 2185–2191.

(7)   Zhang, J. Y.; Fast, D. M.; Breau, A. P. Determination of Valdecoxib and Its Metabolites in Human Urine by Automated Solid-Phase Extraction–liquid Chromatography–tandem Mass Spectrometry. *J. Chromatogr. B* **2003**, *785* (1), 123–134.

(8)   Yuan, J. J.; Yang, D.; Zhang, J. Y.; Bible, R.; Karim, A.; Findlay, J. W. A. Disposition of a pecific Cyclooxygenase-2 Inhibitor, Valdecoxib, in Human. *Drug Metab. Dispos.* **2002**, *30* (9), 1013–1021.

(9)   Zhou, P.; Natale, N. R. Lateral Lithiation of Ethyl 4-Acetyl-5-Methyl-3-Isoxazolyl Carboxylate with 5,5-Dimethyl-1,3-Dioxanyl as a Directing Group. *Tetrahedron Lett.* **1998**, *39* (45), 8249–8252.

(10) Burkhart, D. J.; Zhou, P.; Blumenfeld, A.; Twamley, B.; Natale, N. R. An Improved Procedure for the Lateral Lithiation of Ethyl 4-Acetyl-5-Methyl-3-Isoxazolyl Carboxylate. *Tetrahedron* **2001**, *57* (38), 8039–8046.

(11) Han, X.; Li, C.; Rider, K. C.; Blumenfeld, A.; Twamley, B.; Natale, N. R. The Isoxazole as a Linchpin for Molecules That Target Folded DNA Conformations: Selective Lateral Lithiation and Palladation. *Tetrahedron Lett.* **2002**, *43* (43), 7673–7677.

(12) Rider, Kevin C.; Burkhart, David J.; Li, Chun; McKenzie, Andrew R.; Nelson, Jared K.; Natale, Nicholas R. Preparation of Chiral Isoxazole Carbinols via Catalytic Asymmetric Corey-Bakshi-Shibata Reduction. *ARKIVOC* **2010**, *viii*, 97–107.

(13) Zanger, U. M.; Schwab, M. Cytochrome P450 Enzymes in Drug Metabolism: Regulation of Gene Expression, Enzyme Activities, and Impact of Genetic Variation. *Pharmacol. Ther.* **2013**, *138* (1), 103–141.

(14) Lipinski, C. A.; Lombardo, F.; Dominy, B. W.; Feeney, P. J. Experimental and Computational Approaches to Estimate Solubility and Permeability in Drug Discovery and Development Settings. *Adv. Drug Deliv. Rev.* **2012**, *64, Supplement*, 4–17.

(15) *Calculator Plugins Were Used for Structure Property Prediction and Calculation*; ChemAxon, 2015.

(16) Viswanadhan, V. N.; Ghose, A. K.; Revankar, G. R.; Robins, R. K. Atomic Physicochemical Parameters for Three Dimensional Structure Directed Quantitative Structure-Activity Relationships. 4. Additional Parameters for Hydrophobic and Dispersive

Interactions and Their Application for an Automated Superposition of Certain Naturally Occurring Nucleoside Antibiotics. *J. Chem. Inf. Comput. Sci.* **1989**, *29* (3), 163–172.

(17) Boyland, E.; Kimura, M.; Sims, P. Metabolism of Polycyclic Compounds. 26. The Hydroxylation of Some Aromatic Hydrocarbons by the Ascorbic Acid Model Hydroxylating System and by Rat-Liver Microsomes. *Biochem. J.* **1964**, *92* (3), 631–638.

(18)   Schöllkopf, U.; Groth, U.; Deng, C. Enantioselective Syntheses of (R)-Amino Acids Using L-Valine as Chiral Agent. *Angew. Chem. Int. Ed. Engl.* **1981**, *20* (9), 798–799.

(19) Kalgutkar, A. S.; Nguyen, H. T.; Vaz, A. D. N.; Doan, A.; Dalvie, D. K.; McLeod, D. G.; Murray, J. C. In Vitro Metabolism Studies on the Isoxazole Ring Scission in the anti-inflammatory agent Leflunomide to its Active α-cyanoenol Metabolite A771726: Mechanistic Similarities with the Cytochrome P450-Catalyzed Dehydration of aldoximes. *Drug Metab. Dispos.* **2003**, *31* (10), 1240–1250.

(20) Macsari, I.; Sandberg, L.; Besidski, Y.; Gravenfors, Y.; Ginman, T.; Bylund, J.; Bueters, T.; Eriksson, A. B.; Lund, P.-E.; Venyike, E.; Arvidsson, P. I. Phenyl Isoxazole Voltage-Gated Sodium Channel Blockers: Structure and Activity Relationship. *Bioorg. Med. Chem. Lett.* **2011**, *21* (13), 3871–3876.

(21) Zhang, K. E.; Hee, B.; Lee, C. A.; Liang, B.; Potts, B. C. M. Liquid Chromatography-Mass Spectrometry and Liquid Chromatography-NMR Characterization of in Vitro Metabolites of a Potent and Irreversible Peptidomimetic Inhibitor of Rhinovirus 3C Protease. *Drug Metab. Dispos.* **2001**, *29* (5), 729–734.

(22) Shirota, K.; Kaneko, M.; Sasaki, M.; Minato, K.; Fujikata, A.; Ohta, S.; Hisaka, A.; Suzuki, H. Analysis of the Disposition of a Novel p38 MAPK Inhibitor, AKP-001, and Its

Metabolites in Rats with a Simple Physiologically Based Pharmacokinetic Model. *Drug Metab. Dispos.* **2015**, *43* (2), 217–226.

(23) Zhang, J. Y.; Yuan, J. J.; Wang, Y.-F.; Bible, R. H.; Breau, A. P. Pharmacokinetics and Metabolism of a COX-2 Inhibitor, Valdecoxib, in Mice. *Drug Metab. Dispos.* **2003**, *31* (4), 491–501.

(24) Wempe, M. F.; Anderson, P. L. Atazanavir Metabolism According to CYP3A5 Status: An In Vitro-In Vivo Assessment. *Drug Metab. Dispos.* **2011**, *39* (3), 522–527.

(25) Wempe, M. F.; Rice, P. J.; Lightner, J. W.; Jutabha, P.; Hayashi, M.; Anzai, N.; Wakui, S.; Kusuhara, H.; Sugiyama, Y.; Endou, H. Metabolism and Pharmacokinetic Studies of JPH203, an L-Amino Acid Transporter 1 (LAT1) Selective Compound. *Drug Metab. Pharmacokinet.* **2012**, *27* (1), 155–161.

(26) Li, C.; Twamley, B.; Natale, N. R. Preparation and Crystal Structures of Two 3-Anthracenyl Isoxazolyl Sulfonamides. *J. Heterocycl. Chem.* **2008**, *45* (1), 259–264.

(27) Sevrioukova, I. F.; Poulos, T. L. Structure and Mechanism of the Complex between Cytochrome P4503A4 and Ritonavir. *Proc. Natl. Acad. Sci.* **2010**, *107* (43), 18422–18427.

(28) Trott, O.; Olson, A. J. AutoDock Vina: Improving the Speed and Accuracy of Docking with a New Scoring Function, Efficient Optimization, and Multithreading. *J. Comput. Chem.* **2010**, *31* (2), 455–461.